ATTENUATION STUDIES FROM INVERSION OF STRONG MOTION DATA

Ph.D. THESIS

by

PARVEEN KUMAR

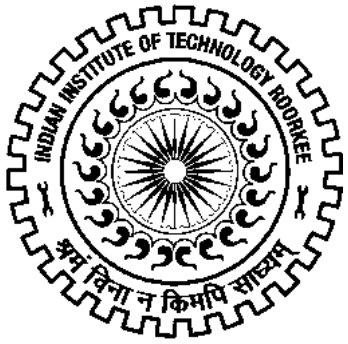

DEPARTMENT OF EARTH SCIENCES
INDIAN INSTITUTE OF TECHNOLOGY ROORKEE
ROORKEE-247 667 (INDIA)

JANUARY, 2014

ATTENUATION STUDIES FROM INVERSION OF STRONG MOTION DATA

A THESIS
Submitted in partial fulfillment of the
requirements for the award of the degree
of
DOCTOR OF PHILOSOPHY
in
EARTH SCIENCES

by
PARVEEN KUMAR

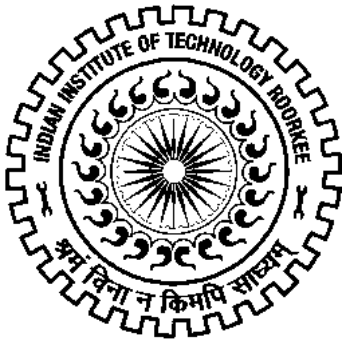

DEPARTMENT OF EARTH SCIENCES
INDIAN INSTITUTE OF TECHNOLOGY ROORKEE
ROORKEE-247 667 (INDIA)

JANUARY, 2014

INDIAN INSTITUTE OF TECHNOLGY ROORKEE
ROORKEE

CANDIDATE'S DECLARATION

I hereby certify that the work, which is being presented in this thesis entitled "**ATTENUATION STUDIES FROM INVERSION OF STRONG MOTION DATA**" in partial fulfillment of the requirements for the award of the Degree of **Doctor of Philosophy** and submitted in the **Department of Earth Sciences** of the Indian Institute of Technology Roorkee is an authentic record of my own work carried out during a period from December, 2010 to January, 2014 under the supervision of **Dr. Anand Joshi**, Department of Earth Sciences, Indian Institute of Technology Roorkee.

The matter presented in the thesis has not been submitted by me for the award of any other degree of this or any other Institute.

(PARVEEN KUMAR)

This is to certify that the above statement made by the candidate is correct to the best of my knowledge.

Dated: January , 2014 (Dr. ANAND JOSHI)
Supervisor

The Ph.D. Viva-Voce Examination of **Mr. Parveen Kumar**, Research Scholar, has been held on . . . . . .

Signature of Supervisor (s) **Signature of External**

Chairman, SRC/CRC **Head of the Deptt./Centre**

ABSTRACT

The amplitude of seismic energy recorded at recording sites is influenced by the source characteristics, medium characteristic and local site conditions. The effects of travel path on earthquake ground motion are directly related to the attenuation property of medium. The knowledge of attenuation characteristic is an essential requirement for determination of the earthquake source parameters and simulation of strong ground motions. It plays an important role in estimation of the seismic hazard of a region. Attenuation property of earth medium is quantitatively defined by a dimensionless quantity know as quality factor 'Q' which defined as the fractional loss of energy per cycle (Knopoff, 1964). It is observed from analysis of strong motion accelerogram that peak ground acceleration is associated with the arrival of S-waves (Hadley et al., 1982). In this thesis shear wave quality factor (Q_β) is used to characterize the attenuation studies of Kumaon Himalaya, India and Central Honshu, Japan region.

The inversion of strong motion data has been used for determination of the attenuation studies in the different parts of the Himalayan region by Joshi (2006a, 2006b and 2007) and Joshi et al. (2010). Joshi (2006a and 2007) and Joshi et al. (2010) have used inversion technique to determine three dimensional attenuation structure based on the shear wave quality factor. The inversion algorithm given by Joshi et al. (2010) for estimation of three dimensional distribution of attenuation property uses strong motion data from limited number of events. Modification in this technique has been made in the present thesis to consider large number of events for better estimation of attenuation characteristic of the region. Various numerical experiments have been made to check the stability of this inversion algorithm. In this work three dimensional attenuation structures have been determined for the Central Honshu, Japan and Kumaon Himalaya, India region to validate the present modified technique. Strong motion data has been used by Joshi (2006b) to obtain frequency dependent shear wave quality factor from inversion of spectral acceleration data. This algorithm estimates simultaneously both the frequency dependent attenuation relation and site effect. Seismic moment is used as one of the main input in the algorithm developed by Joshi (2006b) for the estimation of frequency dependent shear wave quality factor from inversion of strong motion data. Seismic moment used in this algorithm is computed or assumed from independent sources of well studied earthquakes. Modification in this algorithm is made to compute seismic moment directly from the records and refine its value in the inversion scheme.

Three dimensional frequency dependent S-wave quality factor ($Q_\beta(f)$) values for the central Honshu region of Japan have been determined in this thesis using modified algorithm based on inversion of strong motion data. Twenty one earthquakes digitally recorded on strong motion stations of KiK-net network have been used in this work. The borehole data at rock sites having high signal to noise ratio and minimum site effect has been used in this work. The attenuation structure is determined by dividing the entire area into 25 three dimensional blocks of uniform thickness having different frequency dependent shear wave quality factor. Values of shear wave quality factor have been determined at different frequencies. The obtained attenuation structure is compared with the major tectonic features in the region. The comparison shows that the obtained attenuation structure is capable of resolving major tectonic features present in the area. The proposed attenuation structure is further compared with the probabilistic seismic hazard map of the region and shows that it bears some remarkable similarity in the patterns seen in seismic hazard map though two approaches of obtaining hazards are totally different. In this thesis, the frequency dependent shear wave quality factor ($Q_\beta(f)$) has been calculated using strong motion data of the Kumaon Himalaya. A dense network of strong ground motion recorders in the Kumaon region of the Uttarakhand Himalaya is operating since 2006. This network has recorded 294 earthquakes upto July, 2013. A total of forty events recorded on this network have been used for this work. The developed algorithm for inversion of strong motion data gives simultaneously both the shear wave quality factor and the site effect. The site effects obtained from the inversion are compared with the technique given by Lermo and Chavez-Garcia (1993). The comparison of site effect from inversion and H/V technique proposed by Lermo and Chavez-Garcia (1993) indicate that the obtained site effects are well within the standard limit of error. The $Q_\beta(f)$ values at different stations are calculated by using both the North South (NS) and East West (EW) component of acceleration records. The $Q_\beta(f)$ values obtained from both NS and EW components at 16 stations have been used to compute a regional relationship for the Kumaon Himalaya of form $Q_\beta(f) = (28\pm2.1)f^{(1.2\pm0.09)}$. Kumar et al. (2005b) suggests that low Q_o (<200) and high n (>0.8) value indicate high tectonic and seismic active region. Therefore obtained $Q_\beta(f)$ relation revealed that Kumaon region lies in tectonic and seismic active region.

In this thesis, three dimensional attenuation structures based on the frequency dependent shear wave quality factor values have been determined for the Kumaon Himalaya region. Eighteen events recorded on Kumaon network have been used for the present work. Shear wave quality factor values have been estimated at different frequencies for two different rectangular blocks of

surface dimension 85×55 km and 90×30 km which lie in the Kumaon Himalaya region. Both blocks are divided into 25 three dimensional blocks of uniform thickness having different $Q_\beta(f)$ values. The three dimensional distributions of frequency dependent shear wave quality factor values in two different blocks provide attenuation property of the region. The observed contours of shear wave quality factor show comparable trends with the major tectonic units present in the region. The site amplification and frequency dependent shear wave quality factor determined at 16 stations from inversion of strong motion data have been used to compute the source parameters of the Sikkim earthquake (M_w = 6.9) of 18 September, 2011. This earthquake is recorded on six stations of strong motion network in the Uttarakhand Himalaya located about 900 km away from the epicenter of this earthquake. In this work the spectrum of S-phase recorded at these far field stations has been corrected for site amplification term and anelastic attenuation at source and recording site, respectively. The obtained source spectrum from acceleration records is compared with the theoretical source spectrum defined by Brune (1970) at each station for both horizontal components of the records. Iterative forward modeling of theoretical source spectrum give the average estimate of seismic moment (M_o), source radius (r_o) and stress drop ($\Delta\sigma$) as (3.2 ±0.8) $\times 10^{26}$ dyne-cm, 13.3 ±0.8 km and 59.2 ±8.8 bars, respectively for the Sikkim earthquake.

ACKNOWLEDGEMENT

It gives me great pleasure to thank all the persons who helped me in one way or other for the completion of this research work.

It gives me a great pleasure to express my deepest gratitude to my Ph.D. supervisor **Dr. Anand Joshi** from Department of Earth Sciences, for his guidance, encouragement and providing a professional environment in tenure of my research work. I highly appreciate all his contributions of time, ideas, persistence in high quality results, and make my Ph.D. experience productive and stimulating.

I also thankful to **P.K. Gupta** (former Head) and **A.K. Saraf**, Head of the Department of Earth Sciences, Indian Institute of Technology Roorkee, for providing departmental facilities for carrying out my research work. I sincerely thanks **Ministry of Earth Sciences** (MoES), Government of India supported project (Grant no: MoES/P.O.(Seismo)/1(42)/2009) entitled as "Subsurface imaging of Uttaranchal Himalaya using a dense network of strong ground motion recorders". The financial funding for carrying this work from **Ministry of Earth Sciences** (MoES), Government of India supported project (Grant no: MoES/P.O.(Seismo)/1(42)/2009) is thankfully acknowledged.

I feel very happy to thank my colleagues and friends, **Ashvini Kumar, Pushpa, Chinmoy, Sandeep Arora, Piu, Monu, Kamal**, **Rakesh** and (Late) **Mr. Om Prakash** for their sincere support and encouragement through my stay at IIT Roorkee.

I would like to thank my father, Sh. **Satpal Saini**, mother, Smt. **Sunita**, sister, **Nisha** for their constant love and moral support. Last but not the least I express love and gratitude to my wife, **Reena**, for her unending love, patience, understanding and constant personal support.

(Parveen Kumar)

CONTENTS

LIST OF FIGURES

LIST OF TABLES

LIST OF SYMBOLS AND ABBREVIATIONS

$A(f)$	Acceleration spectra
$A_{op}^{'}(f)$	Spectral acceleration at observation point 'op'
$A_{op}^{cal}(f)$	Calculated spectral acceleration at observation point 'op'
$A_{op}^{obs}(f)$	Observed spectral acceleration at observation point 'op'
C	Covariance matrix
D(f)	Frequency-dependent diminution function
D_{ijk}	Attenuation coefficient of ijk^{th} block
E	Computational error
f	Frequency
f_c	Corner frequency
f_m	High frequency cutoff range of the high-cut filter
FS	Amplification due to the free surface
g	Amplifying effects
G_R	Geometrical factor
I	Unit matrix
M_o	Seismic moment
M_s	Surface-wave magnitude
n	Parameter represent level of tectonic activity of a region
$P(f,f_m)$	High cut filter
PRTITN	Reduction factor that accounts for the partitioning of total shear-wave energy into two horizontal components
Q	Quality factor
$Q_{\beta 1}$	Quality factor of the source region
$Q_{\beta 2}$	Quality factor of the site region
Q(f)	Frequency dependent quality factor

Q_c	Coda wave quality factor
Q_o	Parameter represent heterogeneities of a region
Q_α	P-wave quality factor
Q_β	Shear wave quality factor
$Q_\beta(f)$	Frequency dependent Shear-wave quality factor
R	Hypocentral distance
R_m	Resolution matrix
rms_{dat}	Root mean square error for data matrix
RMSE	Root Mean Square Error
rms_{mod}	Root mean square error for model matrix
r_o	Source radius
R_{op}	Ratio of observed and calculated spectral acceleration at observation point ‘op’
$R_{\theta\varphi}$	Radiation pattern coefficient
$S(f)$	Source acceleration spectrum
$S_{op}^{cal}(f)$	Source spectra at observation point ‘op’
$S(f,f_c)$	Source spectrum
$S_D(f)$	Source displacement spectrum
$S_o(f)$	Actual earthquake source strength
T_{ijk}	Time spent in ijk^{th} block
T_{pad}	Length of zero pad
X(k)	Complex series in frequency domain
X(n)	Real time signal
$X_I(k)$	Imaginary part of the complex function
$X_R(k)$	Real part of the complex function
β	Shear wave velocity

β_1	Shear wave velocity of source region
β_2	Shear wave velocity of site region
δD_{ijk}	Difference between the initial and final attenuation coefficient in the ijk^{th} block
λ	Damping factor
μ	Mean value
ρ	Density of earth medium
Σ	Summation
σ	Standard deviation
σ^2_d	Variance of error in data
Ω_o	Long term flat level
Δf_c	Small change in the corner frequency
$\Delta\sigma$	Stress drop

LIST OF PUBLICATIONS FROM THE RESEARCH WORK

[1] A. Joshi, **Parveen Kumar** and S. Arora, (2014), Use of site amplification, anelastic attenuation for determination of source parameters of the Sikkim earthquake of 18 September, 2011 using far field strong motion data, Natural Hazard, vol. 70, 217-235.

[2] **Parveen Kumar**, A. Joshi and O. P. Verma, (2013), Attenuation tomography based on strong motion data: Case study of central Honshu region, Japan, Pure and applied Geophysics, vol. 170, 2087-2106.

[3] **Parveen Kumar** and A. Joshi, (2013), Stability of algorithm for determination of three-dimensional attenuation structures, International conference on Challenges in Disaster mitigation and Management.

[4] **Parveen Kumar** and A. Joshi, (2013), Regional velocity model in Kumaon Himalaya from localization of strong motion events, National conference on Earth Sciences in India: Challenges and Emerging Trends.

[5] A. Joshi, **P. Kumar**, M. Mohanty, A. R. Bansal, V. P. Dimri, and R. K. Chadha, (2012), Determination of $Q_{\beta}(f)$ in different parts of Kumaon Himalaya from the inversion of spectral acceleration data, Pure and applied Geophysics, vol. 169, 1821-1845.

[6] **P. Kumar** and A. Joshi, (2012), Attenuation tomography of Kumaon Himalaya in Pithoragarh region using strong motion data, Nation conference on Engineering Geophysics for Civil Engineering and Geo-Hazards.

[7] **Parveen Kumar** and A. Joshi, (2014), Three-dimensional attenuation structure in the region of Kumaon Himalaya, India based on inversion of strong motion data, Pure and applied Geophysics (Under review).

[8] **Parveen Kumar** and A. Joshi, (2014), Attenuation characteristics of shear waves in Kumaon Himalaya, India using the inversion of strong motion data, Seismological Research Letters (Communicated).

Chapter – 1

Introduction

Seismic energy released from earthquake attenuates while it travels through earth medium. Attenuation characteristics of medium decide the decay of the amplitude of ground acceleration at various sites. Attenuation relation is one of the simple relations to describe decay rate of peak ground acceleration for an earthquake. It is a mathematical expression relating specific parameters of ground shaking to one or more seismological parameters of an earthquake (Campbell, 2001). The seismological parameters used in the attenuation relation characterize the earthquake source, path of seismic wave between the source and the observation point, soil and geological formation beneath the site (Campbell, 2001). Several attenuation relations obtained by different workers are presented by Douglas (2001). One of the major problems of attenuation relation is its dependency on data set of specific region and has always possibilities of improvement with advancement of data acquisition techniques. Attenuation property of earth medium is also quantitatively defined by a dimensionless quantity know as quality factor 'Q' given by Knopoff (1964). The quality factor 'Q' is defined as the fractional loss of energy per cycle (Knopoff, 1964). It is also defined as a ratio of stored energy to dissipated energy during one cycle of the wave (Johnston and Toksoz, 1981).

Different quality factors are assigned to different seismic waves. Attenuation coefficient in any region can be quantified by P-wave quality factor (Q_α); shear wave quality factor (Q_β) and coda wave quality factor (Q_c). Midorikawa (1980) has suggested that S-wave quality factor (Q_β) and S-wave velocity 'β' is empirically related with each other. Therefore, the estimate of Q_β is directly related to the rock properties and seismic hazard. Numbers of different techniques have been used to quantify these attenuation coefficients from different parts of the seismogram. At regional distances (<10°) and high frequencies (>1.0 Hz), the most frequent techniques include (1) those that parameterized the source and fit the body-wave spectra (Boatwright, 1978; Hough et al., 1988); (2) methods that cancel the seismic source through the spectral ratio of different parts of the seismograms (Aki, 1980; Frankel et al., 1990); (3) methods that measure coda amplitude decay with increasing lapse time (Aki, 1969; Aki and Chouet, 1975); (4) methods that use a nearby smaller event as an empirical Green's function (Hough, 1997); and (5) methods that invert the

spectra of recorded ground motion to estimate Q and source parameters (Boatwright et al., 1991; Fletcher, 1995). While it is expected that these different techniques supposed to lead to a uniform explanation of attenuation properties, they often do not provide the same results (Sarker and Abers, 1998a).

This chapter discusses the literature survey related to computation of attenuation coefficient in various seismic environments. This chapter also discusses various techniques for computation of attenuation coefficient which leads to find research gap and objectives of present study.

1.1 Attenuation studies from worldwide data-Literature Review

The attenuation characteristics of a region provide essential information, regarding earthquake hazard of the region. Various techniques have been developed to study the attenuation characteristic of seismic waves using different parts of the seismogram (e.g., Aki, 1969; Aki and Chouet, 1975; Hermann, 1980; Mitchell, 1995). Most frequent methods which are used to quantify the attenuation characteristic are backscattering method, coda normalization method and gernalized inverse method.

Ground motion in the vicinity of earthquakes often dies away slowly leaving a coda wave following the direct body waves and surface waves because of inhomogeneities in the earth. These seismic coda waves are backscattering waves from numerous randomly distributed heterogeneities in the earth (e.g., Aki, 1969; Aki and Chouet, 1975; Rautian, 1976; Rautian and Khalturin, 1976). Aki and Chouet (1975) proposed two extreme models for back-scattered waves to calculate the coda wave quality factor (Q_c). The first single scattering model considers the scattering as a weak process without loss of seismic energy and in the second one, the seismic energy transfer is considered to be a diffused process. The single backscattering model proposed by Aki and Chouet (1975) is a frequently used model for describing the behaviour of the coda waves from small local earthquakes. According to this model the coda waves are interpreted as backscattered body waves generated by the numerous heterogeneities present in the Earth's crust and upper mantle. It implies that scattering is a weak process and outgoing waves are scattered only once before reaching the receiver. Under this assumption the coda amplitudes for a central frequency is related to the source function, lapse time and quality factor at same central frequency. They presented the evidence for supporting their assumption that coda waves are backscattering waves generated from

heterogeneities. They also described the method of interpreting the observed coda spectra based on single-scattering and diffusion theory.

Aki (1980) developed the coda normalization method to estimate the shear wave quality factor (Q_β). The coda normalization method is being designed to normalize the spectral amplitude of the earthquake source by that of coda waves at a fixed lapse time, enabling to measure 'Q_β' from a data set obtained at a single station. It is based on the idea that coda waves consist of scattered S-waves from random heterogeneities in the Earth (Aki, 1969; Aki and Chouet, 1975; Sato, 1977). Aki (1980) modified the Aki and Chouet (1975) and Rautian and Khalturin (1978) method and describe the coda normalization method. The ratio of observed spectra of shear waves and that of coda waves was used by Aki (1980) to eliminate the source effect from observed spectra of shear waves. Aki (1980) describe that, for lapse time greater than roughly twice the direct S-wave travel time, the spectral amplitude of the coda at a given lapse time is independent of the hypocentral distance in the regional distance range.

Boatwright et al. (1991) proposed the gernalized inverse method that inverts the spectra of recorded ground motion to estimate quality factor and source parameters. The inversion procedure has been divided into two parts to reduce the number of parameters. The first part consist the entire frequency band to solve attenuation and source parameters, while the second part solves the source residuals and site response independently at each frequency. It is required in this inversion that the residuals to be solved for all frequencies simultaneously. Fletcher and Boatwright (1991) modified the gernalized inverse method with the addition of geometrical spreading term, which was not used in the earlier approach of inversion given by Boatwright et al. (1991). Fletcher and Boatwright (1991) proposed two step inversion procedure based on singular-value decomposition algorithm. The first part computes the source and attenuation terms for all events and the second part compute the residuals from the first part onto the site terms. In this inversion scheme the Brune spectral shape was assumed for the source, frequency-independent quality factor for the mid-crust, a power law for geometrical spreading, average site attenuation and the individual site responses.

Fletcher (1995) further modified this technique, he applied nonlinear least-square algorithm using Newton's method to provide an unbiased estimate of spectral parameters. Non linear least-square inversion algorithm has been used to estimate source parameters such as stress drop, seismic moment and attenuation parameter. He used the borehole data therefore did not correct the record for site response. Singular value decomposition method given by Press et al. (1992) was

used to find the model parameters. The advantage of using singular value decomposition method was that the variance could also be calculated. Various methods have been used by different researcher to observe the quality factor in different regions of the world (i. e. Aki and Chouet, 1975; Sato, 1977; Roecker et al., 1982; Pulli, 1984; Wu, 1985; Jin and Aki, 1988; Havskov et al., 1989; Ibanez et al., 1990; Pujades et al., 1991; Canas et al., 1991; Atkinson and Mereu, 1992; Akinci et al., 1994; Latchman et al., 1996).

Satoh et al. (1997) have determined the frequency dependent quality factor using the strong motions data of 18 earthquakes in the eastern Tohoku district, Japan. They used the method that invert the spectra of recorded ground motion to estimate frequency dependent quality factor as $Q_{\beta}(f) = 110f^{0.69}$.

Mandal and Rastogi (1998) have estimated the frequency dependent coda-Q values from 30 local earthquakes around Koyna-Warna, India region. The recorded seismic network consists of short-period seismometers, broadband seismometers, digital accelerographs and analog portacorders. Frequency dependent coda-Q was obtained using the single scattering method. They have calculated the frequency dependent coda wave quality factor relation for Koyna-Warna region as $Q_c(f) = 169f^{0.77}$.

Gupta et al. (1998) have estimated $Q_c(f)$ values from 13 local earthquakes recorded between July to August 1996. The data used in this work was recorded on three-component short-period seismometers. They calculated average attenuation relationship, $Q_c(f) = 96f^{1.09}$ using a single back scattering model for Koyna region, India.

Zelt et al. (1999) have estimated the frequency dependent coda-Q relation using the data of short-period recorders for the Southwestern British Columbia, Canada region. Single-scattering method was used to calculate frequency dependent quality factor using the data of 122 local earthquakes. The frequency dependent relation of form $Q_c(f) = 110f^{0.72}$ was estimated for British Columbia region which is applicable in the frequency range of 2-16 Hz.

Chung and Sato (2001) measured $Q_\alpha^{-1}(f)$ and $Q_\beta^{-1}(f)$ by applying the extended coda normalization method i.e. $0.009(\pm0.003)f^{-1.05(\pm0.14)}$ for Q_α^{-1} and $0.004(\pm0.001)f^{-0.70(\pm0.14)}$ for Q_β^{-1}. Data was recorded on three component velocity seismographs for the Southeastern South Korea region.

Castro et al. (2002) have used local earthquakes recorded on three-component geophones in Central Italy to analyze the frequency dependent S-wave quality factor $Q_\beta(f)$ and coda wave quality factor $Q_c(f)$. The relation for Q_β and Q_c were determined using non parametric approach (i.e. study of decay of spectral amplitudes with distance) and the single-scattering model, respectively. Frequency dependence S-wave quality factor was determined as $Q_\beta(f) = 18f^{2.0}$ for the frequency range of 1-10 Hz. The coda wave quality factor of form $Q_c(f) = 55f^{0.8}$ was obtained for the Colfiorito basin, the Marche and the Apennines region of Central Italy.

Gupta and Kumar (2002) have studied the seismic wave attenuation characteristics of the Garhwal Himalaya, Koyna region and North East region of Indian subcontinent. Frequency dependent coda wave quality factor was determined by implementing the single backscattering model for these three regions. Digitally recorded earthquakes were used to determine Q_c for the Garhwal and the Koyna region while strong motion data was used for north east India region. In this work, frequency dependent relationship was obtained as $Q_c(f) = (110\pm5.15)f^{(1.02\pm0.025)}$, $Q_c(f) = (97\pm7.18)f^{(1.09\pm0.036)}$ and $Q_c(f) = (86\pm4.04)f^{(1.01\pm0.026)}$ for the Garhwal Himalaya, Koyna region and northeast India, respectively.

Polatidis et al. (2003) have determined shear wave quality factor for the Hellenic arc, Greece. Velocity records were used in this work. The Q_β values were computed as 47, 79, 143, 271 and 553, respectively for five centered frequencies at 0.8, 1.5, 3.0, 6.0 and 12.0 Hz, respectively. The generalized spectral inversion approach was used for computation of frequency dependent shear wave quality factor. Frequency dependent shear wave quality factor $Q_\beta(f) = 51f^{0.91}$ was estimated in this work.

Dutta et al. (2004) have studied the shear-wave attenuation using the strong motion data in the South-central Alaska region. They estimated S-wave quality factor (Q_β) and coda wave quality factor (Q_c) by generalized inversion and single backscattering methods, respectively. Shear wave quality factor $Q_\beta^{-1}(f) = 0.0097\ f^{-1.19}$ and $Q_\beta^{-1}(f) = 0.0104\ f^{-1.06}$ for the transverse and radial component, respectively have been computed for South-central Alaska region. Similarly, they computed $Q_c^{-1}(f) = 0.0063\ f^{-0.79}$ and $Q_c^{-1}(f) = 0.0066\ f^{-0.84}$ for the transverse and radial component, respectively for South-central Alaska region.

Kim et al. (2004) have determined Q_α^{-1} and Q_β^{-1} using the data of broad-band and short-period seismometers for the Choongchung Provinces, central South Korea region. They calculated $Q_\alpha^{-1} = (3.0\pm0.1) \times 10^{-3}\ f^{-0.54\pm0.01}$ and $Q_\beta^{-1} = (3.0\pm0.1) \times 10^{-3}\ f^{-0.42\pm0.02}$ by implementing the extended coda normalization method.

Mamada and Takenaka (2004) have studied the attenuation characteristic of North western Kagoshima Prefecture, Japan region using the strong motion data. They estimated the value of Q_β^{-1} as function of frequency i.e. $Q_\beta^{-1}(f) = (9.93\times10^{-2})f^{-0.95}$ by applying the coda normalization method.

Bindi et al. (2006) have estimated the frequency dependent P and S wave quality factor for the region of Northwestern Turkey. Data used in this work record on the SABO and GTF seismological networks installed in the East part of Istanbul, which contains seismometers and accelerometers. Generalized spectral inversion scheme was used to determine $Q_\alpha(f) = 56f^{0.25}$ for $2.5 \leq f \leq 10$ Hz and $Q_\beta(f) = 17f^{0.80}$ for $1.0 \leq f \leq 10$ Hz.

Maeda and Sasatani (2006) have used seismic data to compute the shear wave quality factor (Q_β) for the region of southern Kurlie trench. The Shear-wave quality factor $Q_\beta(f) = 38.6f^{1.03}$ and $Q_\beta(f) = 65.6f^{0.69}$ were computed for the southern Kurlie trench region which lies 100 to 150 km away from the southern Hokkaido coast of Japan by using spectral inversion method and coda normalization method, respectively.

Kumar et al. (2007) have studied the attenuation characteristic of the Dharwar Craton, Cuddapah basin and Godavari graben, India. Broadband data was used to determine the coda wave quality factor for these three regions. Single scattering method given by Aki and Chouet (1975) was used for estimation of coda-Q relations. The coda-Q relations $Q_c(f) = (730.62 \pm 0.09)\ f^{(0.54 \pm 0.01)}$, $Q_c(f) = (535.06 \pm 0.13)\ f^{(0.59 \pm 0.01)}$ and $Q_c(f) = (150.56 \pm 0.08)\ f^{(0.91 \pm 0.01)}$ were obtained for Dharwar Craton, Cuddapah basin and Godavari graben region, respectively.

Sharma et al. (2007) have computed the P-wave (Q_α), S-wave (Q_β) and coda-wave (Q_c) quality factors for the Koyna region, India. A total 37 local earthquake recorded on short-period three-component seismometers was used in this work. The extended coda normalization method was used to determine Q_α and Q_β and single back-scattering method was used to determine Q_c. The obtained relationship for $Q_\alpha(f)$, $Q_\beta(f)$ and $Q_c(f)$ are $Q_\alpha(f) = (59.0 \pm 1.0)\ f^{(1.04 \pm 0.04)}$, $Q_\beta(f) = (71.0 \pm 1.0)\ f^{(1.32 \pm 0.08)}$ and $Q_c(f) = (117.0 \pm 2.0)\ f^{(0.97 \pm 0.07)}$, respectively.

Sharma et al. (2008) have estimated the P-wave (Q_α), S-wave (Q_β) and coda-wave (Q_c) quality factor for Kachchh region, Gujarat, India by using broadband data. The extended coda normalization method was used to determine Q_α and Q_β and single back-scattering method was used to determine Q_c. The obtained relationship for $Q_\alpha(f)$, $Q_\beta(f)$ and $Q_c(f)$ are $Q_\alpha(f) = (77.0 \pm 2.0)\ f^{(0.87 \pm 0.03)}$, $Q_\beta(f) = (100.0 \pm 4.0)\ f^{(0.86 \pm 0.04)}$ and $Q_c(f) = (148.0 \pm 3.0)\ f^{(1.01 \pm 0.02)}$, respectively.

Sahin (2008) has estimated the quality factor Q_c in the Southwest Anatolia region using coda wave normalization method. Broadband data recorded at two stations of KOERI array (Kandilli Observatory and Earthquake Research Institute) was used in this work. The coda $Q_c(f)$ relation for this region is obtained as $Q_c(f) = (102 \pm 8) f^{(0.82 \pm 0.07)}$.

Ford et al. (2008) have reported that the attenuation can depend on the method used for its determination. They applied five different attenuation methods to a Northern California broadband dataset. They used (1) coda normalization (2) coda-source normalization (3) two station (4) source/receiver pair and (5) two station method. All methods were used to find out the range of the parameters i.e. 'Q_o' and 'n' of the relation $Q_o f^n$. In this work, they were estimate 'Q_o' = 85±40 and 'n' = 0.65±0.35 for the Northern California region.

Raghukanth and Somala (2009) have estimated shear wave quality factor values using strong motion records from the northeast India. In this work $Q_\beta(f)$ were calculated as $431f^{0.7}$ and $224f^{0.93}$ for Indo-Burma tectonic domain and Bengal basin-Shillong plateau region, respectively, using the generalized inversion scheme.

Padhy (2009a) has determined the frequency depended P and S wave quality factor in the Bhuj area. Data used in this work was that recorded on the short-period three component velocity seismometers and broadband three component velocity seismometers. The extended coda normalization method was used to determine the value of $Q_\alpha^{-1} = (0.052 \pm 0.019)f^{-(1.1 \pm 0.06)}$ and $Q_\beta^{-1} = (0.02 \pm 0.01)f^{-(1.0 \pm 0.04)}$ for this region.

Abdel-Fattah (2009) has used the data set of short-period seismographs, to calculate the attenuation of body waves in the crust at the surrounding area of Cairo Metropolitan region by using the coda normalization method. In this work the frequency-dependent relation for P and S waves was determined as $Q_\alpha^{-1} = (19.0\pm2.0) \times10^{-3}f^{-(0.8\pm0.1)}$ and $Q_\beta^{-1} = (7.0\pm1.0)\times10^{-3}f^{-(0.85\pm0.1)}$, respectively.

Rahimi et al. (2009) have estimated the shear and coda wave quality factor in South East Sabalan Mountain, North West Iran by using 65 local events recorded on five accelerographs. Spectral decay and Coda normalization methods were used to determine the frequency dependent shear wave quality factor and single back scattering method for coda waves. The frequency dependent Q_β at Nir station determined by coda normalization and Spectral decay methods are $Q_\beta(f) = (17.74\pm1.22)f^{(0.95\pm0.04)}$ and $Q_\beta(f) = (10.82\pm1.13)f^{(0.83\pm0.03)}$, respectively and the frequency dependent Q_β at Eslam-abad station determined by coda normalization and Spectral decay methods are $Q_\beta(f) = (22.17\pm1.3)f^{(0.83\pm0.06)}$ and $Q_\beta(f) = (12.76\pm1.96)f^{(0.74\pm0.17)}$, respectively. They also estimated the frequency dependent $Q_c(f)$ relation viz. $Q_c(f) = (48\pm6)f^{(0.88\pm0.05)}$, $Q_c(f) = (49\pm5)f^{(0.97\pm0.03)}$, $Q_c(f) = (51\pm7)f^{(1.02\pm0.06)}$, $Q_c(f) = (53\pm7)f^{(0.97\pm0.03)}$ and $Q_c(f) = (44\pm5)f^{(0.96\pm0.03)}$ at Sarein, Ardebil, Kariq, Eslam-abad and Nir stations, respectively.

Cantore et al. (2011) have studied the S-wave attenuation properties using generalized inversion technique for the Irpinia-Basilicata region (southern Apennines, Italy). Data used in this

work was that recorded on short-period seismometers. In this work frequency dependent shear wave quality factor $Q_\beta(f)$ was estimated as $28.3f^{0.87}$.

Padhy et al. (2011) have determined body waves (Q_α^{-1} and Q_β^{-1}) and coda waves (Q_c^{-1}), quality factor by using the extended coda-normalization method and the single isotropic scattering theory, respectively, in the Andaman Sea region. The average Q_c^{-1} varies from $0.02f^{-1.1}$ to $0.01f^{-0.94}$ with an increase in lapse time window from 10 s to 40 s, respectively. The computed values of Q_α^{-1} and Q_β^{-1} are $0.02f^{-1.01}$ and $0.01f^{-1.0}$, respectively, for this region.

Gupta et al. (2012) have studied the attenuation characteristics of coda waves for mainland Gujarat, India. In this work single backscattering method was implemented on the broadband data to determine the coda-Q. The computed average coda-Q relations are: $Q_c(f) = (87.0\pm13.0)f^{(1.01\pm0.06)}$, $Q_c(f) = (112.0\pm20.0)f^{(0.94\pm0.08)}$ and $Q_c(f) = (120.0\pm22.0)f^{(0.76\pm0.07)}$ for the lapse time of 30s, 40s and 50s, respectively.

Brahma (2012) has estimated coda wave attenuation using the broadband data in the Northeast India. Using the single backscattering model frequency dependent attenuation relation was estimated as $Q_c(f) = (21.49\pm1.17)f^{(1.48\pm0.08)}$, $Q_c(f) = (48.6\pm1.11)f^{(1.29\pm0.06)}$ and $Q_c(f) = (88.86\pm1.12)f^{(1.19\pm0.06)}$, respectively, for the time window of 20s, 30s and 40s, respectively.

Mandal et al. (2013) have determined frequency dependent shear wave quality factor for the central India tectonic zone and its surroundings region using broadband data. They estimated $Q_\beta(f) = 332f^{0.59}$ for the central India region by using double spectral ratio method.

1.1.1 Attenuation studies from Garhwal and Kumaon Himalaya data

Himalaya, the highest mountain chain at the earth, is mainly characterized by a marked concentration of interplate seismicity and high rate of upliftment as well as convergence (Molnar and Chen, 1983; Nakata, 1989; Demets et al., 1990). An attenuation study plays an important role to produce the hazard map of any region. Garhwal and Kumaon Himalaya region having high density of population and hence attenuation study in these regions plays an important role. Several workers have performed attenuation studies related to body and coda waves using different techniques from available data in the Garhwal and the Kumaon Himalaya, India.

Gupta et al. (1995) estimated Q_c by analyzing coda waves of vertical component of velocity sensor of the seven local earthquakes recorded in the Garhwal Himalaya. Single backscattering model was used in this study. They obtained frequency dependence Q_c relationship as $Q_c(f) = 126f^{0.95}$ for Garhwal Himalaya.

Mandal et al. (2001) have used 48 well-located Chamoli aftershocks to estimate frequency dependence Q_c relationship for the Chamoli region. The aftershocks data used in this work were recorded on broadband seismometers and short-period seismometers. They have used scattering method to compute frequency dependence Q_c relationship. The frequency dependent relation of $Q_c(f) = (30\pm0.8)f^{(1.21\pm0.03)}$ was estimated for the Chamoli region in this study.

Gupta and Ashwani Kumar (2002) have used the data of velocity sensor installed in the Garhwal Himalaya to estimate frequency dependent coda wave quality factor. Single backscattering method was employed to determine frequency dependent quality factor. A relation of form $Q_c(f) = (110\pm5.15)f^{(1.02\pm0.025)}$ for the Garhwal Himalaya was obtained in this study.

Paul et al. (2003) have calculated coda wave quality factor for the Kumaon Himalaya region. Eight events recorded on digital telemetered seismic network were used in this work. Single backscattering model given by Aki and Chouet (1975) was used in this study. Coda wave quality factor $Q_c(f) = (92\pm4.73)f^{(1.07\pm.023)}$ was computed for the Kumaon region.

Joshi (2006b) used two main shocks of Uttarkashi and Chamoli earthquakes and several aftershocks to estimate shear wave quality factor for the Garhwal Himalaya. Strong motion data was used in this study. Inversion algorithm was used to obtain shear wave quality factor from strong motion data. A frequency dependent shear wave quality factor $Q_\beta(f) = 112f^{0.97}$ was obtained for the Garhwal region.

Sharma et al. (2006) have computed frequency dependent relationships of quality factors for P waves (Q_α) and for S waves (Q_β) using extended coda normalization method. Strong motion data of seven local earthquakes recorded in Garhwal was used for this purpose. The estimated frequency dependent relations for Garhwal Himalaya are $Q_\alpha(f) = 37f^{1.06}$ and $Q_\beta(f) = 63f^{1.03}$.

Mukhopadhyay et al. (2008) have used 30 aftershock data of the 29th March 1999 Chamoli earthquake to estimate the Q_c values by using single back scattering model. Data used in this work was recorded on the network of short-period seismometers. They determined the coda-Q as $Q_c(f) = (33\pm2)f^{(1.17\pm0.03)}$, $Q_c(f) = (55\pm6)f^{(1.16\pm0.05)}$, $Q_c(f) = (78\pm15)f^{(1.12\pm0.08)}$, $Q_c(f) = (93\pm18)f^{(1.07\pm0.08)}$ and $Q_c(f) = (122\pm20)f^{(0.98\pm0.07)}$, respectively for average lapse time 19.1, 24.0, 29.3, 34.0 and 40.7s, respectively.

Sharma et al. (2009) have estimated frequency dependent relationships of quality factors for P-waves (Q_α) and for S-waves (Q_β) simultaneously using the extended coda normalization method. Data of broadband seismometers and short-period seismometers was used for this purpose. The estimated frequency dependent relations for quality factors are $Q_\alpha(f) = (44 \pm 1)f^{(0.82\pm.04)}$ and $Q_\beta(f) = (87 \pm 3)f^{(0.71\pm.03)}$, respectively, for the Chamoli region, Himalaya.

Padhy (2009b) have computed the scattering attenuation Q_s^{-1} and intrinsic attenuation Q_i^{-1} from inversion of coda envelopes of 1999 Chamoli earthquake data. Short-period and broadband data was used in this work. The scattering attenuation and intrinsic attenuation of value $Q_s^{-1} = (0.006\pm0.004)f^{-(0.89\pm0.33)}$ and $Q_i^{-1} = (0.003\pm0.0005)f^{-(0.84\pm0.08)}$ are obtained in this study.

Singh et al. (2012a) have analyzed seismic attenuation characteristics of the Kumaon Himalaya by using earthquake dataset of 84 events recorded on three-component broadband seismic stations. Single back scattering technique was used to calculate coda (Q_c) values at frequency range of 1.5, 3.0, 6.0, 8.0, 12.0 and 18.0 Hz, respectively, for different lapse time window. The dependencies of coda waves with lapse time were investigated which indicate that Q_o increases from 64 ± 2 to 230 ± 19 with increasing lapse time from 20 to 50s while parameter n decreases from 1.08 to 0.81.

Singh et al. (2012b) have studied the attenuation characteristics of the Kumaon region using 23 local earthquakes recorded during 2004-2008. The recording network consists of five strong motion seismometers and four three-component short period seismometers. Frequency dependent Q_α and Q_β were determined using the extended coda-normalization method. Frequency-dependent relationships of quality factors for P waves and for S waves in this study were obtained as $Q_\alpha(f) = (22.0\pm5.0)f^{(1.35\pm0.04)}$ and $Q_\beta(f) = (104.0\pm10.0)f^{(1.3\pm0.03)}$, respectively.

Singh et al. (2012c) have estimated the coda wave attenuation characteristic using the data of 75 earthquakes in the Garhwal region. Broadband data was used in this study. Single backscattering model was applied to estimate coda wave quality factor. The coda wave quality factor $Q_c(f) = 61.8f^{0.992}$ and $Q_c(f) = 161.1f^{0.998}$ for 10s and 40s coda window length, respectively, were obtained in this study.

Tripathi et al. (2012) studied the coda-Q using the broadband data in the Garhwal region. The single backscattering method was used to estimate coda wave attenuation (Q_c^{-1}). It is found that 'Q_o' varies from 50 to 350 for the lapse time 10s to 60s while 'n' ranges from 1.2 to 0.7 in this study.

Garhwal and Kumaon are the major parts of the Uttarakhand Himalaya. The Garhwal Himalaya having two major earthquakes in the past i.e. Uttarkashi earthquake of 20th October 1991 (M_s = 7.0) and Chamoli earthquake of 28th March 1999 (M_s = 6.6) and hence because of these two earthquake many studies regarding the attenuation characteristic have been performed out in the Garhwal Himalaya region as compared to the Kumaon Himalaya. However, due to limited database available in the rough and difficult terrain of Kumaon Himalaya few work has been done

to estimate attenuation properties of the medium in this part of Himalaya. The attenuation relation developed for Garhwal and Kumaon Himalaya revealed that these two regions have distinct attenuation rates (Joshi et al., 2013) and hence due to these reasons it is important to estimate attenuation characteristic of Kumaon region.

1.1.2 Three dimensional attenuation studies

Detail attenuation study is required for estimation of accurate seismic hazard of the region. This can be achieved from three dimension attenuation studies. Various workers have determined the three dimensional attenuation structures worldwide by using various techniques. The depth dependent Q structures have been obtained using inversion usually prepared by spectral techniques. In this technique, model of earth has been determined by using the observed dispersion of wave's spectrum. It was achieved by using a perturbation scheme which was based on the Rayleigh's principle. According to this principle an initial test model is assumed and then perturbed until its theoretical dispersion matches with the observed dispersion (Archambeau and Anderson, 1963; Anderson and Archambeau, 1964; Anderson et al., 1965; Teng, 1968 and Sekiguchi, 1991). The H/V spectral ratio technique has been used to estimate Q structure using strong motion digital data by Phinney (1964) and Langston (1979). Ward and Young (1980) and Young and Ward (1980) estimated three-dimensional Q structure of geothermal area by using an inversion of the differential attenuation data derived from a reduced spectral technique from teleseismic P-waves. According to this method, effect of seismic attenuation can be observed qualitatively from the seismograms by a shift in the dominant frequency of the seismogram. Ratio of two P-wave spectrums from an earthquake recorded at two different stations solved by using the inversion to get the three-dimensional attenuation structure. Umino and Hasegawa (1984) have estimated the three-dimensional Q structure beneath the Tohoku region by inversion technique using S/P method in which constant ratio of Q_α to Q_β and the identical source spectra of P and S waves are assumed.

It has been shown by Hashida and Shimazaki (1984) by numerical experiment that a quantitatively reliable Q structure and earthquake source strength can be obtained in a region using intensity data, which is assumed to be dependent on strong motion parameters. Hashida and Shimazaki (1984) have formulated the inversion of seismic intensities and later (Hashida and Shimazaki, 1985, 1987) estimated the three dimensional attenuation structures beneath the Kanto

and Tohoku regions in Japan, respectively. Later on Nakamura et al. (1994 and 1995) obtained the three dimensional attenuation structure by using the approach suggested by Hashida and Shimazaki (1984) in the whole Japanese island with the help of large quantity of previous data.

Tsumura et al. (1996) have determined the attenuation (Q_α) structure in the northeast region of Honshu, Japan. They implemented the modified gernalized inverse method proposed by Boatwright et al. (1991) on the data of micro-earthquake network which consist of three component velocity seismometer to obtain 'Q_α' structure in the northeast region of Honshu, Japan.

Sarker and Abers (1998b) have studied the attenuation characteristic using the P- and S-waves of Caucasus region. The data from three component intermediate-period sensor was used in this study. Least square inversion scheme was used to determine frequency independent attenuation parameter which was further used to calculate body wave quality factor. The obtained body wave quality factor values have been used to determine three dimensional attenuation structures for Caucasus region.

Tsumura et al. (2000) have estimated the three dimensional 'Q_α' structures using the data of velocity seismometers in the North eastern Japan region. Earlier approach of inversion proposed by Tsumura et al. (1996) was performed to get the 'Q_α' structure of North eastern Japan region.

Ji-chang and Sato (2001) have studied Q values at different depth levels using the seismic wave record during 1998 in Jiashi earthquake region. Data used in this work was recorded on the seismographs which have the frequency band range 4-40 Hz. Three dimensional seismic inversion processes have been used in this study to estimate Q values in Xinjiang region.

Schlotterbeck and Abers (2001) have determined the three dimensional attenuation structures for the Southern California. Least-square Inversion was applied on the broad banddata to determine the frequency independent attenuation parameter. This parameter was further used to compute attenuation structure based on Q_α and Q_β of the Southern California region.

Nakamura and Uetake (2004) have determined the three dimensional attenuation structures of Tohoku region, Japan by the inversion scheme suggested by Hashida and Shimazaki (1984) using the strong motion data.

Nakamura et al. (2006) have used the strong motion records of the K-NET and KiK-net network to determine the three dimensional S-wave attenuation (Q_β) structure beneath the Kanto plain. Inversion technique of seismic intensities similar to Hashida and Shimazaki (1984) except an unknown site amplification factor was used to estimate the three-dimensional Q_β structure of the Kanto, Japan region.

Joshi (2006a) has estimated three dimensional shear wave attenuation structural using the intensity data in Central Himalaya gap region by using damped least square inversion scheme. Spatial and vertical distribution of shear wave quality factor 'Q_β' were studied for Garhwal Himalaya in this study.

Joshi (2007) has used the inversion technique of intensity data to determine the three-dimensional attenuation structure based on S-wave quality factor 'Q_β' value for a part of the central seismic gap region of Himalaya. The spatial distribution of destruction caused by two major earthquakes i.e. Uttarkashi (20 October 1991) and the Chamoli (29 March 1999) earthquakes was studied by using the obtained Q_β structure.

Joshi et al. (2010) determined the three-dimensional attenuation structure in the Pithoragarh region of Kumaon Himalaya using spectral acceleration data. The data from a local strong motion network installed in the Pithoragarh region of Kumaon Himalaya have been used for this purpose. The final three dimensional attenuation structure was obtained using the inversion of strong motion data.

1.2 Research Gap

The literature survey revealed that there are several methods which can be used to determine attenuation property of a region using broadband, teleseismic, strong motion and micro earthquake data. Attenuation studies related to estimation of quality factor can be divided into two classes. In one class of approach, single frequency dependent quality factor is estimated for entire region while in another class of approach, three dimensional distribution of quality factor is estimated for entire region of study. It is seen that there are very few studies, where estimation of $Q_\beta(f)$ is made directly from strong motion data. Strong motion data is one of the most useful data which is directly used for designing of earthquake resistant structures. It is seen that the ground acceleration in the horizontal component of strong ground motion is mainly affected by shear waves. Therefore, shear wave attenuation described by $Q_\beta(f)$ plays direct role in deciding property of strong ground motion at a particular site. Joshi (2006b) has modified the Fletcher's (1995) technique of inversion of strong motion data to estimate the frequency dependent shear wave quality factor. Joshi (2006b) has used a nonlinear least-squares algorithm using Newton's method. Joshi (2006b) has considered seismic moment as an input to this algorithm. This input parameter of inversion algorithm was used from the independent sources. The three dimensional distribution of frequency dependent shear wave attenuation has been estimated by Hashida and Shimazaki (1984). This algorithm was modified by Joshi (2006a, 2007) and Joshi et al. (2010) to estimate three-dimensional distribution of shear wave quality factor using strong motion data from limited events. Following research gaps have been identified in the techniques to determine the attenuation studies:

1) Most of the attenuation studies are made through broadband, teleseismic and micro earthquake data. Very few attenuation studies are there which directly use strong motion data for determination of attenuation coefficient.

2) Strong motion data has been directly used by Joshi (2006b) to obtain frequency dependent attenuation relation using an inversion algorithm. Seismic moment is used as one of the main input in the algorithm developed by Joshi (2006b) for estimation of frequency dependent shear wave quality factor from inversion of strong motion data. Seismic moment used in this algorithm is computed or assumed from independent sources of well studied earthquakes. Estimation of seismic moment for earthquake recorded in regional network is practically

difficult task. Modification in this algorithm is required to compute seismic moment directly from the records and refine its value in the inversion scheme for each iteration.

3) Computation of seismic moment is strongly affected by shear wave quality factor. Therefore, modification in algorithm given by Joshi (2006b) is required to correct initial value of seismic moment from obtained value of shear wave quality factor in each iteration.

4) The inversion algorithm given by Joshi et al. (2010) for estimation of three dimensional distribution of attenuation property uses strong motion data from limited number of events. Modification in this technique is required to consider large number of events for better estimation of attenuation characteristic of the region.

5) Peak ground acceleration is mainly controlled by shear waves in the strong motion record. Stochastic simulation technique makes use of this concept to calculate peak ground motion at given site due to propagation of shear wave. Shear wave quality factor control the medium characteristics. Though this concept has been frequently used for forward modelling its use for inversion to determine shear wave quality factor and seismic moment is very limited.

6) Kumaon Himalaya is one of the seismically active regions. This region experienced 294 earthquakes in last 6 years. However very few attenuation studies are available for this part of Himalaya. The attenuation study in this part of Himalaya is required for better assessment of seismic hazard potential of the region.

1.3 Objectives identified for research

The amplitudes of earthquake ground motion at recording sites are influenced by the source characteristics, medium characteristic and local site conditions. The effects of travel path on earthquake ground motion are related directly to the attenuation property of medium. The knowledge of attenuation characteristic is an essential requirement for determination the earthquake source parameters and simulation of strong ground motions. It plays an important role in estimation of the seismic hazard of a region.

Site effect is very significant term in the study of strong ground motion. The seismic amplification is increased due to soft deposits overlaid on the bedrock and cause more damage during the large earthquake and this is called site effect (Kuo et al., 2012). The Local site effect

plays an important role in damage distribution during earthquakes. Throughout history, destructions due to many of the earthquakes have been influenced by local site effects. Some noticeable examples are: the Andalusian earthquake of 1884 in southern Spain; the San Francisco (USA) earthquakes in 1906 and 1957; those of Kanto, Tonankai, Niigata and Kobe (Japan) in 1923, 1944, 1964 and 1995, respectively (Luzon et al., 2004). Very few studies have been carried out to understand the effect of attenuation and site effect simultaneously on destruction patterns from earthquakes. Present work in this thesis is aimed to study the shear wave attenuation characteristics and site effect simultaneously from strong motion data. The estimation of three dimensional attenuation structures from strong motion data using inversion algorithm require strong motion data that should be free from site effects. Present work is divided into two parts, first part deal with estimation of frequency dependent shear wave quality factor and site effect from inversion of strong motion data. In the second part, the site effects obtained from inversion of strong motion data from first part is used to correct the strong motion record. The corrected strong motion record is further used for estimation of three-dimensional attenuation structure in the second part. The research work in this Ph.D. degree is targeted with the following objectives:

1. Development of an algorithm and software for inversion of strong motion data for determination of frequency dependent shear wave quality factor and site effect simultaneously at given site.

2. Use of determined site effect for understanding the source characteristics of strong motion earthquakes in the region.

3. Development of an algorithm and software for inversion of strong motion data to determine the three dimensional attenuation tomography of a region.

4. Application of developed algorithm for determination of three dimensional attenuation structure of well studied region and comparison of obtained results with the available tectonic features of the region.

5. Application of algorithm developed in the present work for determination of attenuation structure of the Kumaon Himalaya using strong motion data from a dense network installed in this region.

1.4 Thesis outline

Present thesis consists of eight chapters. Literature review regarding the attenuation studies is presented in Chapter 1. Different techniques used by various workers to determine the attenuation property are discussed in this chapter. Various research gaps are identified on the basis of literature presented in this chapter. This chapter also discusses objectives of present work.

The methodology and algorithm of inversion of strong motion data for the determination of three dimensional attenuation structure is described in Chapter 2. Various numerical experiments have been performed in this chapter to check the stability of the solution and dependency of the obtained solution from developed algorithm.

The complete methodology and algorithm of inversion of strong motion data for determination of site effect and frequency dependent shear wave quality factor $Q_\beta(f)$ simultaneously is described in Chapter 3. This chapter also describes various numerical experiments about the dependency of the result on input data and the stability of the solution obtained in the developed inversion algorithm.

The application of inversion algorithm for determination of three-dimensional attenuation structure of the central Honshu region, Japan is present in Chapter 4. In this chapter three dimensional attenuation structures have been determined at different frequencies and obtained attenuation structure is compared with the available data of the region.

The application of inversion algorithm to determine frequency dependent shear wave quality factor $Q_\beta(f)$ in different parts of Kumaon Himalaya is discussed in Chapter 5. The frequency dependent shear wave quality factor $Q_\beta(f)$ values and site effect have been computed at various stations in Kumaon region, Himalaya. The frequency dependent quality factor obtained at different stations from both NS and EW components have been used to compute a regional average relationship for the region of the Kumaon Himalaya.

The application of inversion algorithm for determination of three-dimensional attenuation structure of the Kumaon Himalaya region, India is present in Chapter 6. In this chapter three dimensional attenuation structures have been determined at different frequencies and obtained attenuation structure is compared with the available geological and tectonic features of the region.

Application of site effects and attenuation studies for determination of source parameters of the Sikkim earthquake of 18 September, 2011 is discussed in Chapter 7.

Conclusion of present research work is given in Chapter 8. This chapter summarizes the research works done in this thesis and its conclusions.

Chapter – 2

Inversion Technique for Estimation of Three Dimensional Attenuation Structure

2.1 Introduction

It is observed that different types of propagation material behave differently during the same earthquake; therefore, the properties of rocks have an important role to affect the amplitude of earthquake ground motion in a particular region. The property of medium which control the attenuation of seismic energy is defined by the quality factor. In this work inversion of strong motion data has been performed to obtain the three dimensional estimate of frequency dependent shear wave quality factor. This chapter describes the complete algorithm of inversion of strong motion data to obtain attenuation structure and various numerical experiments to support the algorithm.

2.2 Inversion Technique

In order to determine three dimensional attenuation structure the entire study area is divided into several three dimensional blocks of different frequency dependent shear wave quality factor '$Q_\beta(f)$' values as shown in Fig. 2.1. The subscripts 'i' and 'j' are used for identification of blocks along two perpendicular X and Y axes in the horizontal plane, respectively, and is shown in Fig. 2.1. The subscript 'k' is used for identification of block in the downward direction as shown in Fig. 2.1. Generally the peak ground acceleration 'A' is associated with arrival of S-waves generated from the point source in the subsurface (Hadley et al., 1982). Following relation given by Hashida and Shimazaki (1984) has been used for computing spectral acceleration value at given frequency 'f':

$$A(f) = S(f) G_R g e^{-\pi f \sum \frac{T_{ijk}}{Q_{ijk}}} \tag{2.1}$$

In above equation, 'A(f)' represents spectral acceleration value, 'S(f)' is the source spectral acceleration value at frequency 'f', 'G_R' is the geometrical factor which is assumed in the present work as inverse of hypocentral distance, 'T_{ijk}' is the time spent in ijkth block of shear wave quality factor 'Q_{ijk}' at particular frequency 'f' and 'g' denotes the amplifying effects at the surface of the

earth and is used as 2.0 (Hashida and Shimazaki, 1984). The term '$1/Q_{ijk}$' in equation (2.1) is replaced with 'D_{ijk}', which modified equation (2.1) as:

$$A(f) = S(f) G_R g e^{-\pi f \sum D_{ijk} T_{ijk}} \tag{2.2}$$

In above equation 'D_{ijk}' is attenuation coefficient which characterizes the property of medium and it is the inverse of the quality factor.

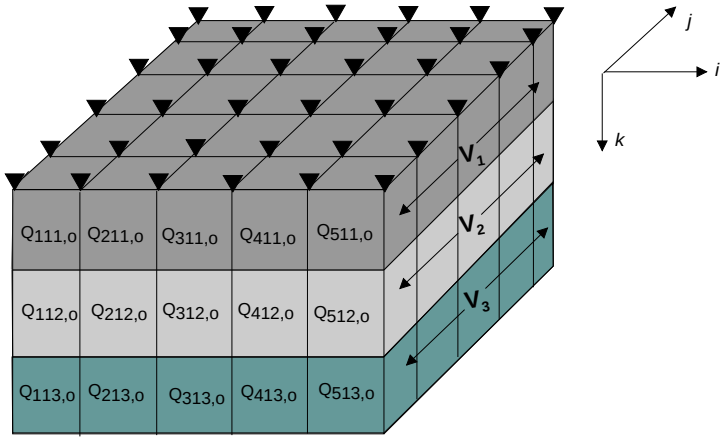

Figure 2.1: Initially $Q_{ijk,o}$ has been used in each block. The subscripts i, j and k describe the position of the blocks in respect of x, y and z directions, respectively.

The iterative inversion process assumes an initial distribution of '$Q_{ijk,o}(f)$' within each block. This initial distribution can be assumed from the available geophysical information of the region. The value of 'S(f)' is required for the forward modeling using equation (2.2). This 'S(f)' is average of several frequency dependent source strength 'S_{op}^{cal} (f)' calculated at different observation point 'op' and is given by following relation (Joshi, 2007):

$$S_{op}^{cal}(f) = \frac{A'_{op}(f)}{G_R g e^{-\pi f \sum D_{ijk,0} T_{ijk}}} \tag{2.3}$$

where, in the above equation 'A'_{op} (f)' is the calculated spectral acceleration value at frequency 'f' at the observation point, located in the surface grid denoted by subscripts 'op' shown in Fig. 2.2. For computing '$S_{op}^{cal}(f)$' from equation (2.3) initial subsurface model defined by velocity 'β' and 'Q_β' in each layer is required. Layered velocity model is used as an input model as used by Hashida and Shimazaki (1984) and Joshi (2007) to limit the number of independent parameters.

The '$S^{cal}(f)$' is calculated by using average value of '$S_{op}^{cal}(f)$' obtained from all observation points. Initial model having attenuation coefficient '$D_{ijk,o}$' and '$S^{cal}(f)$' is used to calculate A_{op}^{cal} and is given by following relation (Joshi 2007):

$$A_{op}^{cal}(f) = S^{cal}(f) G_R g e^{-\pi f \sum D_{ijk,0}, T_{ijk}} \tag{2.4}$$

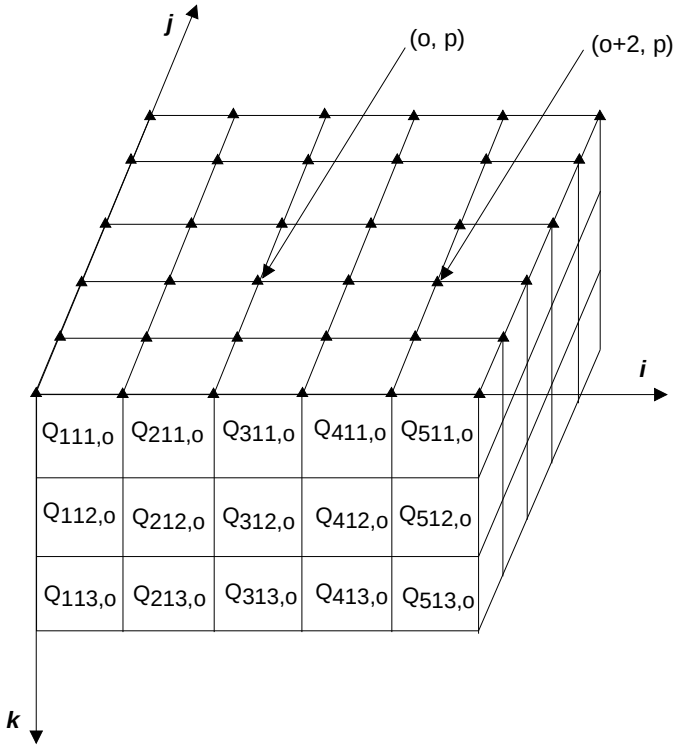

Figure 2.2: Location of observation points at the corner of the grid.

If the observed spectral acceleration value at 'ij' observation point (i. e. 'op') is $A_{op}^{obs}(f)$ then the relation between observed spectral acceleration '$A_{op}^{obs}(f)$', actual earthquake source strength '$S_o(f)$' and actual attenuation coefficient 'D_{ijk}' is given by the following expression:

$$A_{op}^{obs}(f) = S_o(f) G_R g e^{-\pi f \sum D_{ijk}, T_{ijk}} \tag{2.5}$$

Parameter 'T_{ijk}' is the actual time spent by the ray from the source to the observation point in the three dimensional block defined by subscript 'ijk'. Following expression is obtained by dividing equation (2.5) by (2.4).

$$\frac{A_{op}^{obs}(f)}{A_{op}^{cal}(f)} = \frac{S_o(f)}{S^{cal}(f)} e^{-\pi f \sum (D_{ijk} - D_{ijk,0}) T_{ijk}} E \tag{2.6}$$

where, the parameter 'E' defines the computational error that can be due to inadequate model parameterization. Equation (2.6) can be simplified as:

$$\frac{A_{op}^{obs}(f)}{A_{op}^{cal}(f)} = \frac{S_o(f)}{S^{cal}(f)} e^{-\pi f \sum \delta D_{ijk} T_{ijk}} E \tag{2.7}$$

In above equation 'δD_{ijk}' represents the difference between the actual and assumed attenuation coefficient in the ijkth block and can be written as $\delta D_{ijk} = D_{ijk} - D_{ijk,o}$. Equation (2.7) is a non linear equation which can be linearized by taking its natural logarithm. This gives following form of above equation:

$$\ln\left(\frac{A_{op}^{obs}(f)}{A_{op}^{cal}(f)}\right) = \ln\left(\frac{S_o(f)}{S^{cal}(f)}\right) - \pi f \sum \delta D_{ijk} T_{ijk} + e \tag{2.8}$$

Assuming $R_{op} = \ln\left(\frac{A_{op}^{obs}(f)}{A_{op}^{cal}(f)}\right)$, as acceleration residual, equation (2.8) can be modified as:

$$R_{op} = \ln\left(\frac{S_o(f)}{S^{cal}(f)}\right) - \pi f \sum \delta D_{ijk} T_{ijk} + e \tag{2.9}$$

In this equation, left hand side is known and the parameter 'T_{ijk}' can be calculated by using ray theory. A method given by Lee and Stewart (1981) has been used for tracing ray from source to observation point in the layered earth model. The method has already been used by Joshi et al. (2010). Several equations have been obtained for a particular earthquake at different observation point. Equation corresponding to the data of 1st earthquake can be written as (Joshi 2007):

$$R_{op,1}(f) = \ln\left(\frac{S_o(f)}{S^{cal}(f)}\right)_1 - \pi f \sum (\delta D_{ijk})\ T_{ijk,1}^{op} + e \tag{2.10}$$

The parameter ‘e’ in the equation (2.10) represents the estimate of error. The parameter ‘$T^{op}_{ijk,1}$’ represents time spent by the ray released from first event in various blocks to reach the station identified by superscript ‘op’ from event 1. Above set of equation can be written in the matrix given by Joshi (2007) for the data of ‘N’ earthquake as:

$$
\begin{vmatrix}
1 & 2\ldots & N & 1 & 2 & \ldots.. & N_b & 1 \\
1 & 0\ldots & 0 & -\pi f T^{11}_{111,1} & -\pi f T^{11}_{121,1} & \ldots.. & -\pi f T^{11}_{LMK,1} & 1 \\
1 & 0\ldots & 0 & -\pi f T^{21}_{111,1} & -\pi f T^{21}_{121,1} & \ldots.. & -\pi f T^{21}_{LMK,1} & 1 \\
\vdots & \vdots & \vdots & \vdots & \vdots & \vdots & \vdots & \vdots \\
1 & 0\ldots & 0 & -\pi f T^{op}_{111,1} & -\pi f T^{op}_{121,1} & \ldots.. & -\pi f T^{op}_{LMK,1} & 1 \\
\vdots & \vdots & \vdots & \vdots & \vdots & \vdots & \vdots & \vdots \\
1 & 0\ldots & 0 & -\pi f T^{LsMs}_{111,1} & -\pi f T^{LsMs}_{121,1} & \ldots.. & -\pi f T^{LsMs}_{LMK,1} & 1 \\
\text{For } N^{th} \text{ earthquake} & & & & & & & \\
0 & 0\ldots & 1 & -\pi f T^{11}_{111,N} & -\pi f T^{11}_{121,N} & \ldots.. & -\pi f T^{11}_{LMK,N} & 1 \\
0 & 0\ldots & 1 & -\pi f T^{21}_{111,N} & -\pi f T^{21}_{121,N} & \ldots.. & -\pi f T^{21}_{LMK,N} & 1 \\
\vdots & \vdots & \vdots & \vdots & \vdots & \vdots & \vdots & \vdots \\
0 & 0\ldots & 1 & -\pi f T^{op}_{111,N} & -\pi f T^{op}_{121,N} & \ldots.. & -\pi f T^{op}_{LMK,N} & 1 \\
\vdots & \vdots & \vdots & \vdots & \vdots & \vdots & \vdots & \vdots \\
0 & 0\ldots & 1 & -\pi f T^{LsMs}_{111,N} & -\pi f T^{LsMs}_{121,N} & \ldots.. & -\pi f T^{LsMs}_{LMK,N} & 1
\end{vmatrix}
\begin{vmatrix}
In(S_o(f)/S^{cal}(f))_1 \\
\cdot \\
\cdot \\
\cdot \\
\cdot \\
\cdot \\
\cdot \\
In(S_o(f)/S^{cal}(f))_N \\
\\
\delta D_{111} \\
\delta D_{121} \\
\cdot \\
\cdot \\
\cdot \\
\cdot \\
\delta D_{LMK} \\
\\
e
\end{vmatrix}
=
\begin{vmatrix}
R_{11,1}(f) \\
R_{12,1}(f) \\
\cdot \\
\cdot \\
\cdot \\
R_{LsMs,1}(f) \\
\cdot \\
\cdot \\
\\
R_{11,N}(f) \\
R_{12,N}(f) \\
\cdot \\
\cdot \\
\cdot \\
\cdot \\
R_{LsMs,N}(f)
\end{vmatrix}
$$

The above matrix equation can be written in the following form:

$$G\ m = d \tag{2.11}$$

Matrix ‘m’ and ‘d’ contains the model parameters and data, respectively. The range of subscripts i, j and k varies from 1 to L, M and K, respectively, and the range of superscript o and p varies from 1 to L_s and M_s, respectively. Now $N_b = L \times M \times K$ and $N_s = L_s \times M_s$ are the total number of blocks and the total number of observation points, respectively. Therefore complete set of matrix contain $N_e = N_s \times N$ equations and $N_p = N + N_b + 1$ parameters. Matrix ‘G’ is a rectangular matrix; therefore Newton’s method can be used to obtain the following form of model matrix:

$$m = (G^T G)^{-1} G^T d \tag{2.12}$$

where, matrix 'G^T' defines the transpose of matrix 'G'. In actual case some of the eigen values of G^TG are very small so that the variance of solution becomes unacceptably large. To avoid this difficulty, damped least square method of Levenberg (1944) can be used, which does not require eigen values analysis. The inversion using damped least square method is given as:

$$m^{est} = (G^T G + \lambda I)^{-1} G^T d \tag{2.13}$$

In above equation matrix 'I' is a unit matrix and 'λ' is damping factor. The solution of above equation can be obtained by minimizing $|d\text{-}Gm| + m^T(\lambda I)m$ instead of $|d\text{-}Gm|^2$, where (λI) is a diagonal matrix with damping factors. The choice of 'λ' is based on the method modified after Dimiri (1992) and used by Joshi (2007). Various possibilities of fraction of largest eigen value have been checked to choose the value of 'λ'. Damping factor is changed in an iterative manner by using several iterations and final 'λ' is selected on the basis of minimum root mean square error for a particular inversion in data matrix. The root mean square error in the data matrix is calculated by using following equation:

$$RMSE_{dat} = \left[\frac{1}{M} \sum_{i=1}^{M} (d_i^o - d_i^c)^2 \right]^{\frac{1}{2}} \tag{2.14}$$

where, M, d_i^o and d_i^c are the total number of data point, observed data and computed data, respectively. The entire scheme of inversion in the form of flow graph is shown in the Fig. 2.3.

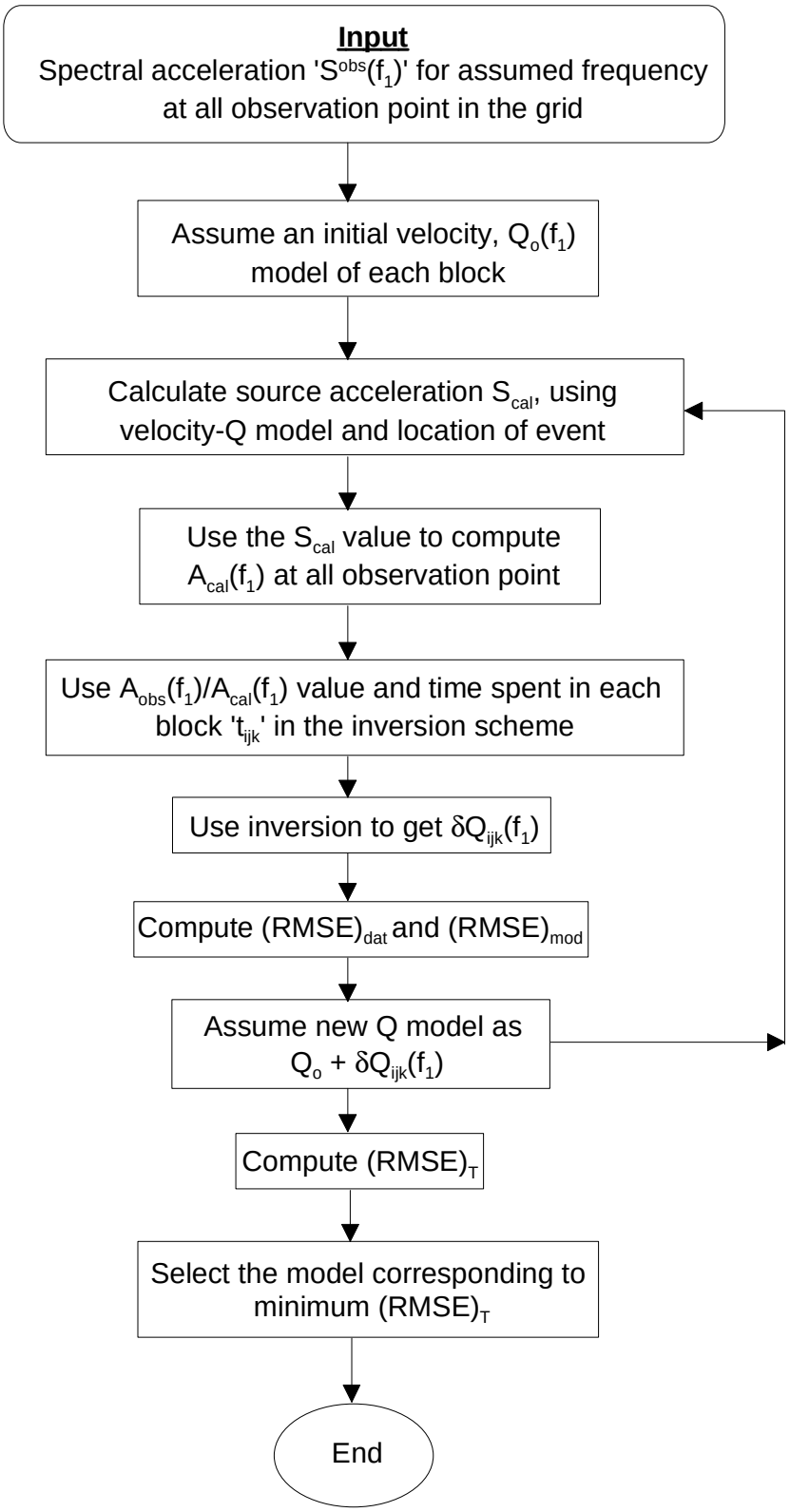

Figure 2.3: Flow chart of the process of inversion (Figure modified after Joshi et al., 2010).

The inversion algorithm gives the estimate of unknown quantities like $\ln(S_o(f)/S^{cal}(f))$ and δD_{ijk}. In this iterative procedure, after each inversion initial model '$Q_{ijk,o}$' is replaced by 'Q_{ijk}' which is given by following expression:

$$Q_{ijk}(f) = \delta Q_{ijk}(f) + Q_{ijk,0}(f) \tag{2.15}$$

where, '$\delta Q_{ijk}(f)$' represents small incremental change in quality factor. In each successive iteration the value of '$Q_{ijk}(f)$' is assumed as initial model in place of '$Q_{ijk,o}(f)$'. Using this modified initial model, '$S_o(f)$' is again computed at all observation points and its average value is used to compute '$A^{cal}(f)$' at these observation points. This again gives a new set of equations for inversion. This iteration is performed until the solution corresponding to the minimum error is obtained. The complete iterative inversion process is shown in Fig. 2.4.

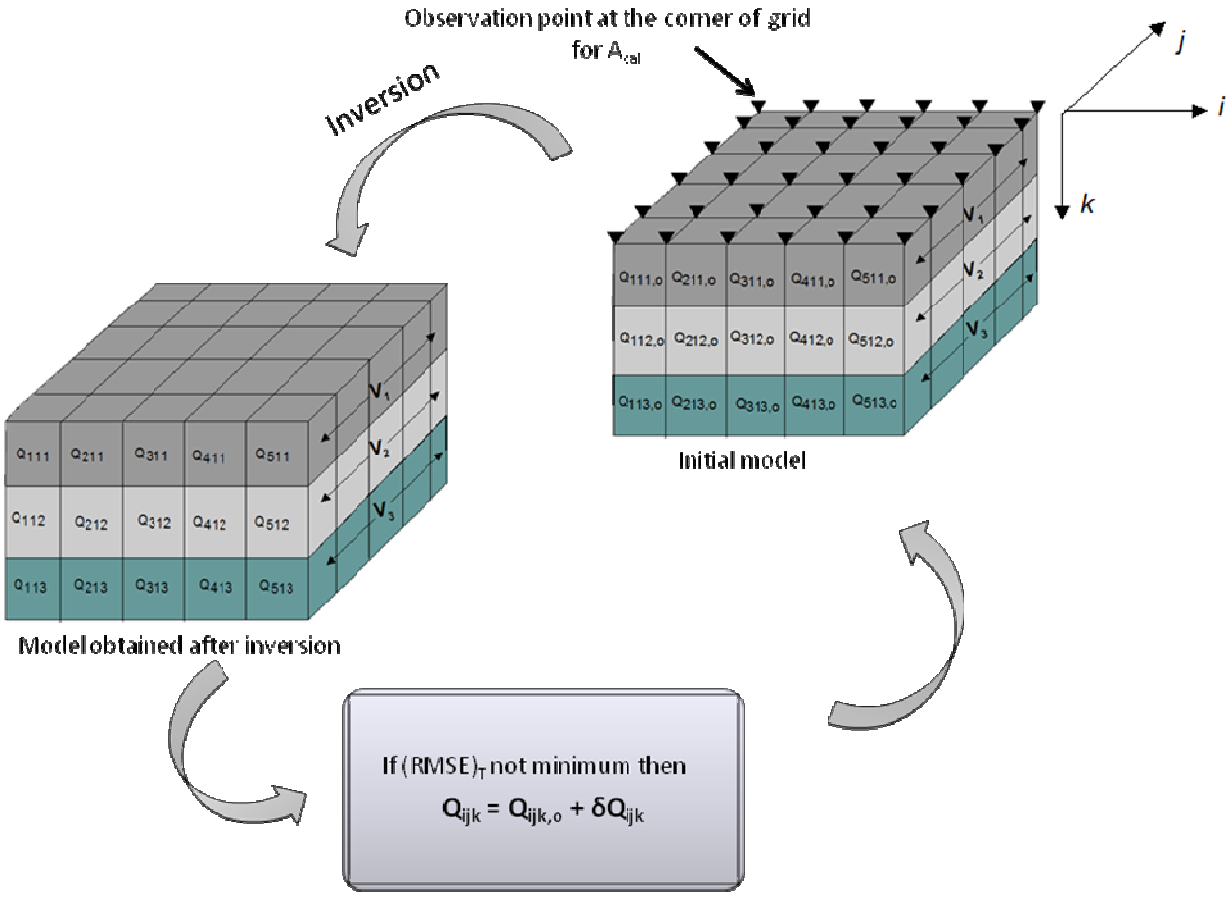

Figure 2.4: Initially $Q_{ijk,o}$ has been used in each block and after first iteration a new model having quality factor value (Q_{ijk}) in different blocks is obtained. The subscripts i, j and k describe the position of the blocks in respect of x, y and z directions, respectively (Figure modified after Joshi, 2007).

2.3 Numerical Experiments

Numerical experiments have been performed on the developed algorithm to check the stability of the solution and dependency of the obtained solution on input dataset. The computer software named three dimensional frequency dependent Q structure (Joshi et al., 2010) based on inversion of strong motion data has been modified in this present work. Input to this algorithm are initial velocity model, initial $Q_\beta(f)$ model, coordinates of hypocenters of input earthquakes, spectral acceleration value at observation points and a reference frequency at which attenuation structure is estimated. The spectral acceleration values at the corner of the grid are obtained from contours prepared from observed spectral acceleration data at different recording stations. The values of spectral acceleration at 36 observation point are calculated from observed spectral acceleration contours. The data of 12 earthquakes provided total 432 spectral acceleration values at 36 observation point for a particular frequency.

The output of the software gives the ratio of observed and calculated spectral acceleration and final value of '$Q_\beta(f)$' at different blocks. Root mean square error for data $(RMSE)_{dat}$ and model matrix $(RMSE)_{mod}$ has been calculated for each iteration. The suitability of model matrix which determined using the damped least square inversion scheme is checked by the resolution matrix and covariance matrix. The resolution matrix 'R_m' and covariance matrix 'C' are given by the following expression (Haydar et al., 1990) as.

$$R_m = (G^T G + \lambda I)^{-1} G^T G \tag{2.16}$$

$$C = \sigma_d (G^T G + \lambda I)^{-1} R_m \tag{2.17}$$

where, σ^2_d is the variance of error in data which is given as:

$$\sigma^2_d = (G_e m - d)^2 / N_p \tag{2.18}$$

$$G_e = (G^T G + \lambda I) \tag{2.19}$$

The resolution of model parameter is given by resolution matrix. Deviation of 'R_m' from the unit matrix indicates the poor resolution. The i^{th} diagonal element of 'R_m' gives us a good measure of the uniqueness of the i^{th} component of the solution parameter (Wiggins 1972). In the present work the total number of parameter (Np) is 88. Among these 88 parameters, 12 represent the ratio of source acceleration spectra of studied events, one represent the error and remaining 75 parameters represent quality factor of different blocks. A model that minimizes all errors

simultaneously gives a reliable solution. Following normalized value of $(RMSE)_{mod}$ and $(RMSE)_{dat}$ has been used in the present work to get a model where $(RMSE)_{mod}$ and $(RMSE)_{dat}$ are minimized simultaneously as given by Joshi (2006a).

$$(RMSE)_T = [(Nor\ (RMSE)_{mod} + Nor\ (RMSE)_{dat}] /2 \quad (2.20)$$

The scenario where $RMSE_{mod}$ and $RMSE_{dat}$ are not minimized for same model the idea of using $(RMSE)_T$ may be helpful for selecting a reliable solution. Various numerical experiments have been made to check the stability and dependency on input events of the present inversion algorithm. Number of local events recorded on strong motion stations of KiK-net network in the Central Honshu region, Japan have been used for these numerical experiments. Various numerical experiments verify the efficacy of the present inversion algorithm to obtain three dimensional frequency dependent 'Q' structure. In the preceding section, following experiments have been applied:

- Dependency of result on number of input events
- Dependency of result on depth of input events
- Stability of solution: Test by Bootstrap method
- Stability of solution: Test by changing the order of input events

2.3.1 Dependency of result on number of input events

In this experiment the developed algorithm is tested for its dependency on number of input events. In this numerical experiment two data sets named as data set 1 and data set 2 have been used. These data sets have different number of input events. The number of input events for data set 1 and data set 2 are twelve and eight, respectively. The parameters of events in data set 1 and data set 2 are given in Table 2.1. The attenuation contours is determined by dividing the entire study area into small three dimensional blocks of uniform thickness of 5 km. The data set 2 contain less number of events as compared to data set 1. The effect of the removal of input events is clearly observed in the final result of inversion and is shown in Fig. 2.5. It is observed from Fig. 2.5 that the contours obtained using the data set 1 coincides well with major geological trends in the area as compared to data set 2. The contour lines of quality factor values obtained using data set 1 are nearly parallels to the Itoigawa-Shizuoka Tectonic Line (ISTL) as shown in Fig. 2.5. It is further observed that rms error for data set 1 is comparatively smaller than that for data set 2.

Table 2.1: Parameters of the events used in data set 1 and data set 2.

Data set 1				
Events	**Origin time h:m:s**	**Depth (km)**	**Epicenter (In Degree)**	
			Latitude	**Longitude**
05/10/2003	00:29:42.52	15	35.99N	137.58E
01/04/2003	09:25:36.42	6	36.36N	137.30E
22/05/2003	07:09:34.25	15	35.71N	138.03E
04/06/2003	02:52:51.06	11	36.01N	137.58E
11/01/2004	16:57:59.57	9	36.40N	137.75E
14/02/2004	20:19:39.37	10	35.85N	137.25E
03/06/2004	19:04:36.87	8	35.98N	137.37E
30/06/2004	06:35:56.14	11	35.98N	137.20E
02/01/2005	01:30:58.66	5	36.04N	137.20E
07/01/2005	23:38:07.86	20	35.67N	137.20E
24/03/2005	20:08:00.86	10	36.20N	137.37E
05/05/2005	07:38:13.27	15	35.51N	137.31E
Data set 2				
11/01/2004	16:57:59.57	9	36.40N	137.75E
14/02/2004	20:19:39.37	10	35.85N	137.25E
03/06/2004	19:04:36.87	8	35.98N	137.37E
30/06/2004	06:35:56.14	11	35.98N	137.20E
02/01/2005	01:30:58.66	5	36.04N	137.20E
07/01/2005	23:38:07.86	20	35.67N	137.20E
24/03/2005	20:08:00.86	10	36.20N	137.37E
05/05/2005	07:38:13.27	15	35.51N	137.31E

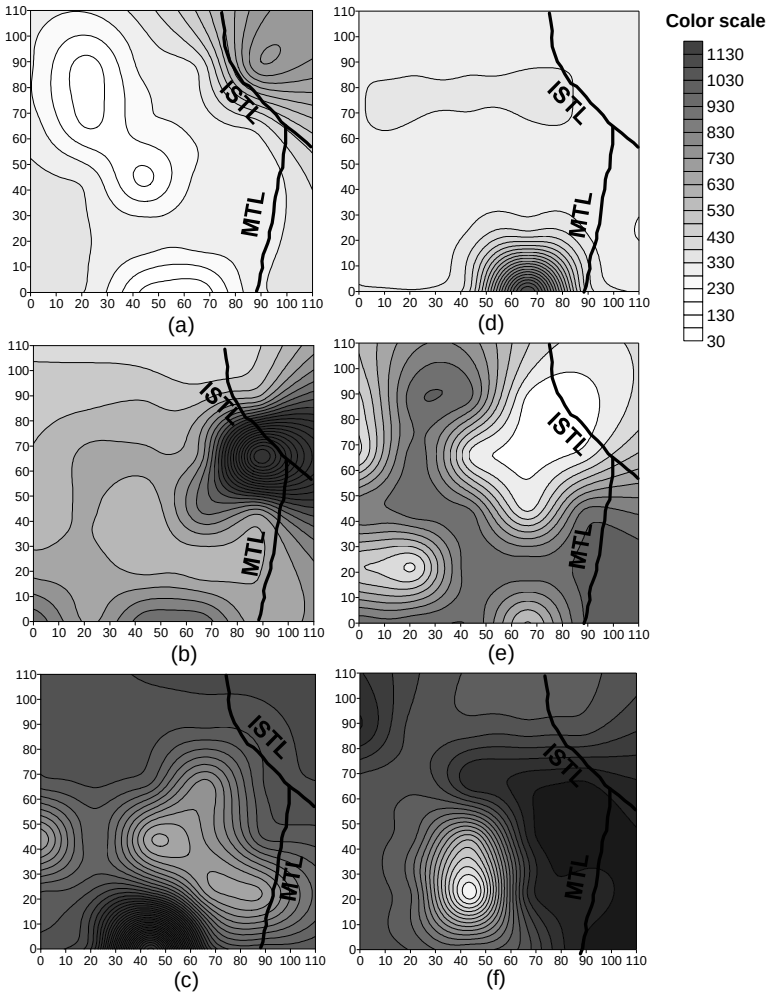

Figure 2.5: Contour of shear wave quality factor for 5 Hz frequency obtained using the data set 1 at (a) 0-5 km, (b) 5-10 km and (c) 10-15 km depth. Contour of quality factor values for 5 Hz frequency obtained using the data set 2 at (d) 0-5 km, (e) 5-10 km and (f) 10-15 km depth. ISTL and MTL describe the Itoigawa-Shizuoka Tectonic Line and Median Tectonic Line, respectively.

The resolution matrix of 88 and 84 parameters obtained from inversion of data set 1 and data set 2, respectively is shown in Fig. 2.6. Unit value in the resolution matrix indicates the high resolution. Deviation from unit value in the resolution matrix indicates the poor resolution. It is observed that high resolution is observed in the results obtained from inversion for data set 1 as compared to data set 2. The depth wise resolution of attenuation parameters is shown in Fig. 2.7 and it shows that the attenuation parameters in data set 1 are mostly resolved in the last layer as compared to data set 2. This shows that the resolution of attenuation parameters become poor as number of input events decreases. The reason of poor resolution is the loss of information due to less number of input earthquake data and attenuation structure of the region depends on the distance travelled by energy from focus of an earthquake to reach the observation point. This

experiment clearly shows that the obtained attenuation structure is strongly dependent on number of input events and rms error increases as the number of input event is decreases. The trend of contours obtained using data set 2 which consist of less number of event clearly shows deviation of contours of $Q_\beta(f)$ value from major tectonic unit of the region.

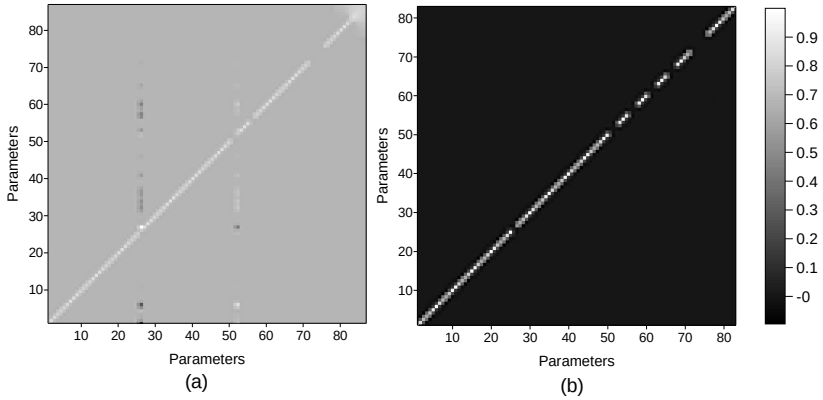

Figure 2.6: Total Resolution matrices of 88 and 84 parameters at 5 Hz for (a) data set 1 and (b) data set 2, respectively.

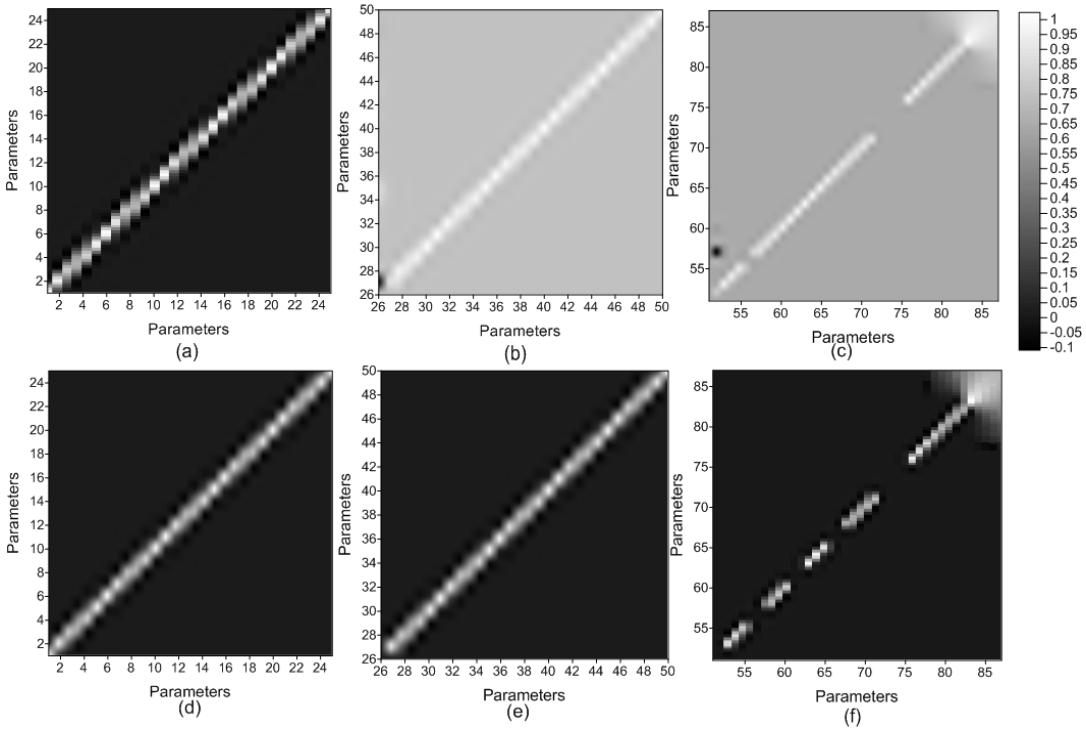

Figure 2.7: The resolution matrix of attenuation parameters at 5 Hz for data set 1 at (a) 0-5 km, (b) 5-10 km and (c) 10-15 km depth. The resolution matrix of attenuation parameters at 5 Hz for data set 2 at (d) 0-5 km, (e) 5-10 km and (f) 10-15 km depth.

2.3.2 Dependency of result on depth of input events

In order to check the dependency of obtained structure on the depth of input earthquakes, two data set having different depth range have been used. These two data sets are named as data set 1 and data set 3 having twelve earthquakes in each data set. The parameters of earthquakes included in data set 1 and 3 are given in Table 2.1 and Table 2.2, respectively. The attenuation contours for 5 Hz frequecy at different depth obtained using these two data sets are shown in Fig. 2.8. It is observed from Fig. 2.8 that data set 1 and 3 gives the different trend of attenuation contour. The depth ranges for data set 1 and 3 are 5-20 km and 5-11 km, respectively. These different depths of the events are responsible to get different trend of attenuaiton contours for the data set 1 and 3, respectively. It is seen that trends of contours of first layer obtained using the data set 1 and 3 are comparable but trends of second and third layers are not comparable with each other. This may be due to less number of events prsent in second and third layer in data set 3 as compared to data set 1 therefore energy coming from events penetrate less number of blocks in second and third layer in data set 3 as compared to data set 1.

Table 2.2: Parameters of the events used in data set 3.

Data set 3				
Events	**Origin time h:m:s**	**Depth (km)**	**Epicenter (In Degree)**	
			Lat.	**Long.**
04/12/2002	08:08:25.06	6	36.37	136.90
01/04/2003	09:25:36.42	6	36.36	137.30
03/12/2010	17:10:43.29	10	35.72	137.58
04/06/2003	02:52:51.06	11	36.01	137.58
11/01/2004	16:57:59.57	9	36.40	137.75
14/02/2004	20:19:39.37	10	35.85	137.25
03/06/2004	19:04:36.87	8	35.98	137.37
30/06/2004	06:35:56.14	11	35.98	137.20
02/01/2005	01:30:58.66	5	36.04	137.20
18/05/2003	03:22:43.82	8	35.93	137.36
13/06/2003	10:06:38.66	9	35.89	137.60
27/02/2011	21:46:54.00	5	36.32	137.30

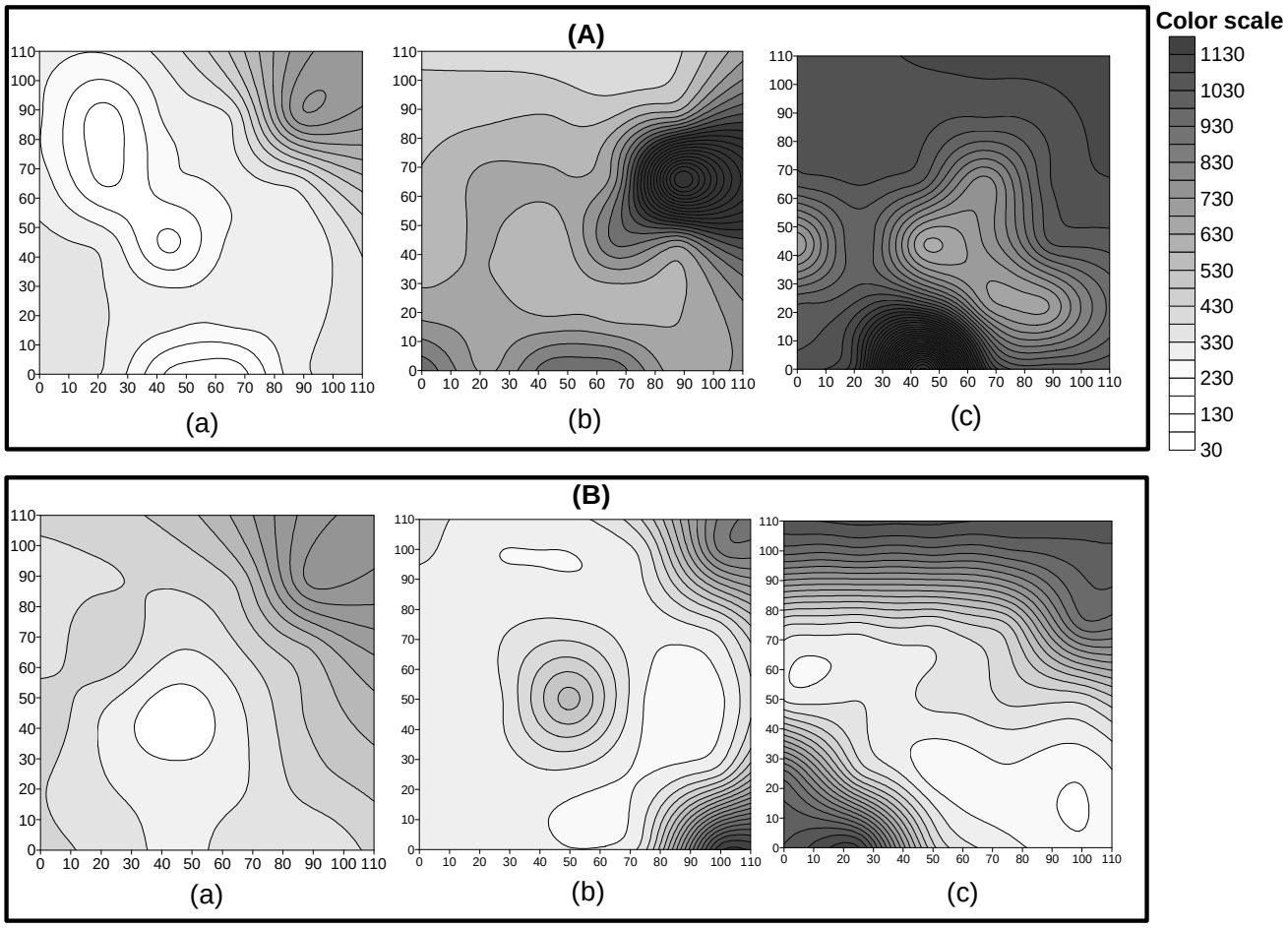

Figure 2.8: Contour of shear wave quality factor for 5 Hz at (a) 0-5 km, (b) 5-10 km and (c) 10-15 km depth for (A) data set 1 and (B) data set 3.

In order to check the dependency of input data having earthquake with similar hypocentral depth range on obtained attenuation structure data set named as data set 4 is prepared which has same depth range as data set 1. The hypocentral parameters used in data set 1 and 4 are given in Table 2.1 and Table 2.3, respectively. The depth ranges for data set 1 and 4 are similar i.e. 5-20 km.The obtained attenuation contours for 5 Hz at different depth using data set 1 and 4 are shown in Fig. 2.9. It is observed from this experiment that data set having similar depth range gives almost similar attenuation structure from inversion algorithm. This experiment shows that input data with different depth range tends to give different attenuation structure while the input data having similar depth range gives almost similar attenuation structure.

Table 2.3: Parameters of the events used in data set 4.

Data set 4				
Events	**Origin time h:m:s**	**Depth (km)**	**Epicenter (In Degree)**	
			Lat.	**Long.**
04/12/2002	08:08:25.06	6	36.37	136.90
18/05/2003	03:22:43.82	8	35.93	137.36
12/06/2003	20:39:54.53	11	35.88	137.40
13/06/2003	10:06:38.66	9	35.89	137.60
24/06/2006	23:09:40.31	11	35.91	137.58
13/06/2008	11:20:41.93	15	35.80	137.55
03/12/2010	17:10:43.29	10	35.72	137.58
06/02/2011	07:24:41.68	10	35.80	137.37
27/02/2011	21:46:54.00	5	36.32	137.30
22/05/2003	07:09:34.25	15	35.71	138.03
05/05/2005	07:38:13.27	15	35.51	137.31
07/01/2005	23:38:07.86	20	35.67	137.20

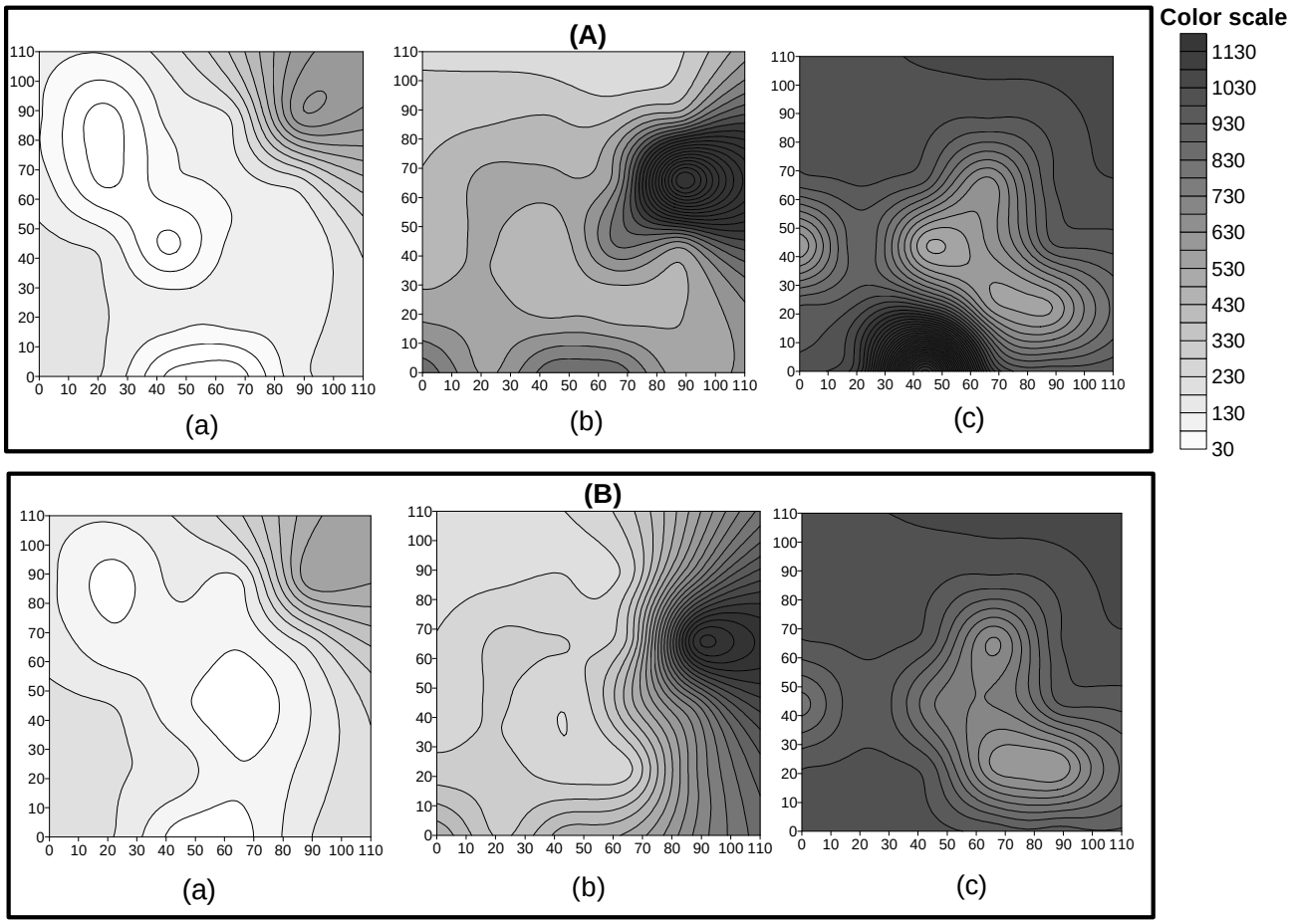

Figure 2.9: Contour of shear wave quality factor for 5 Hz at (a) 0-5 km, (b) 5-10 km and (c) 10-15 km depth for (A) data set 1 and (B) data set 4.

2.3.3 Stability of solution: Test by Bootstrap method

In an attempt to check the dependency of obtained solution on random selection of input data bootstrap method has been implemented in the present work. In this numerical experiment, data set 5 having twelve input earthquake has been used. The random selection of the events have been made from the data set 1 and 4 to generate the data set 5. The hypocentral parameters used in data set 5 are given in Table 2.4. The comparison of attenuation contour at different depth using the data set 1, 4 and 5 are shown in Fig. 2.10. It is observed from Fig. 2.10 that the attenuation contour obtained using the data set 5 is comparable with the attenuation contour obtained using the data set 1 and 4. The depth range of the events used in data set 5 is same with that in the data set 1 and 4. It is seen from the contour map of quality factor that the value of quality factor is almost similar for these three data sets.

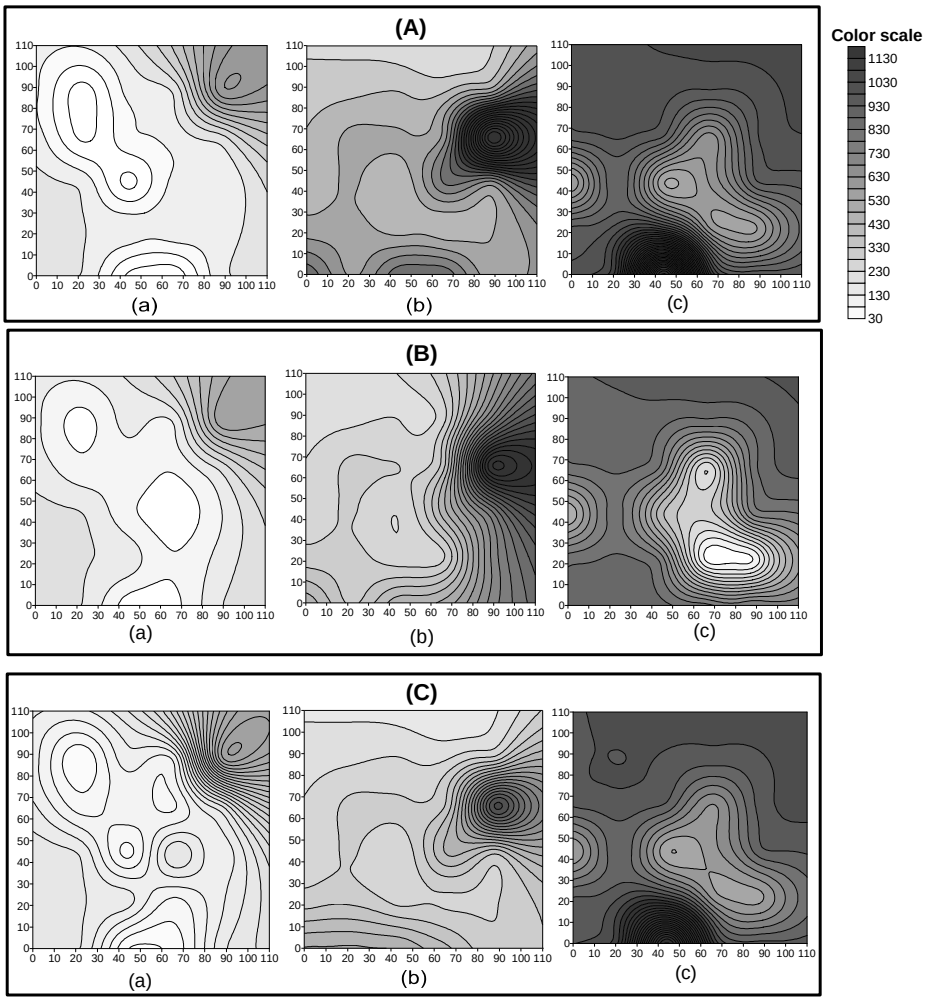

Figure 2.10: Contour of shear wave quality factor for 5 Hz at (a) 0-5 km, (b) 5-10 km and (c) 10-15 km depth for (A) data set 1, (B) data set 4 and (C) data set 5, respectively.

Table 2.4: Parameters of the events used in data set 5.

Data set 5				
Events	**Origin time h:m:s**	**Depth (km)**	**Epicenter (In Degree) Lat. Long.**	
04/12/2002	08:08:25.06	6	36.37N	136.90E
03/06/2004	19:04:36.87	8	35.98N	137.37E
12/06/2003	20:39:54.53	11	35.88N	137.40E
11/01/2004	16:57:59.57	9	36.40N	137.75E
24/06/2006	23:09:40.31	11	35.91N	137.58E
05/10/2003	00:29:42.52	15	35.99N	137.58E
03/12/2010	17:10:43.29	10	35.72N	137.58E
24/03/2005	20:08:00.86	10	36.20N	137.37E
02/01/2005	01:30:58.66	5	36.04N	137.20E
22/05/2003	07:09:34.25	15	35.71N	138.03E
05/05/2005	07:38:13.27	15	35.51N	137.31E
07/01/2005	23:38:07.86	20	35.67N	137.20E

2.3.4 Stability of solution: Test by Changing the order of input events

In order to check the stability of the solution two data set named as data set 1 and data set 6 are considered. The informations of the input events used in data set 6 is given in Table 2.5. In both data set same input events have been used. The only difference is that the order of input events are different in both data set. In this way the same data of earthquakes with same depth range have been obtained in these data set. The attenuation contours at 5 Hz obtained using data set 1 and data set 6 are shown in Fig. 2.11 and similar attenuation structure has been obtained using these two data set. Results obtained in this inversion show that the obtained attenuation structure does not depend on the order of input data and is a stable algorithm.

Table 2.5: Parameters of the events used in data set 6.

Data set 6				
Events	**Origin time h:m:s**	**Depth (km)**	**Epicenter (In Degree)**	
			Lat.	**Long.**
02/01/2005	01:30:58.66	5	36.04N	137.20E
07/01/2005	23:38:07.86	20	35.67N	137.20E
24/03/2005	20:08:00.86	10	36.20N	137.37E
05/05/2005	07:38:13.27	15	35.51N	137.31E
11/01/2004	16:57:59.57	9	36.40N	137.75E
04/06/2003	02:52:51.06	11	36.01N	137.58E
03/06/2004	19:04:36.87	8	35.98N	137.37E
30/06/2004	06:35:56.14	11	35.98N	137.20E
14/02/2004	20:19:39.37	10	35.85N	137.25E
22/05/2003	07:09:34.25	15	35.71N	138.03E
05/10/2003	00:29:42.52	15	35.99N	137.58E
01/04/2003	09:25:36.42	6	36.36N	137.30E

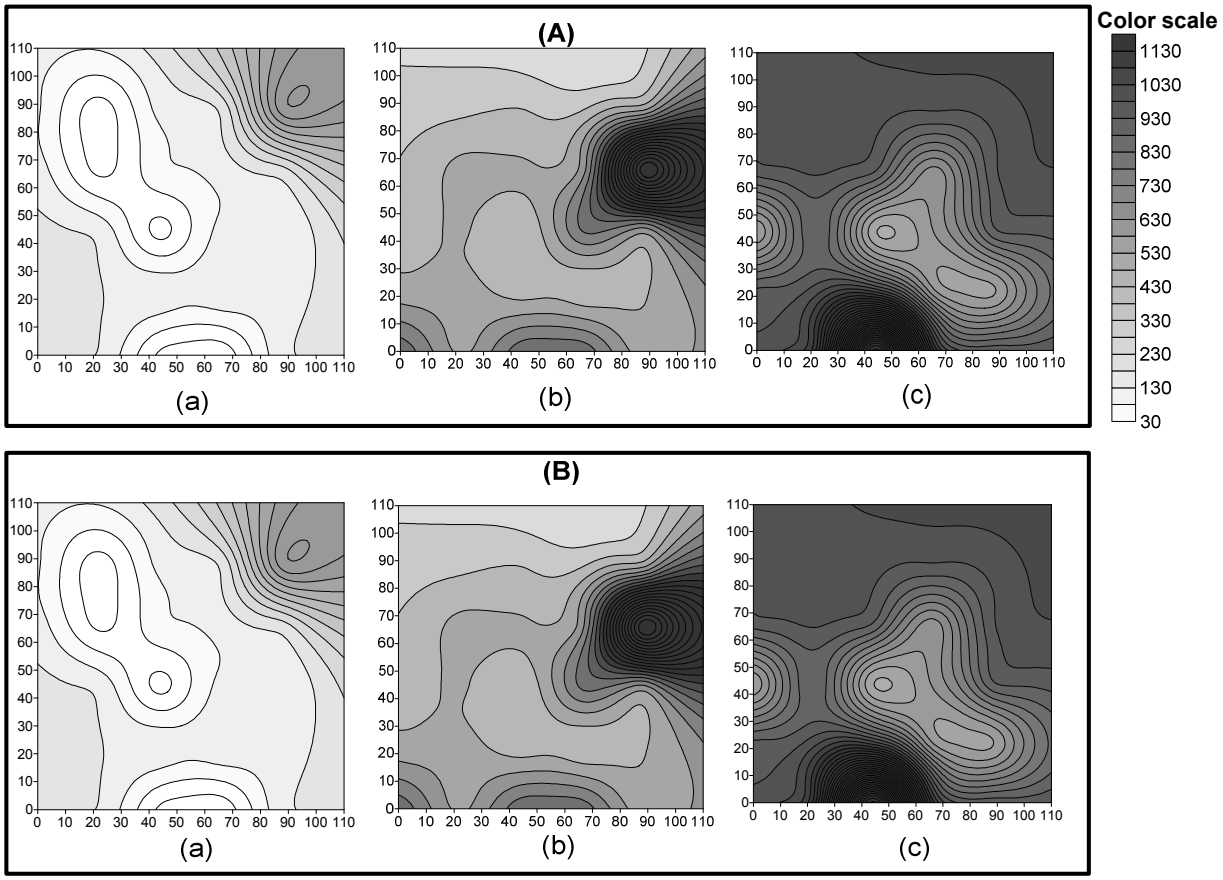

Figure 2.11: Contour of shear wave quality factor for 5 Hz at (a) 0-5 km, (b) 5-10 km and (c) 10-15 km depth for (A) data set 1 and (B) data set 6, respectively.

2.4 Conclusion

This chapter discussed an inversion algorithm to obtain three dimensional attenuation structure of the region initially developed by Hashida and Shimazaki (1984) and modified by Joshi (2006a; 2007) and Joshi et al. (2010). Modification is made in the inversion algorithm in this work by enhancing the number of input events in the inversion algorithm. In earlier algorithm only four earthquakes were used as input, this limitation has been removed and now in the modified algorithm several earthquakes have been used as input events. Various numerical tests have been performed to check the dependency of the inversion algorithm on number of input earthquakes, their depth range and its selection. These numerical tests validate the stability of present software to obtain reliable three dimensional attenuation structures.

Chapter – 3

Inversion Technique for Estimation of Frequency Dependent Shear Wave Quality Factor ($Q_\beta(f)$) and Site effect

3.1 Introduction

Strong motion data includes valuable high-frequency near-field data which is suitable for engineering use. This data contain valuable attenuation characteristics of the medium. The attenuation characteristic of the medium is defined in terms of frequency dependent quality factor. This frequency dependent quality factor is used in various strong motion prediction techniques like composite source modeling technique (Yu et al., 1995), semi empirical modeling technique (Joshi and Midorikawa, 2004) and stochastic simulation technique (Boore, 1983; Boore and Atkinson, 1987). This chapter discusses the direct inversion of strong motion data to estimate frequency dependent shear wave quality factor ($Q_\beta(f)$) and source parameters. The methodology of inversion of strong motion data and various numerical experiments to check the stability of developed methodology has been discussed in this chapter.

3.2 Inversion technique

The acceleration spectra of shear waves at a distance R due to an earthquake of seismic moment M_o can be defined as (Boore, 1983 and Atkinson and Boore, 1998):

$$A(f) = C\, S\,(f)\, D(f) \tag{3.1}$$

where, the 'C' is a constant term at a particular station for a given earthquake, S(f) represents the source acceleration spectra and D(f) represents a frequency dependent diminution function which takes into account the anelastic attenuation and attenuation due to geometrical spreading and is given as (Boore and Atkinson, 1987):

$$D(f) = [e^{-\pi f R/\, Q_\beta(f)\beta} G(R)] P(f, f_m) \tag{3.2}$$

In the above equation $P(f,f_m)$ is a high-cut filter that accounts for the observation that acceleration spectra often show a sharp decrease with increasing frequency, above some cutoff frequency f_m, that cannot be attributed to whole path attenuation (Boore, 1983). Due to rapid fall of acceleration spectra after 25 Hz in most of the acceleration records, f_m = 25 Hz is used in the

present work in the analytical form of $P(f,f_m)$ given by Boore (1983). The function G(R) represents geometrical attenuation term and is taken to be equal to 1/R for R < 100 km and equal to $1/(10\sqrt{R})$ for R > 100 km (Singh et al.,1999). As most of the data used in present work is within R < 100 km, therefore G(R) is used as 1/R. The term $e^{-\pi fR/ Q_\beta(f)\beta}$ represents anelastic attenuation. In this term $Q_\beta(f)$ is the frequency dependent shear wave quality factor. The equation (3.1) serves as the basis for this inversion. For a double-couple seismic source embedded in an elastic medium, considering only S-waves, C is a constant for a given station for a particular earthquake and is given as:

$$C = M_o R_{\theta\phi} \ . FS. \ PRTITN/ (4 \pi\rho\beta^3) \tag{3.3}$$

In the above expression, M_o is the seismic moment, $R_{\theta\phi}$ is the radiation pattern, FS is the amplification due to the free surface, PRTITN is the reduction factor that accounts for partitioning of energy into two horizontal components, and ρ and β are the density and the shear wave velocity, respectively. $S(f,f_c)$ define the source spectrum of the earthquake. In the present work the source acceleration spectra proposed by Aki (1967) and Brune (1970) has been used. This spectrum is based on ω^{-2} decay of high frequency proposed by Aki (1967) and Brune (1970) and is given as:

$$S(f,f_c) = (2\pi f)^2/ (1+(f/f_c)^2) \tag{3.4}$$

In above expression 'f_c' denote corner frequency of earthquake and is dependent on the size of earthquake. Using all defined function in equation (3.2), (3.3) and (3.4), equation (3.1) can be written as:

$$A(f) = \left[\frac{M_o R_{\theta\phi} \ . FS. PRTITN}{4\pi\rho\beta^3} \right] . \left[\frac{(2\pi f)^2}{1+(f / f_c)^2} \right] . \left[e^{-\pi fR/Q_\beta(f).\beta} \right] . G(R) . P(f, f_m) \tag{3.5}$$

Equation (3.5) is a non linear equation and can be linearized by taking its logarithm. This modifies equation (3.1) as:

$$\ln A(f) = \ln C + \ln (S(f, f_c)) - \pi fR/Q_\beta(f)\beta - \ln (R) + \ln P(f,f_m) \tag{3.6}$$

This is now in linearized form with unknown $Q_\beta(f)$ and f_c. The term representing the source filter $S(f,f_c)$ is replaced with equation (3.4). With an assumption of known values of 'f_c', the only

unknown quantity is $Q_\beta(f)$, which can be obtained from inversion by minimizing it in a least-squares sense. The least-squares inversion minimizes as:

$$\chi^2 = \sum [A_s(f) - S(f, f_c)]^2 \quad (3.7)$$

where, $S(f,f_c)$ is the theoretical source acceleration spectrum and $A_s(f)$ is the source spectrum obtained from the record after substituting parameters $Q_\beta(f)$ obtained from the inversion of equation (3.6). Rearranging known and unknown quantities on different sides, following form is obtained from the equation (3.6) as:

$$-\pi f R/ Q_\beta(f)\beta = \ln A(f) - \ln C - \ln (S(f, f_c)) + \ln (R) - \ln P(f,f_m) \quad (3.8)$$

Substituting the term related to the source spectrum $S(f,f_c)$ as $(2\pi f)^2/(1+(f/f_c)^2)$, equation (3.8) can be written as:

$$-\pi f R/ Q_\beta(f)\beta = \ln A(f) - \ln C - \ln (2\pi f)^2 + \ln(1+(f/f_c)^2) + \ln (R) - \ln P(f,f_m) \quad (3.9)$$

In equation (3.9), the dependence on the corner frequency has been linearized by expanding $\ln(1+(f/f_c)^2)$ in a Taylor series around f_c. Accordingly the following expression is obtained:

$$-\pi f R/ Q_\beta(f)\beta = \ln A(f) - \ln C - \ln [(2\pi f)^2/ (1+(f/f_c)^2)] - [2/(1+(f/f_c)^2)](f/f_c)^2(\Delta f_c/f_c) + \ln (R) - \ln P(f,f_m) \quad (3.10)$$

Here Δf_c is the small change in the corner frequency and is an unknown quantity that is obtained from the inversion. In the above expression fourth term in right hand side represent the Taylor series expansion of fourth term in equation (3.9) as given by Fletcher (1995) and Joshi (2006b). Following set of equations is obtained at a particular station for the i^{th} earthquake for frequencies $f_1, f_2, f_3 \ldots f_n$, where n denotes total number of digitized samples in the acceleration record:

$$-\pi f_1 R_{11}/ Q_\beta(f_1)\beta + F(f_1,f_{c1})\,\Delta f_c = D_{11}(f_1)$$

$$-\pi f_2 R_{11}/ Q_\beta(f_2)\beta + F(f_2,f_{c1})\,\Delta f_c = D_{11}(f_2)$$

$$\vdots \qquad \vdots \qquad \vdots$$

$$-\pi f_n R_{11}/ Q_\beta(f_n)\beta + F(f_n,f_{c1})\,\Delta f_c = D_{11}(f_n)$$

where, $F(f,f_c)= 2/(1+(f/f_c)^2)](f/f_c)^2(1/f_c)$ is the term obtained from the expansion of $\ln(1+(f/f_c)^2)$ in terms of Taylor series around f_c. It is found that this function behave linearly for known values of corner frequency 'f_c' and 'f'. For this reason in the present work 'f_c' is used as input parameter and

its several possibilities are checked before the final value is selected on the basis of minimum root mean square error of obtained and calculated data. For an other station, the set of equations will be:

$$
\begin{aligned}
-\pi f_1 R_{12}/\, Q_\beta(f_1)\beta + F(f_1,f_{c1})\,\Delta f_c &= D_{12}(f_1) \\
-\pi f_2 R_{12}/\, Q_\beta(f_2)\beta + F(f_2,f_{c1})\,\Delta f_c &= D_{12}(f_2) \\
\vdots \qquad\qquad \vdots \qquad\qquad &\;\;\vdots \\
-\pi f_n R_{12}/\, Q_\beta(f_n)\beta + F(f_n,f_{c1})\,\Delta f_c &= D_{12}(f_n)
\end{aligned}
\tag{3.11}
$$

Subscripts ‘i’ and ‘j’ represent the event and the station number, respectively. In above equation $D_{ij}(f_i)$ is given as:

$$D_{ij}(f_i) = \ln A_{ij}(f_i) - \ln C_i - \ln\left[(2\pi f)^2/\,(1+(f/f_{ci})^2)\right] + \ln(R_{ij}) - \ln P(f,f_m) \tag{3.12}$$

In the matrix form, the above set of equations can be written as:

$$
\begin{vmatrix}
-\pi f_1R_{11}/\beta & 0 & 0 & \cdots & 0 & F(f_1,f_{c1}) \\
0 & -\pi f_2R_{11}/\beta & 0 & \cdots & 0 & F(f_2,f_{c1}) \\
0 & 0 & -\pi f_3R_{11}/\beta & \cdots & 0 & F(f_3,f_{c1}) \\
\vdots & \vdots & \vdots & & \vdots & \vdots \\
0 & 0 & 0 & \cdots & -\pi f_nR_{21}/\beta & F(f_n,f_{c1}) \\
-\pi f_1R_{12}/\beta & 0 & 0 & \cdots & 0 & F(f_1,f_{c1}) \\
0 & -\pi f_2R_{12}/\beta & 0 & \cdots & 0 & F(f_2,f_{c1}) \\
0 & 0 & -\pi f_3R_{12}/\beta & \cdots & 0 & F(f_3,f_{c1}) \\
\vdots & \vdots & \vdots & & \vdots & \vdots \\
0 & 0 & 0 & \cdots & -\pi f_nR_{12}/\beta & F(f_n,f_{c1}) \\
 & & & \vdots & & \\
 & & & \vdots & & \\
 & & & \vdots & & \\
 & & \text{for } m^{th} \text{ earthquake} & & & \\
-\pi f_1R_{m1}/\beta & 0 & 0 & \cdots & 0 & F(f_1,f_{cm}) \\
0 & -\pi f_2R_{m1}/\beta & 0 & \cdots & 0 & F(f_2,f_{cm}) \\
0 & 0 & -\pi f_3R_{m1}/\beta & \cdots & 0 & F(f_3,f_{cm}) \\
\vdots & \vdots & \vdots & & \vdots & \vdots \\
0 & 0 & 0 & \cdots & -\pi f_nR_{m1}/\beta & F(f_n,f_{cm}) \\
-\pi f_1R_{m2}/\beta & 0 & 0 & \cdots & 0 & F(f_1,f_{cm}) \\
0 & -\pi f_2R_{m2}/\beta & 0 & \cdots & 0 & F(f_2,f_{cm}) \\
0 & 0 & -\pi f_3R_{m2}/\beta & \cdots & 0 & F(f_3,f_{cm}) \\
\vdots & \vdots & \vdots & & \vdots & \vdots \\
0 & 0 & 0 & \cdots & -\pi f_nR_{m2}/\beta & F(f_n,f_{cm})
\end{vmatrix}
\begin{vmatrix}
1/Q_\beta(f_1) \\ 1/Q_\beta(f_2) \\ 1/Q_\beta(f_3) \\ \vdots \\ \vdots \\ \vdots \\ 1/Q_\beta(f_n) \\ \Delta f_c
\end{vmatrix}
=
\begin{vmatrix}
D_{11}(f_1) \\ D_{11}(f_2) \\ D_{11}(f_3) \\ \vdots \\ D_{11}(f_n) \\
D_{12}(f_1) \\ D_{12}(f_2) \\ D_{12}(f_3) \\ \vdots \\ D_{12}(f_n) \\
\vdots \\ \vdots \\ \vdots \\ \vdots \\ \vdots \\
D_{m1}(f_1) \\ D_{m1}(f_2) \\ D_{m1}(f_3) \\ \vdots \\ D_{m1}(f_n) \\
D_{m2}(f_1) \\ D_{m2}(f_2) \\ D_{m2}(f_3) \\ \vdots \\ D_{m2}(f_n)
\end{vmatrix}
$$

This can be represented in the following form:

$$G\,m = d \tag{3.13}$$

Model parameters are contained in the model matrix 'm' and the spectral component in the data matrix 'd'. Inversion of the 'G' matrix gives the model matrix 'm' using the Newton's method as below:

$$m = (G^T G)^{-1} G^T d \tag{3.14}$$

The corner frequency is treated as an input parameter in the inversion algorithm to maintain the linearity in equation (3.12). Different solutions are found for different possibilities of f_c. The final solution is that which gives minimum rmse. In the present inversion scheme several possibilities of corner frequencies are checked by iteratively changing corner frequency 'f_c' in a step of small incremental change of 'Δf'. The small increment 'Δf' considered in the present work is 0.01 Hz. The above inversion is prone to the problems if $G^T G$ is even close to singular and for such a case; the singular value decomposition (SVD) prefer to solve 'm' (Press et al., 1992). Formulation for the SVD is followed after Lancose (1961).

The entire scheme of iterative inversion used for obtaining f_c and $Q_\beta(f)$ is shown in Fig. 3.1 in the form of flow graph. The software QINV developed by Joshi (2006b) has been used in the present work. Seismic moment is one of the most important parameter which is required as input to the present algorithm. This has been computed from the spectral analysis of the recorded data using Brune's model (Keilis Borok, 1959; Brune, 1970). In this process a time window of length which cover entire S phase has been applied to the corrected accelerogram. The sampled window is cosine tapered with 10% at both end (Sharma and Wason, 1994). The spectrum of this time series is obtained using FFT algorithm and spectra has been corrected for anelastic attenuation and geometrical spreading term. The long term spectral level has been computed from obtained source spectrum and is used for calculating seismic moment of an earthquake. Seismic moment 'M_o' of an earthquake can be derived from the long term flat level of the displacement spectrum from Brune's model (1970) and is given as:

$$M_o = 4\pi\rho\beta^3 \Omega_o R / FS.R_{\theta\varphi} \tag{3.15}$$

where, ρ and β are the density and the S-wave velocity of the medium, respectively, Ω_o is the long term flat level of the source displacement spectrum at a hypocentral distance of R, FS is free surface effect and $R_{\theta\varphi}$ is the radiation-pattern coefficient. The value of density and S wave velocity has been used as 2.7 gm/cm^3 and 3.0 km/sec, respectively. As the fault plane solution of the

individual events could not be determined owing to the small number of stations, the radiation pattern $R_{\theta\varphi}$ has been approximately taken as 0.63 for S wave (Atkinson and Boore, 1995).

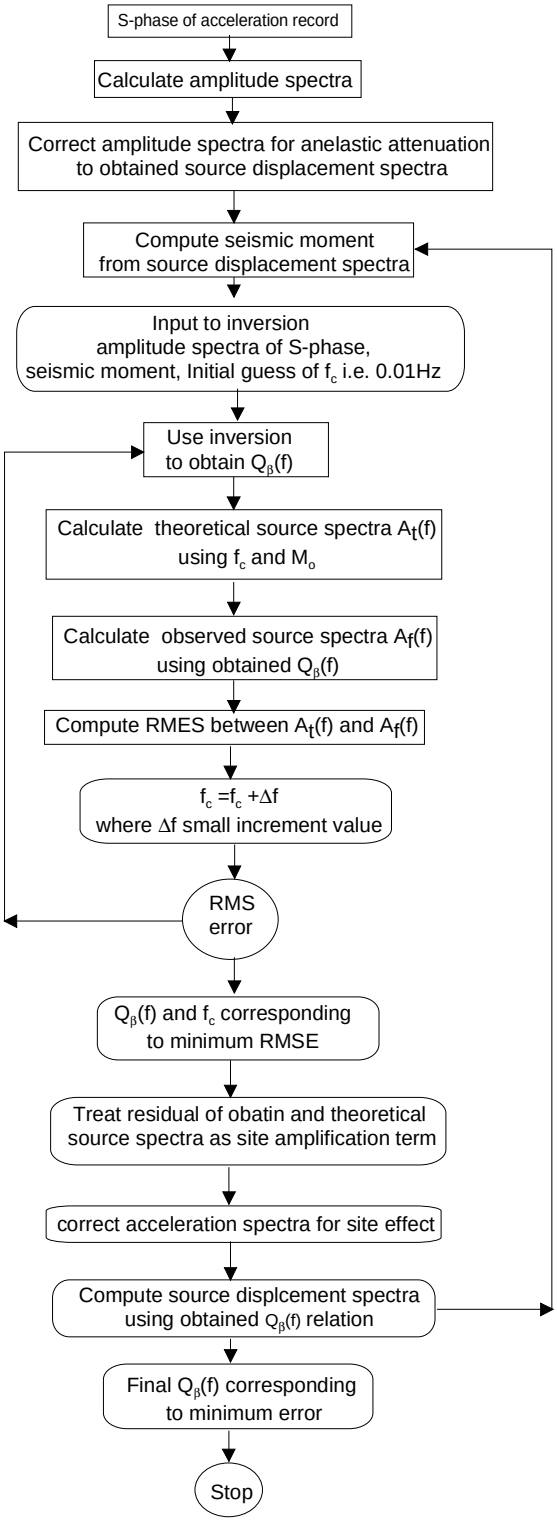

Figure 3.1: Flow diagram of entire process of inversion.

In the first part of inversion process, the acceleration spectra without any correction of site amplification has been used as an input to the algorithm and $Q_\beta(f)$ relation corresponding to minimum error is obtained. The obtained value of seismic moment, corner frequency and $Q_\beta(f)$ from the first part of the inversion are further used for obtaining residual of theoretical and observed source spectra which is treated as site amplification terms (Joshi, 2006b). The site amplifications terms obtained from inversion are used to correct the acceleration spectra which are now used as input in the second part of inversion scheme which is similar to the first part. The final outcome from this part is a new $Q_\beta(f)$ relation together with input values of seismic moment and corner frequency of each input. The obtained value of $Q_\beta(f)$ from second part of inversion is used to calculate source displacement spectra from acceleration record and is further used for computing seismic moment for next inversion. The process of two step inversion is repeated for this new estimate of seismic moment and goes on until minimum rmse is obtained which gives final estimate of $Q_\beta(f)$ at each station. The whole procedure to compute seismic moment after iteratively correcting acceleration spectra is shown in Fig. 3.2.

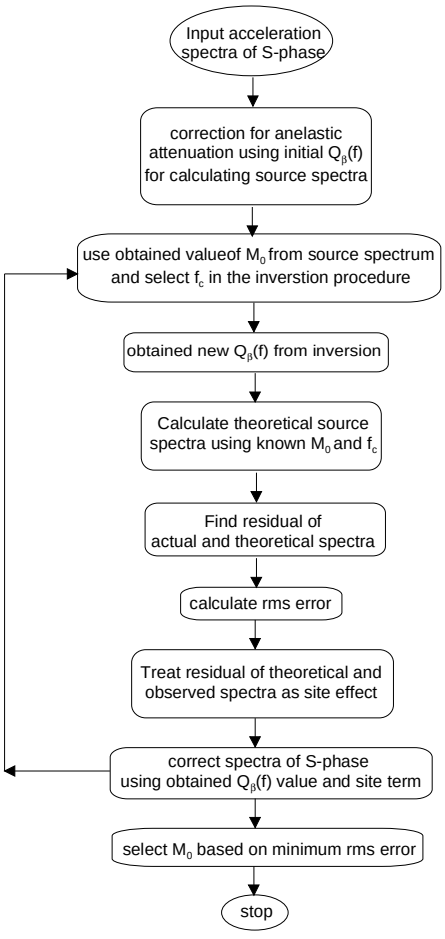

Figure 3.2: Flow diagram of entire process to obtain seismic moment.

In an attempt to check whether the residual make sense as a site amplification term, the technique proposed by Lermo and Chavez-Garcia (1993) has been used to obtain the site amplification curves. In this technique, amplitude spectrum of the horizontal-component of shear wave is divided by the amplitude spectrum of the vertical-component at each station to obtain the frequency dependent site response. This technique is analogous to the receiver function technique applied in the studies of the upper mantle and crust from teleseismic records (Langston, 1979). This method is similar to the Nakamura (1988) method of computing site amplification factors using H/V ratio at single station. Corner frequency of each event obtained from iterative inversion has been used to calculate residual of observed and theoretical source spectra of each event which is used as site amplification term. The site amplifications at Dharchula station obtained after iterative inversion of six events are shown in Fig. 3.3.

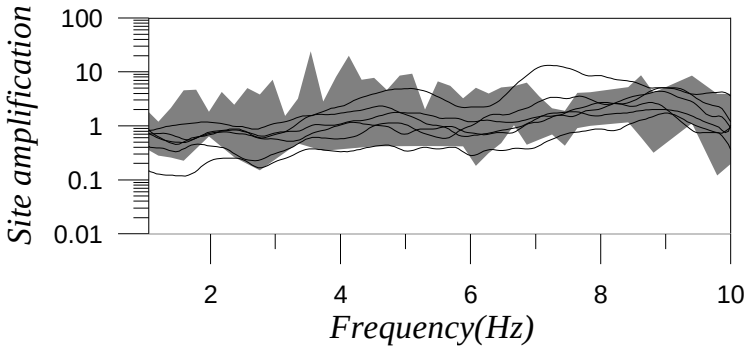

Figure 3.3: Site amplification at Dharchula station. The black lines show the site effects obtained by inversion of acceleration records of input events for NS component at Dharchula station. Different lines indicated site effect obtained from residual of input acceleration and source spectra. The shaded area denotes the region between $\mu+\sigma$ and $\mu-\sigma$ of the site amplification obtained using the technique given by Lermo and Chavez-Garcia (1993). Parameters 'μ' and 'σ' describe the mean and standard deviation, respectively.

3.3 Numerical Experiments

The developed software and algorithm has been numerically experimented to check its stability and its dependency on input data set. Three different set of input data has been used for this numerical experiment to obtain $Q_\beta(f)$ at Dharchula station. The NS component of acceleration record has been used for this numerical test. Each set contain six events and detail of events is shown in Table 3.1. The source parameters of these events were calculated from the source displacement spectra computed using $Q_\beta(f)$ value as given by Joshi et al. (2012a) for the Kumaon Himalaya. After obtaining $Q_\beta(f)$ from inversion of spectral acceleration data, source displacement is again computed using obtained value of $Q_\beta(f)$ from inversion. The process goes on until rms

error is minimized. The residual of obtained and theoretical spectra in each step is treated as site amplification and is used further for correcting acceleration record for site amplification term. Three input data sets from Dharchula station are separately used and site amplification and $Q_\beta(f)$ is calculated for each set.

In order to check the effect of high frequencies on obtained $Q_\beta(f)$ relation the entire data is passed through high cut filter having high cut range of 21, 23, 25 and 30 Hz, respectively. Fig. 3.4 and 3.5 show that almost same site amplification and $Q_\beta(f)$ relation has been obtained in four different cases for three different data set at Dharchula station and minimum error is obtained for high cut corner of 25 Hz frequency. Therefore the input records are filtered at high cut corner of 25 Hz frequency. Almost similar results have been obtained for all three sets at similar cutoff frequency which indicate stability of inversion algorithm.

Table 3.1: Information of events used in the present numerical experiment.

Data Set	Date	Origin time (h:m:s)	Epicenter	Depth (km)	Moment magnitude M_w
Data set I	05/05/06	08:00:28.72	29º38.65',80º 42.16'	30	3.9
	27/10/06	07:55:01.39	29º57.46',80º 15.23'	13	3.8
	05/05/06	08:49:40.48	29º41.43',80º 45.00'	25	3.7
	07/05/06	06:46:13.72	29º57.51',80º 48.80'	35	3.8
	01/04/06	19:42:52.10	30º12.73',80º 24.13'	11	3.9
	27/10/06	08:01:32.23	29º52.35',80º 17.70'	16	3.3
Data set II	12/01/10	09:35:21.62	29º51.73',80º 21.30'	05	3.4
	04/09/08	12:53:10.14	30º8.38',80º 15.28'	15	4.6
	07/02/10	07:16:41.68	29º52.14',80º 21.48'	03	3.5
	06/07/10	19:11:54.09	29º47.73',80º 27.61'	07	3.3
	19/07/10	00:08:41.44	29º52.41',80º 26.38'	11	3.4
	08/10/10	17:10:13.64	29º48.57',80º 35.62'	18	3.3
Data set III	12/04/07	04:59:54.49	29º48.72',80º 22.01'	15	3.1
	30/05/06	18:25:18.03	29º54.14',80º 26.95'	03	3.8
	26/01/10	06:51:13.30	29º51.82',80º 19.89'	03	3.9
	04/09/08	17:38:20.21	29º08.17',80º 20.09'	03	3.2
	08/12/09	07:05:16.70	30º22.39',80º 13.22'	13	4.5
	11/01/10	05:15:14.61	29º48.68',80º 25.06'	12	4.4

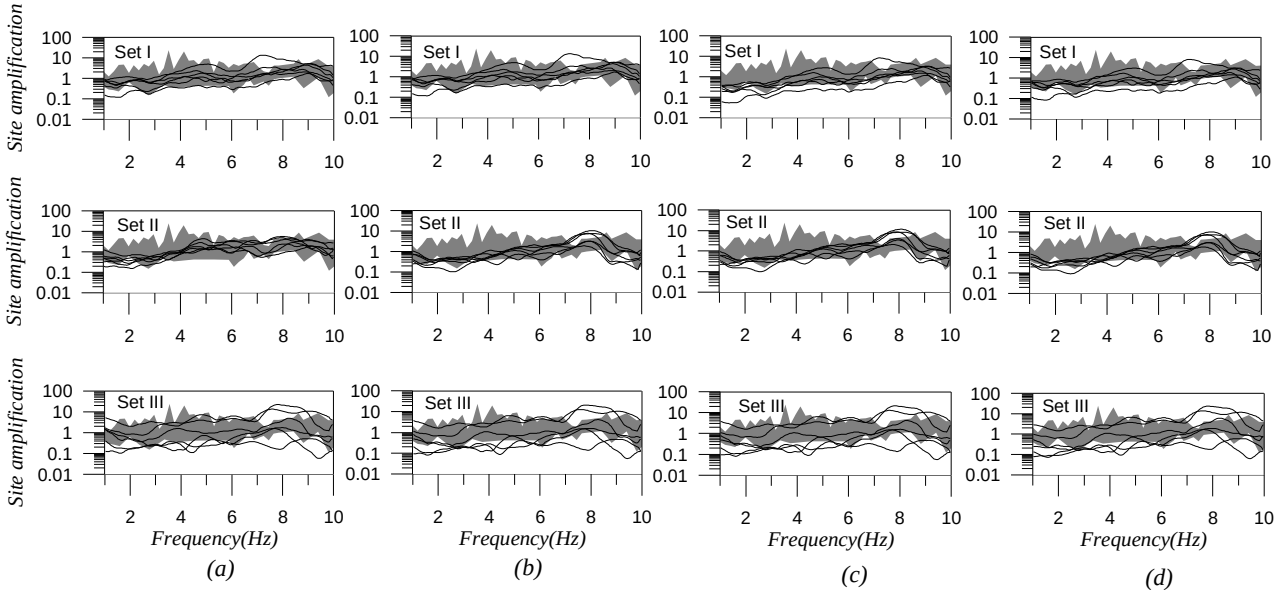

Figure 3.4: Site effects obtained from three different sets for NS component at Dharchula station at frequency range 1 to 21 Hz, 1 to 23 Hz, 1 to 25 Hz and 1 to 30 Hz are shown in (a), (b), (c) and (d), respectively. The shaded area denotes the region between μ +σ and μ –σ of the site amplification obtained using the technique given by Lermo and Chavez-Garcia (1993). Parameters 'μ' and 'σ' describe the mean and standard deviation, respectively.

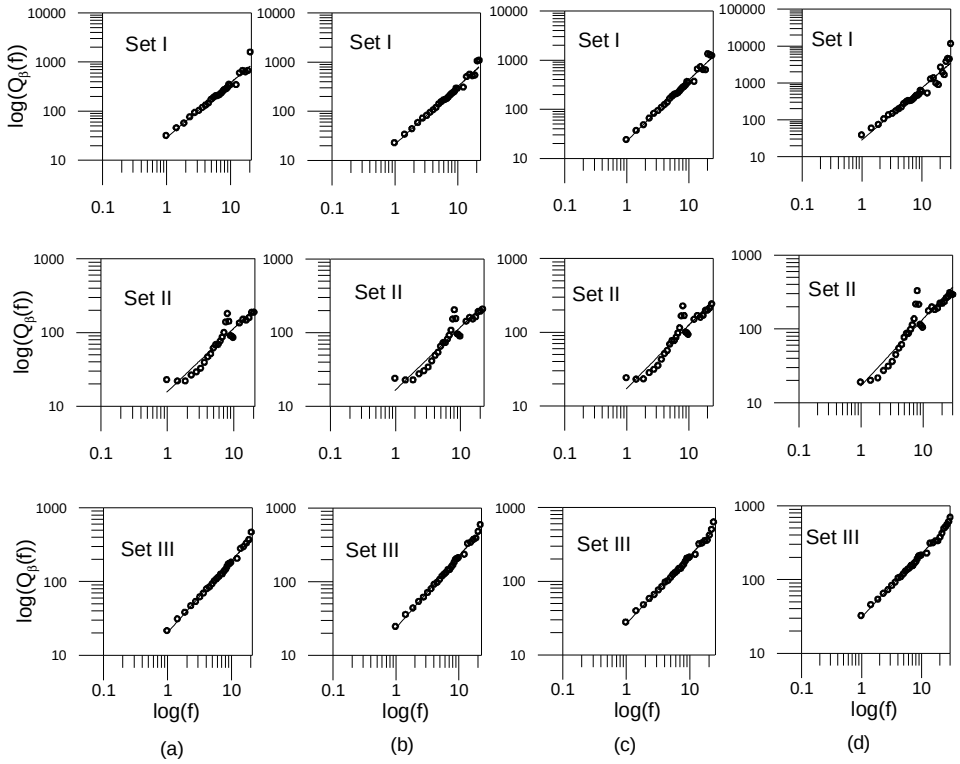

Figure 3.5: The $Q_\beta(f)$ relationship for three different sets for NS component at Dharchula station at frequency range 1 to 21 Hz, 1 to 23 Hz, 1 to 25 Hz and 1 to 30 Hz are shown in (a), (b), (c) and (d), respectively.

The input data, site amplification and $Q_\beta(f)$ obtained from each set at cutoff frequency of 25 Hz is shown in Fig. 3.6. It is found that almost similar $Q_\beta(f)$ and site amplification has been obtained at Dharchula station for this cutoff for all three sets. Root mean square error is also almost similar for all three set at Dharchula station.

In an attempt to check the obtained $Q_\beta(f)$ value by using other horizontal component of acceleration record from same data set, the EW component of acceleration record has been used as input to the inversion algorithm. Table 3.2 gives the value of rms error and obtain $Q_\beta(f)$ relation for both NS and EW horizontal component. It is found that almost similar $Q_\beta(f)$ value is obtained for both NS and EW component of acceleration record. The numerical experiment about dependency of result in cutoff frequency and data set indicate the stability of solution obtained in the inversion algorithm.

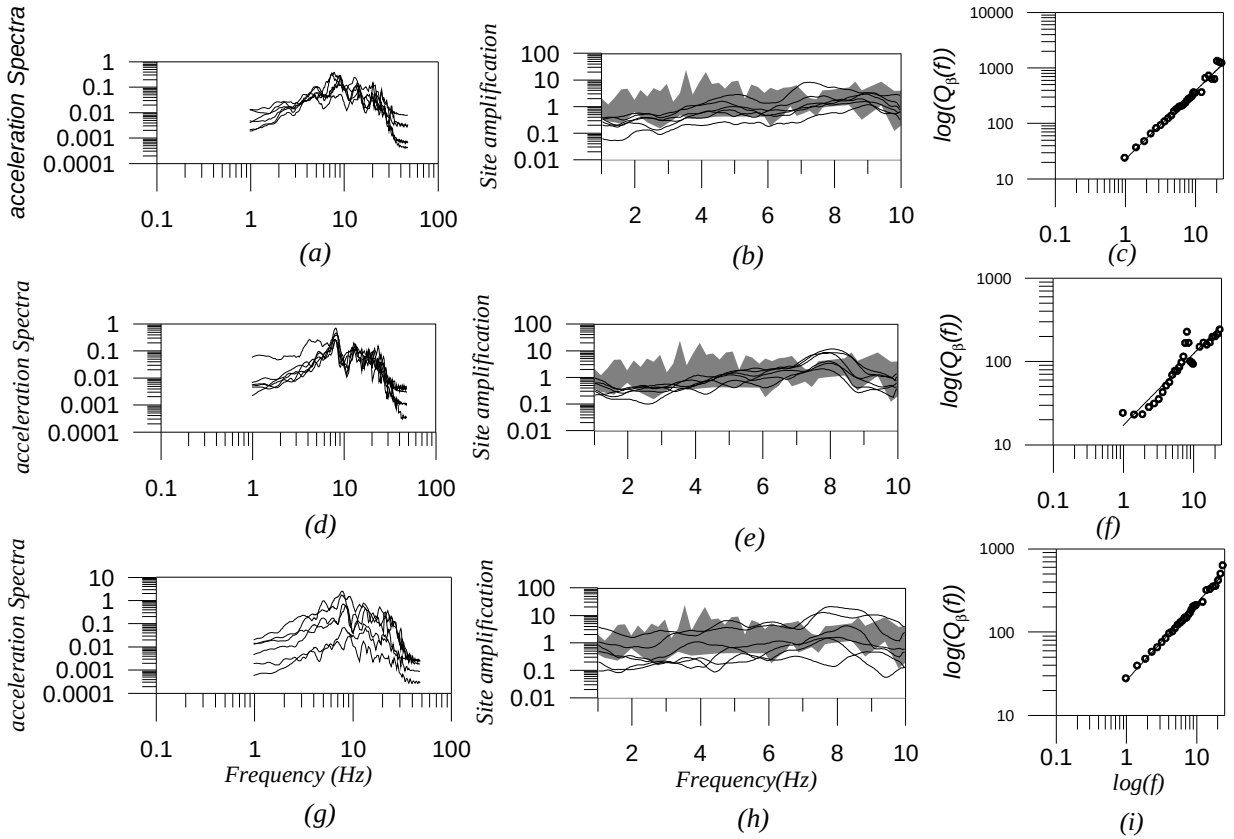

Figure 3.6: Input acceleration spectrum (a), (d) and (g) for complete frequency range for three different sets for NS component at Dharchula. Site effects (b), (e) and (h) obtained from different sets at frequency range of 1 to 10 Hz and (c), (f) and (i) are the $Q_\beta(f)$ relationship for the three different sets at Dharchula station at frequency range of 1 to 25 Hz. The shaded area denotes the region between $\mu+\sigma$ and $\mu-\sigma$ of the site amplification obtained using the technique given by Lermo and Chavez-Garcia (1993). Parameters 'μ' and 'σ' describe the mean and standard deviation, respectively.

Table 3.2: $Q_\beta(f)$ and RMS error at high cut frequency of 21, 23, 25 and 30 Hz obtained from inversion of data for both NS and EW component from three sets of event used at Dharchula station.

Details of data set		Obtained result from Inversion at 21 Hz			Obtained result from Inversion at 23 Hz		Obtained result from Inversion at 25 Hz		Obtained result from Inversion at 30 Hz	
	Date and Origin time	$Q_\beta(f)$		RMS error	$Q_\beta(f)$	RMS error	$Q_\beta(f)$	RMS error	$Q_\beta(f)$	RMS error
Set I	27/10/06 08:01:32.23	NS	$(24\pm9)f^{(1.2\pm0.11)}$	0.1008	$(14\pm7)f^{(1.4\pm0.12)}$	0.0368	$(18\pm9)f^{(1.4\pm0.17)}$	0.0206	$(28\pm12)f^{(1.4\pm0.12)}$	0.0217
	05/05/06 08:49:40.48									
	07/05/06 06:46:13.72	EW	$(16\pm7)f^{(1.3\pm0.13)}$	0.0291	$(18\pm2.4)f^{(1.3\pm0.18)}$	0.0174	$(15\pm10)f^{(1.4\pm0.28)}$	0.0102	$(23\pm9)f^{(1.4\pm0.11)}$	0.0116
	05/05/06 08:00:28.72									
	27/10/06 07:55:01.39									
	01/04/06 19:42:52.01									
Set II	19/07/10 00:08:41.44	NS	$(13\pm3.7)f^{(0.9\pm0.35)}$	0.0843	$(15\pm4)f^{(0.9\pm0.33)}$	0.0580	$(17\pm4.6)f^{(0.8\pm0.33)}$	0.0643	$(19\pm6.5)f^{(0.8\pm0.42)}$	0.0601
	08/10/10 17:10:13.64									
	06/07/10 19:11:54.09									
	12/01/10 09:35:21.62	EW	$(14\pm2)f^{(0.8\pm0.28)}$	0.0307	$(16.4\pm3)f^{(0.8\pm0.36)}$	0.0366	$(18\pm6)f^{(0.7\pm0.11)}$	0.0285	$(16\pm03)f^{(0.9\pm0.17)}$	0.0576
	07/02/10 07:16:41.68									
	04/09/08 12:53:10.14									
Set III	12/04/07 04:59:54.49	NS	$(12\pm3.7)f^{(1.3\pm0.14)}$	0.3269	$(16\pm2.8)f^{(1.2\pm0.07)}$	0.2659	$(16\pm2.5)f^{(1.2\pm0.14)}$	0.1271	$(21\pm3.7)f^{(1.0\pm0.10)}$	0.0741
	04/09/08 17:38:20.21									
	30/05/06 18:25:18.03									
	26/01/10 06:51:13.30	EW	$(15\pm5)f^{(1.2\pm0.25)}$	0.0973	$(16\pm2.5)f^{(1.2\pm0.17)}$	0.1961	$(13\pm6)f^{(1.5\pm0.17)}$	0.0831	$(20\pm4.2)f^{(1.5\pm0.12)}$	0.4853
	11/01/10 05:15:14.61									
	08/12/09 07:05:16.70									

In order to check the dependency of obtained $Q_\beta(f)$ relation on the depth of input earthquakes a numerical experiment has been made. Two data set named as data set I and IV have been used for this experiment. The NS component recorded at Dharchula station has been used as input data to the inversion algorithm for this numerical experiment. The parameters of earthquakes included in data set I and IV are given in Table 3.1 and 3.3, respectively. The obtained site amplification and $Q_\beta(f)$ relation from data set I and IV is shown in Fig. 3.7. The obtained $Q_\beta(f)$

relation using the data set I and IV is reported in Table 3.5. It is seen from Fig. 3.7 that data set I and IV gives different $Q_\beta(f)$ relation. The depth range of the events used in data set I and data set IV are different. The depth ranges for data set I and IV are 11-35 km and 3-7 km, respectively. These different depth range may be responsible for different $Q_\beta(f)$ relation obtained for the data set I and IV, respectively.

In order to check the dependency of input data having earthquake with similar hypocentral depth range on obtained $Q_\beta(f)$ relation data set named as data set V is prepared which has same depth range as data set I. The hypocentral parameters used in data set V are given in Table 3.4. The depth ranges for data set I and V are similar i.e. 11-35 km. The obtained site amplification and $Q_\beta(f)$ corresponding to input data of data set I and V is shown in Fig. 3.8. The obtained $Q_\beta(f)$ relation using the data set I, IV and V is reported in Table 3.5. It is observed from this experiment that data set having similar depth range gives almost similar $Q_\beta(f)$ relation as compare to the data set having different depth range. This experiment shows that input data with different depth range tends to give different $Q_\beta(f)$ relation while the input data having similar depth range gives almost similar $Q_\beta(f)$ relation.

Table 3.3: The hypocentral parameters of events used for Data set IV.

Data set IV			
Date	**Origin time**	**Epicenter**	**Depth(km)**
30/05/06	18:25:18.03	29º54.14',80º 26.95'	3
26/01/10	06:51:13.30	29º51.82',80º 19.89'	3
04/09/08	17:38:20.21	29º08.17',80º 20.09'	3
07/02/10	07:16:41.68	29º52.14',80º 21.48'	3
06/07/10	19:11:54.09	29º47.73',80º 27.61'	7
12/01/10	09:35:21.62	29º51.73',80º 21.30'	5

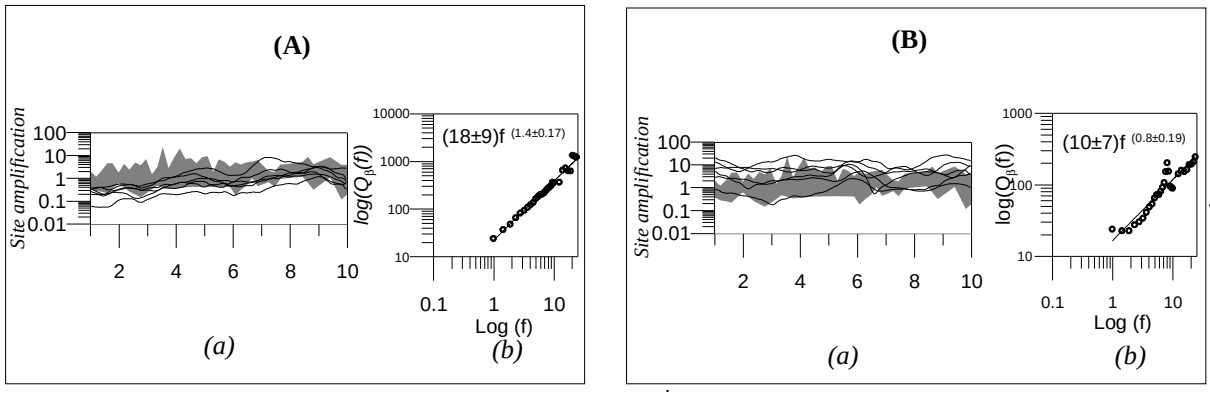

Figure 3.7: (a) Site effects and (b) $Q_\beta(f)$ relationship obtained using the (A) Data set I and (B) Data set IV, respectively. The shaded area denotes the region between $\mu+\sigma$ and $\mu-\sigma$ of the site amplification obtained using the technique given by Lermo and Chavez-Garcia (1993). Parameters 'μ' and 'σ' describe the mean and standard deviation, respectively.

Table 3.4: The hypocentral parameters of events used for Data set V.

Data set V			
Date	**Origin time**	**Epicenter**	**Depth(km)**
19/07/10	00:08:41.44	29º52.41',80º26.38'	11
12/04/07	04:59:54.49	29º48.72',80º22.01'	15
08/12/09	07:05:16.70	30º22.39',80º13.22'	13
19/08/08	10:54:32.17	29º45.16',79º42.27'	35
01/08/11	10:14:23.52	29º58.34',79º58.70'	25
01/10/11	04:26:53.38	29º53.16',80º27.84'	25

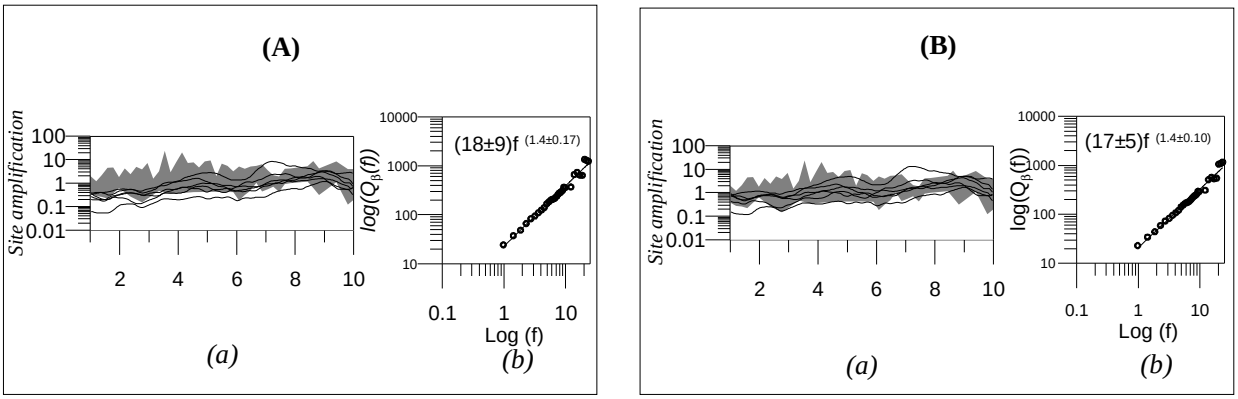

Figure 3.8: (a) Site effects and (b) $Q_\beta(f)$ relationship obtained using the (A) Data set I and (B) Data set V, respectively. The shaded area denotes the region between $\mu+\sigma$ and $\mu-\sigma$ of the site amplification obtained using the technique given by Lermo and Chavez-Garcia (1993). Parameters 'μ' and 'σ' describe the mean and standard deviation, respectively.

Table 3.5: $Q_\beta(f)$ and RMS error obtained from inversion of data for NS component using Data set I, IV and V at Dharchula station.

Data Set	**Obtained result from Inversion**	
	$Q_\beta(f)$	**RMS error**
Set I	$(18\pm9)f^{(1.4\pm0.17)}$	0.0206
Set IV	$(10\pm7)f^{(0.8\pm0.19)}$	0.9180
Set V	$(17\pm5)f^{(1.4\pm0.10)}$	0.0312

In an attempt to check the dependency of obtained solution on random selection of input data, bootstrap method has been implemented in the present work. In this numerical experiment, data set VI has been used. The NS component recorded at Dharchula station has been used for this numerical experiment. The random selection of the events have been made from the data set I and V to generate the data set VI. The hypocentral parameters used in data set VI are given in Table

3.6. The site amplification and $Q_\beta(f)$ relation obtained using the data set I, V and VI are shown in Fig. 3.9. It is observed from Fig. 3.9 that the $Q_\beta(f)$ relation obtained using the data set VI is comparable with the $Q_\beta(f)$ relation obtained using the data set I and V. The depth range of the events used in data set VI are same with that in the data set I and V. The obtained $Q_\beta(f)$ relation using the data set I, V and VI are given in Table 3.7 and it reveals the $Q_\beta(f)$ relation is almost similar for these three data sets.

Table 3.6: The hypocentral parameters of events used for Data set VI.

Data set VI			
Date	**Origin time**	**Epicenter**	**Depth(km)**
01/04/06	19:42:52.10	30º12.73',80º 24.13'	11
01/08/11	10:14:23.52	29º58.34',79º 58.70'	25
27/10/06	07:55:01.39	29º57.46',80º 15.23'	13
19/08/08	10:54:32.17	29º45.16',79º 42.27'	35
27/10/06	08:01:32.23	29º52.35',80º 17.70'	16
01/10/11	04:26:53.38	29º53.16',80º 27.84'	25

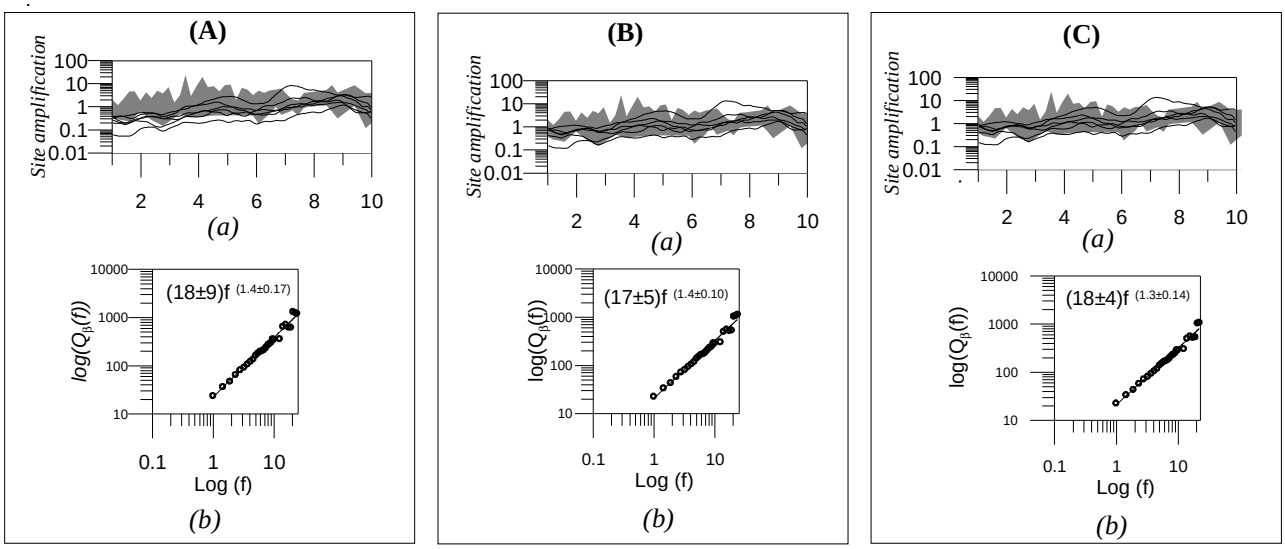

Figure 3.9: (a) Site effects and (b) $Q_\beta(f)$ relationship obtained using the (A) Data set I, (B) Data set V and (C) Data set VI, respectively. The shaded area denotes the region between $\mu+\sigma$ and $\mu-\sigma$ of the site amplification obtained using the technique given by Lermo and Chavez-Garcia (1993). Parameters 'μ' and 'σ' describe the mean and standard deviation, respectively.

Table 3.7: $Q_\beta(f)$ and RMS error obtained from inversion of data for NS component using Data set I, V and VI at Dharchula station.

Data Set	Obtained result from Inversion	
	$Q_\beta(f)$	RMS error
Set I	$(18\pm9)f^{(1.4\pm0.17)}$	0.0206
Set V	$(17\pm5)f^{(1.4\pm0.10)}$	0.0312
Set VI	$(18\pm4)f^{(1.3\pm0.14)}$	0.0217

3.4 Conclusion

This chapter discussed a two step inversion algorithm to obtain frequency dependent S-wave quality factor $Q_\beta(f)$ using the strong motion data. In the earlier study, the input to inversion algorithm like seismic moment was considered from the independent sources. This limitation is incorporated by using seismic moment computed from the acceleration record after properly correcting the record for site amplification and anelastic attenuation term in each iteration. Numerical tests have been performed to check the stability of solution and dependency of results on frequency contents of input data set and the depth range of input events.

Chapter – 4

Three Dimensional Attenuation Structure of Central Honshu region, Japan

4.1 Introduction

Central Honshu is the part of Honshu Island in Japan where three island arcs, the Northeast Japan Arc, the Southwest Japan Arc, and the Izu-Bonin Arc, meet one another. The geomorphological and geological structure of central Honshu region is extremely complicated due to this tectonic activity. Central Honshu is divided by the Itoigawa-Shizuoka Tectonic Line (ISTL), the Median Tectonic Line (MTL). A network of strong motion recorders name as KiK network is operated in this region which is maintained by National Research Institute for Earth Science and Disaster Prevention (NIED). Several local events are recorded frequently in this region by KiK net network. In the present chapter strong motion data acquired by this network have been used to determine the three dimensional attenuation structure of Central Honshu region, Japan using the inversion technique as discussed in Chapter 2.

4.2 Tectonic setting

Honshu is the largest island of Japan which was initiated by tectonic process of rifting and back-arc spreading of the Japan Sea, which is similar to the other arcs in Japan. Arc to arc juncture of East Japan and the West Japan arc systems represent the Central Honshu region (Takeuchi 2008). The main tectonic features of the study area are The Median Tectonic Line (MTL) and The Itoigawa-Shizuoka Tectonic Line (ISTL) and are shown in Fig. 4.1. The ISTL is a major tectonic structure that divides the Honshu island of Japan into NE and SW parts (Yabe, 1918; Kato, 1992). ISTL is basically a major geological boundary and a proxy for the plate boundary between the North American Plate and the Eurasian Plate (Nakamura, 1983; Kobayashi, 1983). The MTL is the Japan's longest fault system. It connects with ISTL and Fossa Magna and the extension of MTL is disappeared towards the northeastern side of ISTL. Fossa Magna zone is the tectonic depression zone lies of the east side of the ISTL. The ISTL is considered as the western boundary of Fossa Magna (Wilson and Kato, 1995). Towards the east side of ISTL the Kanto Plain exists, which is the largest plain in Japan. The Kanto Plain having the depressed area developed during the

Quaternary time. This depressed area is covered with thick Quaternary sediments having a large amount of volcanic ash. The deposited volcanic ash was weathered to become clay known as the Kanto loam. In the region on the west side of the ISTL, the oldest geological belt (Hida Belt), consisting of metamorphic rocks. The metamorphic rocks are gneiss, the parent rocks of which are pre-Cambrian rocks (source: http://www.glgarcs.net).

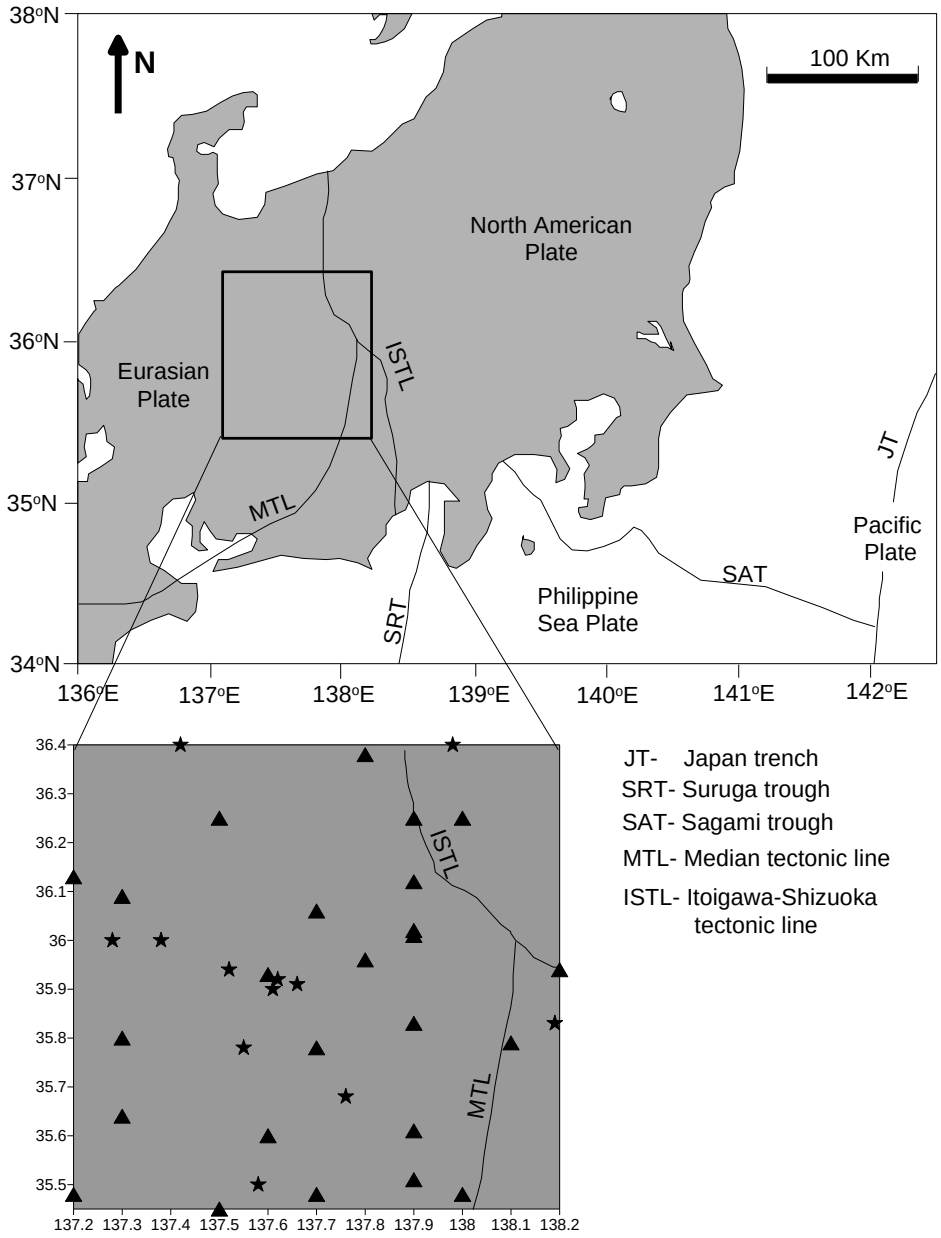

Figure 4.1: Tectonic setting of Central Honshu region, Japan and the block represents the study area. Solid triangles and stars denote the location of recording stations and earthquakes, respectively (Figure modified after Yoshimoto et al., 2004).

4.3 Data

National Research Institute for Earth Science and Disaster Prevention (NIED) has deployed the nation-wide seismic observation networks. KiK-net (KIBAN kyoshin network) is the sub-set of Hi-net (High-sensitivity seismograph network) which consists of 696 strong-motion observation stations. The locations of these sites are shown in Fig. 4.2. The strong motion sensors of KiK-net network are placed at surface as well as borehole. The depth of boreholes in KiK-net network lies between 100m to 200m. Each station has digital strong-motion seismograph with a wide frequency band and wide dynamic range having a maximum measurable acceleration of 2,000 gal. The sampling frequency of data is 200 Hz. The KiK-net stations have two three-component accelerometers at each recording sites. One accelerometer is placed at the surface while other at the hard rock in borehole.

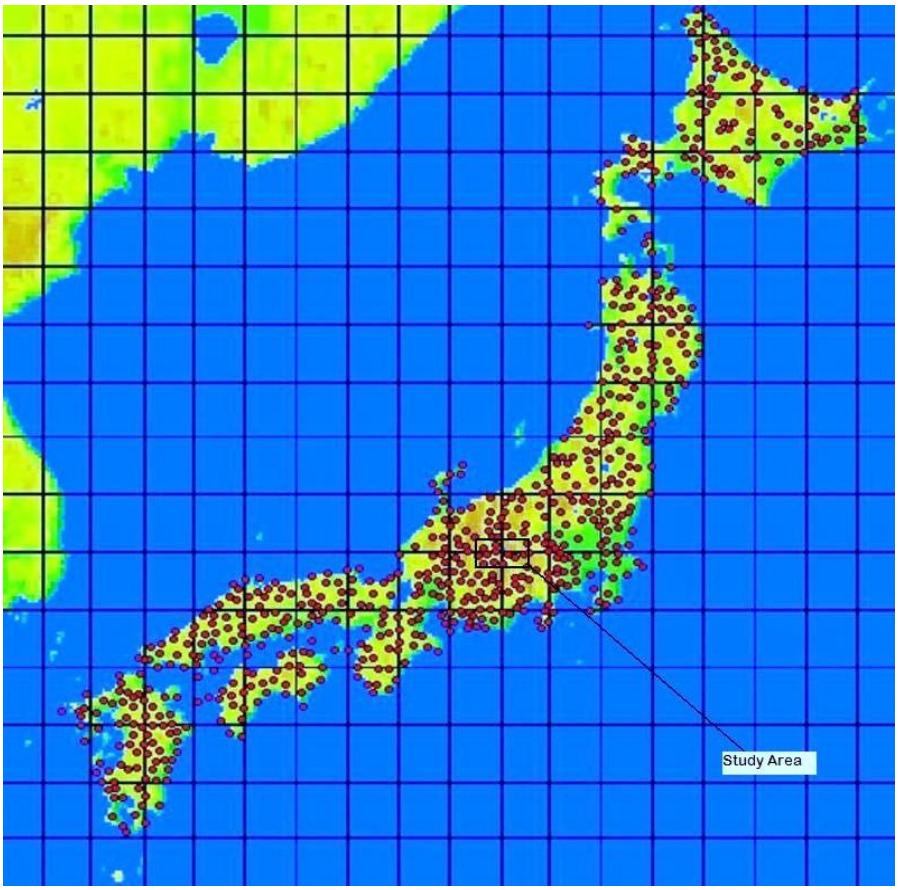

Figure 4.2: Map of Japan showing the locations of sensors deployed all over JAPAN. Study area is shown in the box. (Source: http://www.kik.bosai.go.jp-sitemap).

The acceleration records for present study have been acquired from official website of KiK-net. In order to use record free from site amplification, acceleration records from borehole sensor have been used in this present work. A total of 293 records from twenty one earthquakes are used for numerical experiment related to the developed algorithm discussed in Chapter 2. The final attenuation structure is based on 138 records of twelve earthquakes at 27 different stations in the Central Honshu region. Details of the 27 stations from which data has been used for the present study is reported in Table 4.1. The downloaded acceleration records need to be processed for obtaining attenuation structure. The records have been processed using the procedure suggested by Boore and Bommer (2005). Processing steps used in present work are (i) baseline correction, (ii) instrument scaling (iii) padding and (iv) frequency filtering. These steps are defined in following section.

Table 4.1: Detail of the recording stations (Source: http://www.kik.bosai.go.jp, last accessed 2011).

Station Code	Station Name	Latitude (Degree)	Longitude (Degree)	Depth (meter)
GIFH 04	FURUKAWA	36.2417	137.2013	100
GIFH 10	KAMIOKA	36.3749	137.3746	100
GIFH 11	YAOTSU	35.4833	137.2494	100
GIFH 14	KAMITAKARA	36.2462	137.5204	100
GIFH 15	TAKAYAMA	36.1306	137.2238	104
GIFH 16	ASAHI-KITA	36.0909	137.3468	100
GIFH 19	ASAHIMINAMI	36.0184	137.3936	100
GIFH 20	GERO-N	35.7959	137.2561	128
GIFH 24	HIGASHISHIRAKAWA	35.6369	137.3217	106
GIFH 28	NAKATSUGAWA	35.4539	137.4737	400
NGNH 03	ACHI2	35.4753	137.7376	165
NGNH 08	MISATO	36.25	137.86	250
NGNH 13	TAKAGI	35.51	137.88	124
NGNH 10	KISO	35.96	137.77	104
NGNH 15	TATSUNO	36.0056	137.9336	100
NGNH 16	CHINO	35.9433	138.1879	247
NGNH 18	KAIDA	35.9292	137.598	100
NGNH 20	AGEMATU	35.7839	137.7203	100
NGNH 21	INA	35.8283	137.9267	180
NGNH 22	HASE	35.7914	138.0855	100
NGNH 23	NAGISO	35.6024	137.6135	102
NGNH 24	MATSUKAWA	35.612	137.8827	107
NGNH 30	NAGAWA	36.0609	137.688	101
NGNH 31	SHIOJIRI	36.1153	137.9419	218
NGNH 32	MATSUMOTO	36.26	137.99	100
NGNH 35	HOTAKA	36.3793	137.8231	105
NGNH 54	IIDA	35.4456	138.0088	104

Baseline correction

The baseline correction step involves subtracting of straight line from the input of time series. The line can be linear least square fit to the time series or the mean value of time series. The mean value is determined from the mean of suitable portion of accelerogram. Basically the portion of record prior to P wave is taken for calculating mean and in case of absence of pre event record, entire record can be used. In the high frequency strong ground motion it is very difficult to see the effect of baseline correction in acceleration record and is evident on the velocity record obtained from the integration of acceleration record.

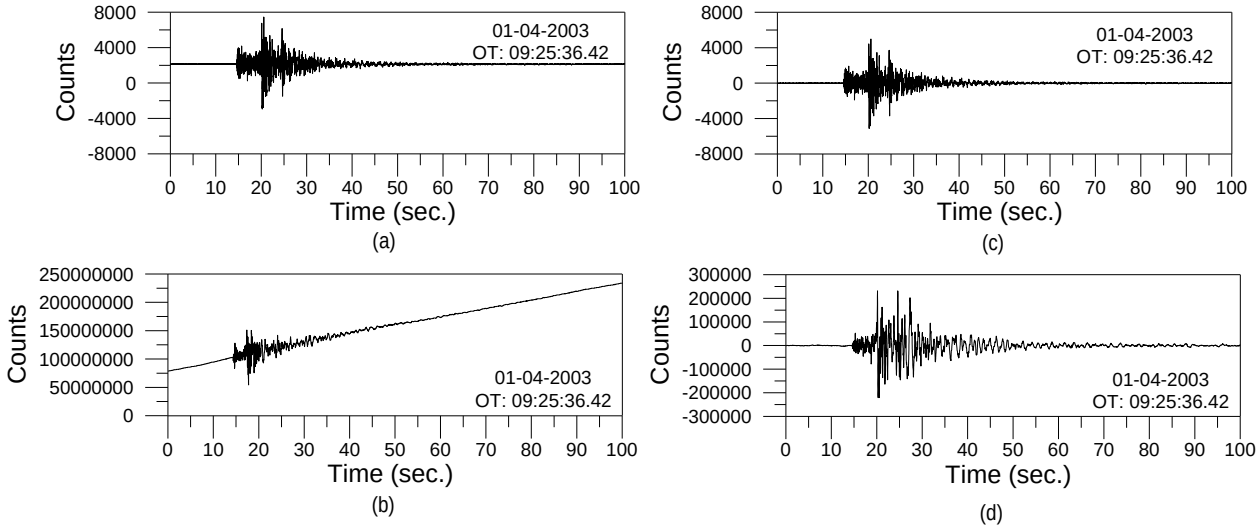

Figure 4.3: (a) Digitized acceleration record without baseline correction, (b) velocity record obtained from the integration of acceleration record (c) Digitized acceleration record with baseline correction, (d) velocity record obtained from the integration of acceleration record from NGNH10 station.

Instrument scaling

This is an important correction, which converts counts or volt recorded by instruments into actual ground motion. Different instruments have different scaling factor and based on the type of sensor used in recording, different value of scaling factor is used for data recorded by different sensors. Without instrument scaling correction recorded data does not have any physical meaning.

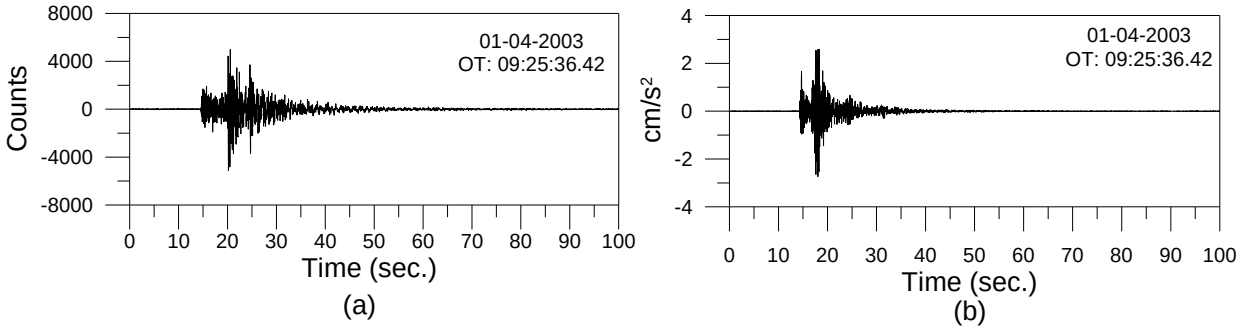

Figure 4.4: Processed (Baseline corrected) NS component at NGNH10 station (a) before (b) after instrument scaling correction.

Padding

The padding-processing step extends the time series in both directions by adding zeros to the leading and trailing ends of the record. This step is used before application of low cut frequency filtering. Zero pads are added symmetrically to the both ends of the records in order to accommodate the filter transient. The length of zero pad 't_{pad}' at each end is calculated using following empirically determined formula:

$$T_{pad} = 1.5 * nroll/f_c \quad (4.1)$$

where, 'nroll' is the rolloff of the acausal low cut Butterworth filter and f_c is the low cut frequency of the filter. The effect of padding is visible in the integrated displacement record obtained from strong motion record. A long term away from zero at the end of the velocity or displacement time series indicates that there may be insufficient padding. The integrated displacement record shows without padding there is long term away from zero at the end of displacement record as shown in Fig. 4.5c and this is removed in the zero padded processed record shown in Fig 4.5f.

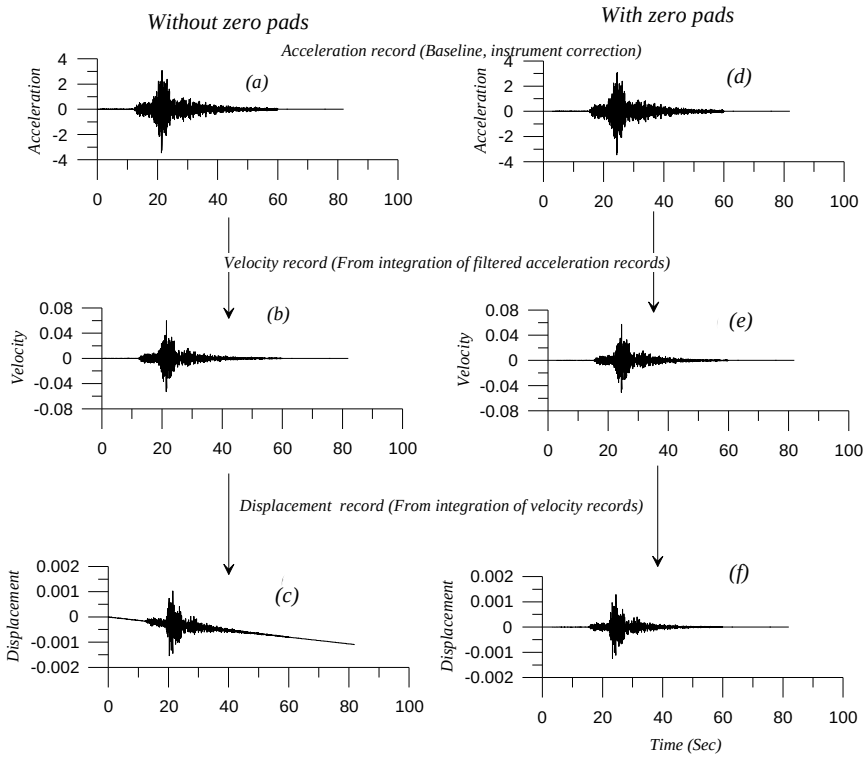

Figure 4.5: (a) Acceleration record without zero pad, (b) Velocity record obtained from integration of acceleration record, and (c) Displacement record obtained from the integration of velocity record. (d) Acceleration record with zero pads, (e) Velocity record obtained from integration of acceleration record, and (f) Displacement record obtained from the integration of velocity record.

Frequency filtering

For routine processing of strong motion data acausal filtering is preferred over causal filtering. One reason for this preference is that at periods much shorter than the corner frequency the waveforms and hence the response spectra is less sensitive to the low cut frequency corner (Boore and Akkar, 2003). The distinguish feature of acausal filter are that they do not produce any phase distortions in the signal, whereas the causal filter do result in phase shifts in the record (Boore and Bommer, 2005). Acausal filters needs to start to act prior to the beginning of the record, which can be accomplished by adding lines of data points of zero amplitude, known as pads, before the start of the record and after the end of record. The length of pads depends on the filter corner frequency and filter order (Boore and Bommer, 2005). The most important parameter in the filtering technique is the choice of low frequency cutoff. This choice is depends on (i) frequency characteristics of the earthquake source and (ii) visual inspection of integrated acceleration time series.

Filter corner can be estimated from the Fourier amplitude spectra of entire record after applying baseline corrections. At low frequencies noise are assumed to fall off roughly as 1/f towards higher frequencies, whereas signal is generally assumed to fall off between f^2 and f towards low frequencies. The low cut filter corner is usually estimated to be at the intersection of these two trends (Stephens and Boore, 2004). After baseline and instrument corrections a filter is applied to remove high frequency noise. In the usual processing of digital records a Butterworth filter with a corner frequency near 80% of final sampling rate (Shakal et al., 2004) is used. Low frequency selection of Butterworth filter remains the most difficult part of strong motion processing. The effect of earthquake magnitude is to raise the response spectrum at low frequencies and subsidize the noise spectrum in the usual strong motion processing band. In order to select the low frequency corner of the Butterworth filter, the data of noise from pre event memory of digital record has been used. The frequency at which the ratio of response spectra of record to noise is equal to 3 (Boore and Bommer, 2005) is assumed as low frequency of the Butterworth filter. Figure 4.6 shows method of selection of low cut filter corner of the bandpass filter used in processing of the records.

Total twelve earthquakes recorded at 27 different stations in Central Honshu region are used in the present work. Thus a total of 138 accelerograms have been used in this work. The hypocentral parameters of earthquakes used in present work are calculated by using HYPO71 program originally developed by Lee and Lahr (1972). The arrival time of primary and secondary phases from these events has been used for localization of events using HYPO71 software. Arrival time of P and S phase, geographical coordinates of recording stations and velocity model are the inputs of this software. The velocity model given by Honda et al. (2005) has been used as input velocity model in the determination of hypocentral parameters in the Central Honshu region. Same velocity model has been used as input in the inversion algorithm developed for determination of three dimensional attenuation structure of central Honshu region. Hypocentral parameter of these events and the obtained error in their localization is reported in Table 4.2. Locations of these earthquakes and recorded stations are shown in Fig. 4.1. In the present work strong motion data recorded by different sensors is processed using baseline correction, instrument scaling, padding and frequency filtering explained in earlier text. Processed records of some of the events used in the present work for determination three dimensional attenuation structure of Central Honshu region, Japan are shown in Fig. 4.7 to 4.18.

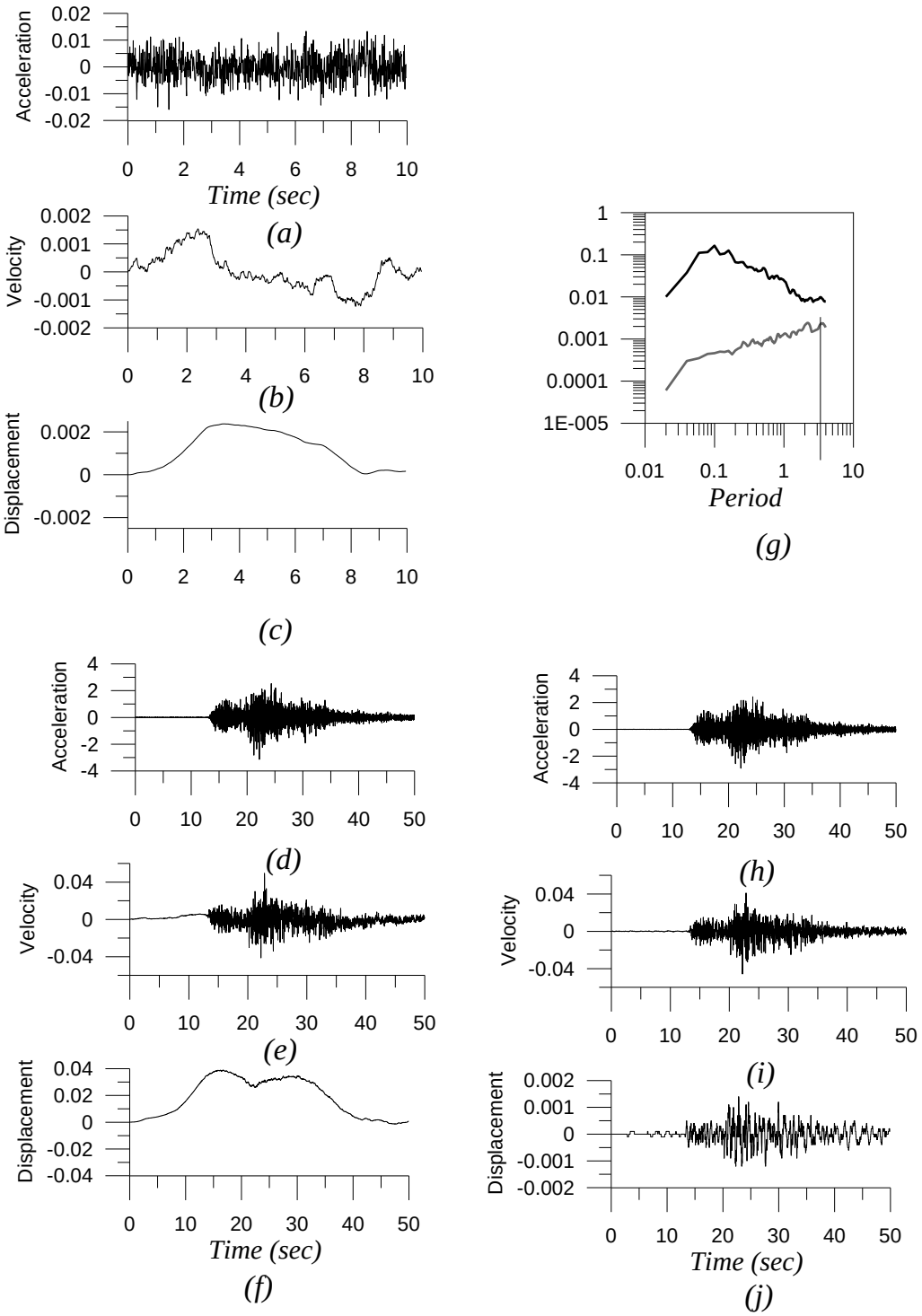

Figure 4.6: (a) Acceleration, (b) velocity and (c) displacement waveform of the digitized record of noise taken from pre-event memory of the record. (d) Acceleration, (e) velocity, and (f) displacement record of signal without filtering. (g) Pseudo velocity response spectra at 5% damping of noise and signal without filtering. (h) Acceleration, (i) velocity and (j) displacement record of signal after filtering.

Table 4.2: Hypocentral parameters of the events used in the present work. ERH and ERZ define the error of epicenter and focal depth, respectively.

Events	Origin time h:min:sec	Depth (km)	Epicenter (In Degree) Latitude	Longitude	ERH (km)	ERZ (km)
05/10/2003	00:29:42.52	15	35.99N	137.58E	3.8	4.7
01/04/2003	09:25:36.42	6	36.36N	137.30E	4.3	1.8
22/05/2003	07:09:34.25	15	35.71N	138.03E	4.2	4.6
04/06/2003	02:52:51.06	11	36.01N	137.58E	3.7	4.4
11/01/2004	16:57:59.57	9	36.40N	137.75E	2.4	3.3
14/02/2004	20:19:39.37	10	35.85N	137.25E	3.2	1.6
03/06/2004	19:04:36.87	8	35.98N	137.37E	3.2	4.1
30/06/2004	06:35:56.14	11	35.98N	137.20E	4.4	4.7
02/01/2005	01:30:58.66	5	36.04N	137.20E	6.2	4.1
07/01/2005	23:38:07.86	20	35.67N	137.20E	6.4	1.6
24/03/2005	20:08:00.86	10	36.20N	137.37E	3.3	3.2
05/05/2005	07:38:13.27	15	35.51N	137.31E	2.2	1.7

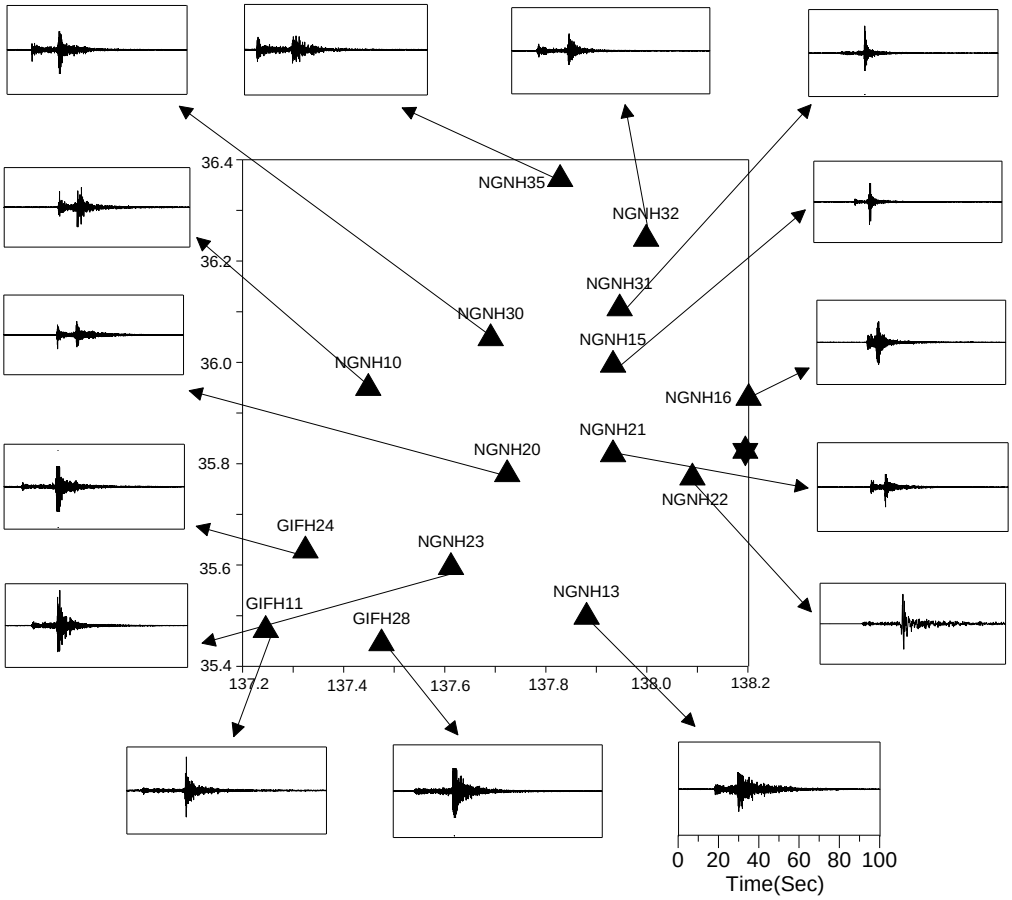

Figure 4.7: Normalize processed accelerograms of an event occurred on 05-05-2005 used for the present work recorded at different stations. Star and triangle denote the location of epicenter and recording station, respectively.

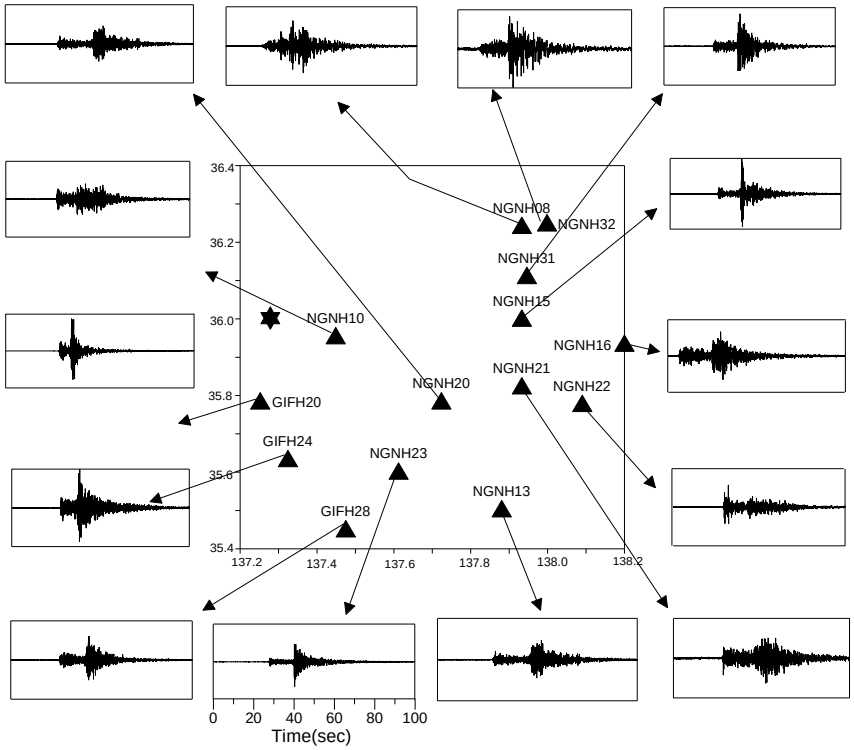

Figure 4.8: Normalize processed accelerograms of an event occurred on 05-10-2003 used for the present work recorded at different stations. Star and triangle denote the location of epicenter and recording station, respectively.

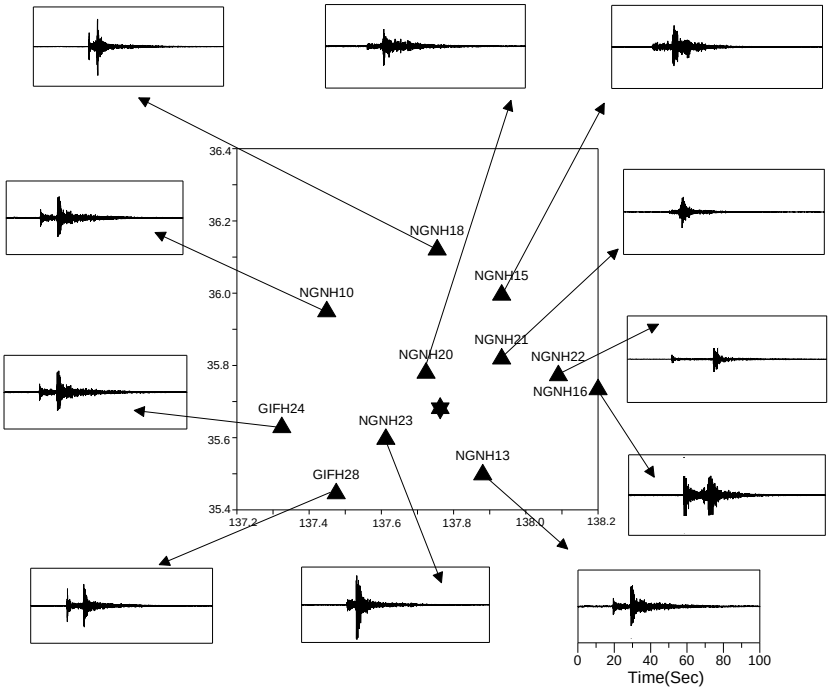

Figure 4.9: Normalize processed accelerograms of an event occurred on 22-05-2003 used for the present work recorded at different stations. Star and triangle denote the location of epicenter and recording station, respectively.

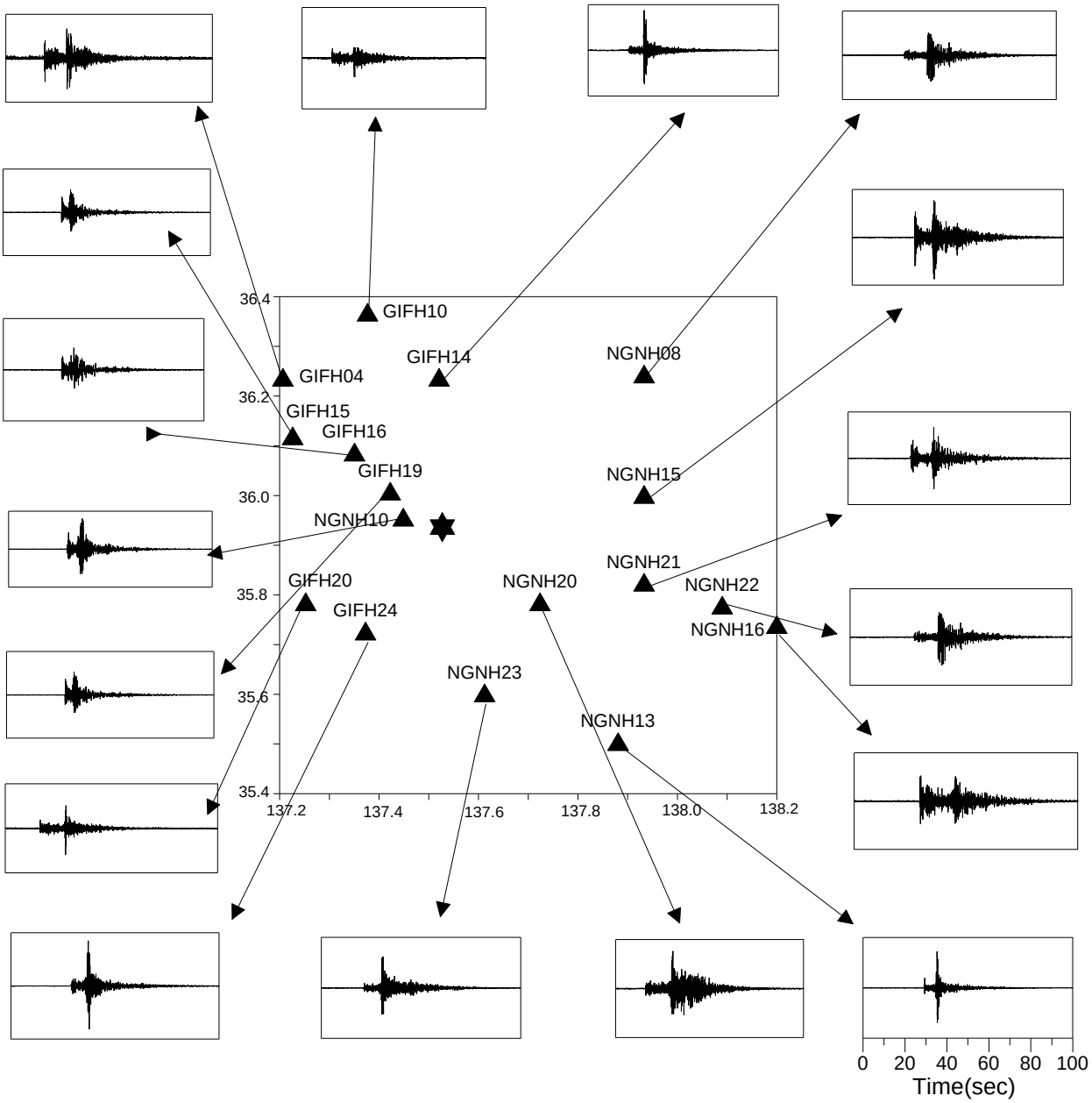

Figure 4.10: Normalize processed accelerograms of an event occurred on 01-04-2003 used for the present work recorded at different stations. Star and triangle denote the location of epicenter and recording station, respectively.

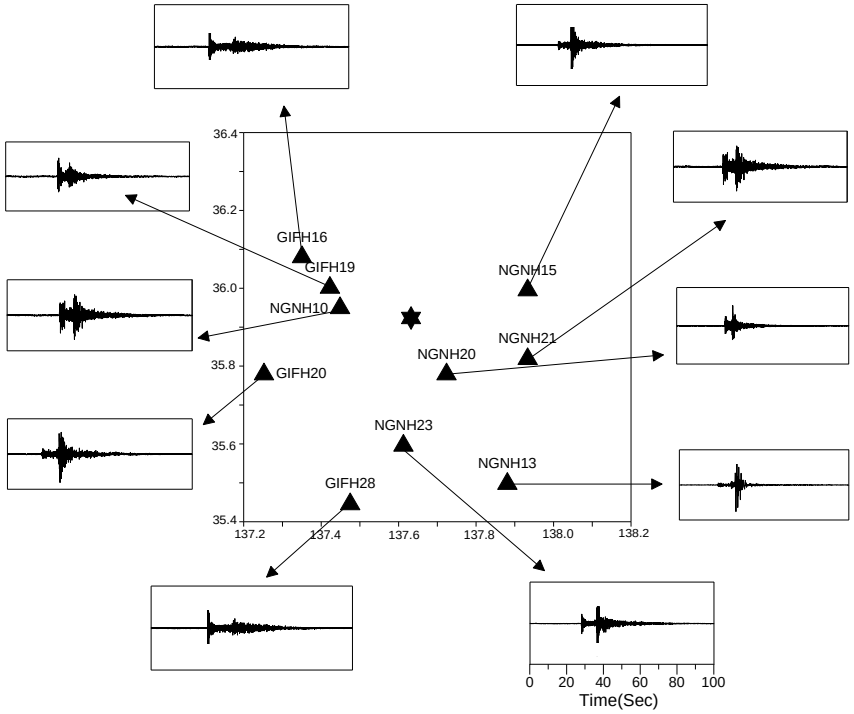

Figure 4.11: Normalize processed accelerograms of an event occurred on 04-06-2003 used for the present work recorded at different stations. Star and triangle denote the location of epicenter and recording station, respectively.

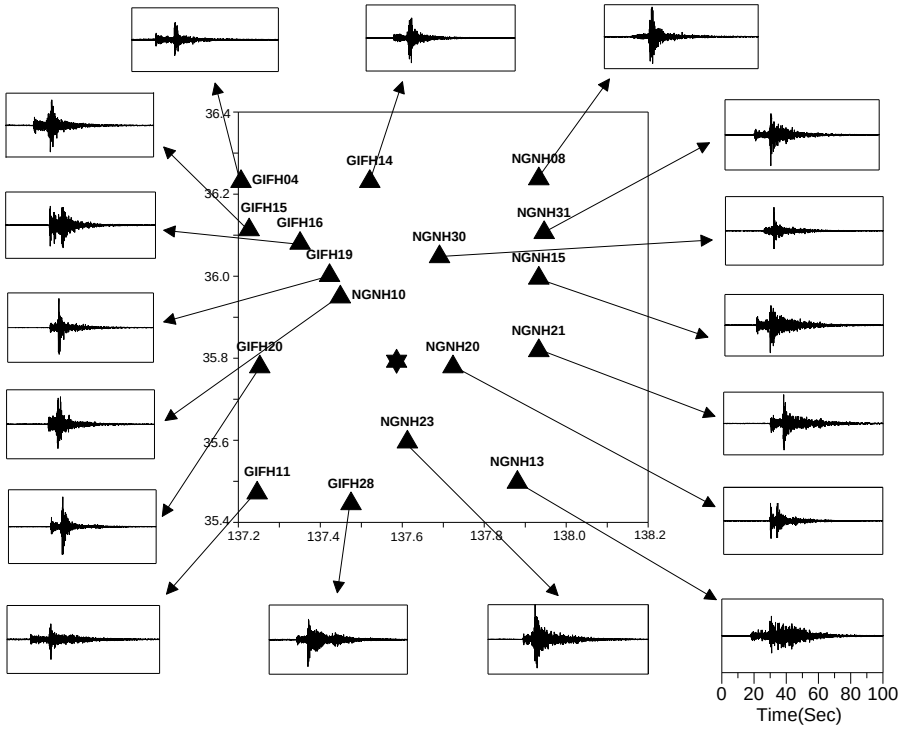

Figure 4.12: Normalize processed accelerograms of an event occurred on 02-01-2005 used for the present work recorded at different stations. Star and triangle denote the location of epicenter and recording station, respectively.

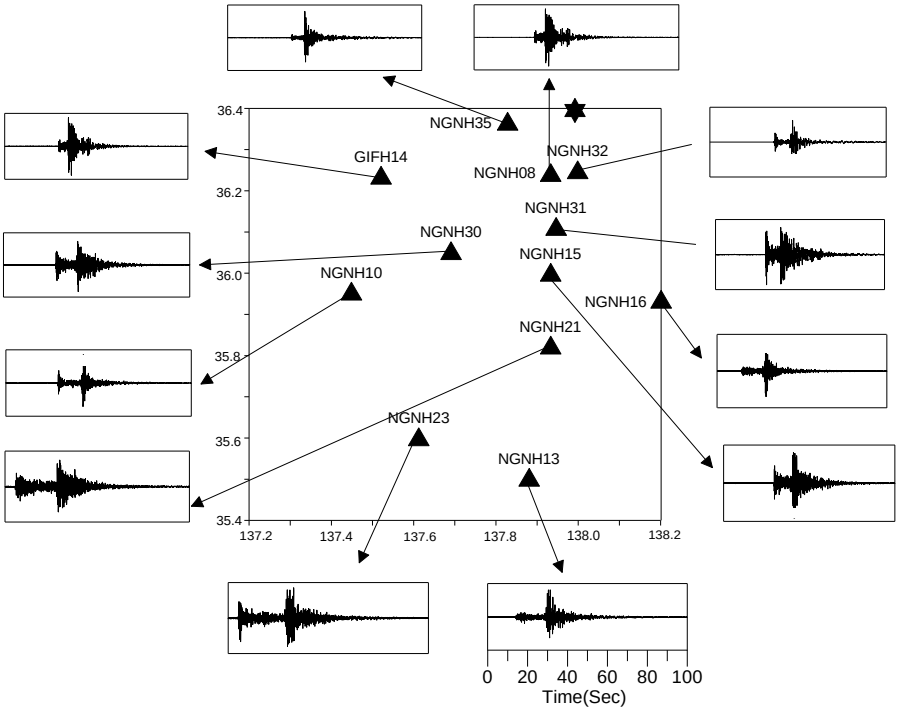

Figure 4.13: Normalize processed accelerograms of an event occurred on 11-01-2004 used for the present work recorded at different stations. Star and triangle denote the location of epicenter and recording station, respectively.

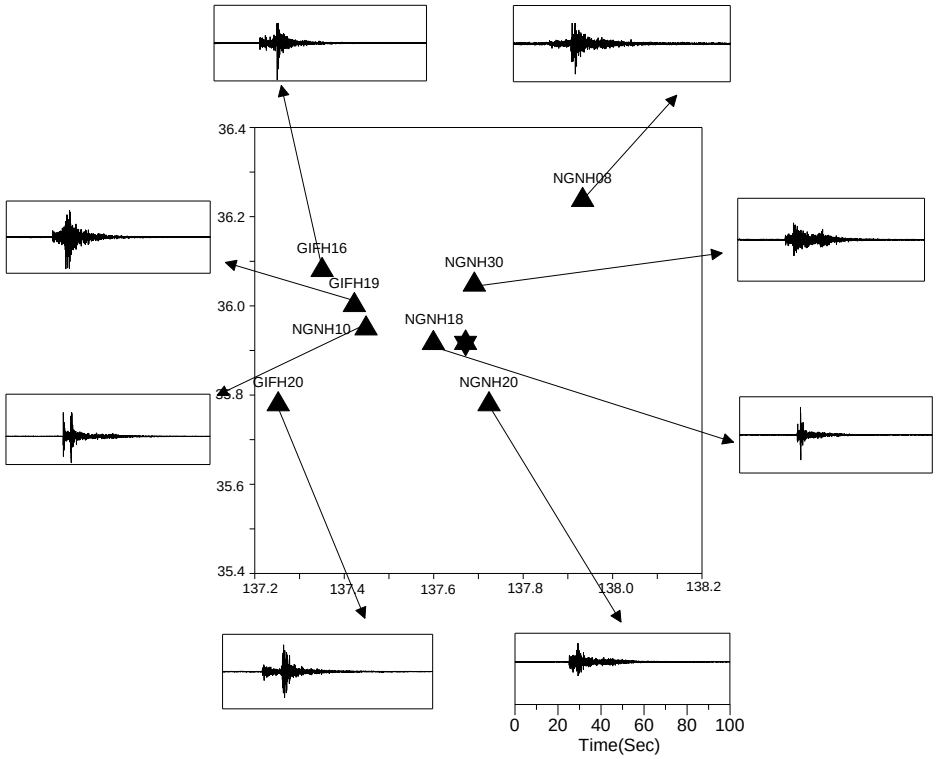

Figure 4.14: Normalize processed accelerograms of an event occurred on 14-02-2004 used for the present work recorded at different stations. Star and triangle denote the location of epicenter and recording station, respectively.

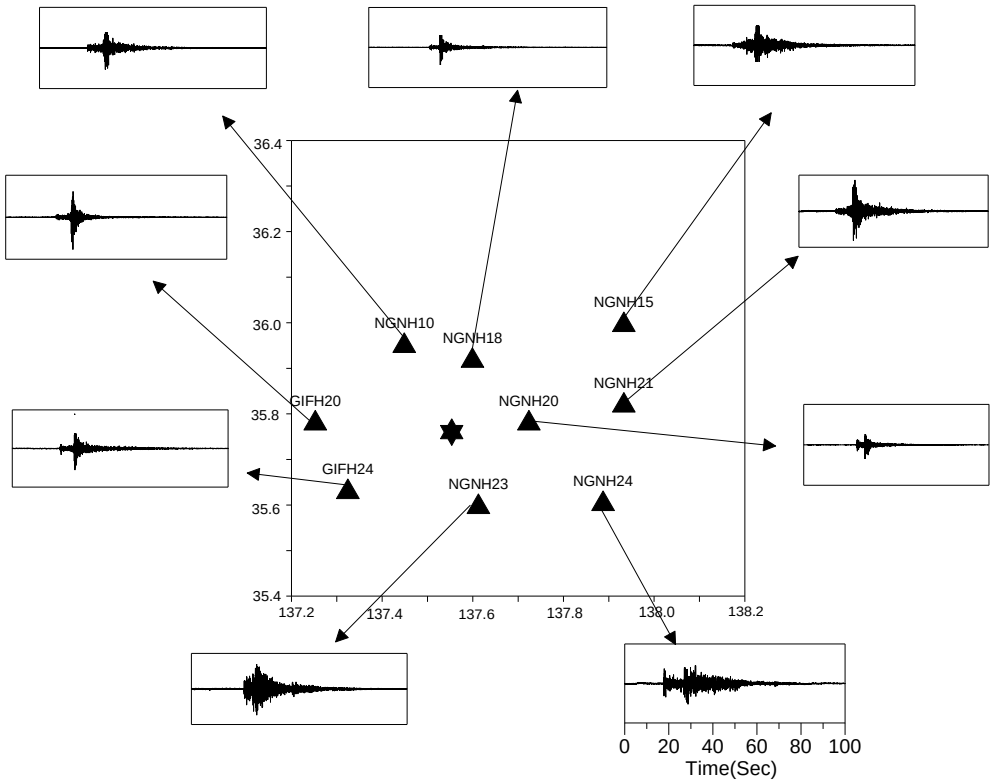

Figure 4.15: Normalize processed accelerograms of an event occurred on 03-06-2004 used for the present work recorded at different stations. Star and triangle denote the location of epicenter and recording station, respectively.

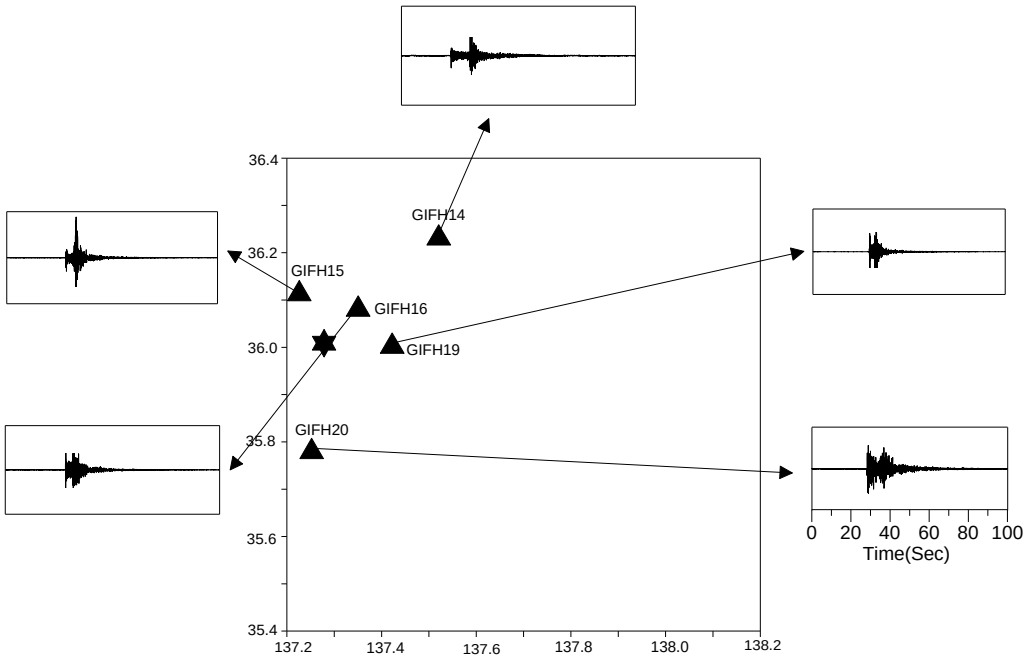

Figure 4.16: Normalize processed accelerograms of an event occurred on 30-06-2004 used for the present work recorded at different stations. Star and triangle denote the location of epicenter and recording station, respectively.

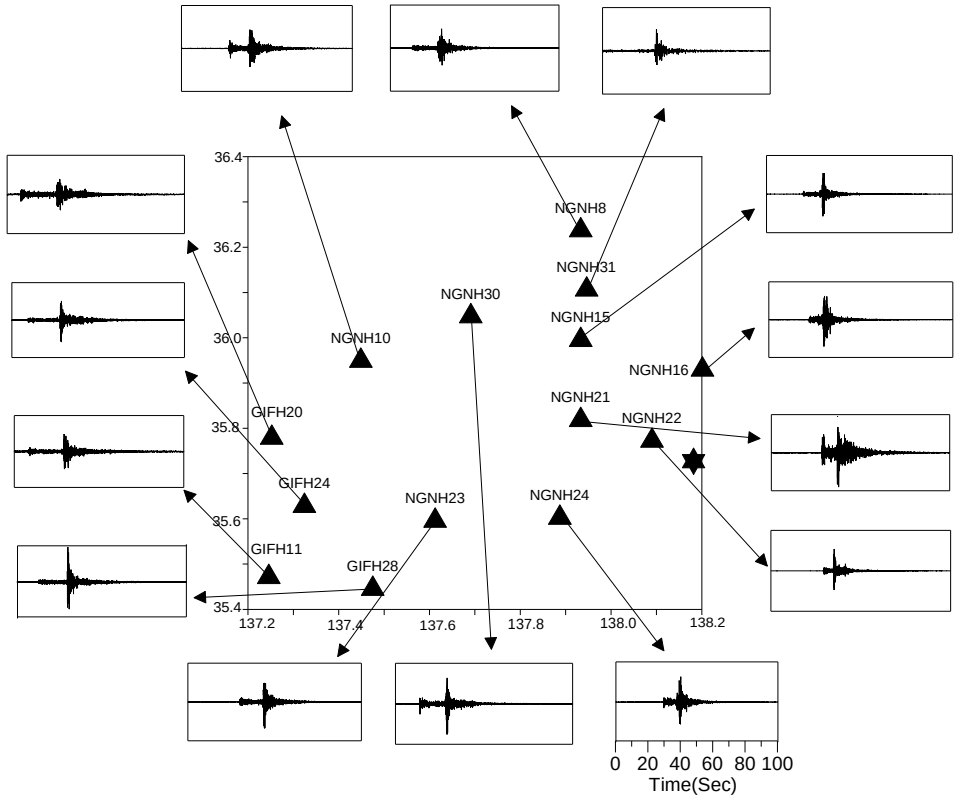

Figure 4.17: Normalize processed accelerograms of an event occurred on 07-01-2005 used for the present work recorded at different stations. Star and triangle denote the location of epicenter and recording station, respectively.

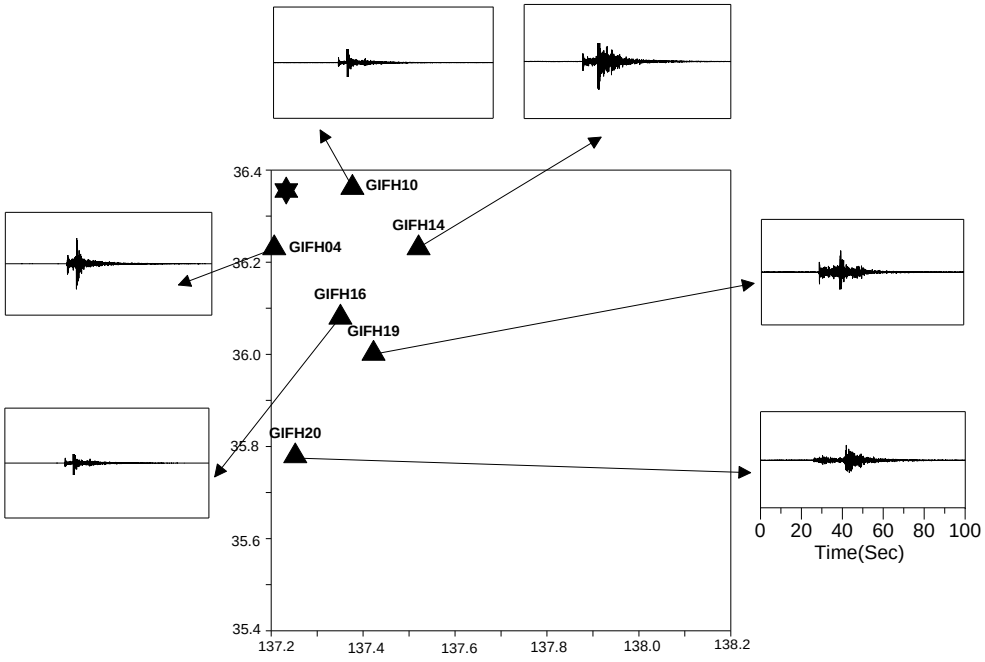

Figure 4.18: Normalize processed accelerograms of an event occurred on 24-03-2005 used for the present work recorded at different stations. Star and triangle denote the location of epicenter and recording station, respectively.

Entire study area shown in Fig. 4.1 is marked by a rectangular block of dimension 110 km × 110 km. This region is represented by three dimensional rectangular Cartesian coordinate system for its use in inversion algorithm discussed in Chapter 2. The origin of this system is at the extreme southern end of block. The X and Y axis follows eastward and northward direction, respectively. For the purpose of attenuation structure entire region is divided into 5 × 5 × 3 rectangular blocks along X, Y and Z axes, respectively as shown in Fig. 4.19. The ray path map from source to the observation point is shown in Fig. 4.20. Each corner of the surface blocks are assumed as the observation point. This gives 36 observation points. The algorithm developed in Chapter 2 requires spectral acceleration values of S-phase at each point. The S-phase from acceleration record is selected by visual inspection. The value of amplitude spectrum at selected frequency at different stations is used as input to prepare spectral acceleration contours. Value of spectra acceleration at various corners of grid calculated from spectral acceleration contour is used as an input to the present algorithm. Various step used to prepare the contour map of spectral acceleration from acceleration record is shown in Fig. 4.21. Spectral acceleration value at 36 observation points within grid is used as input value to the algorithm. Contour map of spectral acceleration obtained from strong motion data of some of the events used in this work is shown in Fig. 4.22 to 4.26.

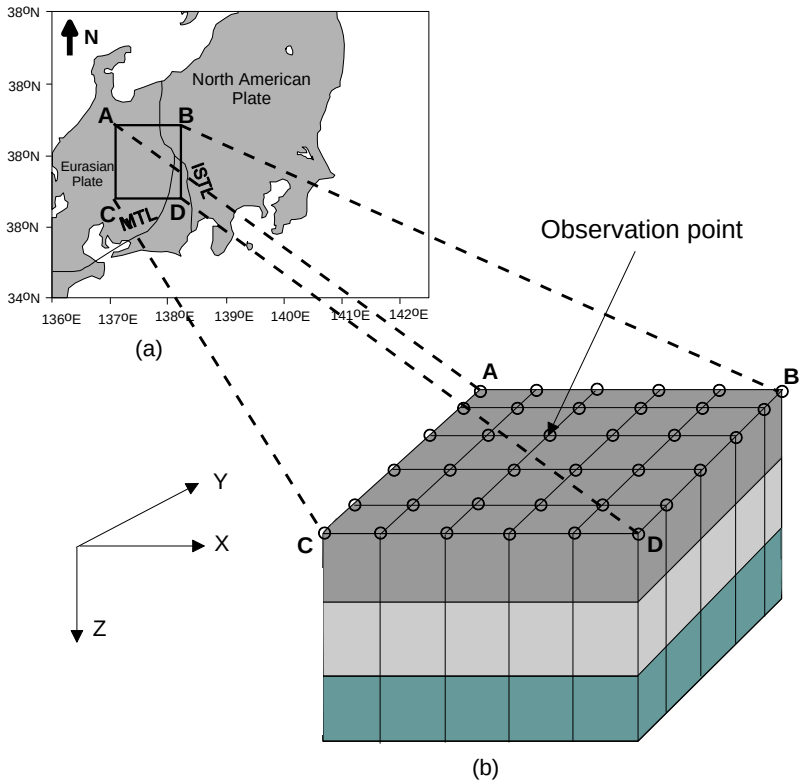

Figure 4.19: (a) Study region denotes by a rectangular box. (b) Entire Study region is divided into 5, 5 and 3 rectangular blocks along X, Y and Z axes, respectively. ISTL and MTL describe the Itoigawa-Shizuoka Tectonic Line and Median Tectonic Line, respectively.

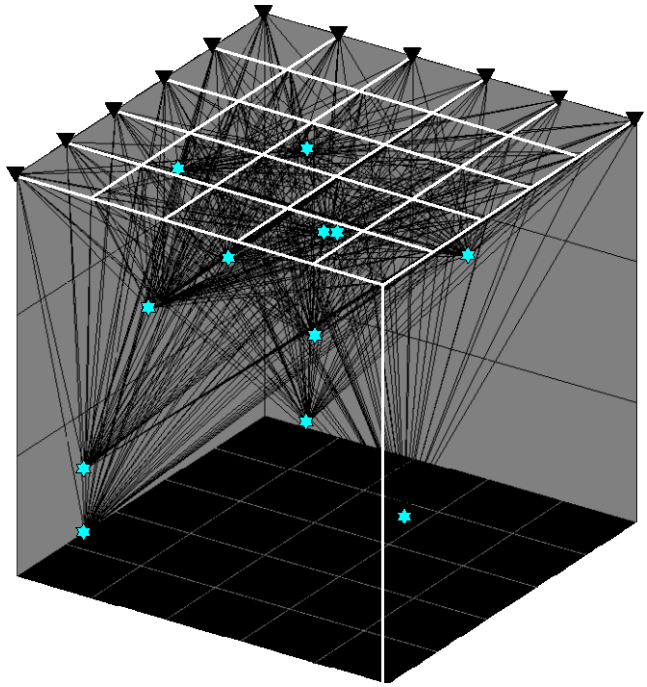

Figure 4.20: Projection of ray path of different events at observation points. Star and triangle denotes the location of epicenter and observation point, respectively.

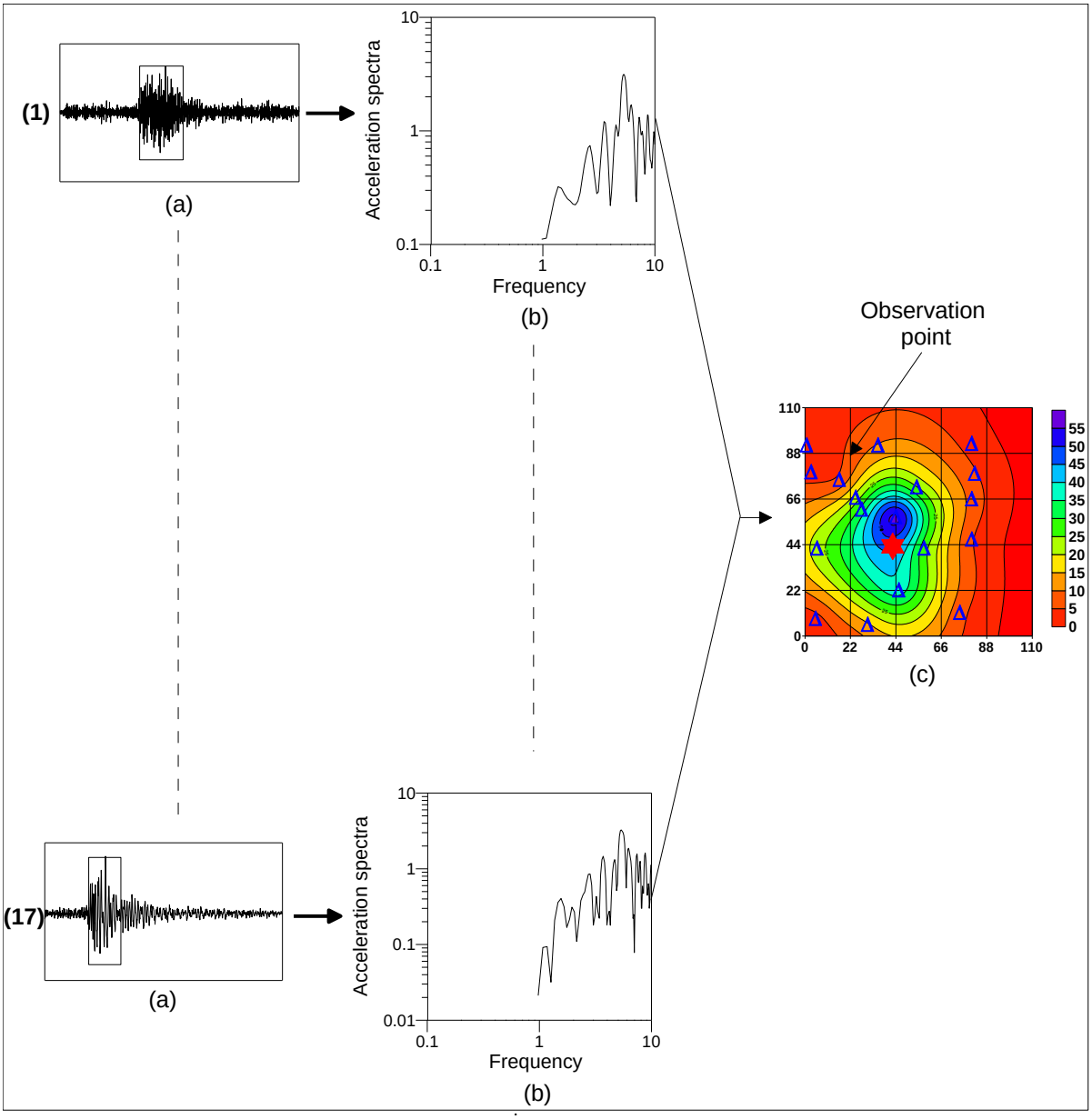

Figure 4.21: (a) The acceleration record of earthquake with S-phase identified by the rectangular block, (b) source acceleration spectrum computed from the S-phase and (c) contour map of acceleration spectra obtained using the acceleration spectra values at selected frequency. Triangles and stars denote the location of recording stations and events, respectively.

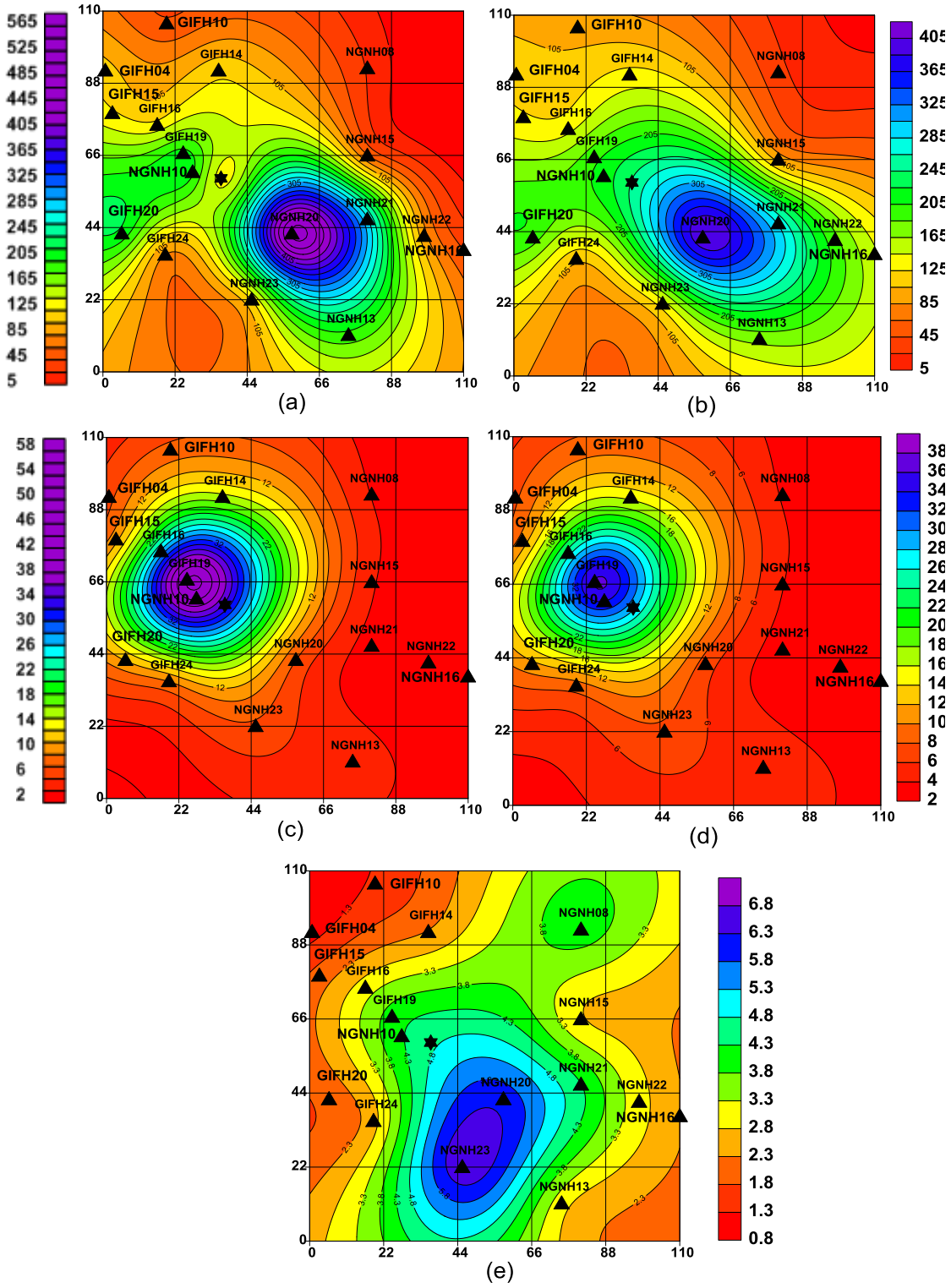

Figure 4.22: Contour map of spectral acceleration of event occurred on 01-04-2003 at (a) 1.5 Hz, (b) 2.5 Hz, (c) 5.0 Hz, (d) 7.0 Hz and (e) 10.0 Hz frequency, respectively. Triangles and stars denote the location of recording stations and events, respectively.

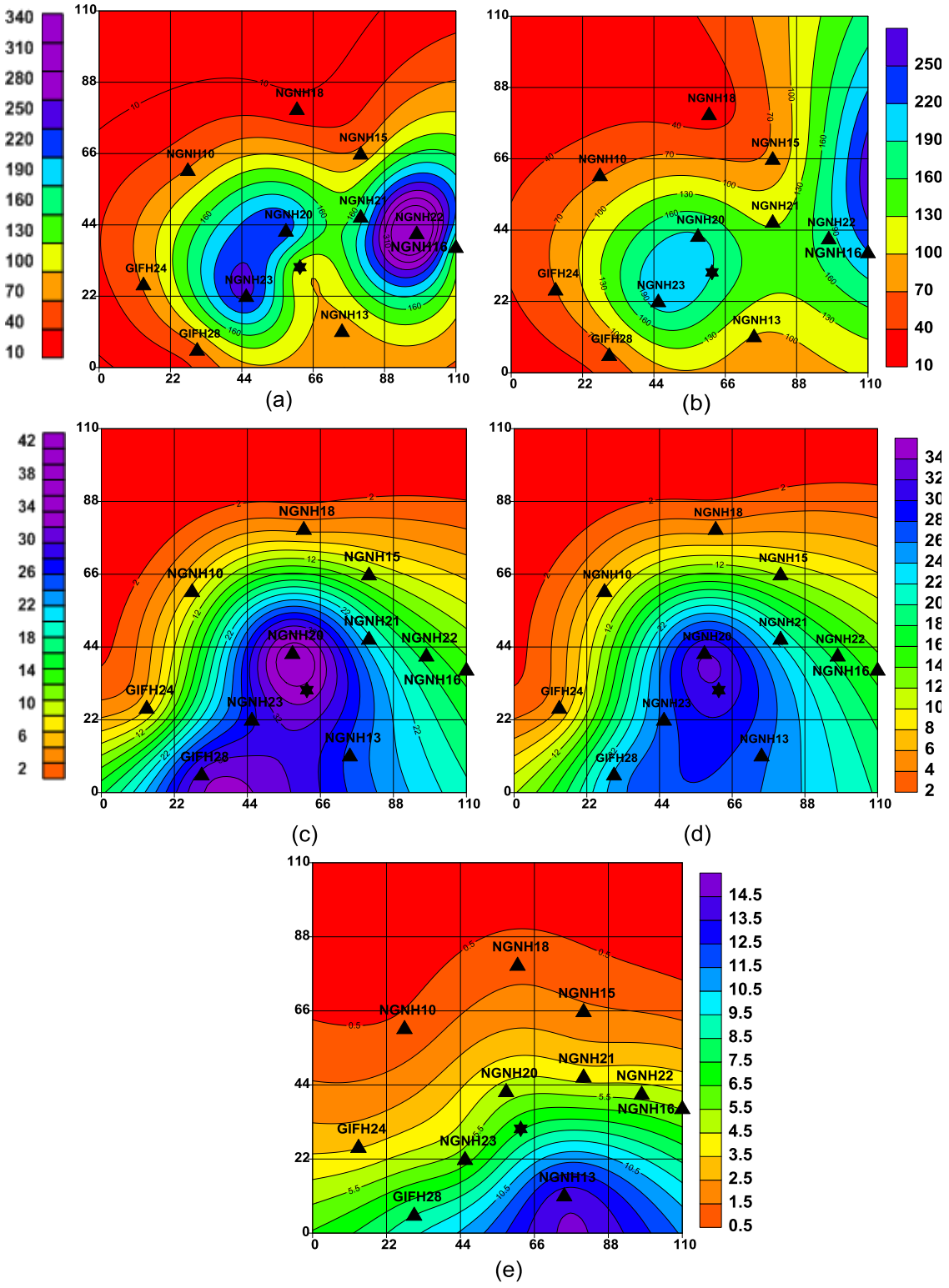

Figure 4.23: Contour map of spectral acceleration of event occurred on 22-05-2003 at (a) 1.5 Hz, (b) 2.5 Hz, (c) 5.0 Hz, (d) 7.0 Hz and (e) 10.0 Hz frequency, respectively. Triangles and stars denote the location of recording stations and events, respectively.

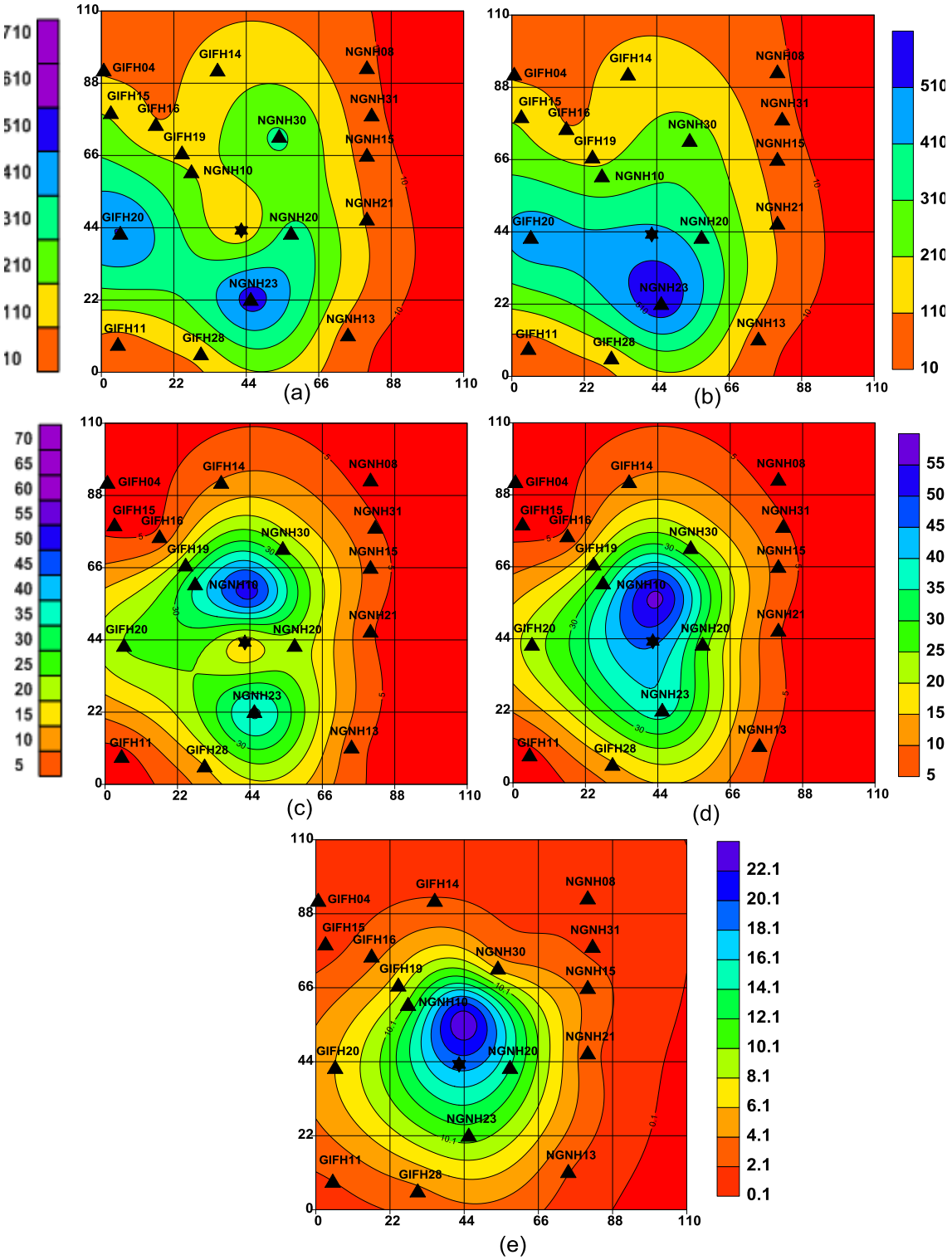

Figure 4.24: Contour map of spectral acceleration of event occurred on 02-01-2005 at (a) 1.5 Hz, (b) 2.5 Hz, (c) 5.0 Hz, (d) 7.0 Hz and (e) 10.0 Hz frequency, respectively. Triangles and stars denote the location of recording stations and events, respectively.

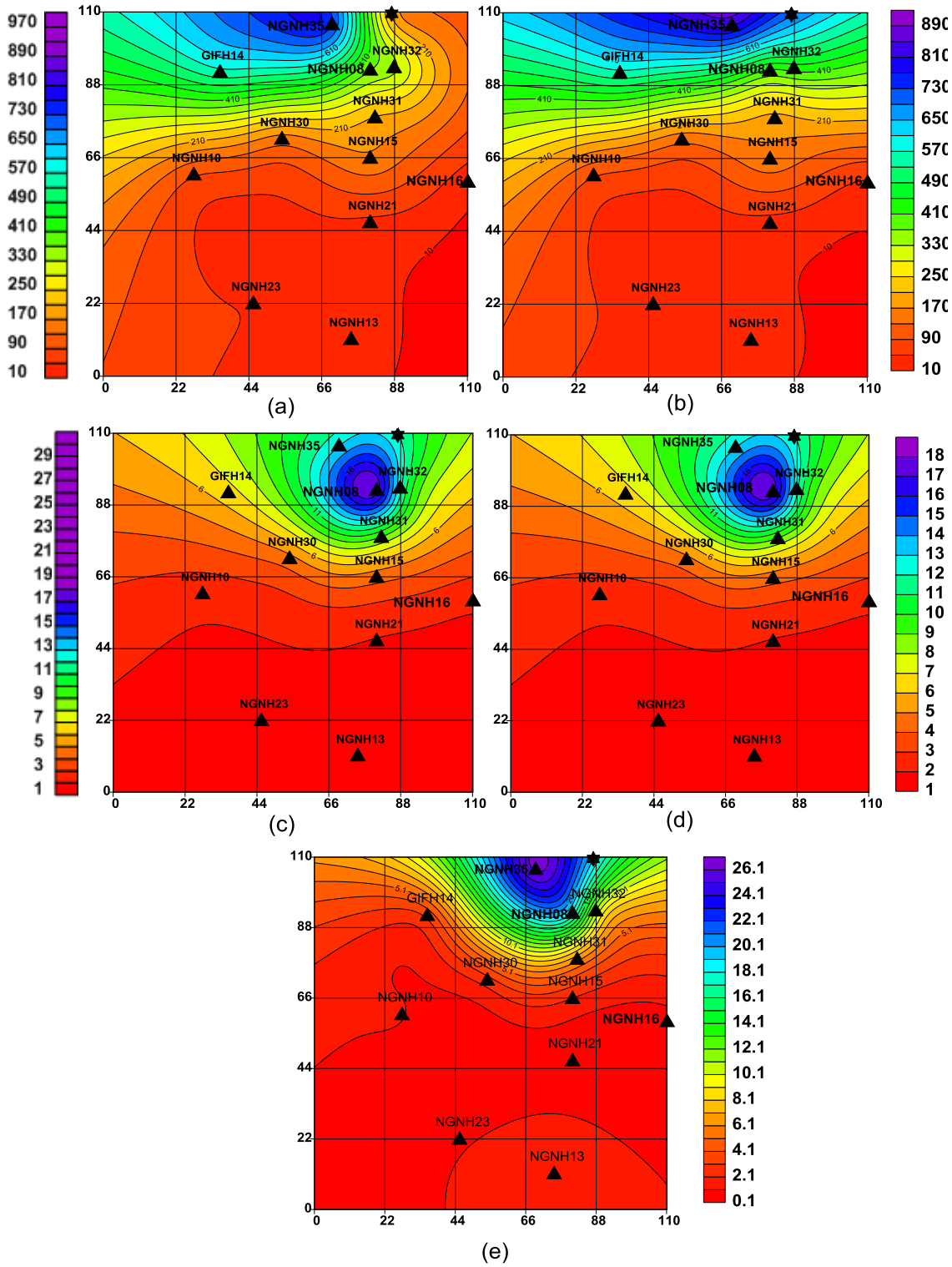

Figure 4.25: Contour map of spectral acceleration of event occurred on 11-01-2004 at (a) 1.5 Hz, (b) 2.5 Hz, (c) 5.0 Hz, (d) 7.0 Hz and (e) 10.0 Hz frequency, respectively. Triangles and stars denote the location of recording stations and events, respectively.

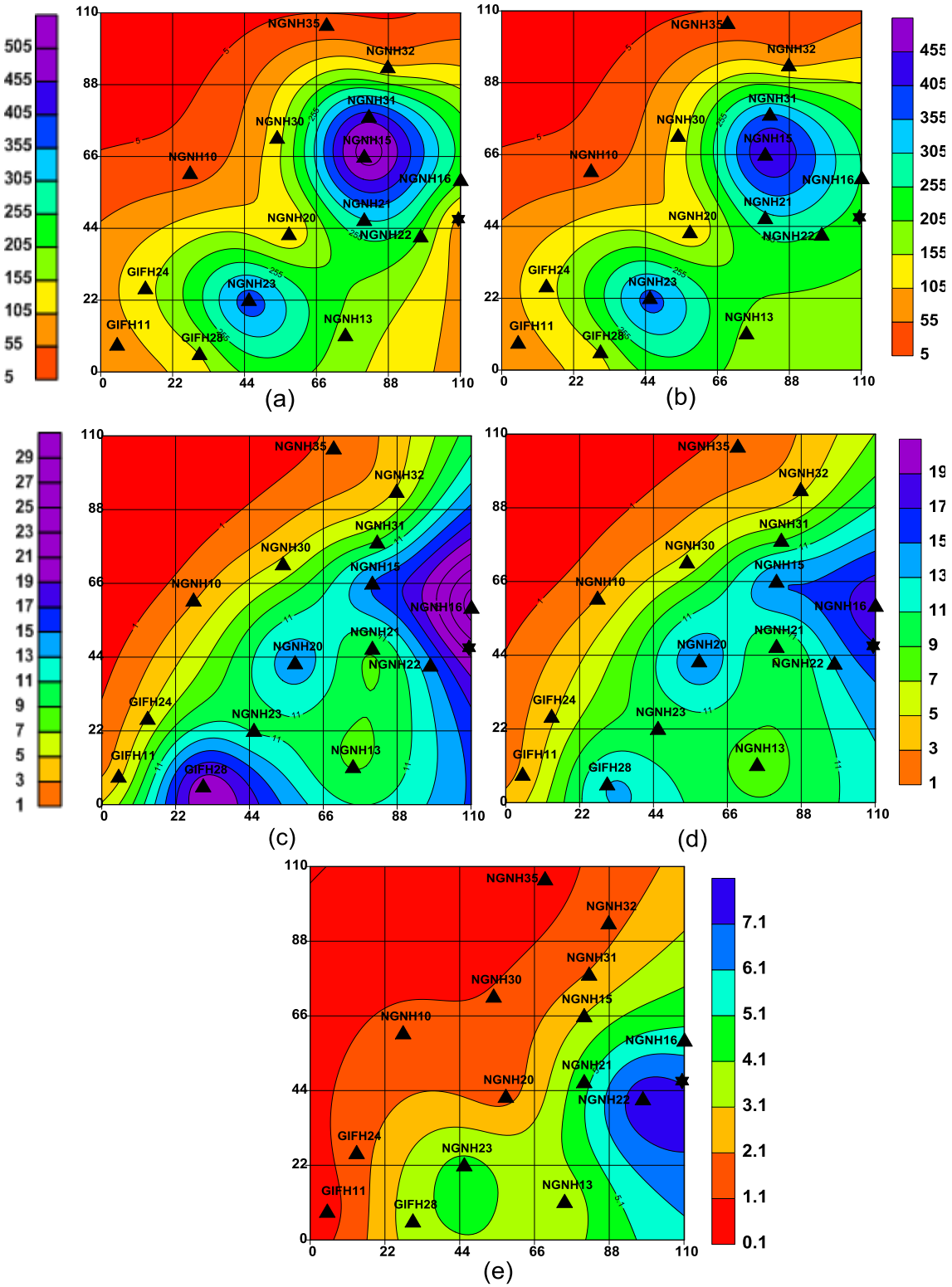

Figure 4.26: Contour map of spectral acceleration of event occurred on 05-05-2005 at (a) 1.5 Hz, (b) 2.5 Hz, (c) 5.0 Hz, (d) 7.0 Hz and (e) 10.0 Hz frequency, respectively. Triangles and stars denote the location of recording stations and events, respectively.

4.4 Results and Discussion

In the present work three-dimensional attenuation structure has been determined at 1.5 Hz, 2.5 Hz, 5.0 Hz, 7.0 Hz and 10 Hz frequency, respectively using the data set of twelve earthquakes. Parameters of twelve earthquakes used for determination of attenuation structure are given in Table 4.2. Present study area consist Itoigawa-Shizuoka Tectonic Line and Median Tectonic Line. The depressed area of eastern side of ISTL is covered with Quaternary sediments including a large amount of volcanic ash derived from volcanoes (source: http://www.glgarcs.net). High quality factor values have been observed in eastern side as compare to western side of ISTL as shown in Fig. 4.27 to 4.31. It is further observed from the Fig. 4.27 to 4.31 that the top most layer (0-5 km) have low quality factor values as compare to the deepest layer. In the deeper layers the trend of contour lines become parallel to the ISTL as shown in Fig. 4.27 to 4.31. Present work revealed that the Q structure at different frequencies matches with the geological and tectonic units at different depth.

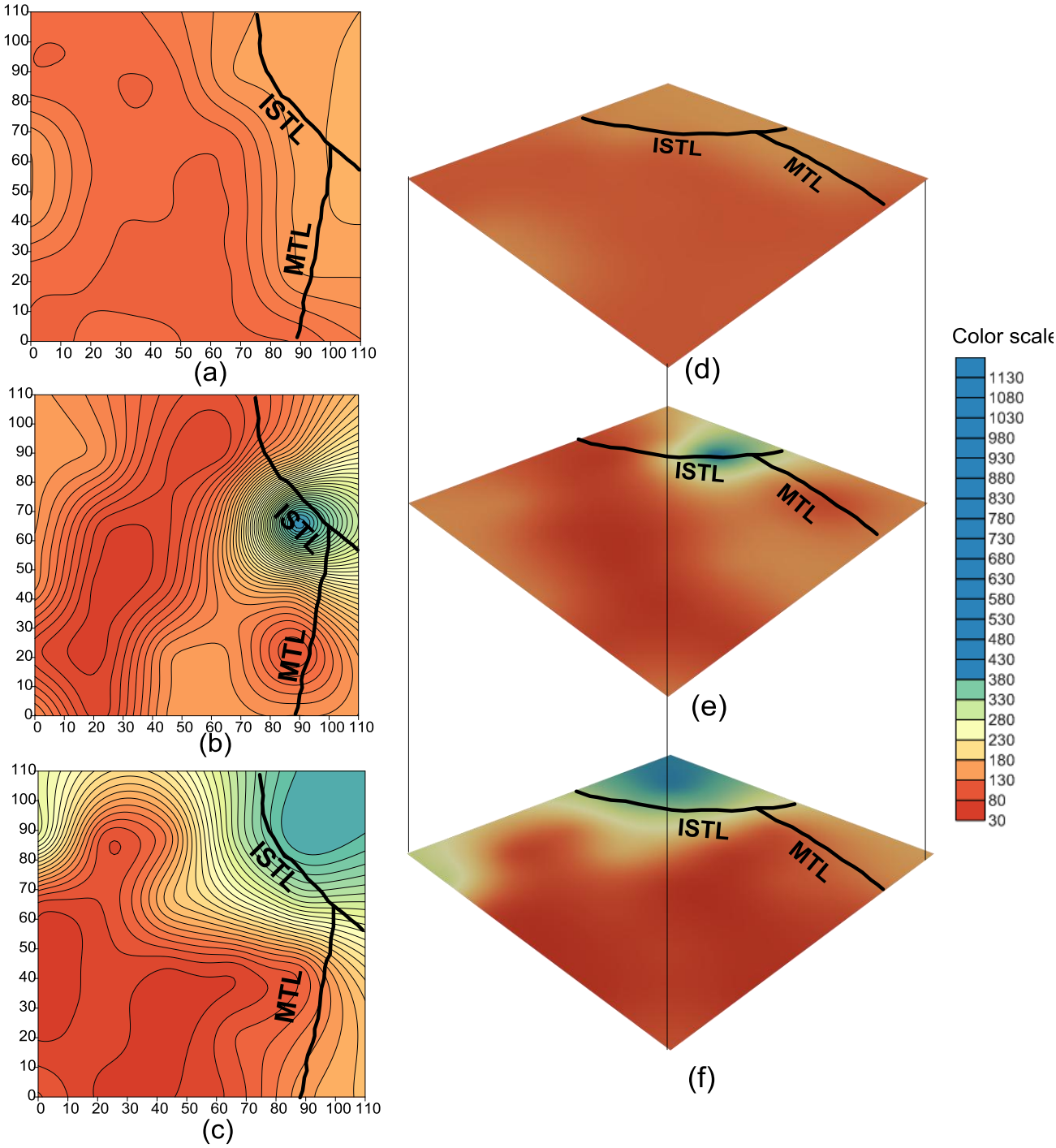

Figure 4.27: Contour of shear wave quality factor with tectonic lines for 1.5 Hz at (a) 0-5 km, (b) at 5-10 km and (c) at 10-15 km depth, respectively. (d), (e) and (f) represent three dimensional distributions of shear wave quality factor for 1.5 Hz at 0-5 km, 5-10 km and 10-15 km depth, respectively. ISTL and MTL describe the Itoigawa-Shizuoka Tectonic Line and Median Tectonic Line, respectively.

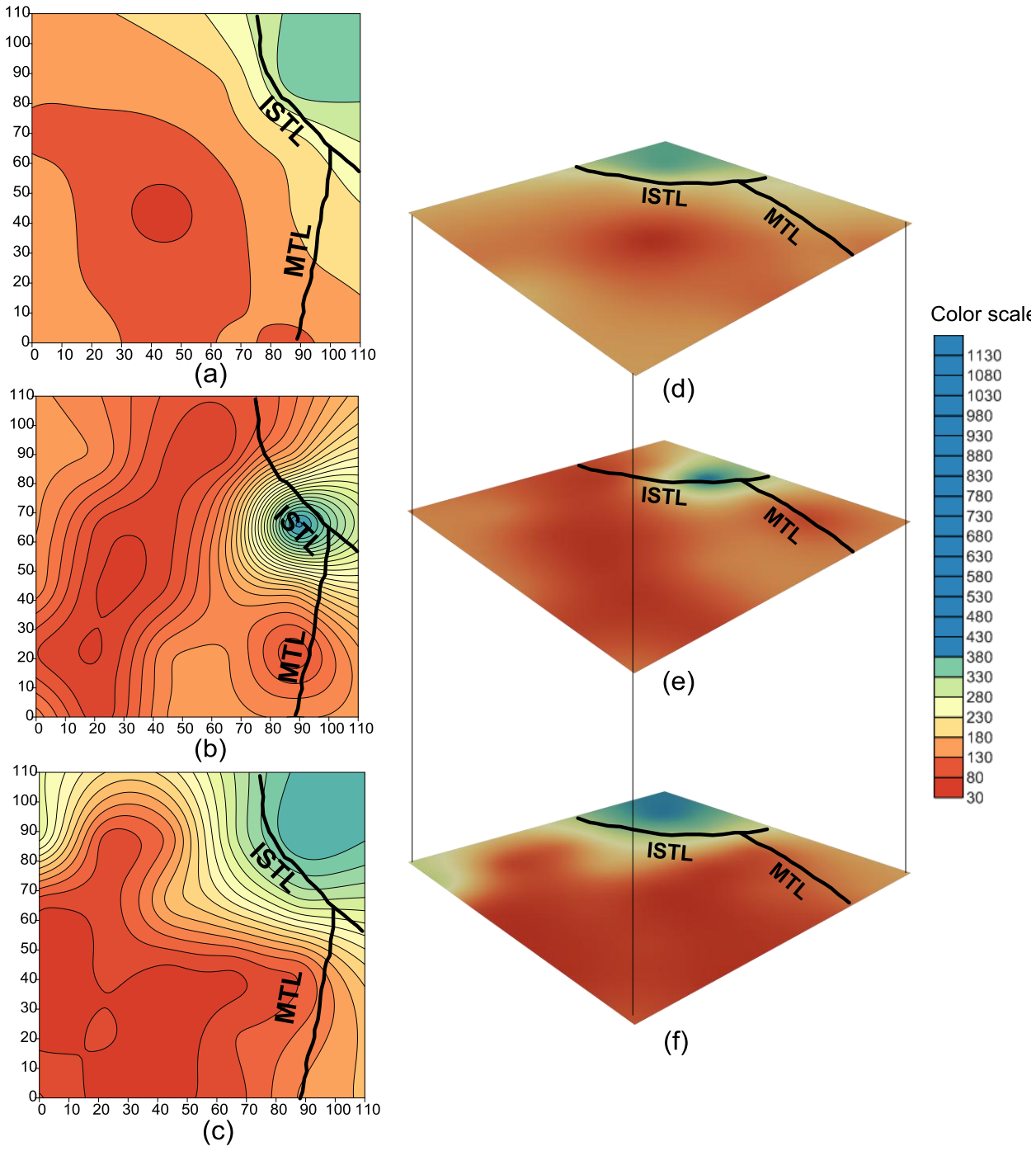

Figure 4.28: Contour of shear wave quality factor with tectonic lines for 2.5 Hz at (a) 0-5 km, (b) at 5-10 km and (c) at 10-15 km depth, respectively. (d), (e) and (f) represent three dimensional distributions of shear wave quality factor for 2.5 Hz at 0-5 km, 5-10 km and 10-15 km depth, respectively. ISTL and MTL describe the Itoigawa-Shizuoka Tectonic Line and Median Tectonic Line, respectively.

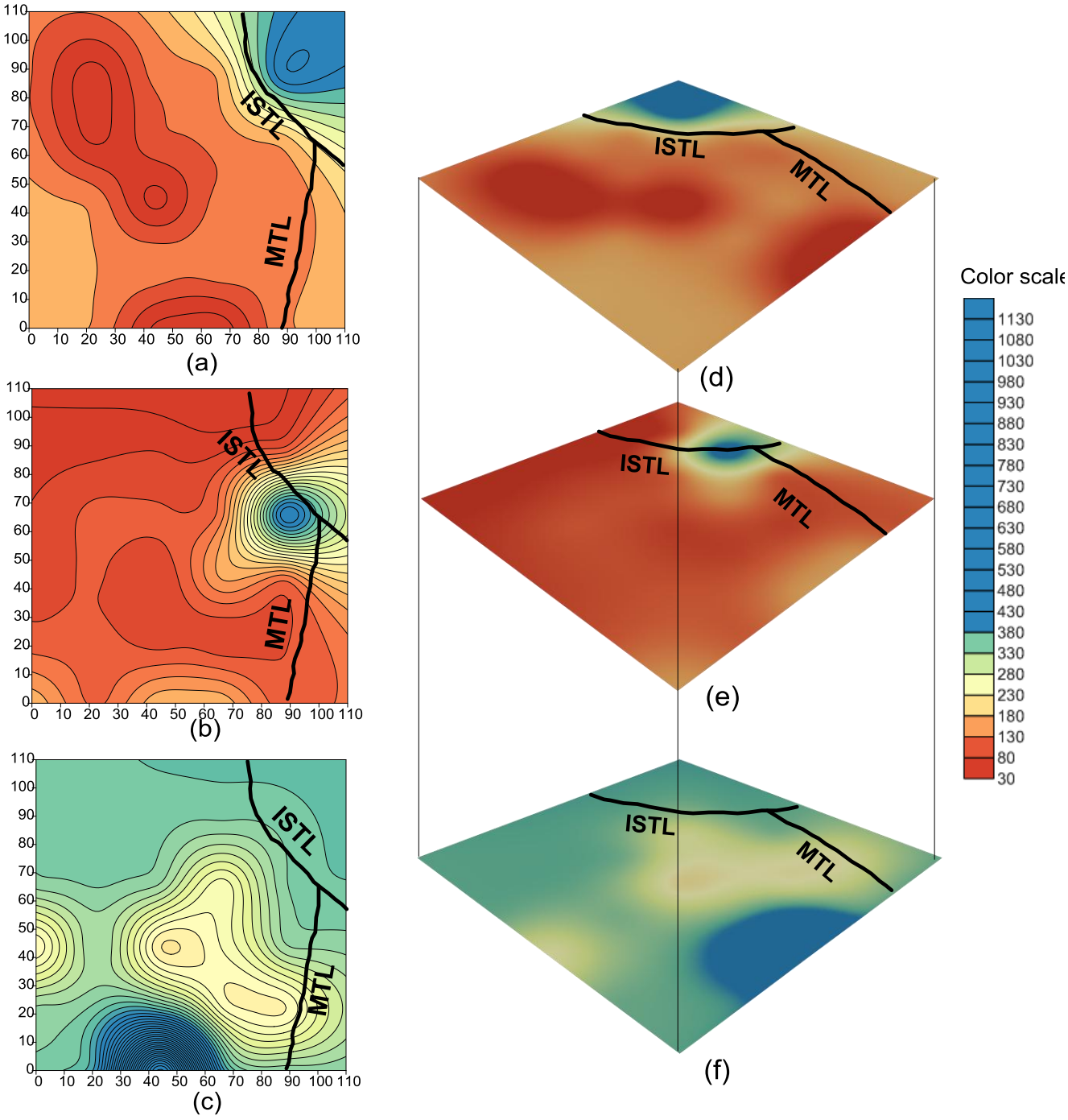

Figure 4.29: Contour of shear wave quality factor with tectonic lines for 5.0 Hz at (a) 0-5 km, (b) at 5-10 km and (c) at 10-15 km depth, respectively. (d), (e) and (f) represent three dimensional distributions of shear wave quality factor for 5.0 Hz at 0-5 km, 5-10 km and 10-15 km depth, respectively. ISTL and MTL describe the Itoigawa-Shizuoka Tectonic Line and Median Tectonic Line, respectively.

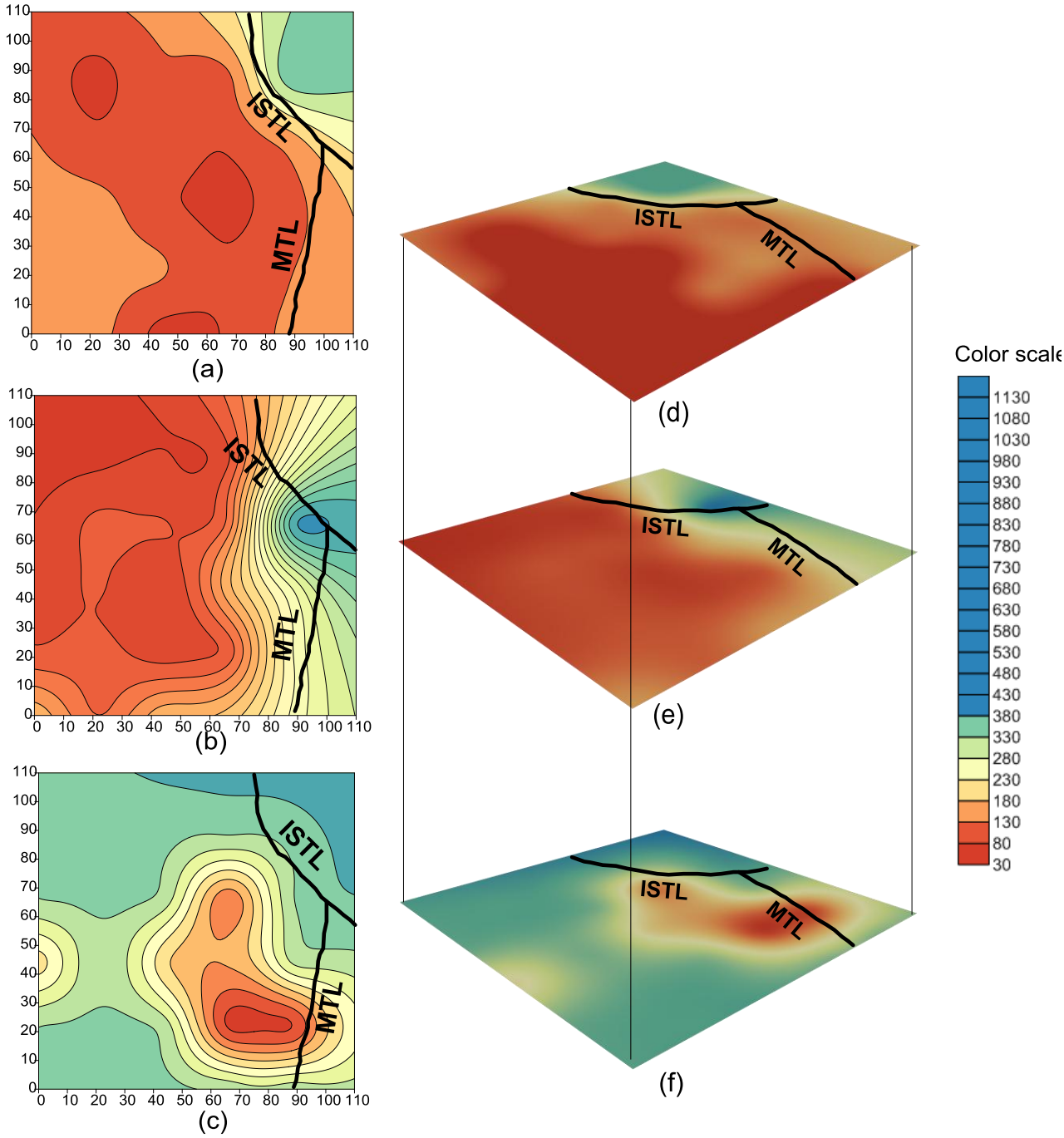

Figure 4.30: Contour of shear wave quality factor with tectonic lines for 7.0 Hz at (a) 0-5 km, (b) at 5-10 km and (c) at 10-15 km depth, respectively. (d), (e) and (f) represent three dimensional distributions of shear wave quality factor for 7.0 Hz at 0-5 km, 5-10 km and 10-15 km depth, respectively. ISTL and MTL describe the Itoigawa-Shizuoka Tectonic Line and Median Tectonic Line, respectively.

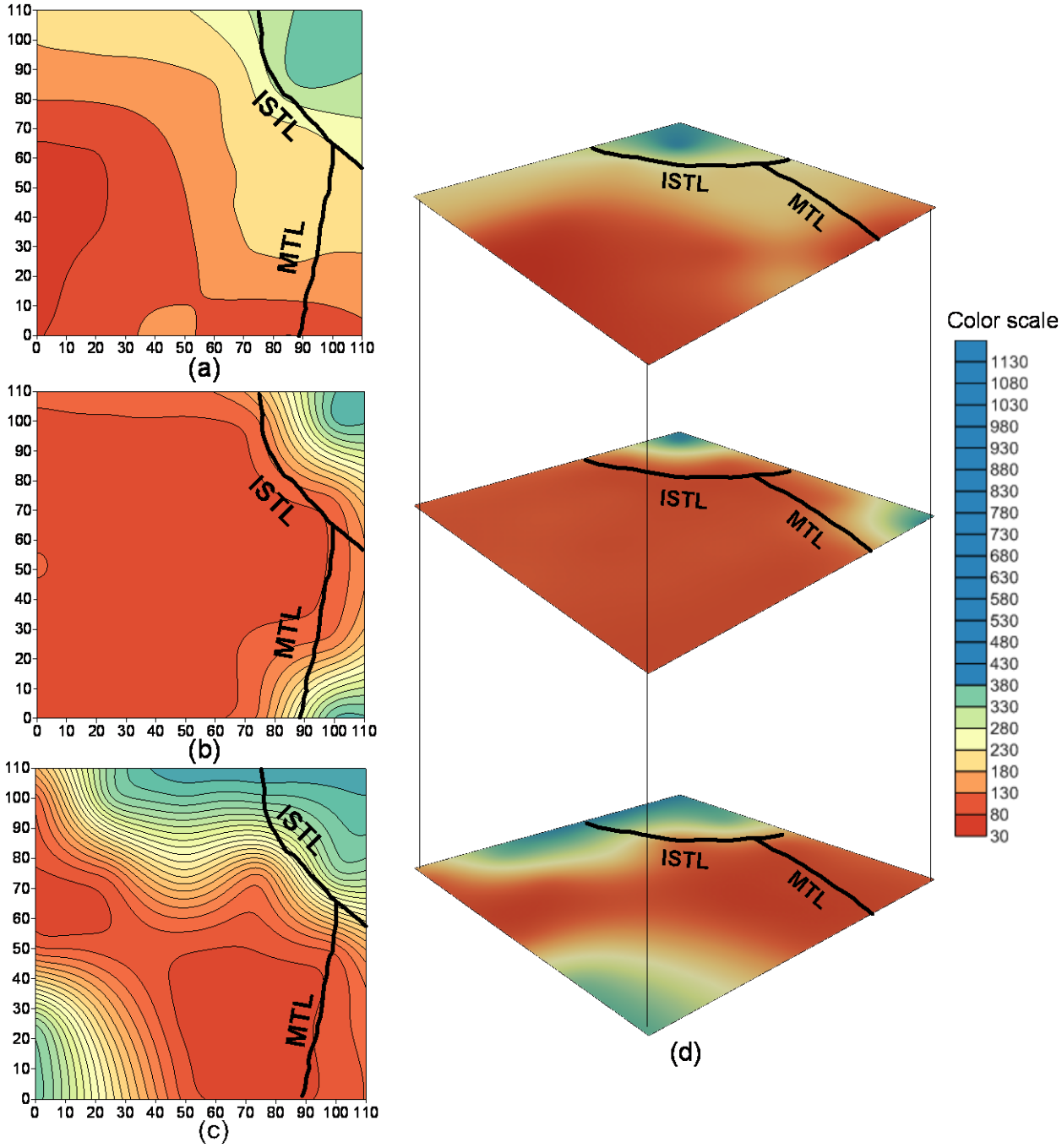

Figure 4.31: Contour of shear wave quality factor with tectonic lines for 10.0 Hz at (a) 0-5 km, (b) at 5-10 km and (c) at 10-15 km depth, respectively. (d), (e) and (f) represent three dimensional distributions of shear wave quality factor for 10.0 Hz at 0-5 km, 5-10 km and 10-15 km depth, respectively. ISTL and MTL describe the Itoigawa-Shizuoka Tectonic Line and Median Tectonic Line, respectively.

High ‘Q’ value accounts for low attenuation and hence zonation of any area on the basis of ‘Q’ value gives idea about high or low seismic hazard in that area. Seismic hazard in a region can also be obtained by probabilistic and deterministic methods. The zone of high seismic hazard obtained from attenuation study is further compared with various zone of seismic hazard obtained from probabilistic approach. The probabilistic seismic hazard map of the Central Japan region is shown in Fig. 4.32. It is seen from Fig. 4.32 that the eastern side of the study area have high probability of seismic hazard as compared to the western side. A comparison has been made between the obtained contours of ‘Q’ values at 0-5 km at different frequencies with the probabilistic seismic hazard map and is shown in Fig. 4.33.

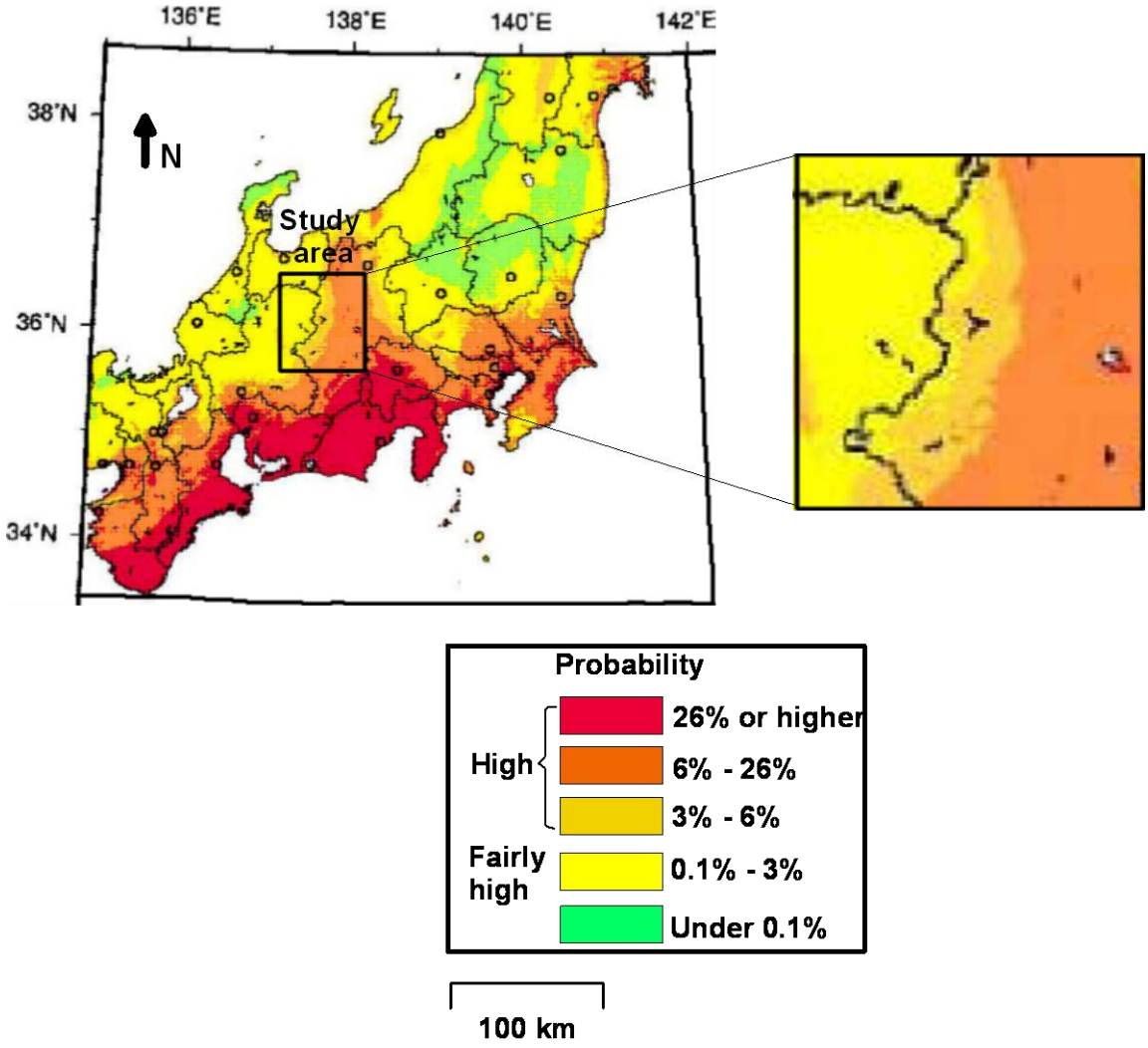

Figure 4.32: Probabilistic seismic hazard map of the Central Japan region (Figure modified after the Headquarters for Earthquake Research Promotion, 2005).

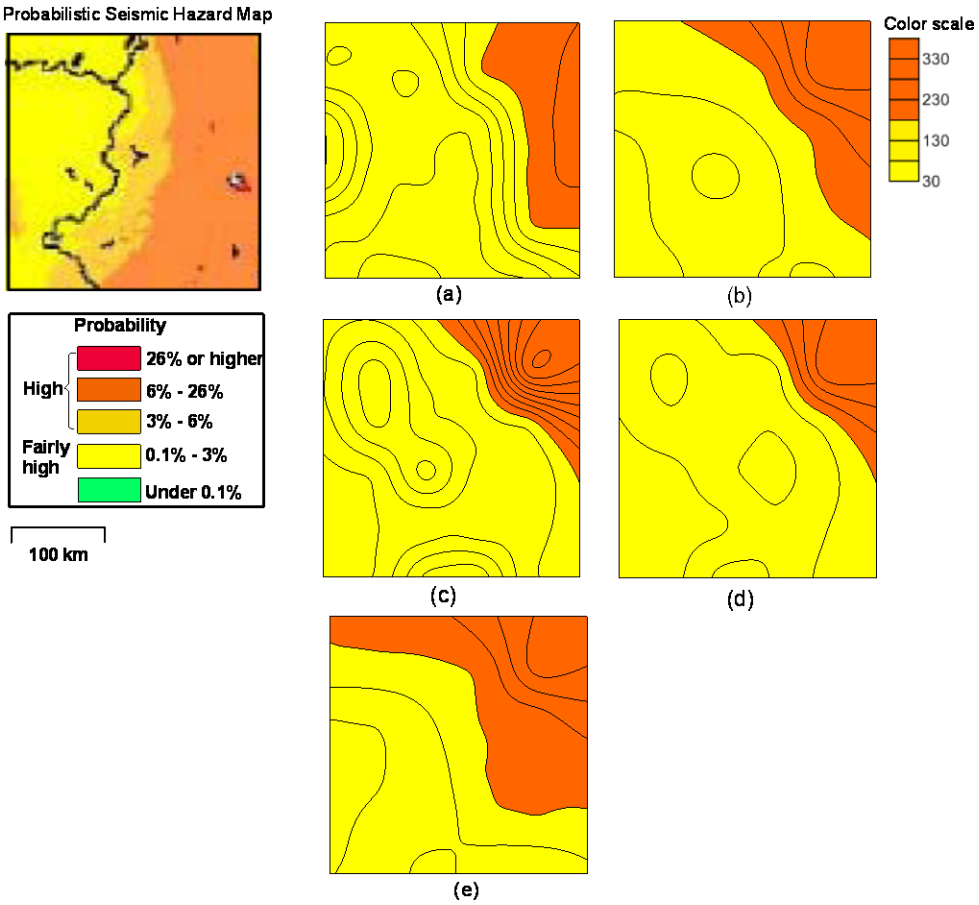

Figure 4.33: Comparison of obtained attenuation structure at 0-5 km with the Probabilistic seismic hazard map for (a) 1.5 Hz, (b) 2.5 Hz, (c) 5.0 Hz, (d) 7.0 Hz and (e) 10.0 Hz.

It is seen from Fig. 4.33 that obtained contour of shear wave quality factor at 0-5 km at different frequencies are almost similar and shows comparable trends with the probabilistic seismic hazard map. It is seen that eastern side of obtained attenuation contours shows low attenuating earth medium and therefore high seismic hazard potential which is similar to the probabilistic seismic hazard map given by the Headquarters for Earthquake Research Promotion, 2005. It is seen that although method of obtaining hazard using probabilistic map is dependent on different inputs and methodologies, the seismic hazard obtained from attenuation structure is comparable with that obtained by probabilistic map. Several studies show that high attenuation is directly related to magma erupted by active volcano (Havskov et al. 1989), Matsunami (1991), Shapiro et al. (2000), Cruz-Atienza et al. (2001), Novelo-Casanova and Martinez-Bringas (2005). However in the present study the region covered by attenuation tomography does not contain any evidence of magma eruption by active volcano in the region.

4.5 Conclusion

This chapter describes the result of inversion of strong motion data to obtain three-dimensional attenuation structure of the central Honshu region, Japan. The complete method and algorithm is discussed in detail in Chapter 2. The shear wave attenuation structure is determined at 1.5, 2.5, 5.0, 7.0 and 10.0 Hz frequency at different depth. The observed attenuation structure is compared with the geological and tectonic structure of the region. The observed attenuation structure gives comparable match with the major tectonic unit present in the Honshu region in almost each frequency selected in this work. The obtained attenuation contours also gives an idea about low and high seismic hazard present in the region.

Chapter – 5

Determination of $Q_\beta(f)$ for Kumaon Himalaya, India

5.1 Introduction

In determination of three dimensional attenuation structure of any region using algorithm defined in Chapter 2 we require strong motion data corrected for site amplification term. As a strong trade off exists between local site amplification terms and shear wave quality factor therefore an algorithm is require which should estimate both shear wave quality factor and site amplification term simultaneously. This algorithm has been defined in Chapter 3. A dense network of strong motion data has been installed in the Kumaon region of the Uttarakhand Himalaya, India. As the strong motion data recorded at different site is expected to have site amplification terms therefore algorithm discussed in Chapter 3 has been used to obtain both the shear wave quality factor and site amplification terms simultaneously which is further used to correct strong motion data for site amplification terms.

5.2 Tectonics and Geology

The Himalayan mountain chain is characterized by a marked concentration of interplate seismicity and high rate of upliftment as well as convergence (Molnar and Chen, 1983; Nakata, 1989; Demets et al., 1990). Many thrust faults lie in the Himalaya regions which are able to produce the earthquakes of magnitude 8.0 or greater (Gitis et al., 2008). Fourteen major earthquakes of magnitude $\geq$ 7.5, including five great earthquakes (including the 1912 Burma earthquake) of magnitude $\geq$8, have occurred in the Himalayan region during 1897 to 1992 (Gupta et al., 1995; Satyabala and Gupta, 1996). Historically many earthquakes have been recorded in this region which are mostly concentrated between main boundary thrust (MBT) and main central thrust (MCT) (Seeber and Armbruster, 1984). In the present work the region of Kumaon Himalaya has been considered which lies in the vicinity of Garhwal Himalaya. Seismicity of this region from 1973 to 2012 is shown in Fig. 5.1. The focal mechanisms of selected regional and teleseismic Himalayan earthquakes indicate thrust faulting as the dominant mode of deformation for Himalaya (Fitch, 1970; Rastogi, 1974; Chandra, 1978). Ni and Barazangi (1984) demonstrated that most of the thrust-type Himalayan earthquakes are concentrated at depth of 10 and 20 km. Additionally Valdiya (1981) suggested that the neotectonics of the Himalaya manifests as movements along

numerous thrusts. Several studies have been carried out to explain the mechanics of these thrust earthquakes in terms of plate tectonic forces which revealed that the regional plate tectonic lithospheric compressive stresses resulting from the northward movement of the Indian plate are prime factor in generation of interplate seismicity in the region (Fitch, 1970; Chandra, 1978; Ni and Barazangi, 1984; Burchfiel and Royden, 1985).

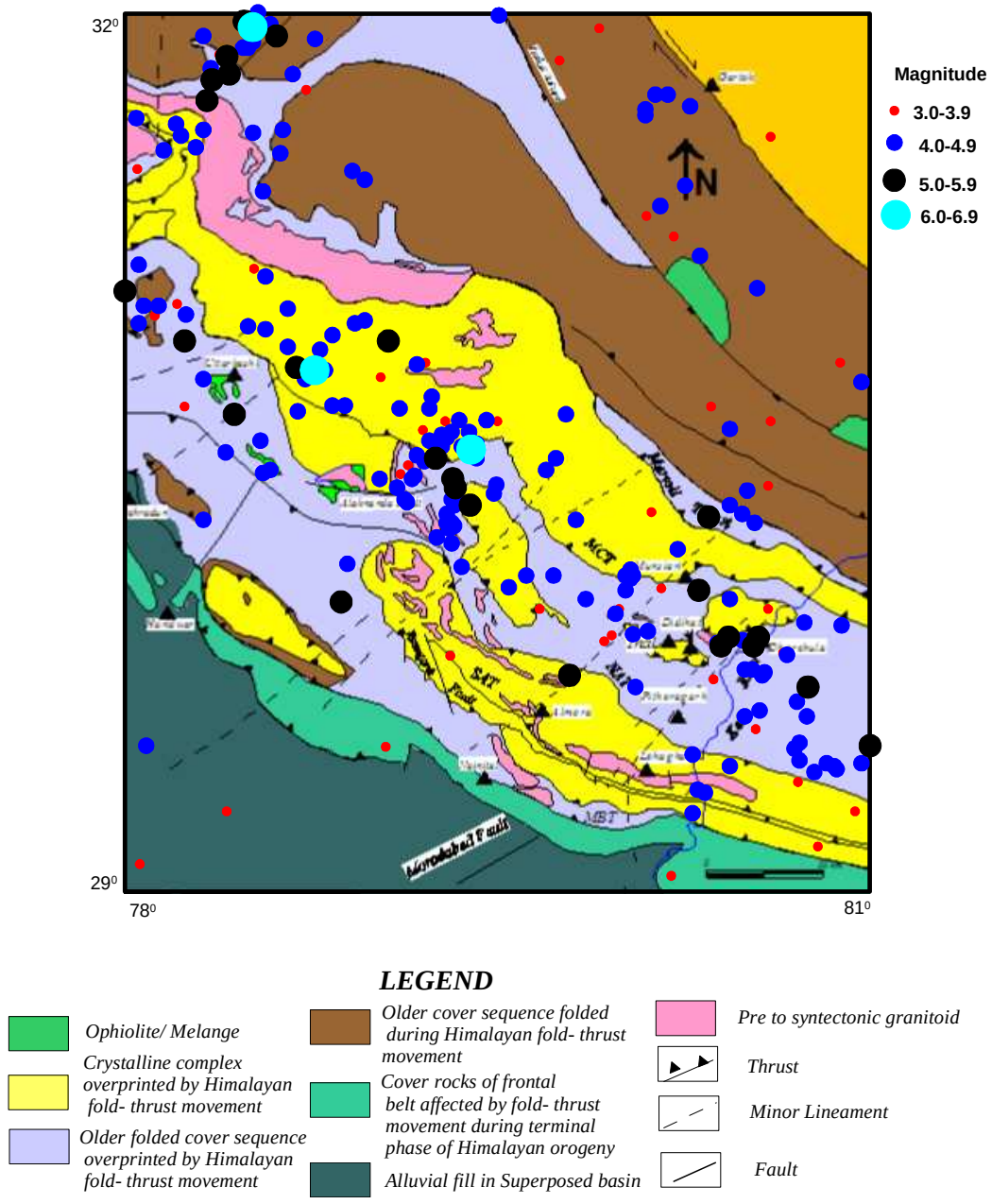

Figure 5.1: Locations of various events in the Garhwal and Kumaon Himalaya during 1973 to 2012 reported by USGS. The geology and tectonics of the region is after GSI (2000).

The Himalaya has been geologically divided into four lithotectonic subdivisions as shown in Fig. 5.2. From south to north these are defined as (Gansser, 1964):

(1) Outer Himalaya: - This part mostly includes the molassic Siwalik Supergroup of Mio-Pliocene ages and is demarcated by two tectonic planes, the Himalayan Frontal Thrust (HFT) to the south and the Main Boundary Thrust (MBT) to the north (Bhattacharya, 2008).

(2) Lesser Himalaya: - This part exposes a thick pile of highly folded Proterozoic sedimentary strata together with a few outcrops of older crystalline rocks; this subdivision is bounded by the MBT in the south and the Main Central Thrust (MCT) in the north. The Main Central Thrust (MCT) is defined by the contact between the Lesser and the Higher Himalayas (Bhattacharya, 2008).

(3) Greater or Higher Himalaya: - This part exposes a massive, north-dipping pile of metamorphic rocks – the Central Crystalline Zone – and is demarcated by the MCT to its south and the Dar-Martoli Fault or Tethys Fault or the South Tibetan Detachment (STD) to the north (Bhattacharya, 2008).

(4) Tethys Himalaya: - This part includes with a thick pile of sedimentary rocks of Cambrian to Lower Eocene ages (Bhattacharya, 2008).

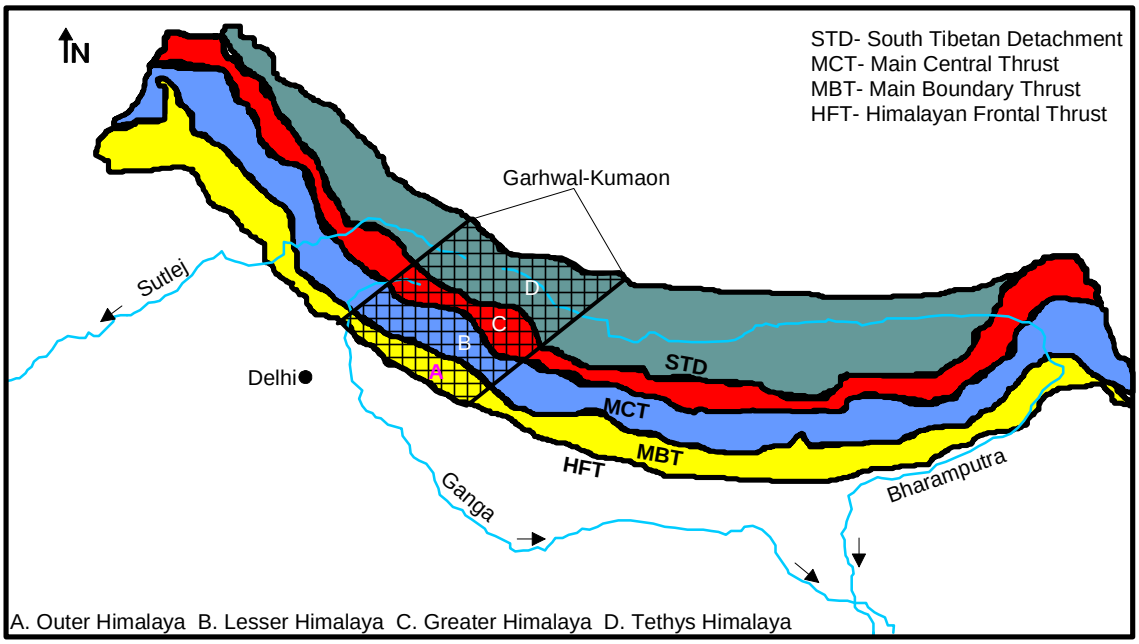

Figure 5.2: Geological sketch map of the Himalaya. A - Outer Himalaya, B - Lesser Himalaya, C - Greater Himalaya and D - Tethys Himalaya (Figure modified after Bhattacharya, 2008).

5.3 Data

Department of Earth Sciences, Indian Institute of Technology Roorkee has deployed a network of fourteen strong motions stations in the highly mountainous terrain of the Kumaon Himalaya, India under a major seismicity project funded by the Ministry of Earth Sciences, Government of India. This region lies along the international boundary of India and Nepal. Frequent seismic activity and thrust system present in this region demonstrate the seismotectonic importance of the region. The Kumaon sector manifests strong deformation and reactivation of some of the faults and thrusts during Quarternary times. This is amply evident by the recurrent seismicity patterns, geomorphic developments and geodetic surveys (Valdiya, 1999). This region shows development of all the four-morphotectonic zones, which are demarcated by intra-crustal boundary thrust of regional dimension. These zones from South to North are: Siwalik or Sub Himalaya, Lesser Himalaya, Great Himalaya and Tethys Himalaya (Paul et al., 2003). The Garhwal-Kumaon region lie in the seismic gap of major earthquakes therefore this region is seismologically important (Khattri and Tyagi, 1983; Bilham et al., 2001). Because of high seismic activity and seismic gap present in this region, this strong motion network has great importance in recording recent seismic activities of the region.

The sites for installation of accelerographs have been selected on the basis of historical seismic activities. The historical events during 1973 to 2012 show a cluster of events in between Main Central Thrust (MCT) and North Almora Thrust (NAT) in Kumaon Himalaya region as shown in Fig. 5.1. Hence most of the accelerographs are installed between MCT and NAT to record all earthquakes occurring in this region. The locations of all stations are shown in Fig. 5.3 and its details are given in Table 5.1. Some stations of this network are mobile and hence Fig. 5.3 shows a total of 16 stations. The minimum inter station distance between these stations is approximately 11 km. This network is installed in highly mountainous terrain of Kumaon Himalaya as shown in Fig. 5.4 where elevation of recording stations from mean sea level lie between 612 to 2239 m. This network is one of the dense networks monitoring strong motion seismic activity in highly mountainous terrain of Himalaya, India. Three-component accelerograph has been installed at each site as shown in Fig. 5.5. The stations Jouljibi and Munsyari have minimum and maximum elevation 612 m and 2239 m, respectively.

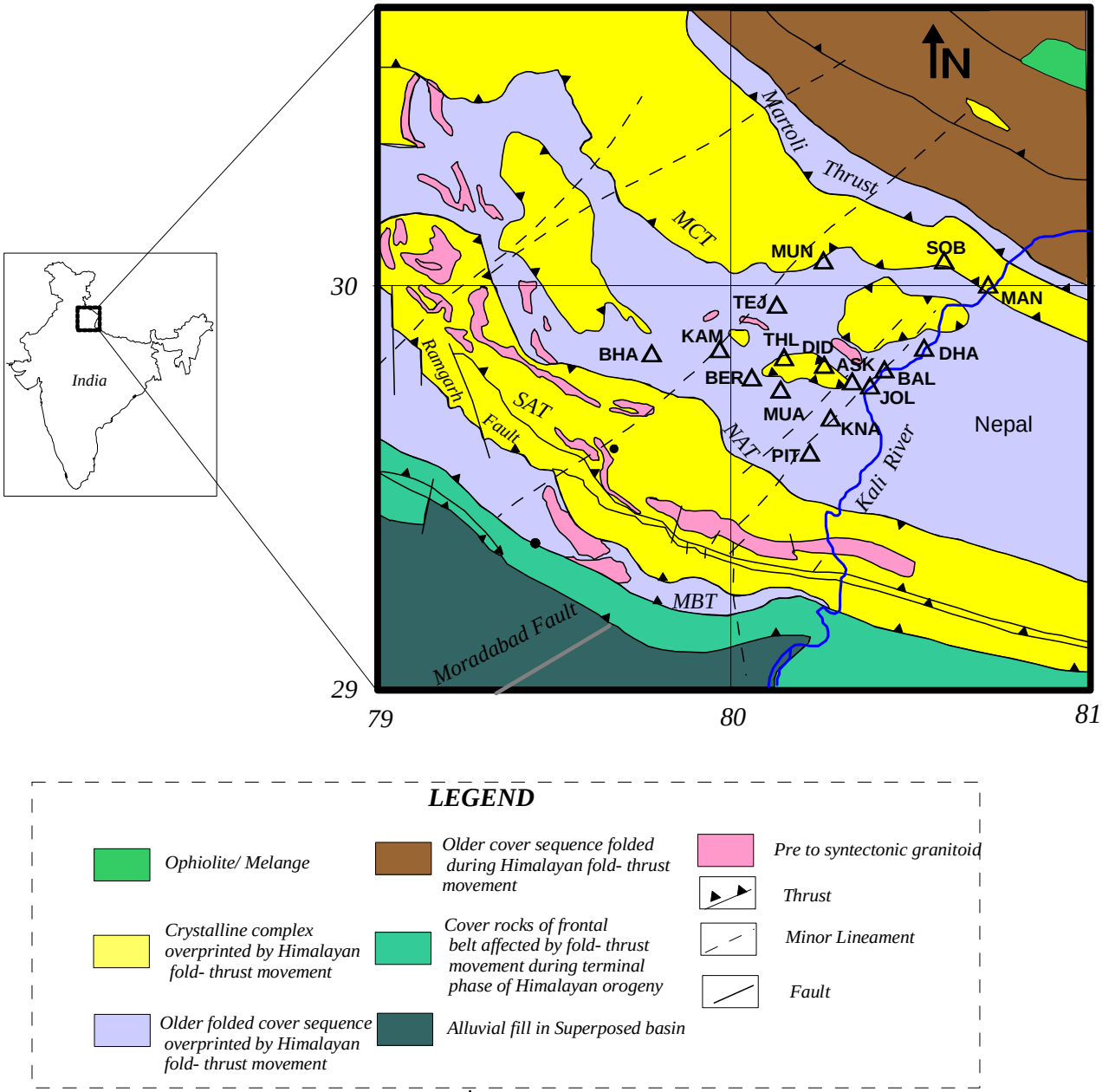

Figure 5.3: Location of strong motion recording stations installed in the Kumaon Himalaya. The geology and tectonics of the region is after GSI (2000).The strong motion stations of local network denoted by hollow triangles.

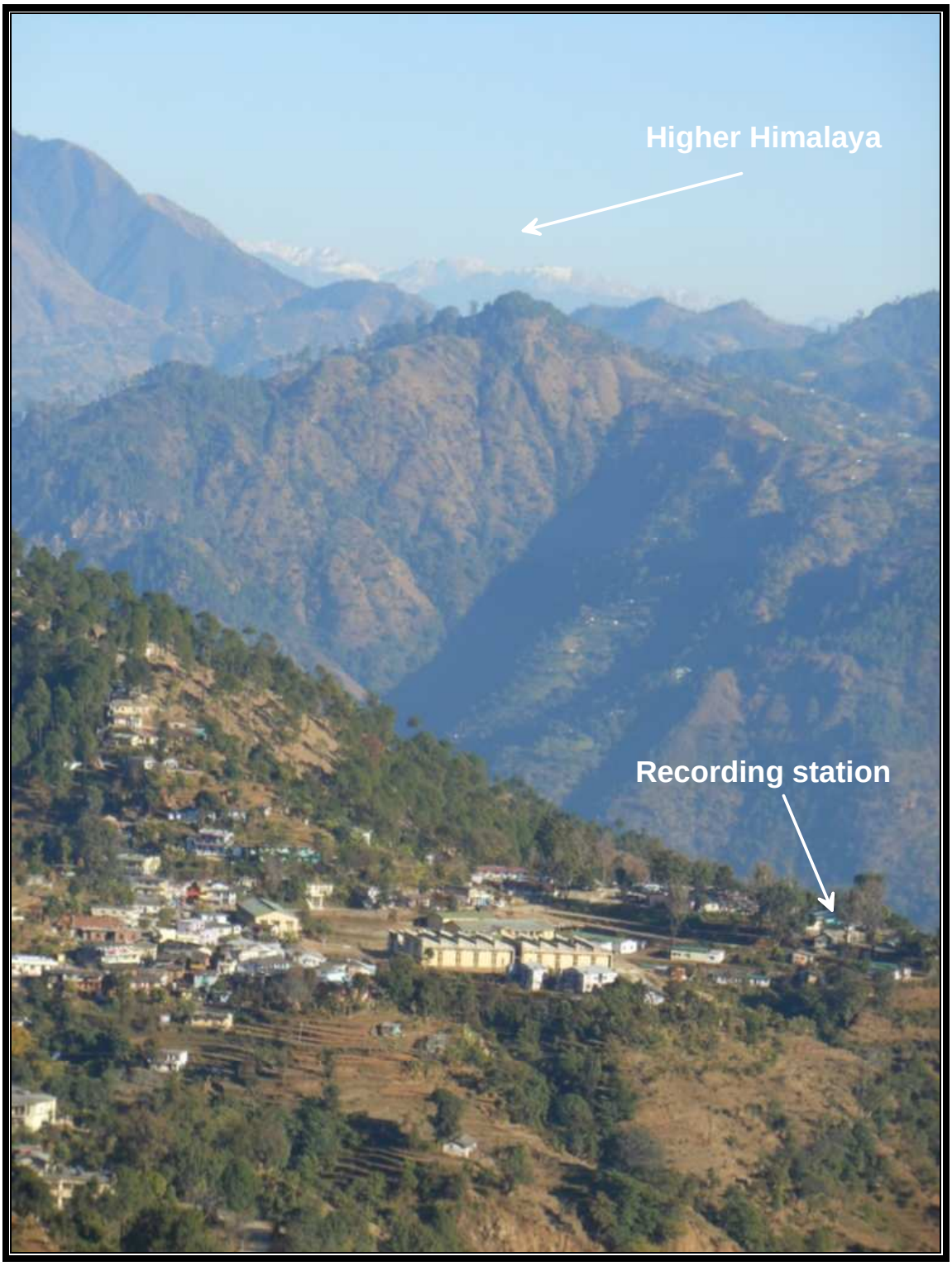

Figure 5.4: Location of recording station in mountainous terrain of Himalaya. Figure showing location of Askot station installed at the elevation of 1258 meter from mean sea level.

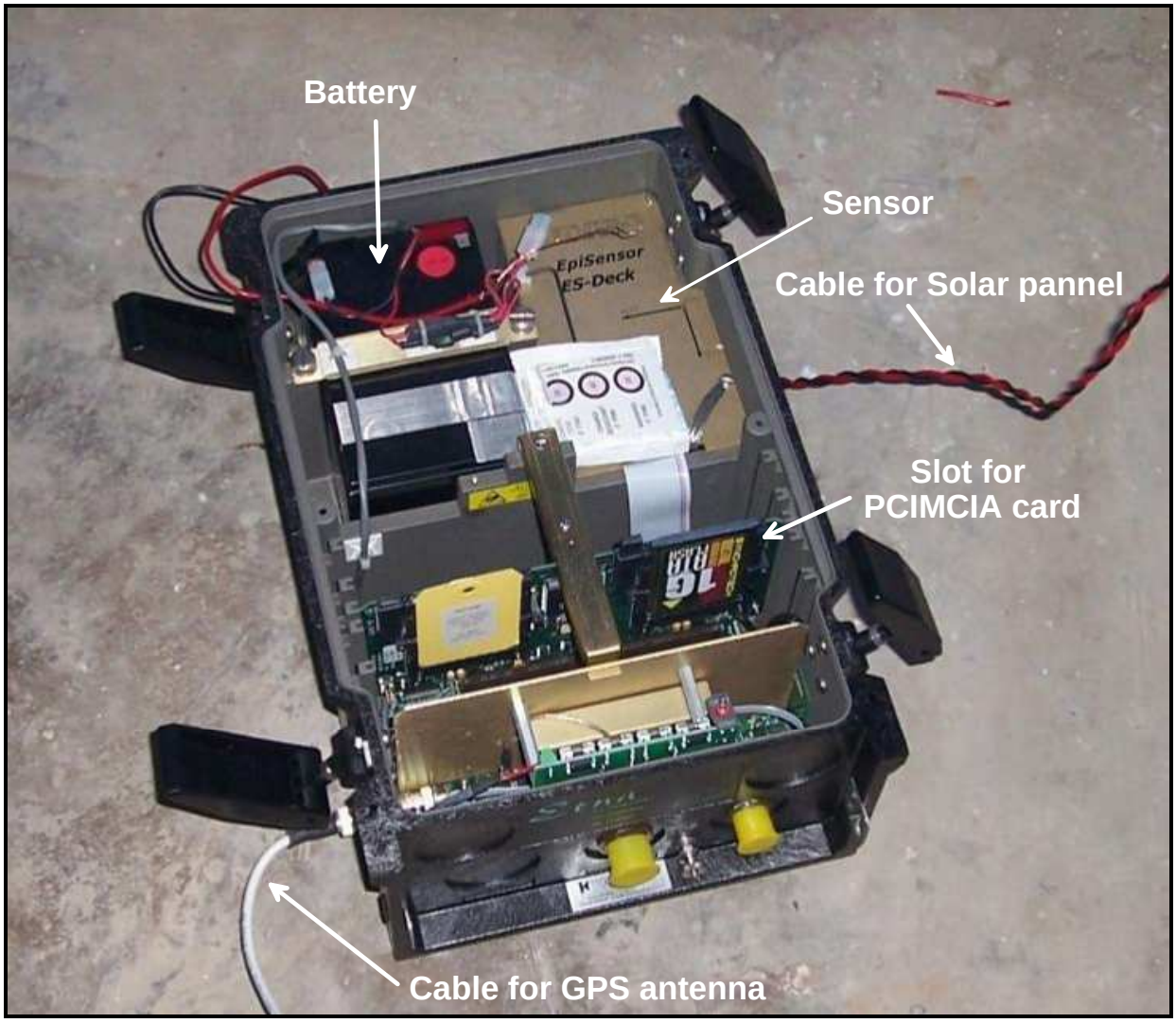

Figure 5.5: Strong motion accelerograph of Kinemetrics, U.S.A. installed at each site.

Three-component force balance, short period accelerometer of Kinemetrics, U.S.A. has been installed at all stations of this network. In order to record events with low energy, the threshold level of instruments were set at very low level of .005% of full scale. The sensitivity of instrument is 1.25 V/g and full scale measurement is 2.5V. Purpose of such low threshold level is to record almost every possible local events occurring in the region. Sampling interval of digital data is kept at 0.01 sec. The major components of entire accelerograph unit are the Sensor, Global positioning system (GPS) antenna, Solar panel, Battery and PCIMCIA card and shown in Fig. 5.6 and 5.7. The entire instrument is in a compact form and consists of sensor, recording unit and battery. The GPS antenna is connect through a cable to the main unit and is used to provide exact

geographical location and time in GMT. Solar panel and battery is used to supply the power backup to the accelerograph. PCIMCIA is the memory card which is used to store the data. Data can be retrieved from the PCIMCIA card or through a cable connected with laptop as shown in Fig 5.8. The data retrieved from the card is obtained in .EVT format. The ASCII conversion of this format give three files with extension .001, .002 and .003 which represent the NS, EW and vertical components, respectively. Three component of an accelerogram recorded at Munsyari station is shown in Fig. 5.9.

Table 5.1: Name, code and location of the recording stations.

Sr. No.	**Station Name**	**Station Code**	**Latitude (Degree)**	**Longitude (Degree)**	**Elevation of the stations from mean sea level (meter)**
1	Didihat	DID	29.80	80.25	1628
2	Pithoragarh	PIT	29.58	80.21	1574
3	Tejam	TEJ	29.95	80.12	968
4	Dharchula	DHA	29.84	80.53	935
5	Munsyari	MUN	30.06	80.25	2239
6	Askot	ASK	29.76	80.33	1258
7	Kamedidevi	KAM	29.84	79.96	1811
8	Jouljibi	JOL	29.75	80.38	612
9	Baluakot	BAL	29.79	80.42	644
10	Knalichhina	KNA	29.67	80.27	1656
11	Muavani	MUA	29.74	80.13	822
12	Berinag	BER	29.77	80.05	1684
13	Mangti	MAN	30.00	80.71	1609
14	Sobla	SOB	30.06	80.59	1628
15	Thal	THL	29.82	80.14	784
16	Bhageshwar	BHA	29.83	79.77	873

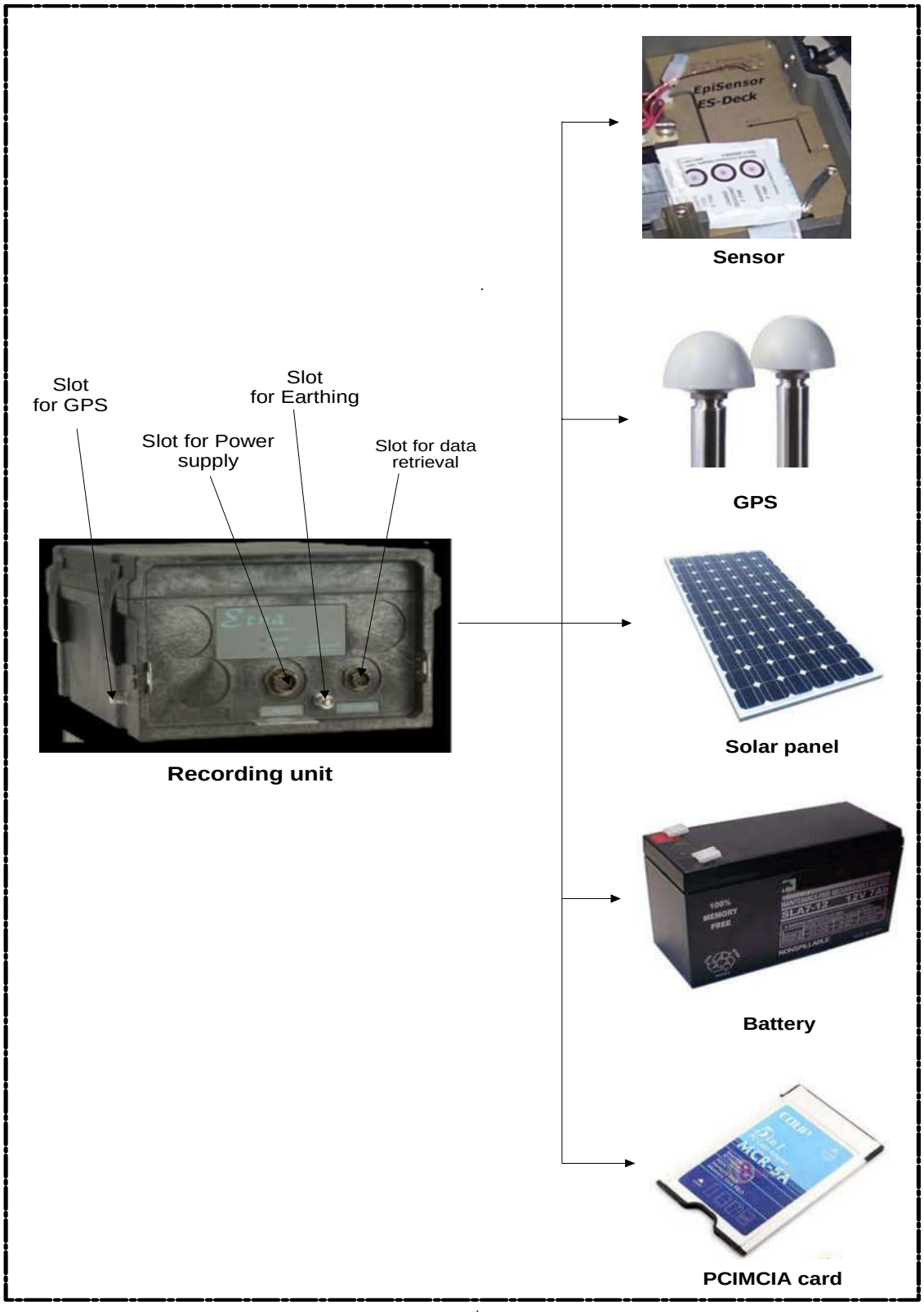

Figure 5.6: Major components of the accelerograph.

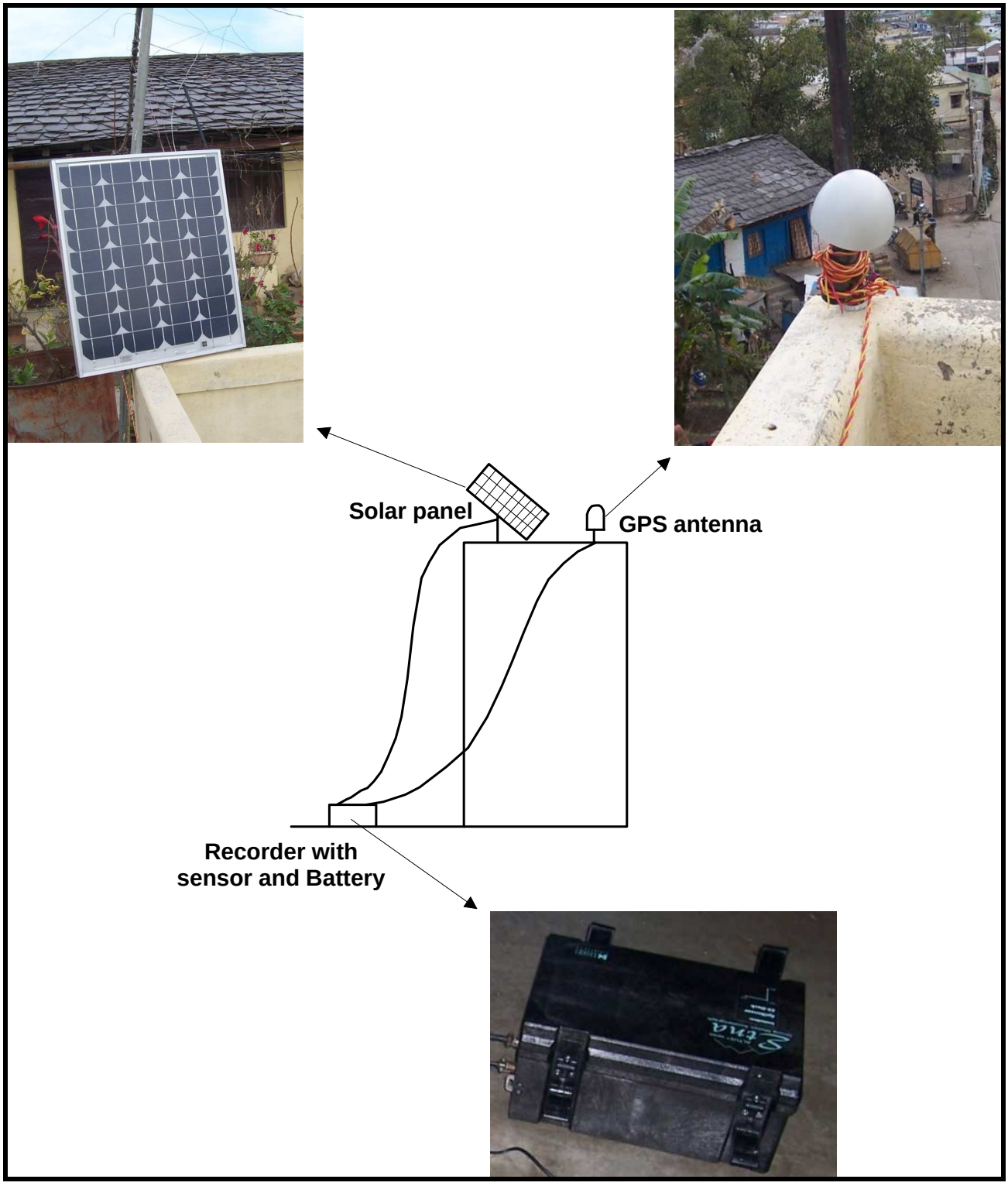

Figure 5.7: A figure showing the major component of accelerograph installed in the field.

Figure 5.8: Retrieval of data recorded in the accelerograph through a cable by using the laptop.

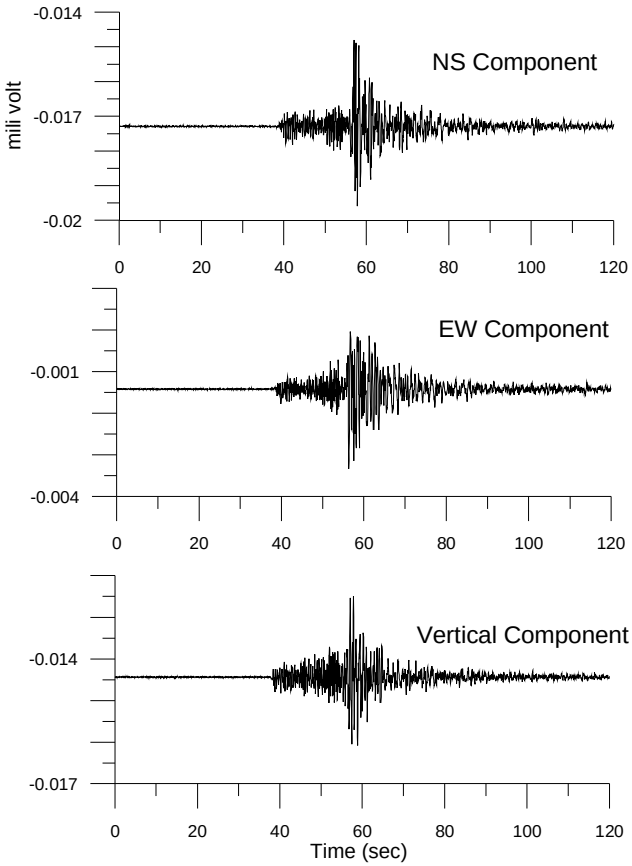

Figure 5.9: Recorded three component of unprocessed accelerogram of an event occurred on 26-02-2012 at Munsyari station.

This network is operational since 2006. It had recorded various earthquakes in this region. A total of 294 events have been recorded by this network in this region during 2006 to 2013. The arrival time of primary and secondary phases from records of these events has been used for localization of events using HYPO71 program originally developed by Lee and Lahr (1972). The velocity model used for localization of events is that given by Yu et al. (1995). A total of 110 events have been localized since 2006 to 2013. In the present work forty local events recorded in this network installed in the Kumaon region has been used. Hypocentral parameter of events used in present work and the obtained error in their localization is reported in Table 5.2. Location of the forty events used in the present work is shown in Fig. 5.10. The records collected from the accelerograph have been processed using the procedure suggested by Boore and Bommer (2005). The processing steps involve baseline correction, instrument scaling, padding and frequency filtering discussed in detail in Chapter 4. In the present work six events have been used at each station. Some of the processed records used in the present work are shown in Fig. 5.11 to 5.26.

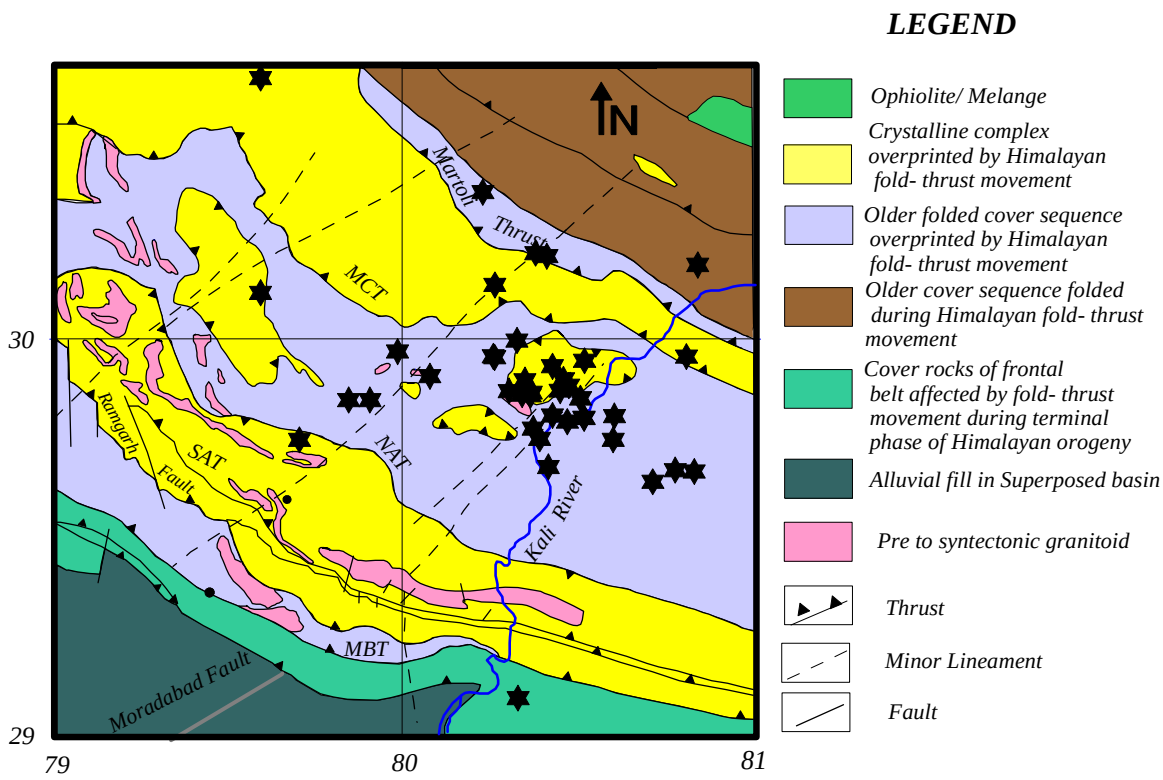

Figure 5.10: Location of the events used in the present work. The geology and tectonics of the region is after GSI (2000). Stars denote the location of the events.

Table 5.2: Hypocentral parameters of events used in the present work and the error obtained in its localization. ERH and ERZ define the error of epicenter and focal depth, respectively.

Sr. No.	Date	Origin time	Epicenter	Depth (km)	ERH (km)	ERZ (km)
1	01/04/06	19:42:52.10	30º12.73',80º 24.13'	11	0.4	1.1
2	05/05/06	08:00:28.72	29º38.65',80º42.16'	30	2.7	1.7
3	05/05/06	08:49:40.48	29º41.43',80º45.00'	25	4.0	3.0
4	07/05/06	06:46:13.72	29º57.51',80º48.80'	35	1.4	4.5
5	30/05/06	18:25:18.03	29º54.14',80º26.95'	03	0.9	1.9
6	27/10/06	07:55:01.39	29º57.46',80º15.23'	13	5.6	3.1
7	27/10/06	08:01:32.23	29º52.35',80º17.70'	16	3.1	1.3
8	12/04/07	04:59:54.49	29º48.72',80º22.01'	15	4.0	8.7
9	19/08/08	10:54:32.17	29º45.16',79º42.27'	35	7.1	8.4
10	04/09/08	12:53:10.14	30º08.38',80º15.28'	15	1.7	1.0
11	04/09/08	17:38:20.21	29º08.17',80º20.09'	03	8.3	3.9
12	17/09/08	16:59:09.12	30º04.49',80º35.62'	25	5.0	4.1
13	08/12/09	07:05:16.70	30º22.39',80º13.22'	13	8.4	5.6
14	11/01/10	05:15:14.61	29º48.68',80º25.06'	12	0.2	0.6
15	12/01/10	09:35:21.62	29º51.73',80º21.30'	05	0.4	7.2
16	26/01/10	06:51:13.30	29º51.82',80º19.89'	03	2.3	1.5
17	07/02/10	07:16:41.68	29º52.14',80º21.48'	03	0.9	0.8
18	06/07/10	19:11:54.09	29º47.73',80º27.61'	07	1.2	1.6
19	19/07/10	00:08:41.44	29º52.41',80º26.38'	11	2.9	2.0
20	08/10/10	17:10:13.64	29º48.57',80º35.62'	18	5.7	3.2
21	11/06/11	02:59:03.70	30º13.08',80º22.11'	20	6.0	4.5
22	20/06/11	06:27:19.53	30º37.72',80º49.80'	25	1.2	6.0
23	12/07/11	01:41:01.54	29º48.26',80º30.45'	12	3.6	1.6
24	12/07/11	01:44:26.07	29º48.32',80º30.43'	11	2.9	1.2
25	01/08/11	10:14:23.52	29º58.34',79º58.70'	25	5.1	5.2
26	19/08/11	01:52:42.91	29º40.89',80º24.37'	08	3.9	9.7
27	06/09/11	08:54:28.61	29º45.16',80º22.91'	02	6.5	5.7
28	01/10/11	04:26:53.38	29º53.16',80º27.84'	25	2.5	5.1
29	09/10/11	07:34:55.69	29º56.93',80º30.53'	22	3.2	4.7
30	06/11/11	18:34:46.05	29º56.09',80º25.07'	17	2.1	3.2
31	18/11/11	09:50:37.56	29º51.00',79º54.02'	31	1.4	9.0
32	09/12/11	08:22:47.12	29º51.25',80º29.84'	10	4.3	2.9
33	09/02/12	19:17:31.65	30º40.00',79º35.62'	25	5.4	6.2
34	26/02/12	22:57:01.35	29º45.16',80º35.62'	25	7.9	4.5
35	26/02/12	23:06:05.92	29º40.42',80º48.93'	16	1.8	3.6
36	17/06/12	07:44:29.32	29º53.87',80º20.34'	19	1.4	8.4
37	16/03/12	15:22:42.07	29º54.67',80º04.02'	12	3.5	5.2
38	16/03/12	19:35:50.36	29º50.84',79º50.52'	20	7.6	4.3
39	08/04/12	07:38:14.81	29º57.69',80º15.93'	14	9.8	4.2
40	10/05/12	22:00:38.82	30º07.20',79º35.14'	17	5.4	3.4

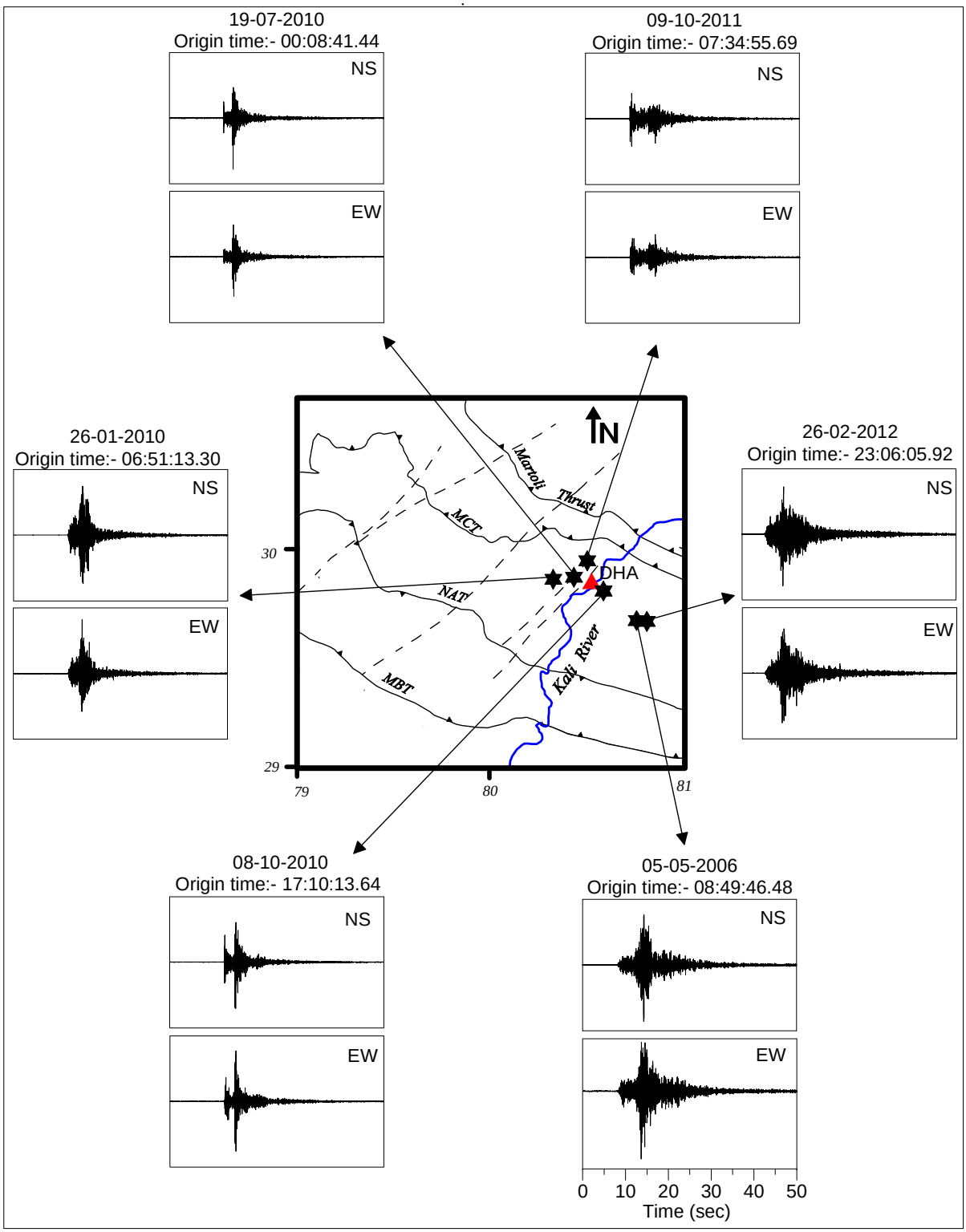

Figure 5.11: Normalize processed NS and EW component of accelerograms of the events used at Dharchula station. Star denotes the epicenter of events. Triangle shows the location of recording station. The tectonics of the region is taken after GSI (2000).

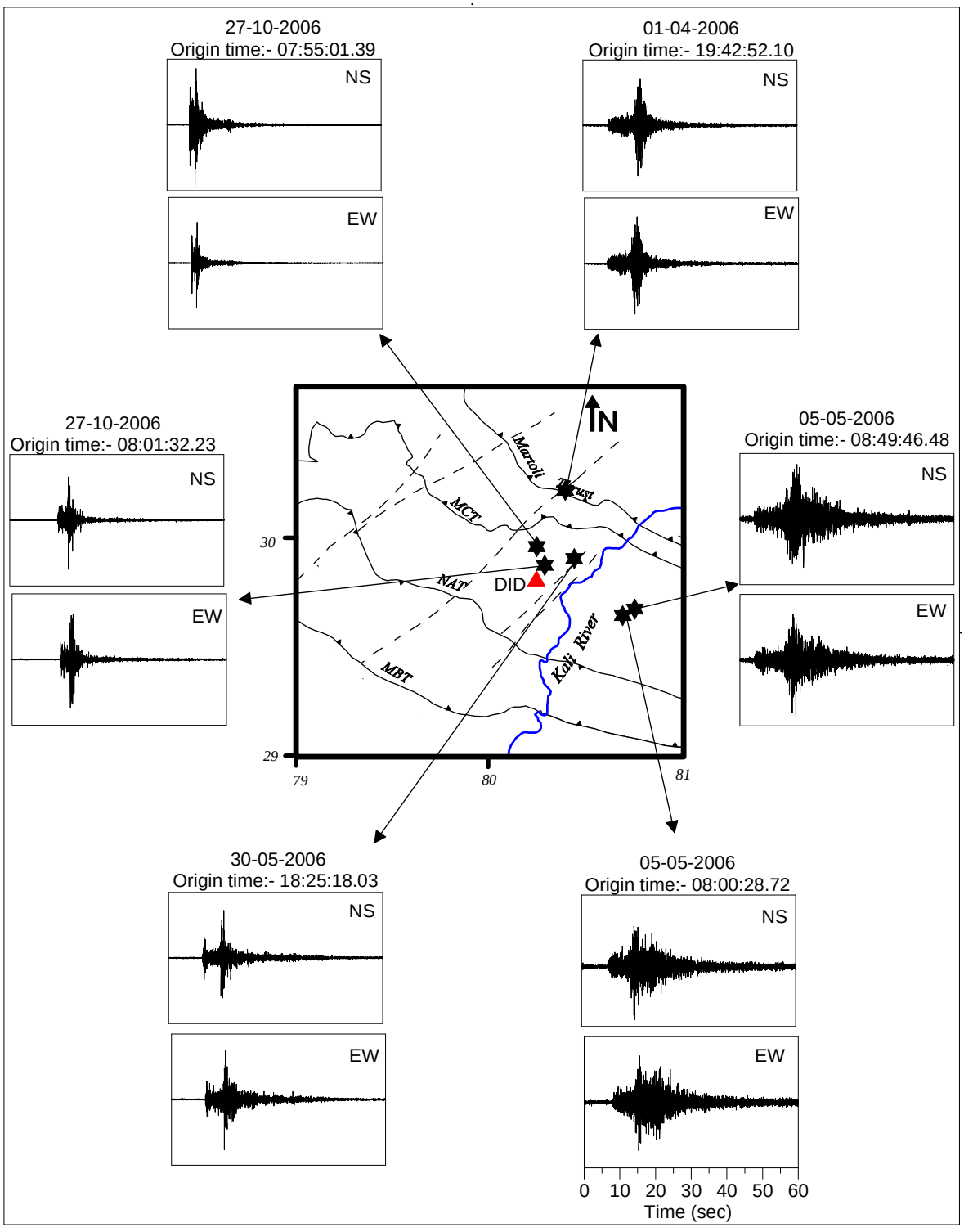

Figure 5.12: Normalize processed NS and EW component of accelerograms of the events used at Didihat station. Star denotes the epicenter of events. Triangle shows the location of recording station. The tectonics of the region is taken after GSI (2000).

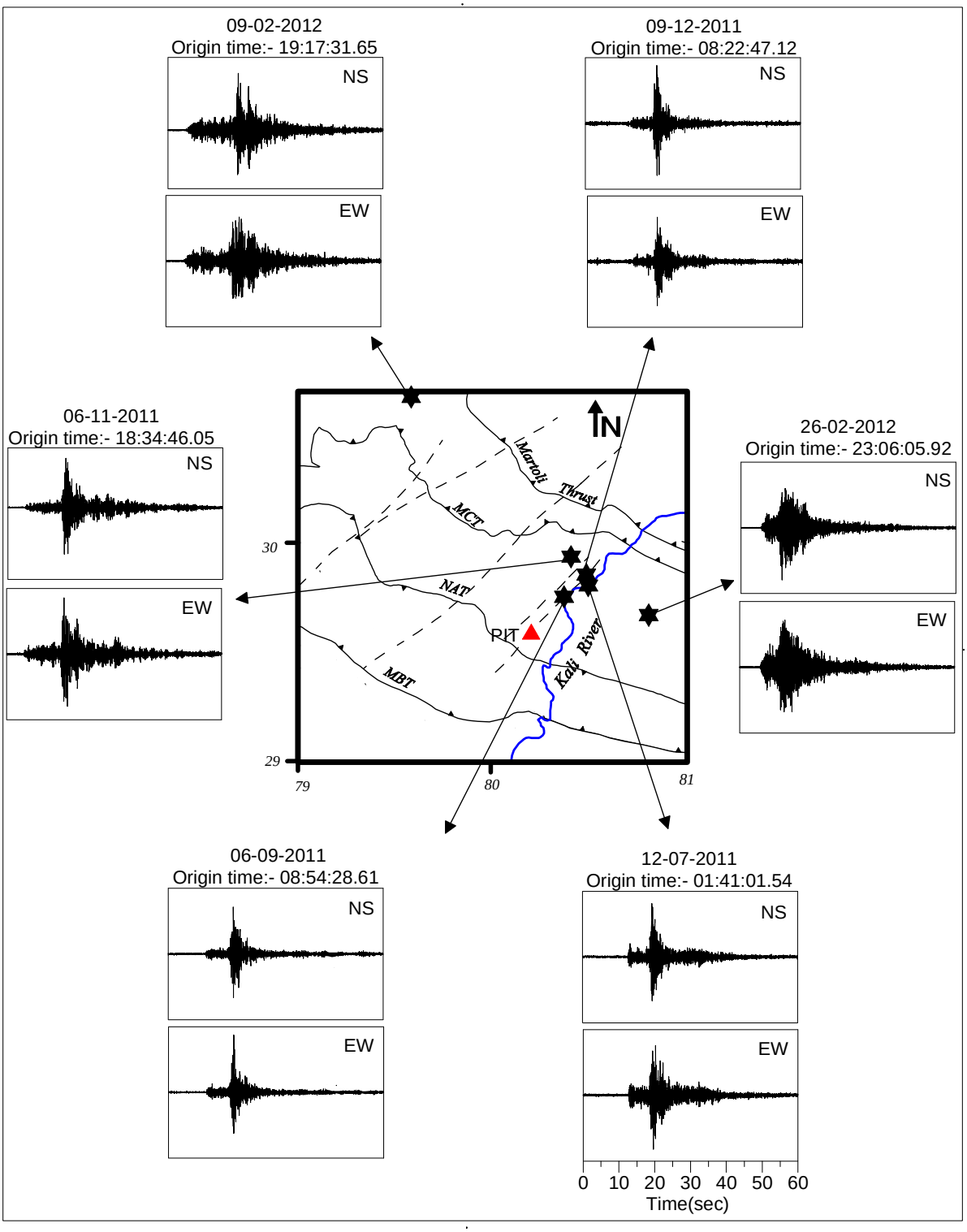

Figure 5.13: Normalize processed NS and EW component of accelerograms of the events used at Pithoragarh station. Star denotes the epicenter of events. Triangle shows the location of recording station. The tectonics of the region is taken after GSI (2000).

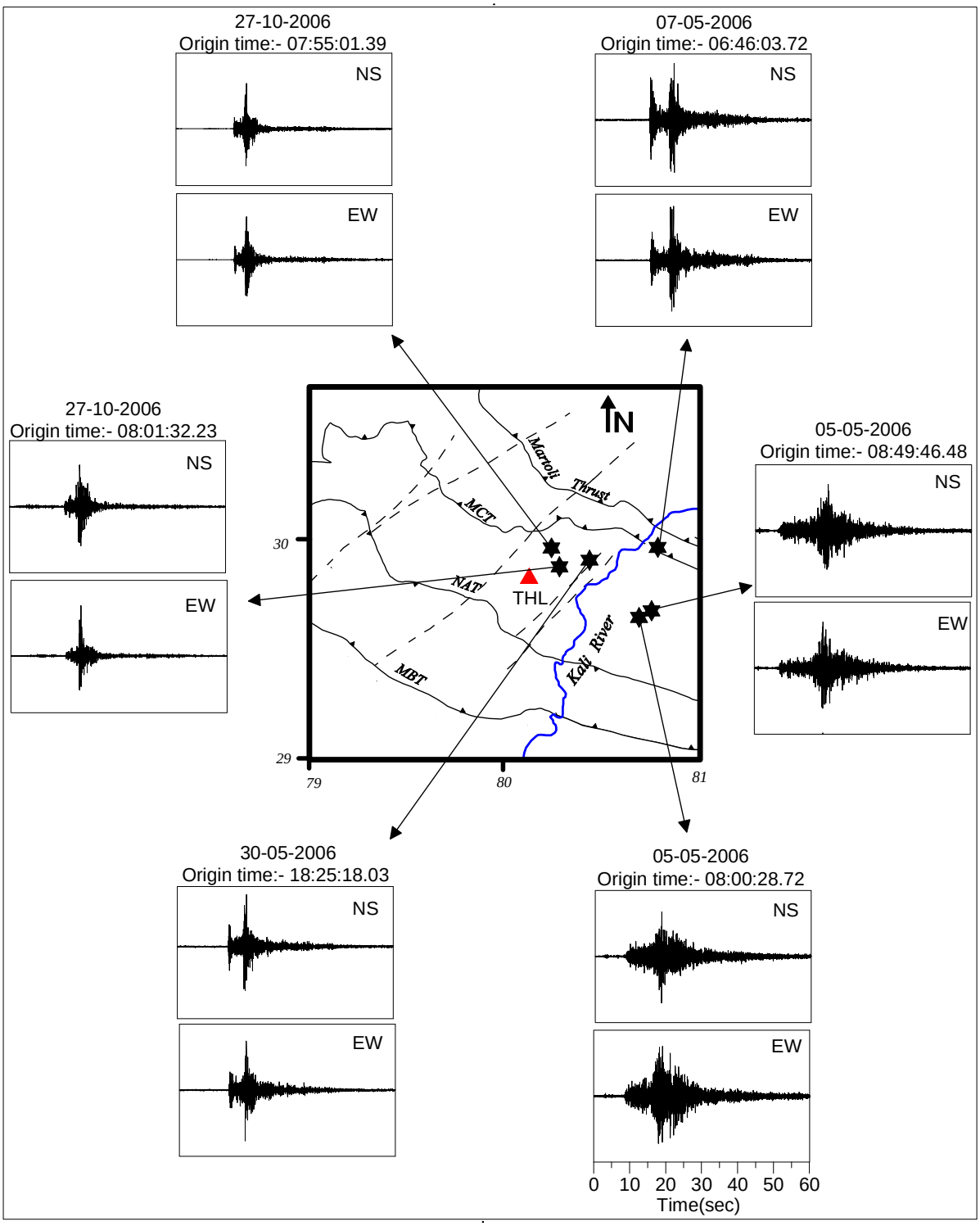

Figure 5.14: Normalize processed NS and EW component of accelerograms of the events used at Thal station. Star denotes the epicenter of events. Triangle shows the location of recording station. The tectonics of the region is taken after GSI (2000).

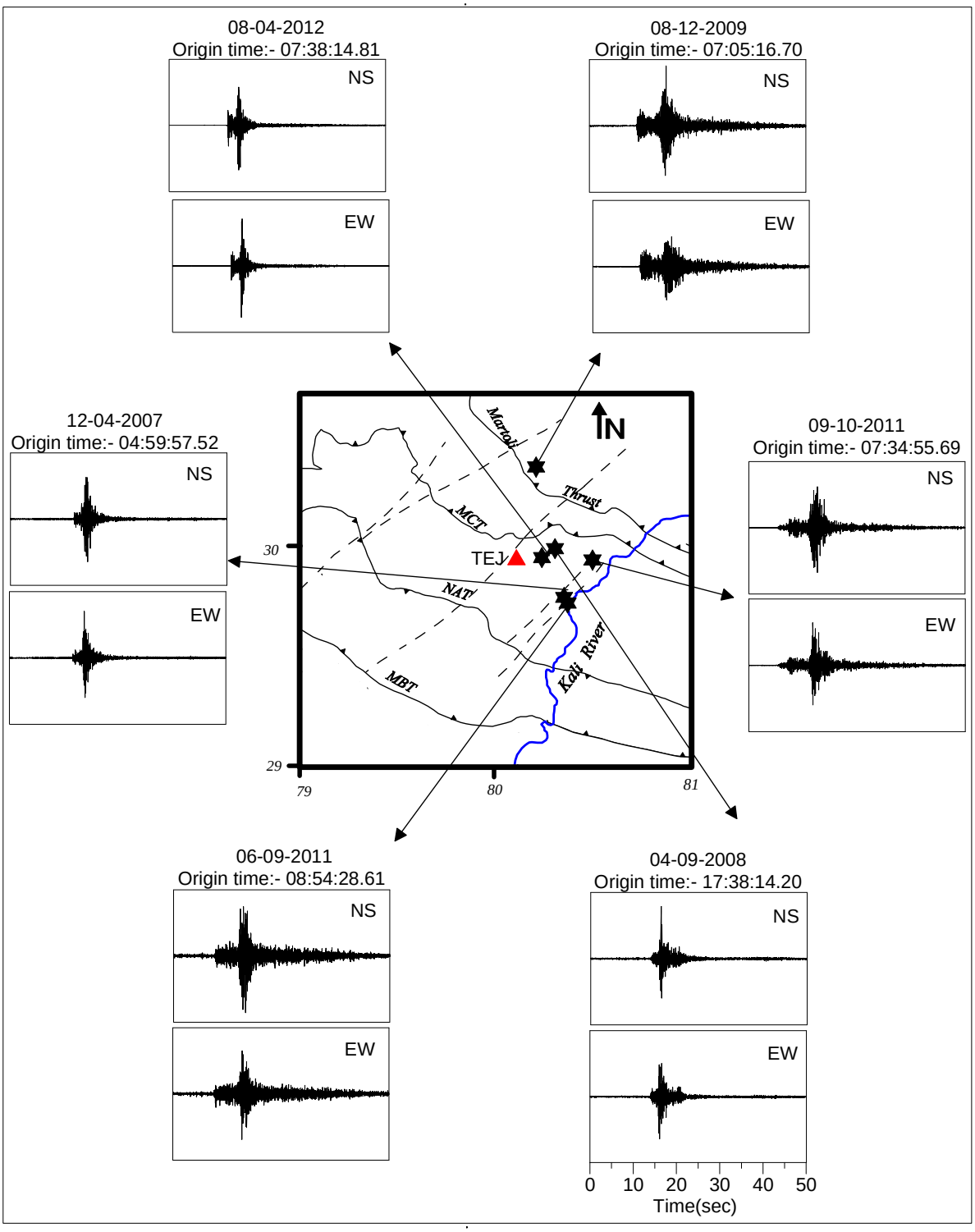

Figure 5.15: Normalize processed NS and EW component of accelerograms of the events used at Tejam station. Star denotes the epicenter of events. Triangle shows the location of recording station. The tectonics of the region is taken after GSI (2000).

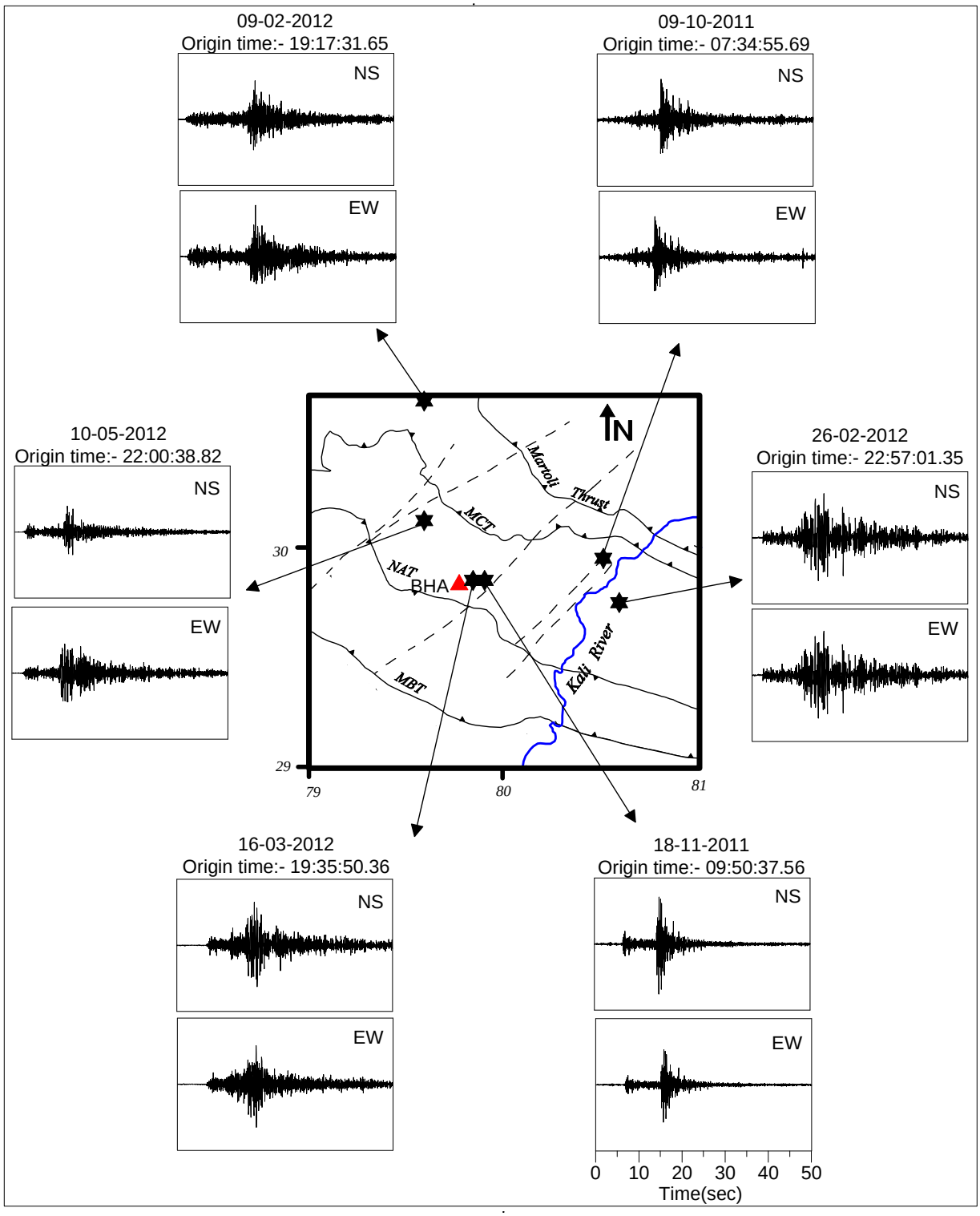

Figure 5.16: Normalize processed NS and EW component of accelerograms of the events used at Bhageshwar station. Star denotes the epicenter of events. Triangle shows the location of recording station. The tectonics of the region is taken after GSI (2000).

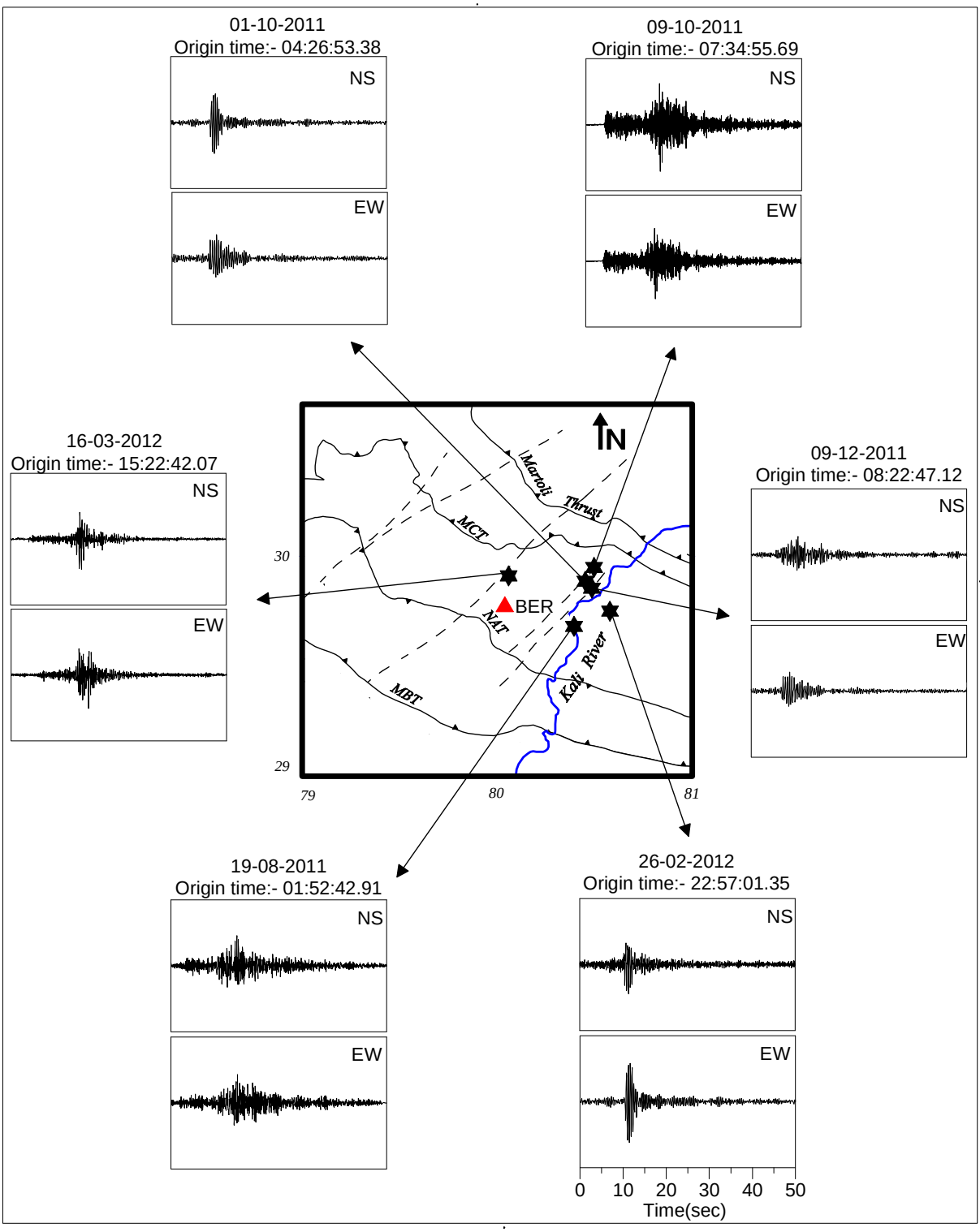

Figure 5.17: Normalize processed NS and EW component of accelerograms of the events used at Berinag station. Star denotes the epicenter of events. Triangle shows the location of recording station. The tectonics of the region is taken after GSI (2000).

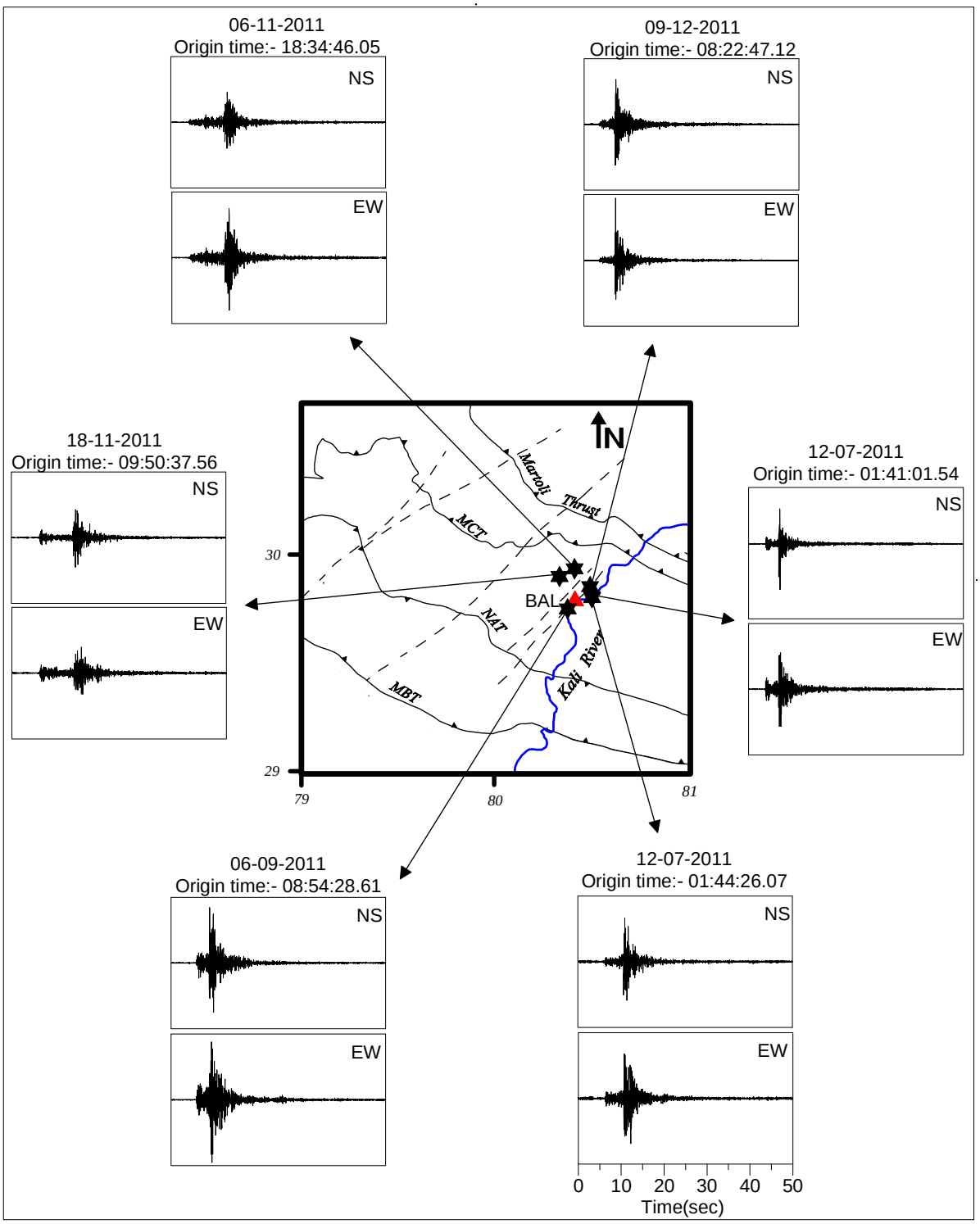

Figure 5.18: Normalize processed NS and EW component of accelerograms of the events used at Baluakot station. Star denotes the epicenter of events. Triangle shows the location of recording station. The tectonics of the region is taken after GSI (2000).

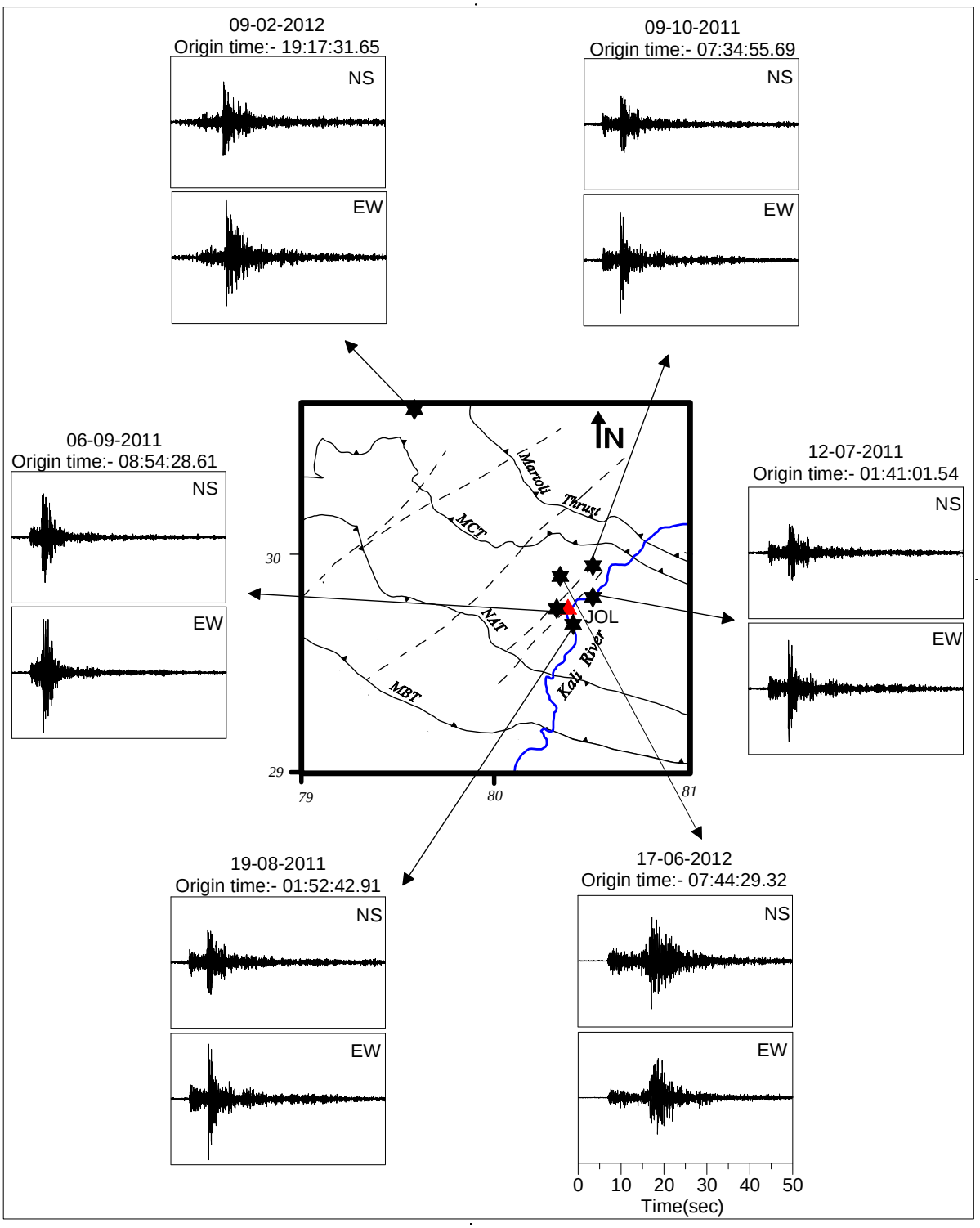

Figure 5.19: Normalize processed NS and EW component of accelerograms of the events used at Jouljibi station. Star denotes the epicenter of events. Triangle shows the location of recording station. The tectonics of the region is taken after GSI (2000).

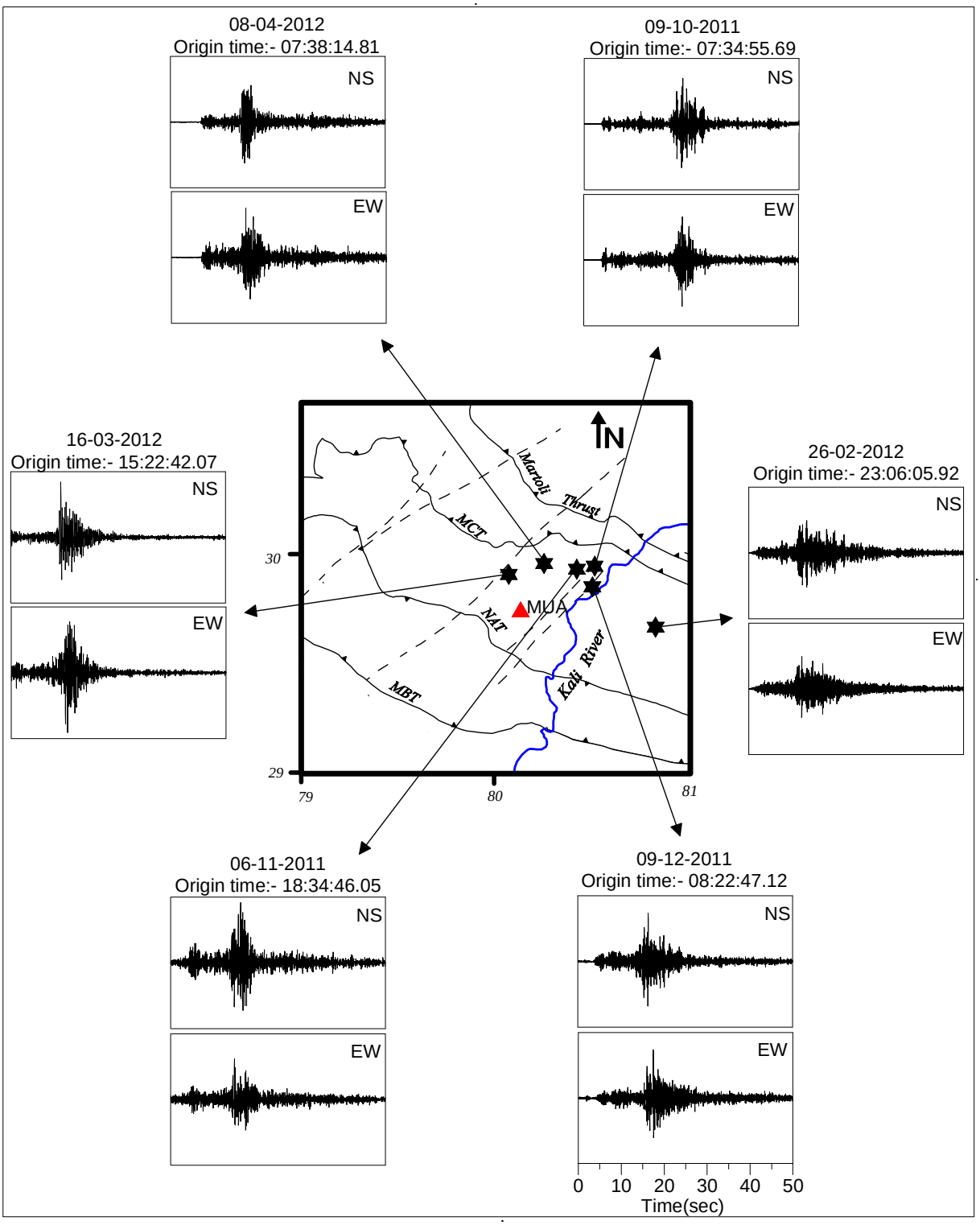

Figure 5.20: Normalize processed NS and EW component of accelerograms of the events used at Muavani station. Star denotes the epicenter of events. Triangle shows the location of recording station. The tectonics of the region is taken after GSI (2000).

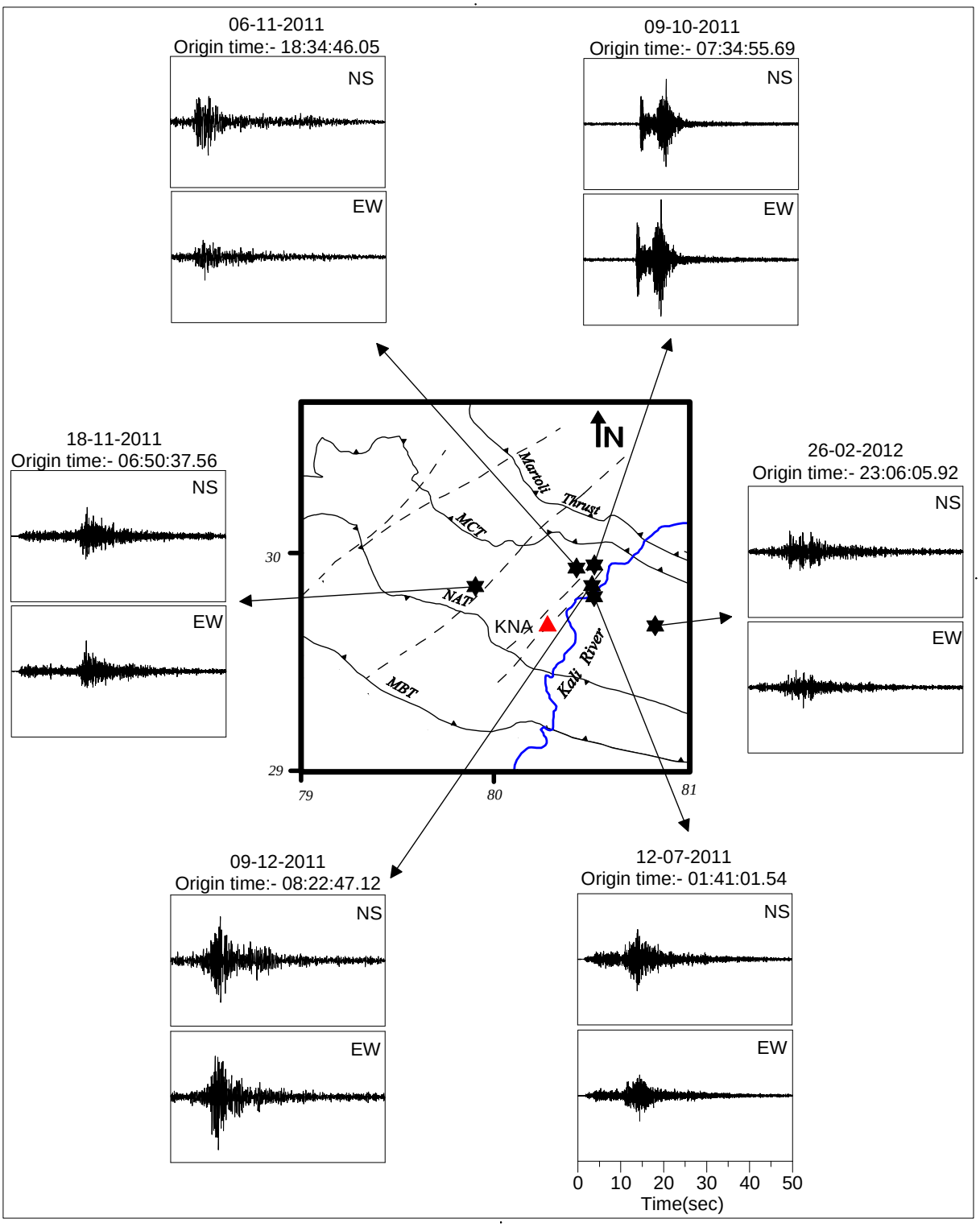

Figure 5.21: Normalize processed NS and EW component of accelerograms of the events used at Knalichhina station. Star denotes the epicenter of events. Triangle shows the location of recording station. The tectonics of the region is taken after GSI (2000).

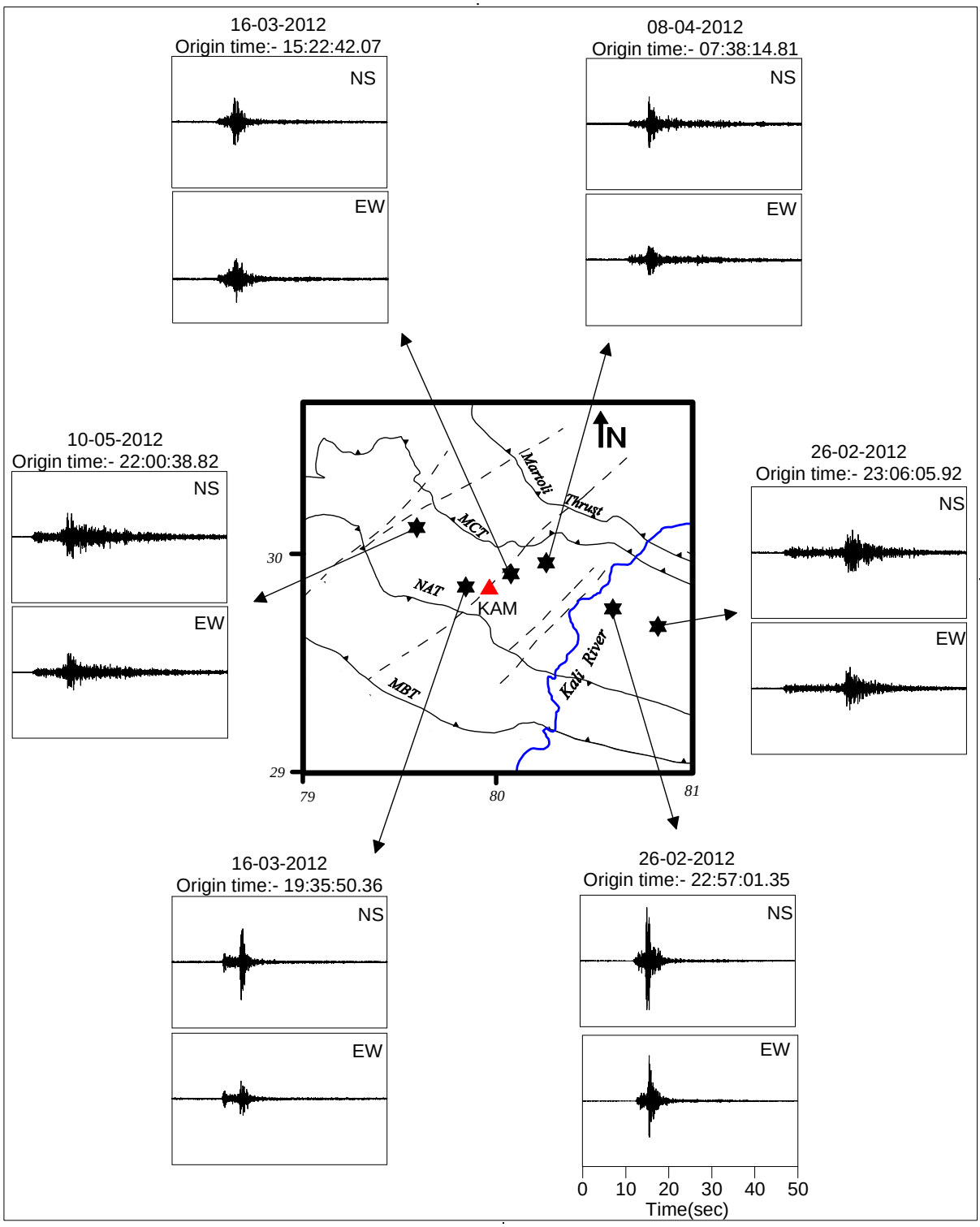

Figure 5.22: Normalize processed NS and EW component of accelerograms of the events used at Kamedidevi station. Star denotes the epicenter of events. Triangle shows the location of recording station. The tectonics of the region is taken after GSI (2000).

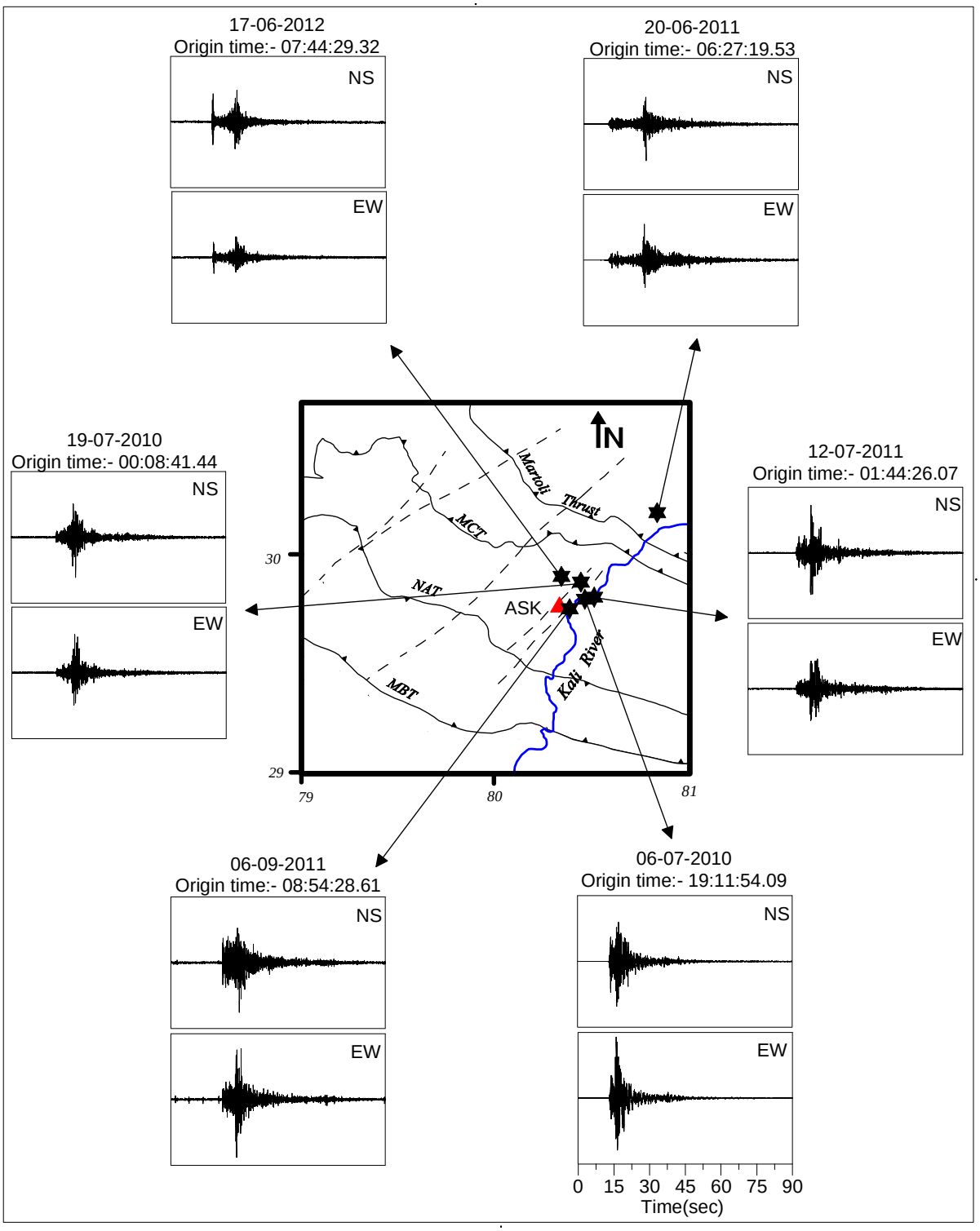

Figure 5.23: Normalize processed NS and EW component of accelerograms of the events used at Askot station. Star denotes the epicenter of events. Triangle shows the location of recording station. The tectonics of the region is taken after GSI (2000).

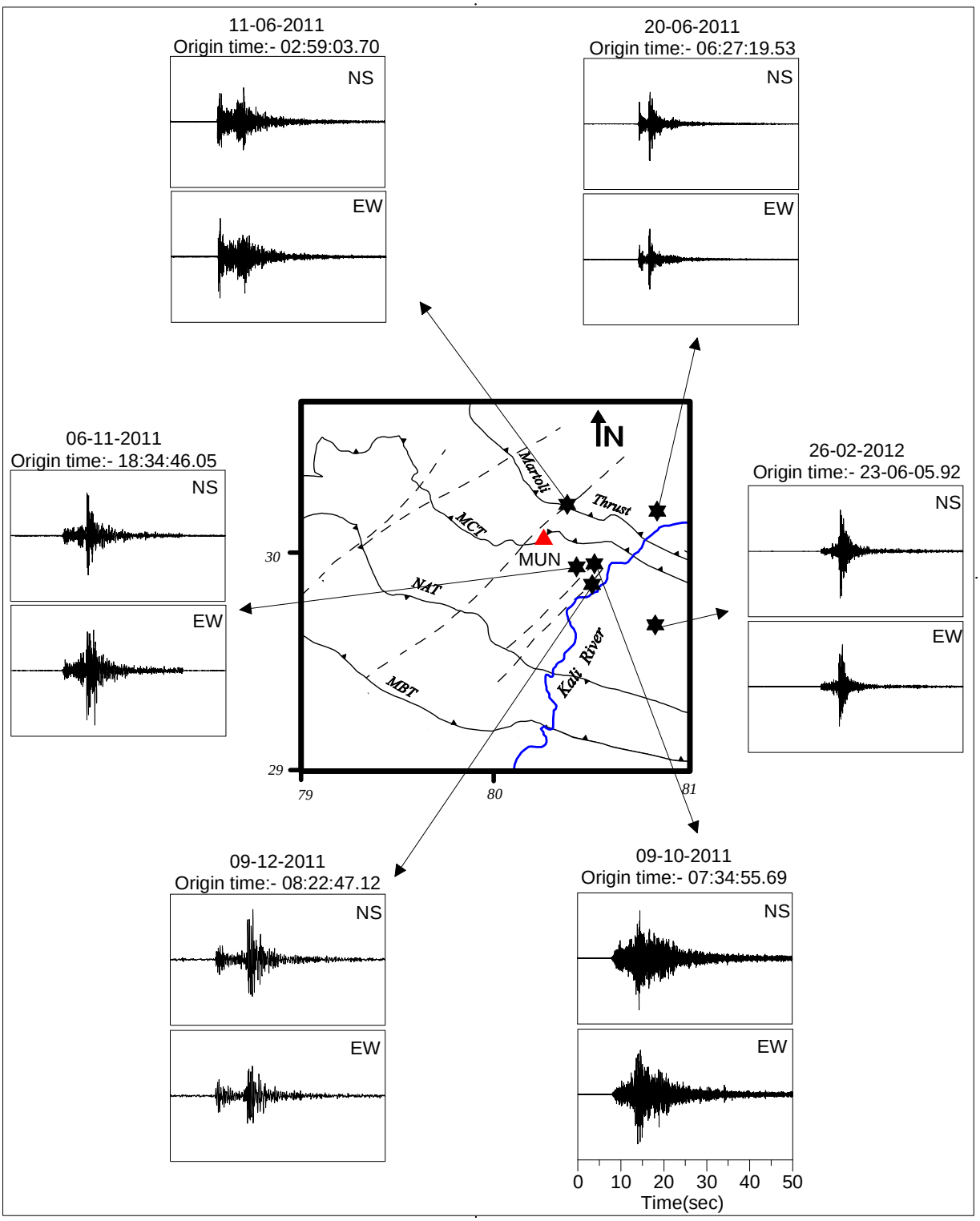

Figure 5.24: Normalize processed NS and EW component of accelerograms of the events used at Munsyari station. Star denotes the epicenter of events. Triangle shows the location of recording station. The tectonics of the region is taken after GSI (2000).

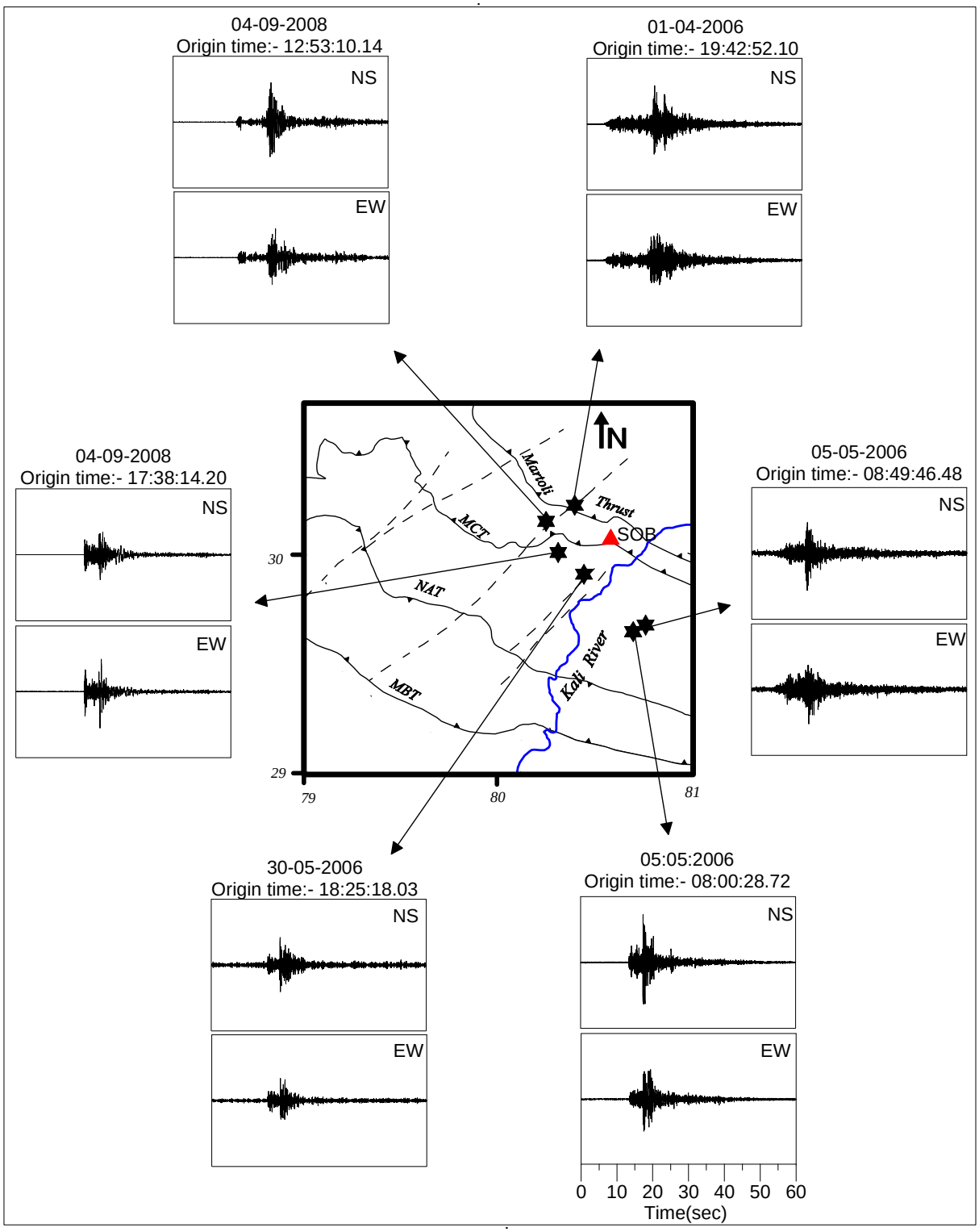

Figure 5.25: Normalize processed NS and EW component of accelerograms of the events used at Sobla station. Star denotes the epicenter of events. Triangle shows the location of recording station. The tectonics of the region is taken after GSI (2000).

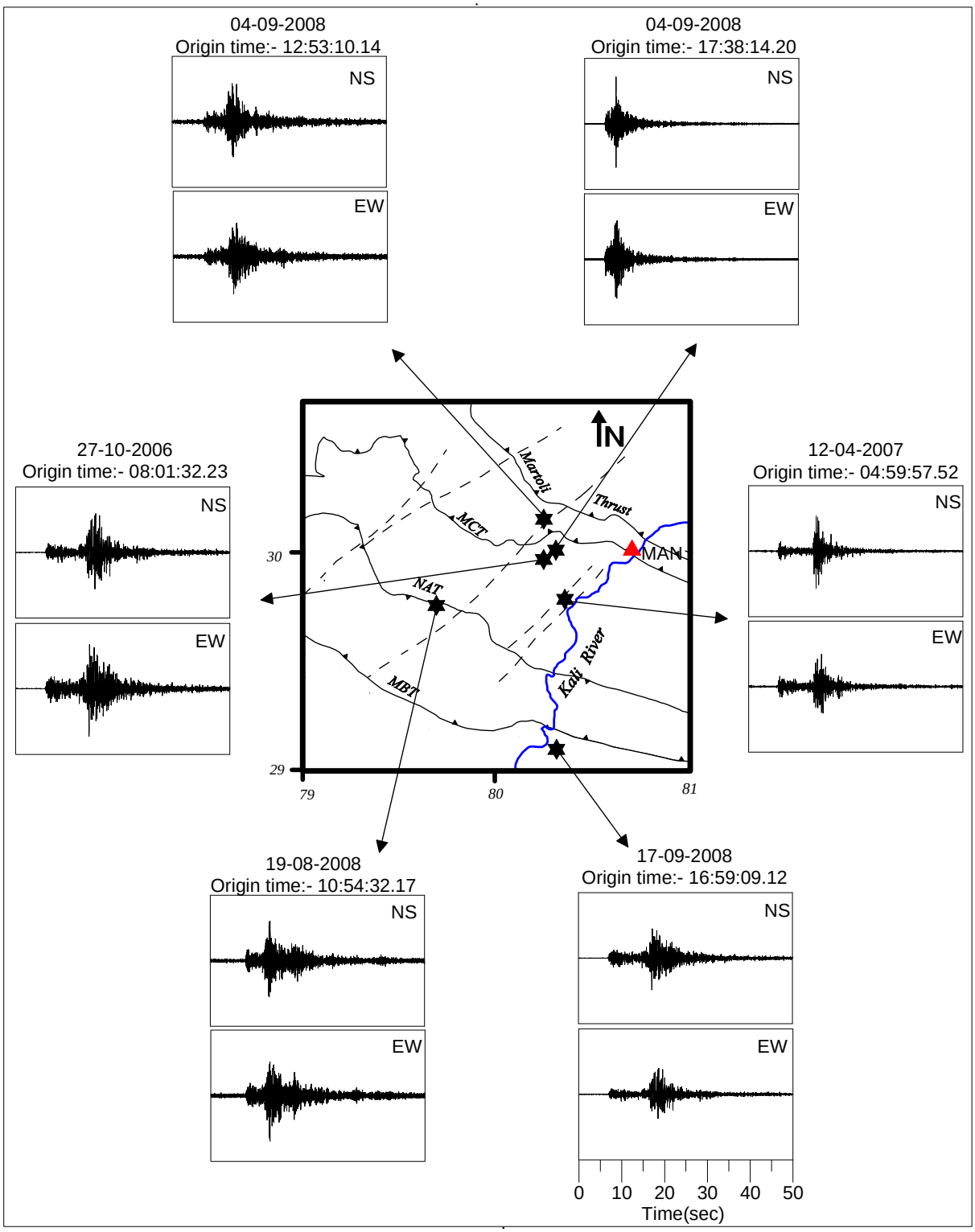

Figure 5.26: Normalize processed NS and EW component of accelerograms of the events used at Mangti station. Star denotes the epicenter of events. Triangle shows the location of recording station. The tectonics of the region is taken after GSI (2000).

A time window which starts from the onset of S phase and end before the arrival of low frequency surface wave in the record and which cover entire S phase has been applied to the corrected accelerogram. Selection of S phase is based on visual inspection of entire accelerogram. This sampled window is cosine tapered with 10% taper at both end (Sharma and Wason, 1994). This windowed time series is passed through a FFT operator for computing its Fourier transform. For computing Fourier transform in the present work, the FFT algorithm given by Cooley and Tukey, (1965) has been used. The FFT algorithm gives Fourier transform 'X(k)' of a real time signal 'x(n)' by following expression:

$$X(k) = \sum_{n=0}^{N-1} e^{\frac{-2\pi i n k}{N}} .x(n) \tag{5.1}$$

where, 'X(k)' represent a complex series in frequency domain and in the present work amplitude spectrum 'A_m(k)' is calculated from 'X(k)' by using following formula:

$$A_m(k) = \sqrt{[X_R(k)]^2 + [X_I(k)]^2} \tag{5.2}$$

where, 'X_R(k)' and 'X_I(k)' represent real and imaginary part of the complex function 'X(k)' obtained in frequency domain. The obtained spectrum is further smoothened using Laplacian operator before using it as an input to the present algorithm. The complete process of obtaining spectral amplitude from processed time series is shown in Fig. 5.27. In the present work both horizontal component i.e. North South (NS) and East West (EW) of strong ground motion has been used for inversion.

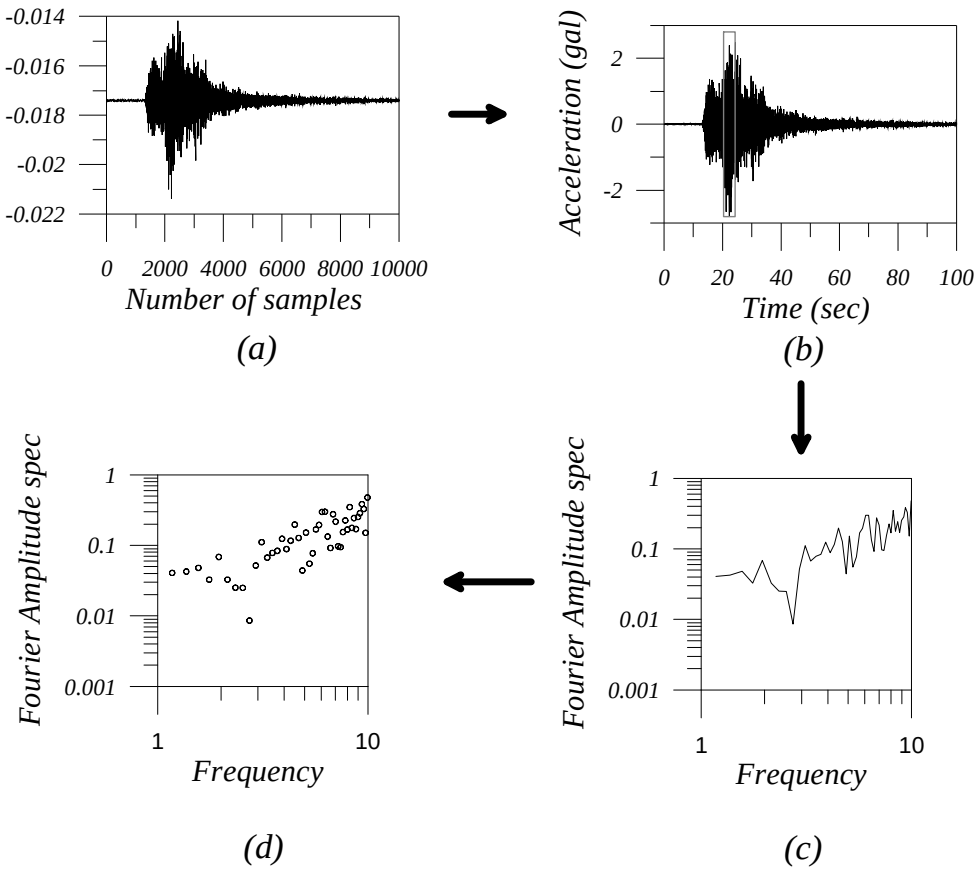

Figure 5.27: (a) Unprocessed accelerogram of 5/05/06 event recorded at Dharchula station, (b) processed accelerogram at Dharchula station with rectangular block showing S-phase, (c) acceleration spectrum of S phase marked by rectangular block with a time window of 4.0 sec, (d) Discrete value of acceleration spectra used for present inversion. The discrete values of acceleration spectra are shown by small circles.

5.4 Results and discussion

The discrete value of acceleration spectrum of S-phase at different frequency is used as input to the algorithm developed for calculation of shear wave quality factor and site effects at each station simultaneously. First part of inversion consist of calculation of seismic moment by using initial value of $Q_\beta(f)$. The obtained seismic moment is further used as input to the algorithm to obtain $Q_\beta(f)$ and site amplification term. In this step of iterative inversion procedure the acceleration spectra is corrected for site effects and $Q_\beta(f)$ obtained from inversion and seismic moment is calculated from source displacement spectra. The process is repeated till minimum root mean square error is obtained. The complete algorithm is already discussed in Chapter 3.

5.4.1 Site effects

The data used in the present work consist of various events which have been recorded at different stations. Seismic moment of input event has been determined from the source displacement spectra of two horizontal components of acceleration record of each event recorded at different stations using the methodology define in Chapter 3. The average seismic moment for each event is calculated by using all values of seismic moment at different stations. The initial value of $Q_\beta(f)$ used for obtaining source spectra is that given by Joshi et al. (2012a) for the Kumaon Himalaya. The obtained source spectra for an event recorded at four different stations are shown in Fig. 5.28.

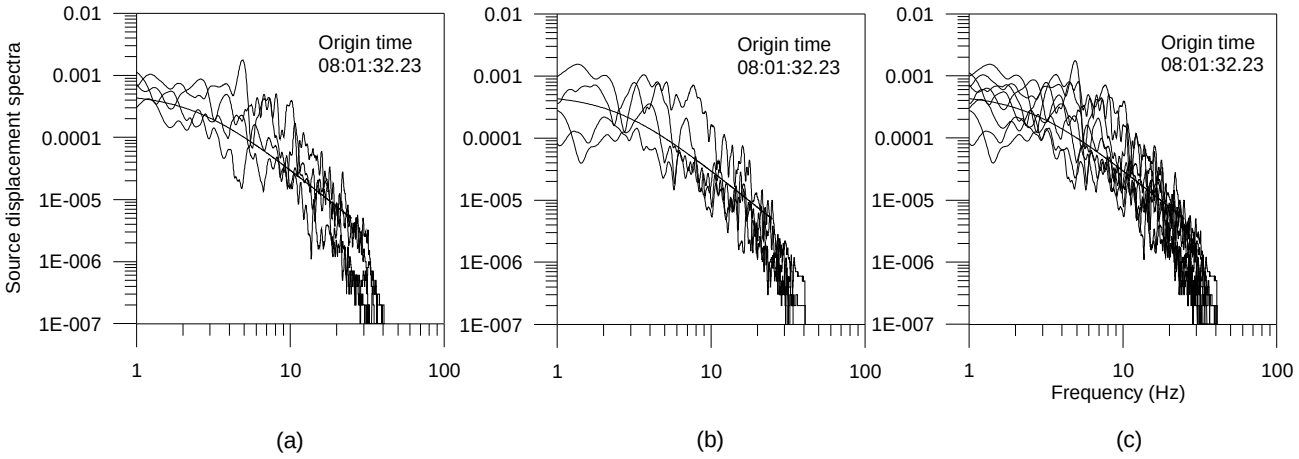

Figure 5.28: (a), (b) and (c) are the obtained source displacement spectra for an event recorded at four different stations for NS, EW and both components, respectively. Solid line indicates the theoretical spectra defined by Aki (1967).

Average value of seismic moment computed from two horizontal components recorded at several stations is used as an input to the first part of inversion together with the spectra of S phase in the acceleration record. Several values of the corner frequency have been selected iteratively and are used as input to the inversion algorithm. Root mean square in the obtained and observed data is calculated for each case and the solution corresponding to minimum RMSE gives direct estimate of $Q_\beta(f)$ relation together with the value of corner frequency. Basic equation of acceleration spectra of shear waves at a distance R due to an earthquake of seismic moment M_o used for present inversion algorithm is given below (Boore, 1983 and Atkinson and Boore, 1998):

$$A(f) = C\, S\, (f)\, D(f) \qquad (5.3)$$

where, the ‘C’ term is constant at a particular station for a given earthquake, S(f) represents the source acceleration spectra and D(f) denotes a frequency-dependent diminution function which takes into account the anelastic attenuation and attenuation due to geometrical spreading. One of the important requirements of using eq. (5.3) for inversion is that the acceleration spectrum shown in the left hand side of equation should be free from site amplifications. This can be achieved in two ways (1) by using records from those stations where site amplifications are not effective within the range of frequencies required for the inversion (i.e. rock site) or (2) by removing the site amplifications directly from the acceleration spectra. The first approach is not feasible in this study, as enough information about the site characteristics is not available at each strong motion site. Use of the second approach is more suitable for this study therefore the inversion process is divided into two sub-inversions to save computer memory and processing time. In the first part of inversion spectral acceleration data, seismic moment and corner frequency is used as input parameters. Several possibilities of corner frequencies are checked for each input event in this part of inversion. Final values are selected on the basis of minimum RMSE. The obtained value of corner frequency is used to compute theoretic source spectrum and residual is treated as site amplification term. Different site amplification curves are obtained at each station depending upon number of input events. Average value of site amplification obtained from inversion is used for correcting the acceleration record.

Shear wave quality factor at each station is calculated using both the NS and EW component of acceleration records. Direct seismological evidences of nonlinear site effects were reported by using spectral ratio techniques (Wen, 1994). Therefore in an attempt to check whether the residual make sense as a site amplification filter, the technique proposed by Lermo and Chavez-Garcia (1993) to obtain site amplification curves have been used. In this technique, the amplitude spectrum of the horizontal-component is divided by the amplitude spectrum of vertical-component at each station to obtain the frequency-dependent site response. This technique is analogous to the receiver function technique applied in the studies of the upper mantle and crust from teleseismic records (Langston, 1979). This method is also similar to the Nakamura (1988) method of computing site amplification factors using H/V ratio at single station. The site amplifications obtained at different stations after inversion and its comparison with H/V ratio method is shown in Fig. 5.29. This comparison clearly shows that residual make sense as site amplification term as it lies within the range of site amplification term obtained by other method.

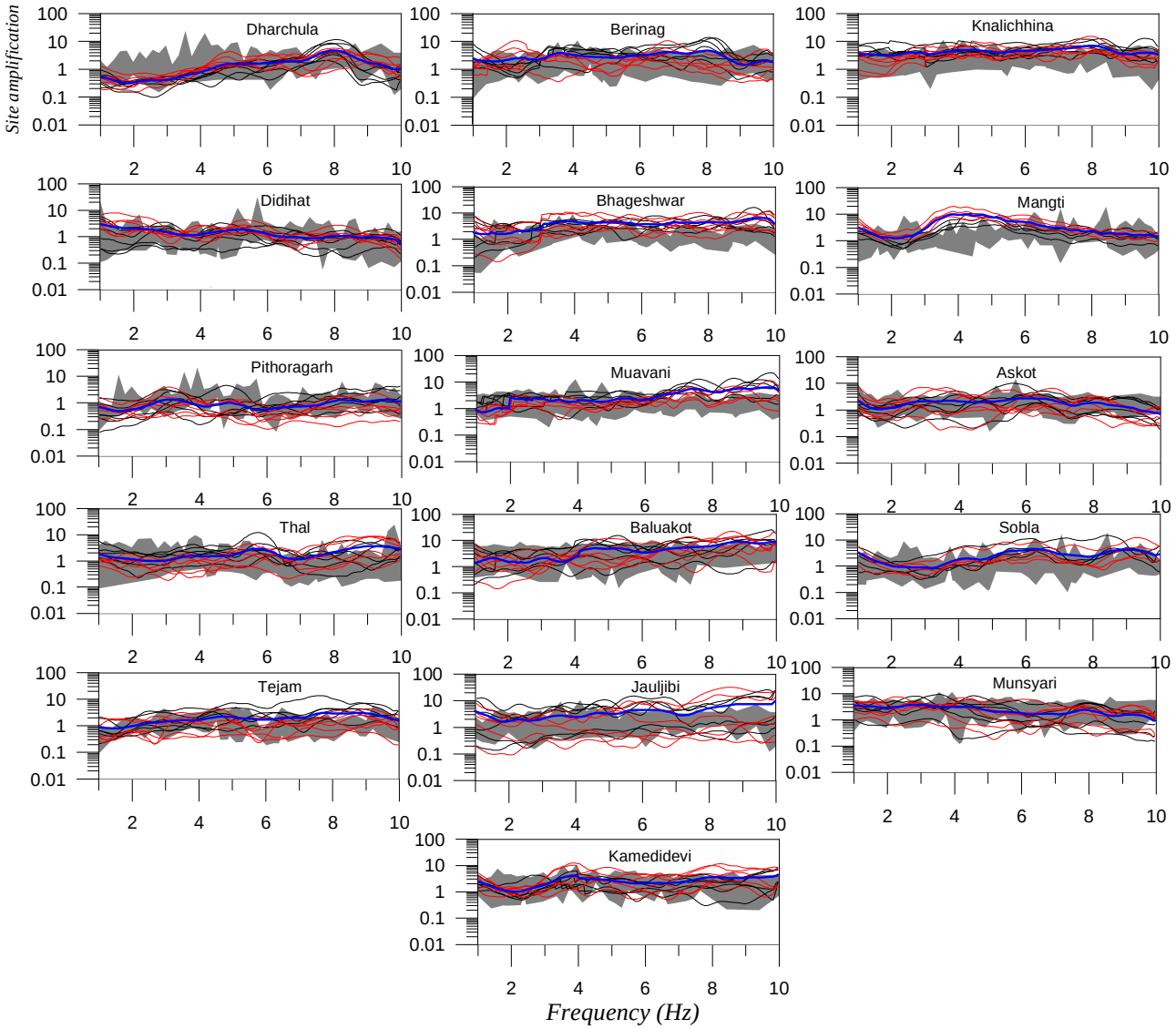

Figure 5.29: Site effect at the sixteen recorded stations. The black and red lines show the site effects obtained by inversion of acceleration records of input events for NS and EW component, respectively. Different lines indicated site effect obtained from residual of input acceleration and source spectra. μ and σ describe the mean and standard deviation. The shaded area denotes the region between μ +σ and μ –σ of the site amplification obtained using technique given by Lermo and Chavez-Garcia (1993). Average site amplification term obtained by inversion is shown by the blue line. Parameters 'μ' and 'σ' describe the mean and standard deviation, respectively.

5.4.2 Frequency dependent shear wave quality factor $Q_\beta(f)$

In the present work six events at each station have been used for inversion process. The iterative inversion is performed at each station independently. The $Q_\beta(f)$ relation of form $Q_o f^n$ obtained by using all value of $Q_\beta(f)$ obtained from inversion of NS and EW record at each station

is shown in Fig. 5.30 and its value is given in Table 5.3. As the study area is covered mostly by sequences of Lesser Kumaon Himalaya a regional relationship for Kumaon Himalaya has been calculated in the present work. In order to calculate regional $Q_\beta(f)$ relation, values of $Q_\beta(f)$ obtained from inversion of NS and EW component data at each station is further used to obtain a best fit line using least square fitting. Plot of $Q_\beta(f)$ at each station is shown in Fig. 5.31(a). The best fit line gives $Q_\beta(f) = (28\pm2.1)f^{(1.2\pm0.09)}$ which represent regional attenuation characteristics of Kumaon Himalaya. The deviation of Q_0 and 'n' with respect to their mean values is shown in Fig. 5.31(b) and (c), respectively. The shaded area in Fig. 5.31(b) and 5.31(c) denotes the region between $(\mu+\sigma)$ and $(\mu-\sigma)$. It is seen that the calculated value of Q_o for shear wave attenuation varies in between 28±2.1 and 'n' varies in between 1.2±0.09 indicating highly heterogeneous and tectonically active region.

Table 5.3: The $Q_\beta(f)$ relationship and RMS error obtained at different stations using NS and EW component data. Final $Q_\beta(f)$ relation at each station is developed by using the value of $Q_\beta(f)$ obtained from NS and EW component separately.

Stations	**Obtained result for NS component**		**Obtained result for EW component**		**Final $Q_\beta(f)$ relation using value of $Q_\beta(f)$ obtained from NS and EW component separately**
	$Q_\beta(f)$ Relation	**RMSE**	**$Q_\beta(f)$ Relation**	**RMSE**	**$Q_\beta(f)$ Relation**
Dharchula	$(17\pm4.6)f^{(0.8\pm0.33)}$	0.0226	$(18\pm6.6)f^{(0.7\pm0.17)}$	0.0166	$(21\pm5.0)f^{(0.7\pm0.23)}$
Didihat	$(24\pm3.3)f^{(1.4\pm0.13)}$	0.0481	$(22\pm7.7)f^{(1.4\pm0.09)}$	0.0680	$(35\pm7.0)f^{(1.1\pm0.15)}$
Pithoragarh	$(40\pm5.0)f^{(0.8\pm0.10)}$	0.0134	$(33\pm8.3)f^{(1.3\pm0.10)}$	0.0478	$(39\pm3.5)f^{(1.1\pm0.15)}$
Thal	$(26\pm8.0)f^{(1.4\pm0.10)}$	0.0652	$(29\pm5.6)f^{(1.4\pm0.14)}$	0.0826	$(35\pm8.0)f^{(1.2\pm0.21)}$
Tejam	$(21\pm3.4)f^{(0.9\pm0.19)}$	0.0478	$(19\pm5.4)f^{(1.3\pm0.16)}$	0.1188	$(20\pm2.6)f^{(1.1\pm0.22)}$
Bhageshwar	$(34\pm4.1)f^{(1.2\pm0.10)}$	0.0328	$(41\pm5.1)f^{(1.2\pm0.12)}$	0.0212	$(39\pm4.7)f^{(1.2\pm0.11)}$
Berinag	$(15\pm2.1)f^{(1.3\pm0.15)}$	0.0566	$(23\pm2.2)f^{(1.2\pm0.09)}$	0.0360	$(21\pm5.7)f^{(1.2\pm0.11)}$
Baluakot	$(16\pm2.6)f^{(1.1\pm0.11)}$	0.0697	$(13\pm2.8)f^{(1.3\pm0.20)}$	0.0881	$(16\pm3.0)f^{(1.2\pm0.12)}$
Jauljibi	$(10\pm0.8)f^{(1.3\pm0.12)}$	0.0425	$(8\pm1.1)f^{(1.3\pm0.12)}$	0.0597	$(10\pm2.9)f^{(1.3\pm0.12)}$
Muavani	$(17\pm2.9)f^{(1.4\pm0.14)}$	0.1946	$(24\pm4.5)f^{(1.3\pm0.17)}$	0.3576	$(19\pm3.5)f^{(1.3\pm0.07)}$
Knalichhina	$(22\pm2.9)f^{(1.3\pm0.10)}$	0.0682	$(19\pm2.9)f^{(1.4\pm0.12)}$	0.0572	$(22\pm3.0)f^{(1.3\pm0.09)}$
Kamedidevi	$(27\pm4.4)f^{(1.0\pm0.09)}$	0.0863	$(24\pm4.2)f^{(0.9\pm0.07)}$	0.0783	$(25\pm5.4)f^{(0.9\pm0.06)}$
Askot	$(25\pm4.6)f^{(0.8\pm0.09)}$	0.0865	$(30\pm4.3)f^{(0.7\pm0.07)}$	0.0621	$(25\pm5.3)f^{(0.8\pm0.09)}$
Munsyari	$(39\pm5.2)f^{(1.4\pm0.08)}$	0.1259	$(35\pm5.2)f^{(1.5\pm0.09)}$	0.1098	$(44\pm5.6)f^{(1.3\pm0.07)}$
Sobla	$(23\pm2.4)f^{(1.2\pm0.12)}$	0.0578	$(27\pm3.5)f^{(1.1\pm0.11)}$	0.0495	$(27\pm2.4)f^{(1.1\pm0.05)}$
Mangti	$(40\pm7.9)f^{(1.2\pm0.22)}$	0.0742	$(42\pm5.1)f^{(1.2\pm0.10)}$	0.1822	$(33\pm3.7)f^{(1.1\pm0.07)}$

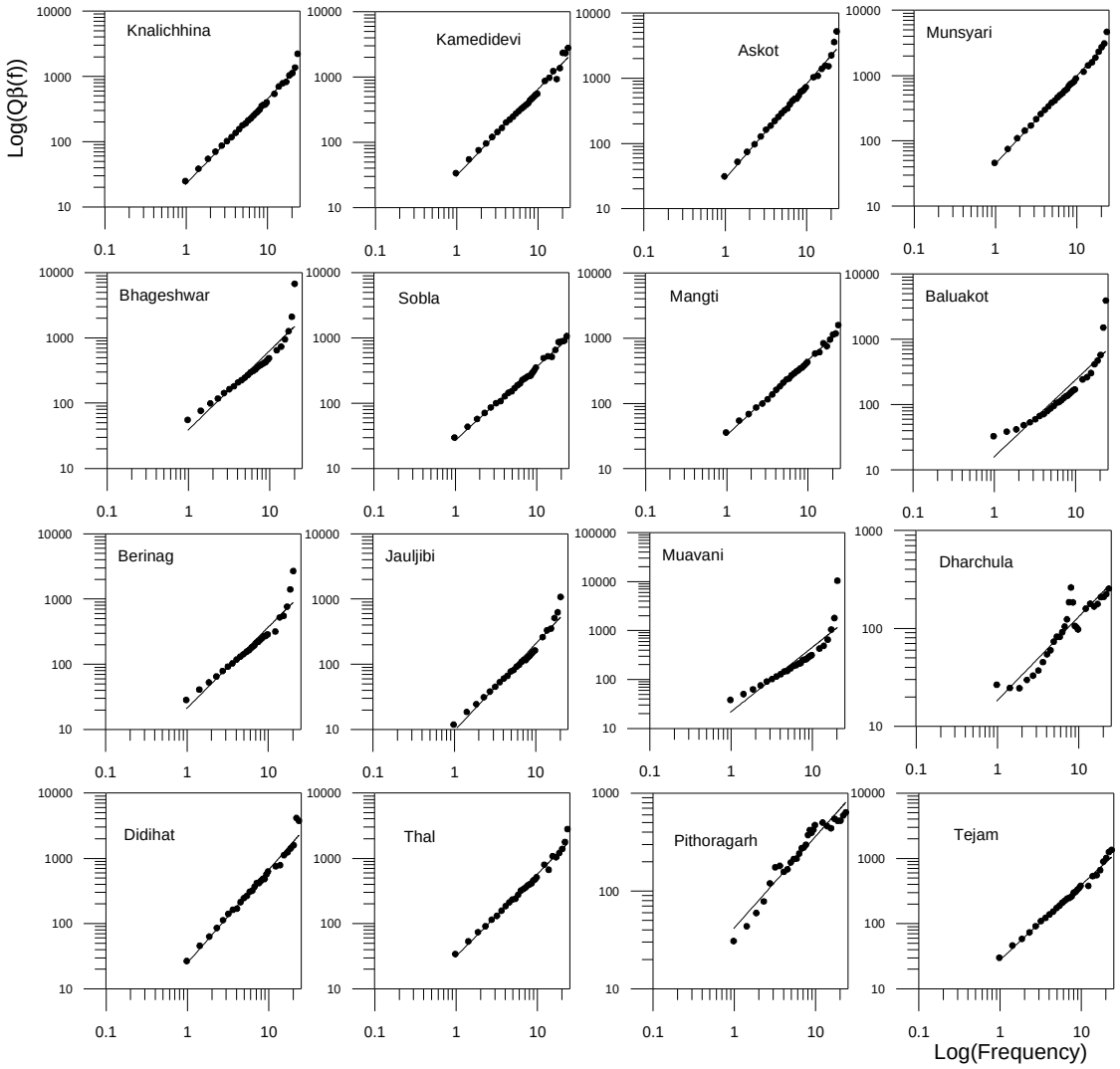

Figure 5.30: Obtained $Q_\beta(f)$ relationship at different stations. The $Q_\beta(f)$ at different frequency is taken from the value obtained after inversion of NS and EW components, respectively.

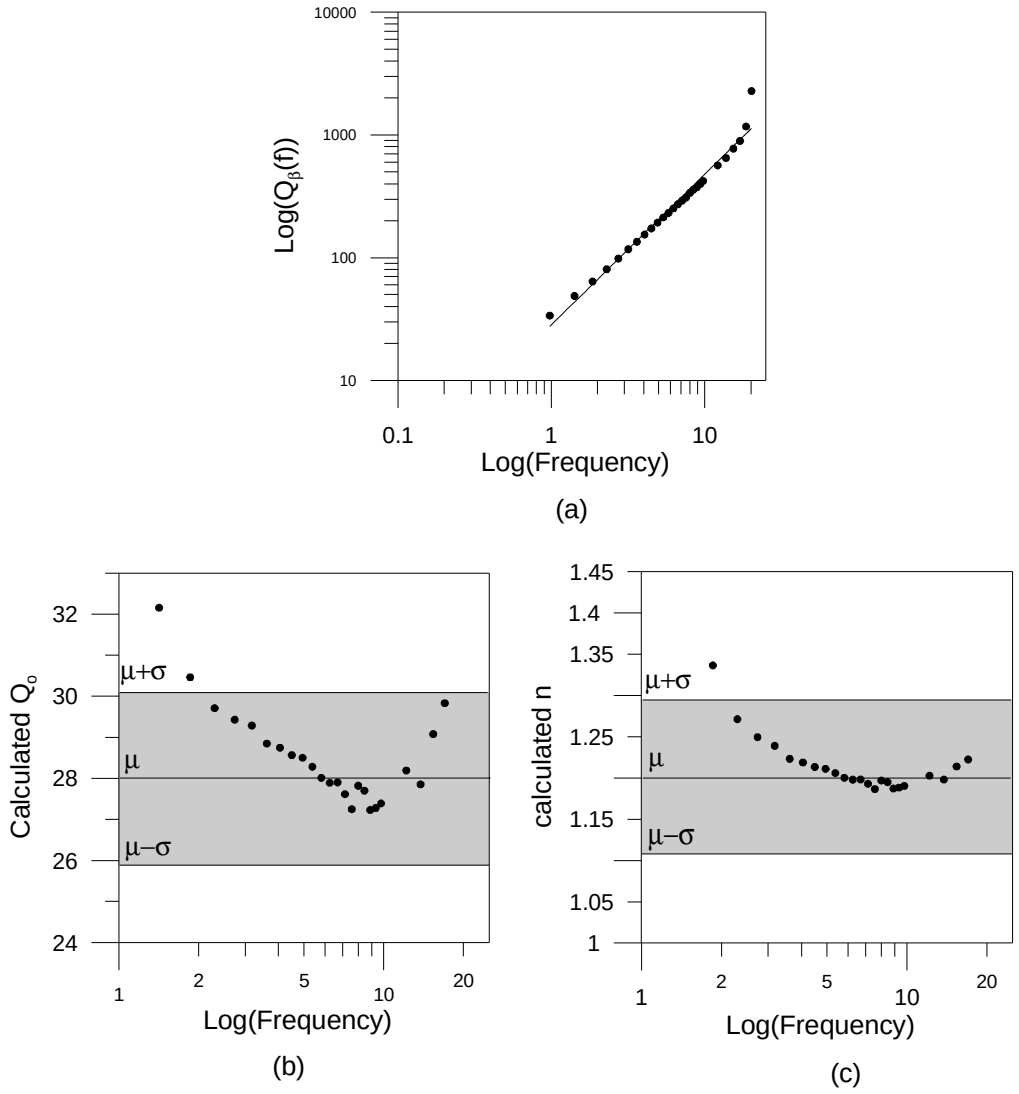

Figure 5.31: (a) Regional $Q_\beta(f)$ relationship for Kumaon Himalaya based on the obtained value of shear wave attenuation at different stations at different frequencies (b) variation of Q_o with respect to its mean value (c) variation of n with respect to its mean value. The shaded area denotes the region between μ +σ and μ -σ. Parameters 'μ' and 'σ' describe the mean and standard deviation, respectively.

The $Q_o f^{n}$ relation can be used for separating different regions into active and stable groups. The parameter 'Q_o' and 'n' in this relation represent heterogeneities and level of tectonic activity of the region, respectively. This relation propose low values of Q_o (<200) for tectonically and seismically active regions and high Q_o (>600) for seismically stable region and intermediate values for moderate regions (Kumar et al., 2005b). Regions with higher 'n' value manifest higher tectonic activity. It is seen from Table 5.4 that for various active regions like Hindukush; Washington; Kagoshima, Japan; Ishikawa, Japan; Mt. Etna Italy and Southern Apennines, Italy etc., Q_o and 'n' varies from 28 to 97 and 0.5 to 1.0, respectively (Roecker et al., 1982; Havskon et

al., 1989; Mamada and Takenaka (2004); Maeda et al., 2008; Giampiccolo et al., 2007 and Cantore et al., 2011). Comparison of present relation with other available relations of Himalaya region is shown in Fig. 5.32(a) and it revealed that the relation obtained in this work falls within the range of values that are justified for tectonically active Himalaya regions. The comparison of the relation developed for the Kumaon Himalaya, India with the world wide active region is shown in Fig. 5.32(b) and suggest that Kumaon Himalaya falls in the active region.

Table 5.4: Q(f) Relationship for Himalaya region, India and worldwide. $Q_c(f)$ and $Q_\beta(f)$ are the Coda-wave quality factor and Shear-wave quality factor, respectively.

Attenuation relation	Region	Reference	Data used
Himalaya region, India			
$\mathbf{Q_c(f)} = 126f^{0.95}$	Garhwal Himlaya, India	Gupta et al. (1995)	Strong motion data
$\mathbf{Q_c(f)} = 30f^{1.21}$	Garhwal, India	Mandal et al. (2001)	Strong motion and broad band data
$\mathbf{Q_c(f)} = 86f^{1.02}$	NE Himalaya, India	Gupta and Kumar (2002)	Strong motion data
$\mathbf{Q_c(f)} = 92f^{1.07}$	Kumaon Himalaya, India	Paul et al. (2003)	Strong motion data
$\mathbf{Q_c(f)} = 158f^{1.05}$	NW Himalaya, India	Kumar et al. (2005b)	Strong motion data
$\mathbf{Q_\beta(f)} = 112f^{.97}$	Garhwal Himlaya, India	Joshi (2006b)	Strong motion data
$\mathbf{Q_c(f)} = 87f^{0.71}$	Garhwal region, India	Sharma et al.(2009)	Strong motion and broad band data
$\mathbf{Q_\beta(f)} = 104f^{1.3}$	Kumaon Himalaya, India	Singh et al. (2012b)	Strong motion data
$\mathbf{Q_c(f)} = 61.8f^{0.992}$	Garhwal Himalaya	Singh et al. (2012c)	Broad band data
$\mathbf{Q_\beta(f)} = 29f^{1.1}$	Kumaon Himalaya, India	Joshi et al. (2012a)	Strong motion data
Worldwide relation			
$\mathbf{Q_c(f)} = 60f$	Hindukush	Roecker et al. (1982)	Smoked paper records
$\mathbf{Q_c(f)} = 63f^{0.97}$	Washington	Havskon et al. (1989)	Strong motion data
$\mathbf{Q_\beta(f)} = 97f^{0.59}$	Kagoshima, Japan	Mamada and Takenaka (2004)	Strong motion data
$\mathbf{Q_c(f)} = 34.5f^{0.95}$	Ishikawa, Japan	Maeda et al. (2008)	Strong motion data
$\mathbf{Q_c(f)} = 32f^{0.5}$	Mt. Etna, Italy	Giampiccolo et al. (2007)	Strong motion data
$\mathbf{Q_c(f)} = 28.3f^{0.87}$	Southern Apennines (Italy)	Cantore et al. (2011)	Strong motion data

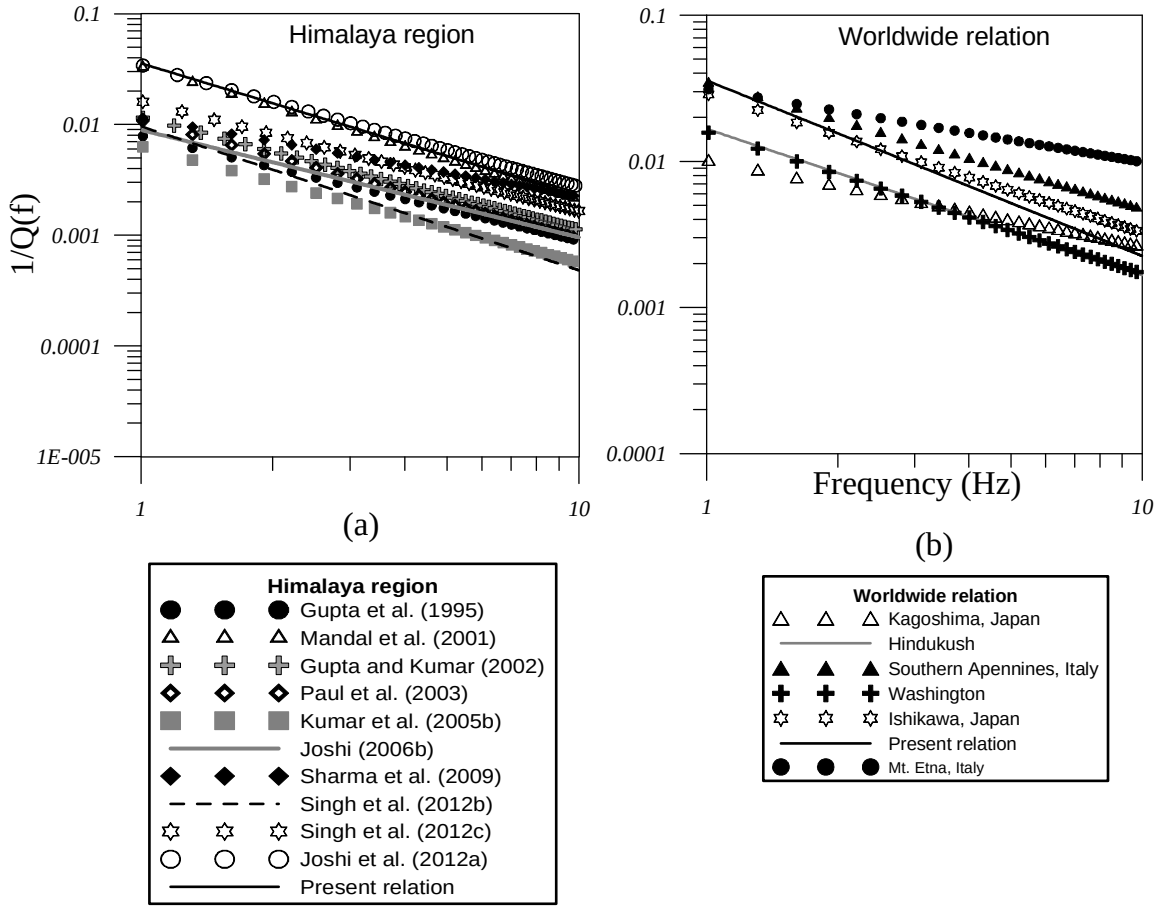

Figure 5.32: Comparison of $Q_\beta(f)$ relation developed in present work with the relation of (a) Himalaya region and (b) worldwide region.

5.5 Conclusion

In this chapter two step modified inversion algorithm has been used for obtaining $Q_\beta(f)$ and site amplification term from inversion of the strong motion data. Data of forty events recorded at sixteen stations located in the Kumaon Himalaya have been used in this study. Site amplification at each station is determined from obtained results of inversion. In this work $Q_\beta(f)$ relation and site amplification at each station is obtained individually. The values of $Q_\beta(f)$ obtained at sixteen different stations further used to obtain a regional regression relation of form $Q_\beta(f) = (28\pm2.1)f^{(1.2\pm0.09)}$ which represent the attenuating property of rocks in the Kumaon Himalaya region. Low value of Q_o and high value of 'n' obtained in the present $Q_\beta(f)$ relation shows that the region is seismically active and characterized by local heterogeneities.

Chapter – 6

Three Dimensional Attenuation Structure of Kumaon Himalaya, India

6.1 Introduction

State of Uttarakhand is among seismically active regions in India. Seismicity map of this region shows that it is locale several earthquakes in recent past. Main Central thrust is a major tectonic unit present in this area. The Kumaon Himalaya forms a part of tectonic belt which consist of Main central thrust in this region. The region of Kumaon Himalaya is covered by a network of fourteen stations under a major research project sponsored by the Ministry of Earth Sciences, Government of India. Strong motion accelerographs of Kinemetrics, USA, have been installed in each station of this network. This network has recorded 294 events in this region since March 2006. In this chapter three-dimensional attenuation structure of Kumaon Himalaya is determined using the strong motion data recorded by this network. Three dimensional attenuation structure of this region is determined by using the inversion algorithm already defined in Chapter 2.

6.2 Geology and Tectonics

The Kumaon Himalaya is located near the central part of the Himalaya. Most part of the Kumaon Himalaya in India is characterized by high seismic activity due to the convergence and collision of the northward-moving Indian plate with the Eurasian plate. The Main Central Thrust (MCT) and North Almora Thrust (NAT) are passing through the study area as shown in Fig. 6.1. The Main Central Thrust (MCT) is defined by the contact between the lesser and the Higher Himalayas (Gansser, 1964). The Almora Thrust describes the tectonic base of the great Almora Nappe built up of medium grade metamorphics and granitoids constituting a major tectonic element of the structural framework of Kumaun. Heim and Gansser (1939) have named the two flanks of this asymmetrically synformal thrust as North Almora thrust and South Almora Thrust, respectively (Valdiya, 1980).

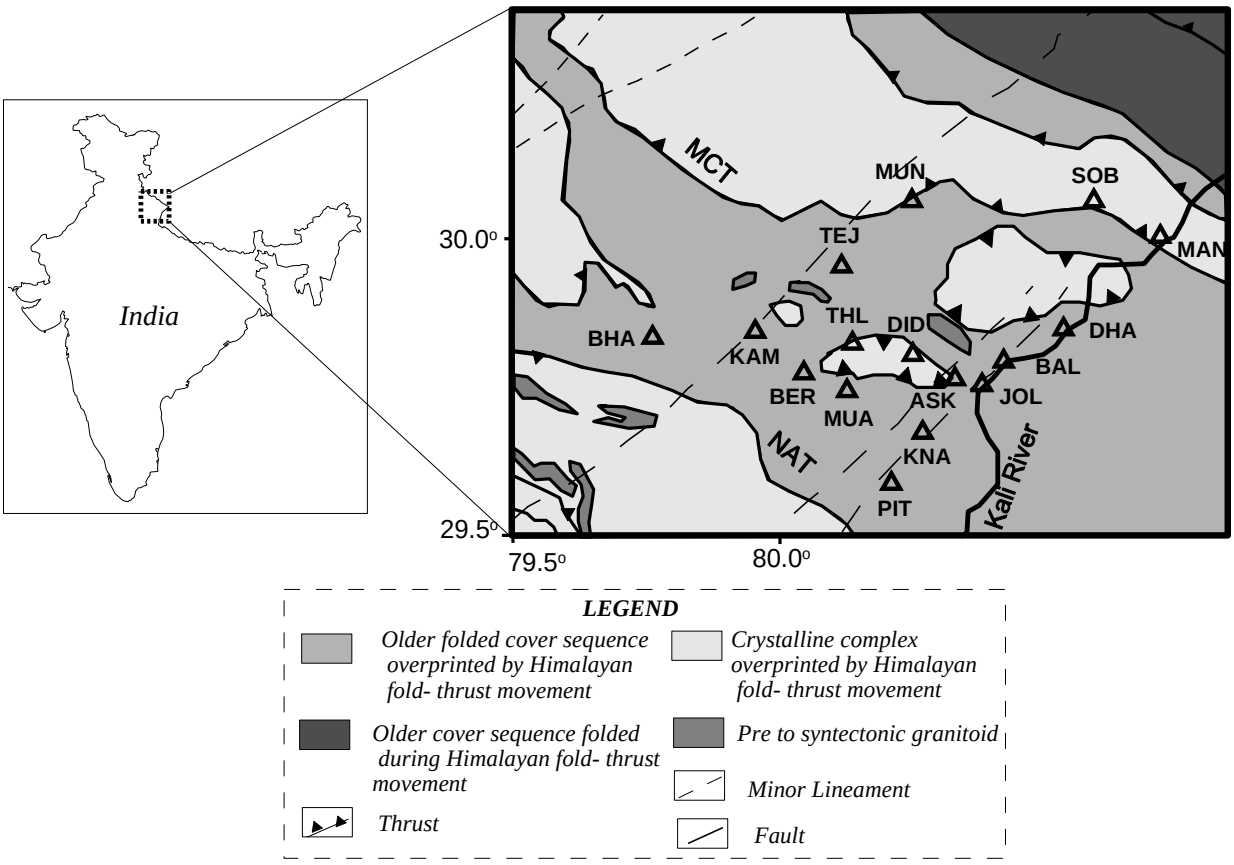

Figure 6.1: Study area lies in the Kumaon Himalaya, India region. MCT and NAT describe the Main central thrust and North Almora thrust. The geology and tectonics of the region is after GSI (2000). The hollow triangles denote the location of recording stations.

6.3 Data

Under the major research project sponsored by the Ministry of Earth Sciences, Government of India network of fourteen strong motion accelerographs of Kinemetrics, USA, have been installed in Kumaon region by department of Earth Sciences IIT Roorkee. Location of stations of this network is shown in Fig. 6.1. Some stations of this network are mobile and hence Fig. 6.1 shows the location of 16 stations. This network has recorded 294 events in this region since March 2006. A total of eighteen earthquakes recorded during April 2006 to April 2012 at various stations of this network have been used in the present work. Hypocentral parameters of events used in present work have been determined using the least square method given by Geiger (1912). The software named as HYPO71 originally developed by Lee and Lahr (1972) is used for localization of events. Important parameters required for determination of hypocentral parameters are the

arrival time of P and S phase, geographical coordinates of recording stations and input velocity model. The P and S phase present in the acceleration record is determined by visual inspection. The velocity structure is an important input parameter that is used for determination of hypocentral parameters using HYPO71 software. The velocity model given by Yu et al. (1995) for modeling of strong motion data due to Uttarkashi earthquake has been used as input velocity model in present work. Same velocity has been used as input in the inversion algorithm developed for determination of three dimensional attenuation structure of Kumaon region. The obtained hypocentral parameters of all recorded events determined using the HYPO71 software is given in Table 6.1. The strong motions data collected from the accelerograph have been processed by applying various processing steps which involve baseline correction, instrument scaling, padding and frequency filtering (Boore and Bommer, 2005). All processing steps are discussed briefly in Chapter 4. Processed records of some of the events used in the present work are shown in Fig. 6.2 to 6.10.

Table 6.1: The hypocentral parameters determined for events used in present work.

Sr. no.	Date (dd/mm/yy)	Origin time (hr:min:sec)	Epicenter		Depth (km)
			Latitude (Degree)	Longitude (Degree)	
1	01/04/06	19:42:52.10	30.212	80.402	11
2	30/05/06	18:25:18.03	29.902	80.449	03
3	05/02/07	07:57:35.08	29.866	80.276	31
4	03/04/07	03:39:14.77	29.753	80.296	25
5	04/09/08	12:53:10.14	30.139	80.255	15
6	17/09/08	16:59:09.12	30.075	80.594	25
7	04/07/10	02:35:57.50	29.857	80.352	13
8	15/12/10	05:33:02.45	29.753	80.45	25
9	05/05/11	07:15:22.18	30.026	80.632	37
10	15/06/11	00:59:22.15	29.959	79.973	4
11	09/10/11	07:34:55.69	29.949	80.509	22
12	18/11/11	09:50:37.56	29.85	79.900	31
13	09/01/12	10:41:15.17	29.856	80.594	25
14	16/01/12	05:01:50.15	29.780	79.991	25
15	16/03/12	15:22:42.07	29.911	80.067	12
16	16/03/12	19:35:50.36	29.847	79.842	20
17	08/04/12	07:38:14.81	29.962	80.266	14
18	19/07/12	22:36:51.30	29.826	80.134	24

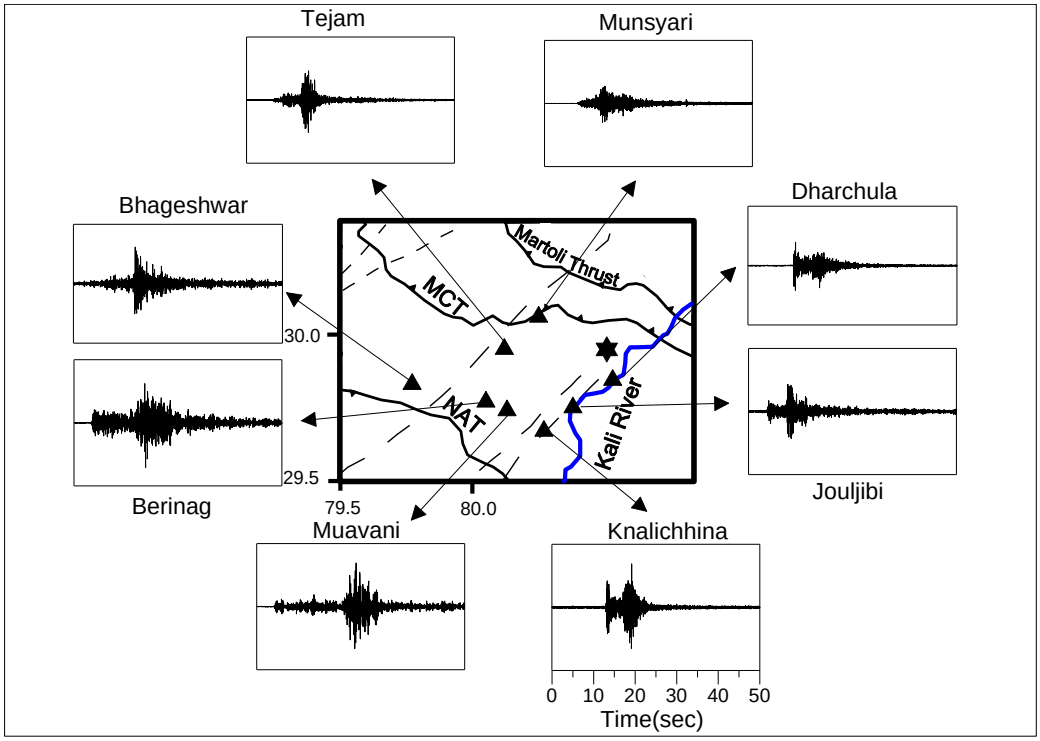

(a)

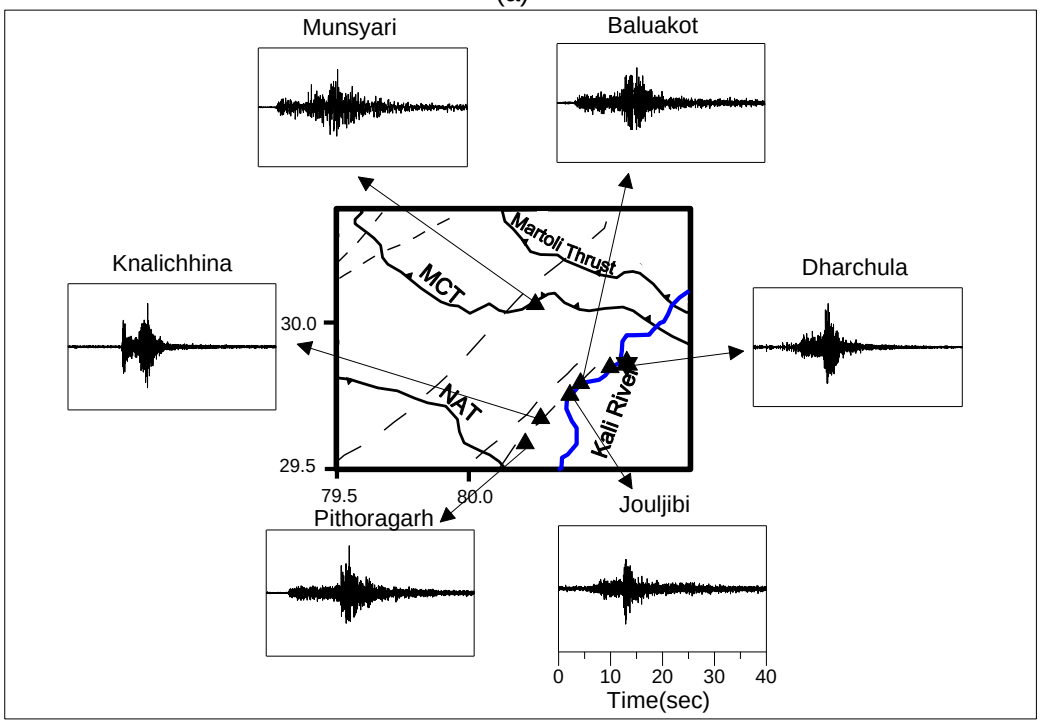

(b)

Figure 6.2: Processed normalized accelerograms of the events occurred on (a) 09-10-2011 and (b) 09-01-2012 recorded at different station. Star denotes the epicenter of events. Triangle shows the location of recording station. The tectonics of the region is taken after GSI (2000).

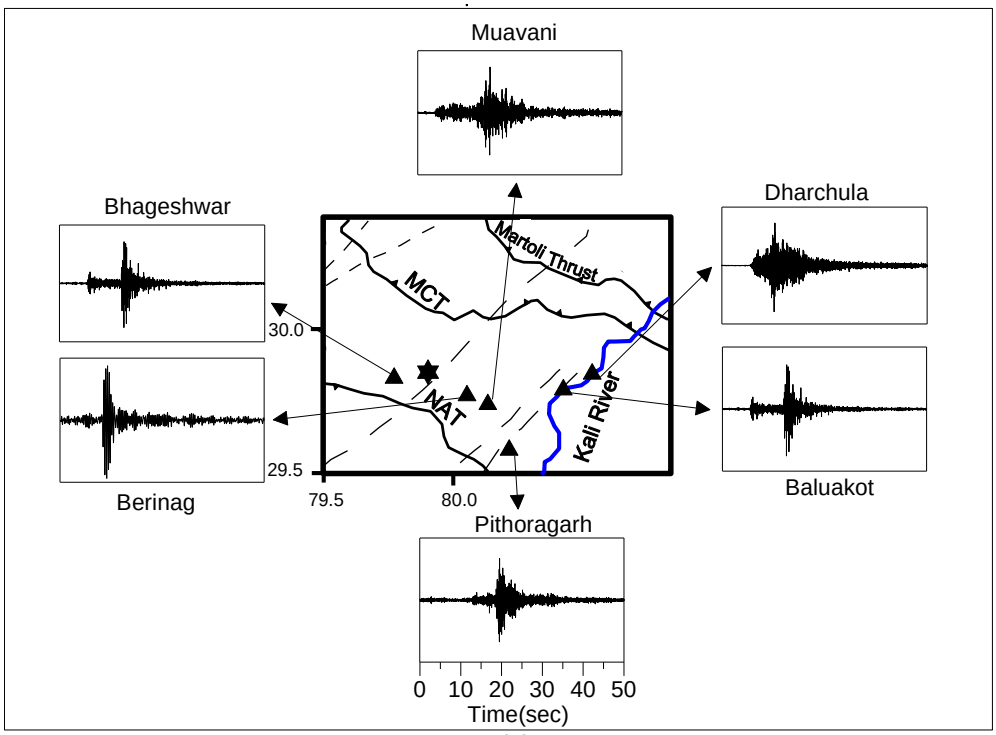

(a)

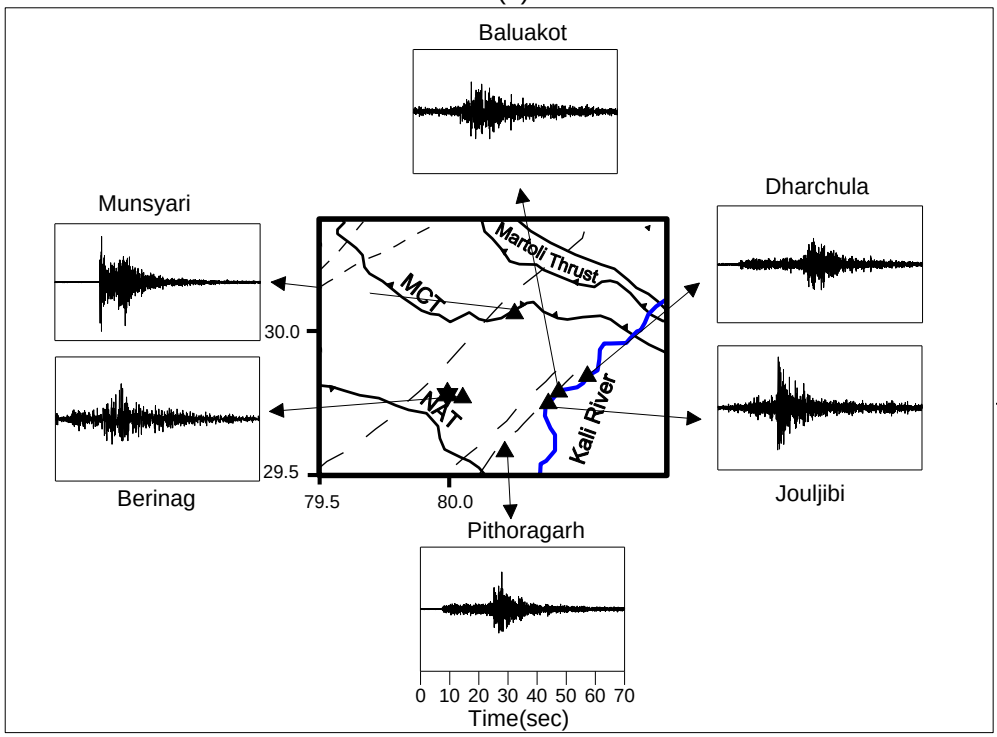

(b)

Figure 6.3: Processed normalized accelerograms of the events occurred on (a) 18-11-2011 and (b) 16-01-2012 recorded at different station. Star denotes the epicenter of events. Triangle shows the location of recording station. The tectonics of the region is taken after GSI (2000).

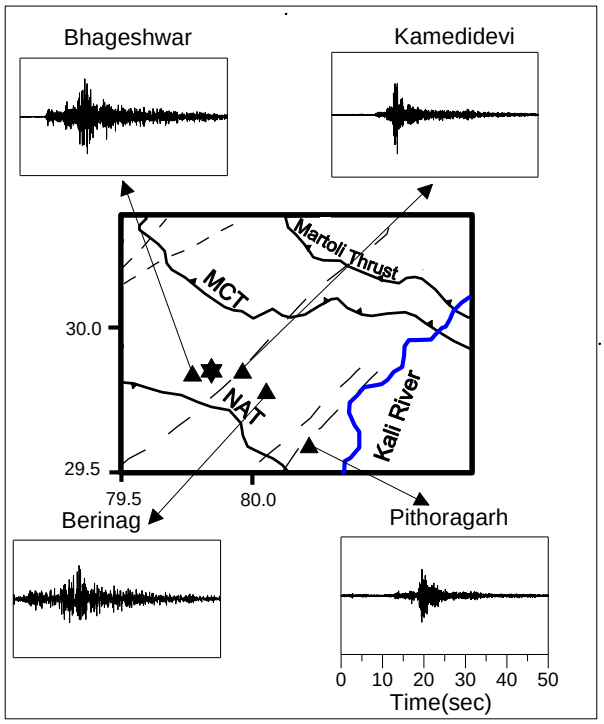

(a)

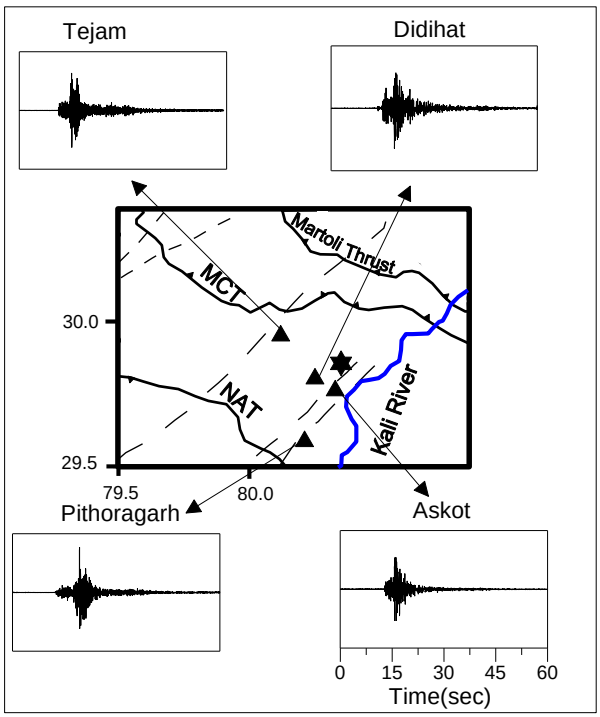

(b)

Figure 6.4: Processed normalized accelerograms of the events occurred on (a) 16-03-2012 and (b) 04-07-2010 recorded at different station. Star denotes the epicenter of events. Triangle shows the location of recording station. The tectonics of the region is taken after GSI (2000).

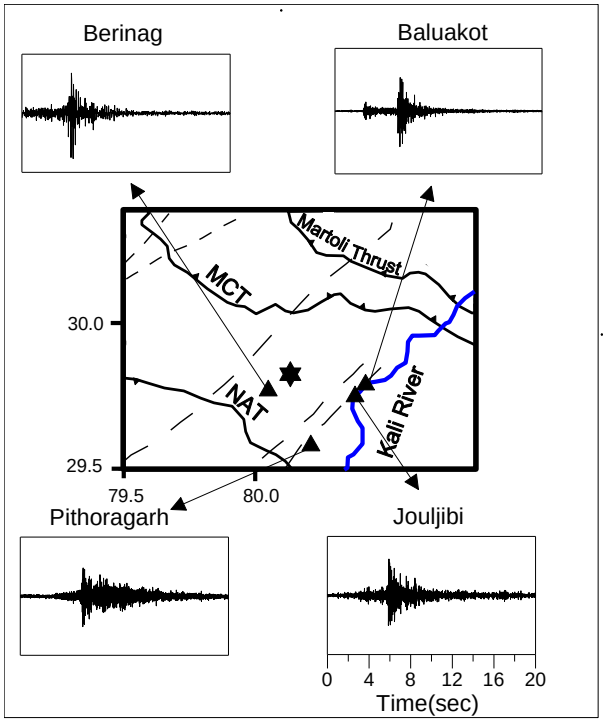

(a)

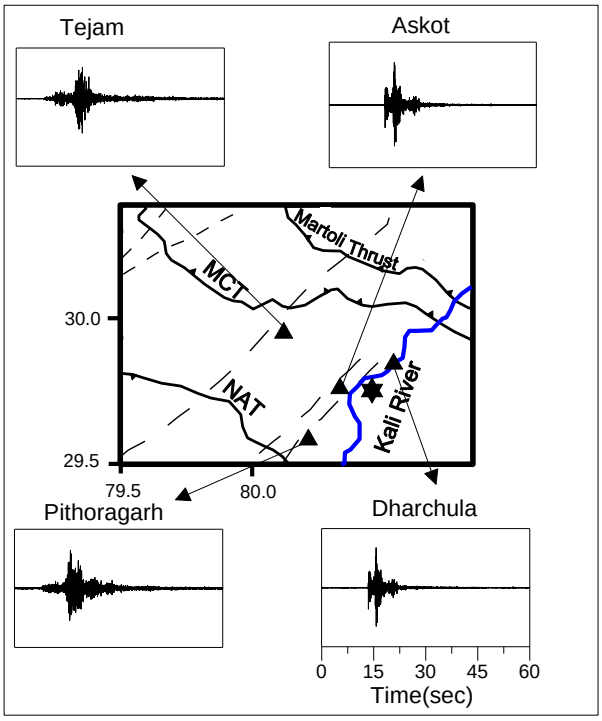

(b)

Figure 6.5: Processed normalized accelerograms of the events occurred on (a) 19-07-2012 and (b) 15-12-2010 recorded at different station. Star denotes the epicenter of events. Triangle shows the location of recording station. The tectonics of the region is taken after GSI (2000).

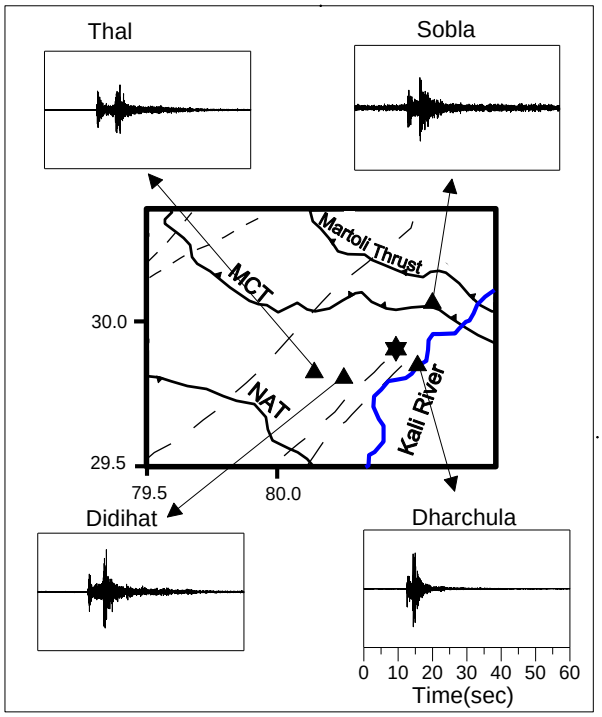

(a)

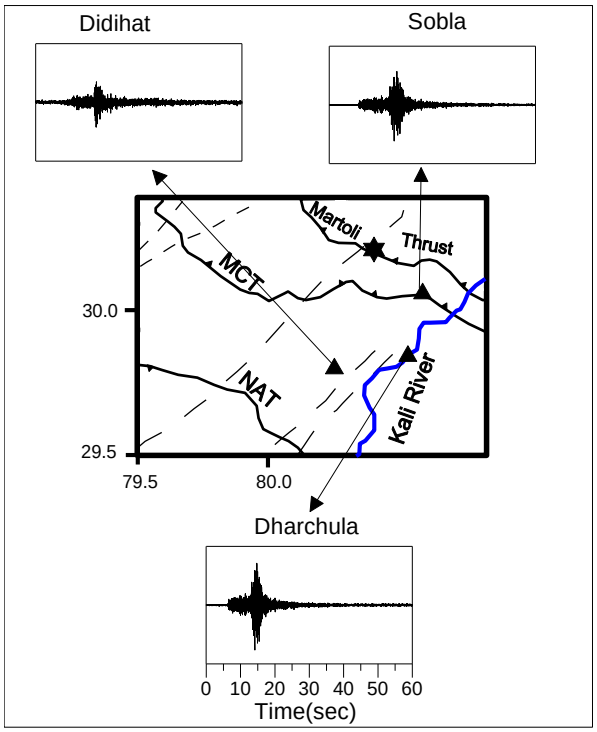

(b)

Figure 6.6: Processed normalized accelerograms of the events occurred on (a) 30-05-2006 and (b) 01-04-2006 recorded at different station. Star denotes the epicenter of events. Triangle shows the location of recording station. The tectonics of the region is taken after GSI (2000).

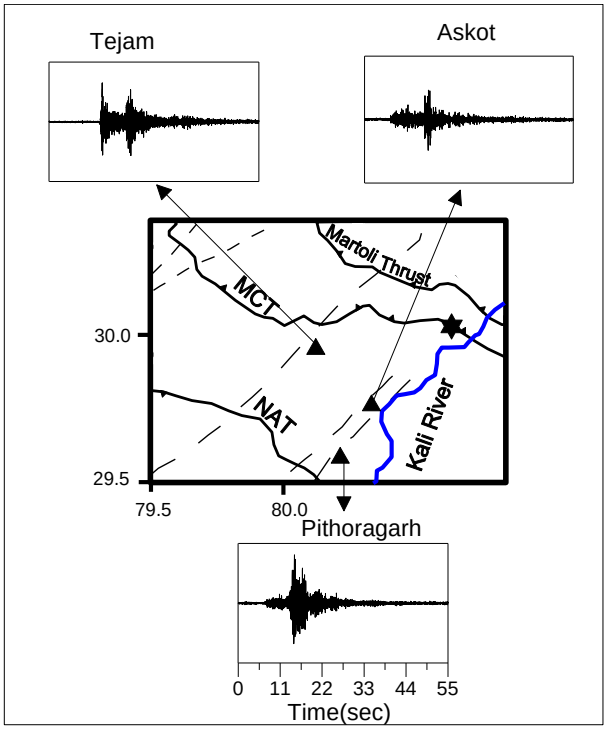

(a)

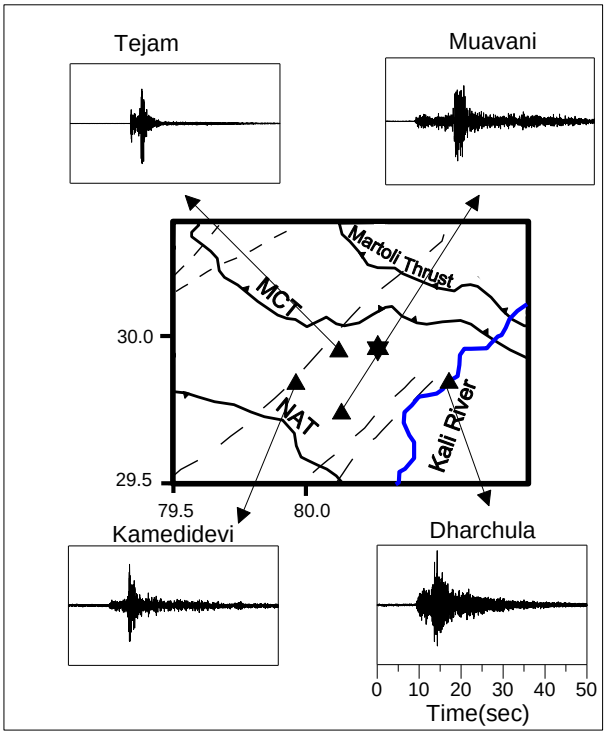

(b)

Figure 6.7: Processed normalized accelerograms of the events occurred on (a) 05-05-2011 and (b) 08-04-2012 recorded at different station. Star denotes the epicenter of events. Triangle shows the location of recording station. The tectonics of the region is taken after GSI (2000).

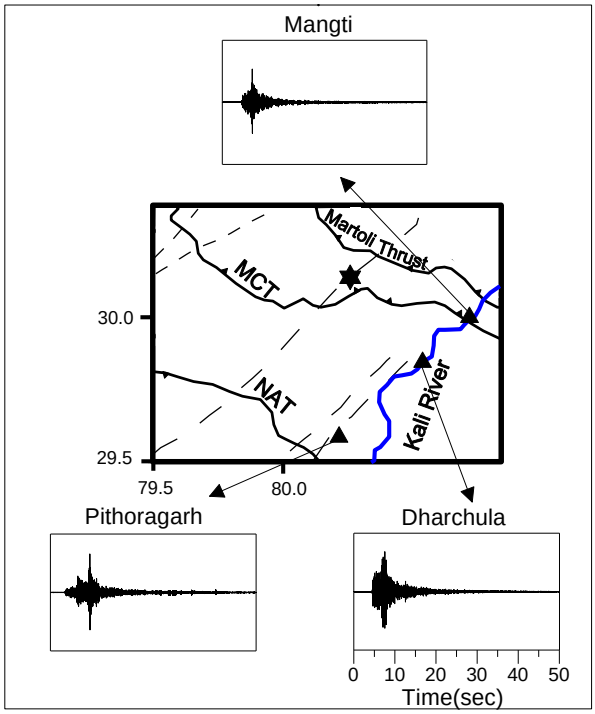

(a)

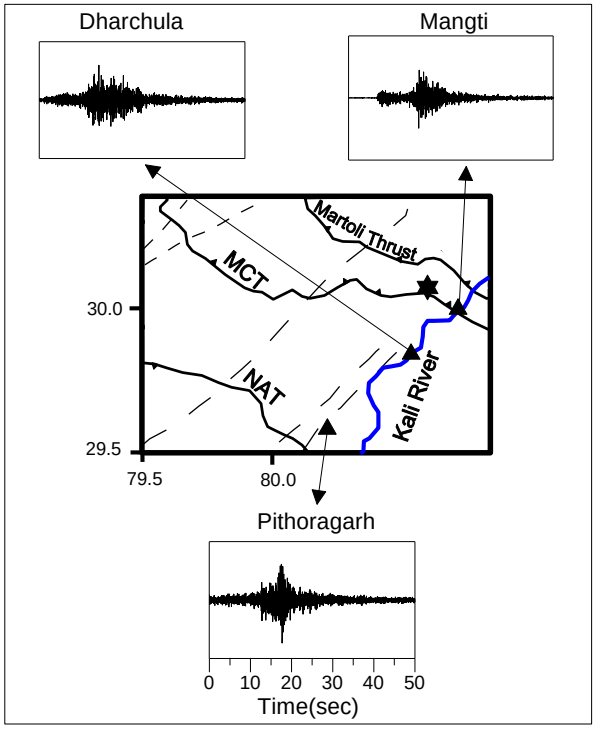

(b)

Figure 6.8: Processed normalized accelerograms of the events occurred on (a) 04-09-2008 and (b) 17-09-2008 recorded at different station. Triangle shows the location of recording station. The tectonics of the region is taken after GSI (2000).

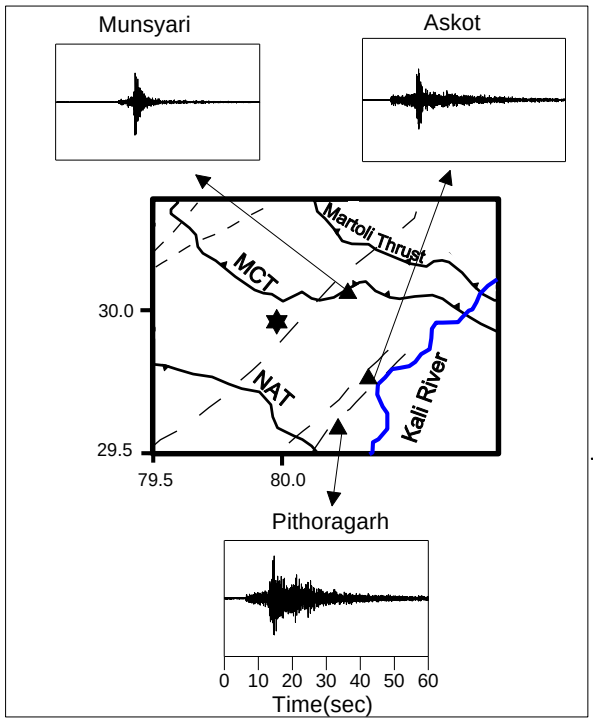

Figure 6.9: Processed normalized accelerograms of the events occurred on (a) 15-06-2011 and (b) 05-02-2007 recorded at different station. Triangle shows the location of recording station. The tectonics of the region is taken after GSI (2000).

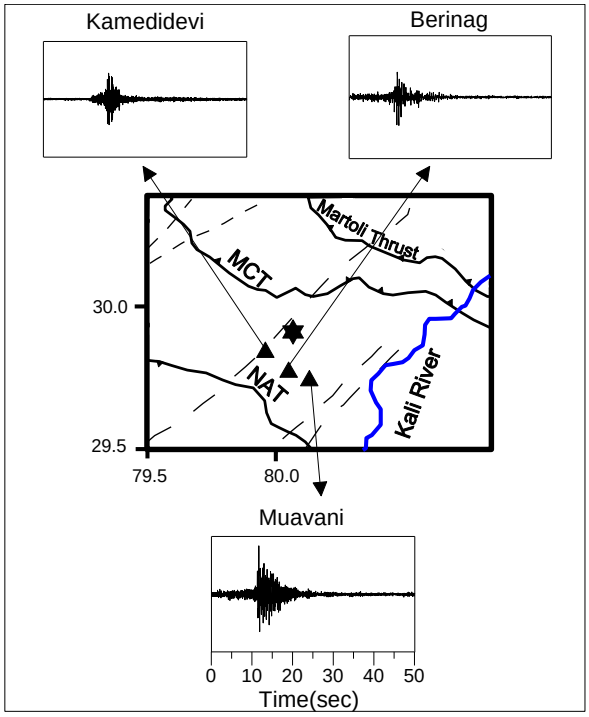

(a)

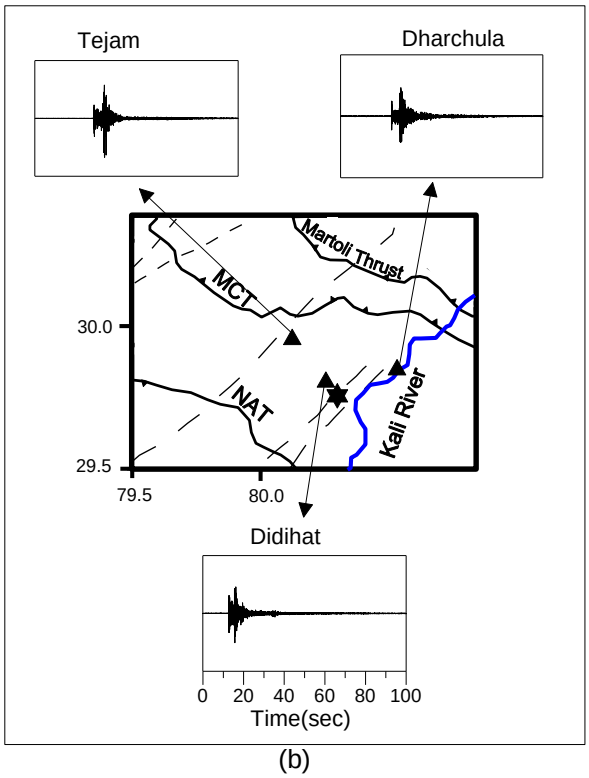

(b)

Figure 6.10: Processed normalized accelerograms of the events occurred on (a) 16-03-2012 and (b) 03-04-2007 recorded at different station. Triangle shows the location of recording station. The tectonics of the region is taken after GSI (2000).

In the present work attenuation structure of region is determined by using data from two blocks having some common area. The choice of common area is made to confirm the reliability of obtained attenuation structure from the inversion of strong motion data of two blocks. These blocks are named as block 1 and block 2. The surface dimensions of block 1 and block 2 are 85×55 km and 90×30 km, respectively. Twelve events within each block that has been recorded by various stations located in each block are used to obtain three-dimensional attenuation structure. Location of events in block 1 used for present work is shown in Fig. 6.11 and given in Table 6.2. The ray path map of energy travelling from source to the observation points in block 1 is shown in Fig. 6.12. Location of events in block 2 used for present work is shown in Fig. 6.13 and given in Table 6.3. The ray path map of energy travelling from source to the observation points in block 2 is shown in Fig. 6.14. A total of eighteen earthquakes recorded during April 2006 to April 2012 at various stations of Kumaon strong motion network have been used in the present work.

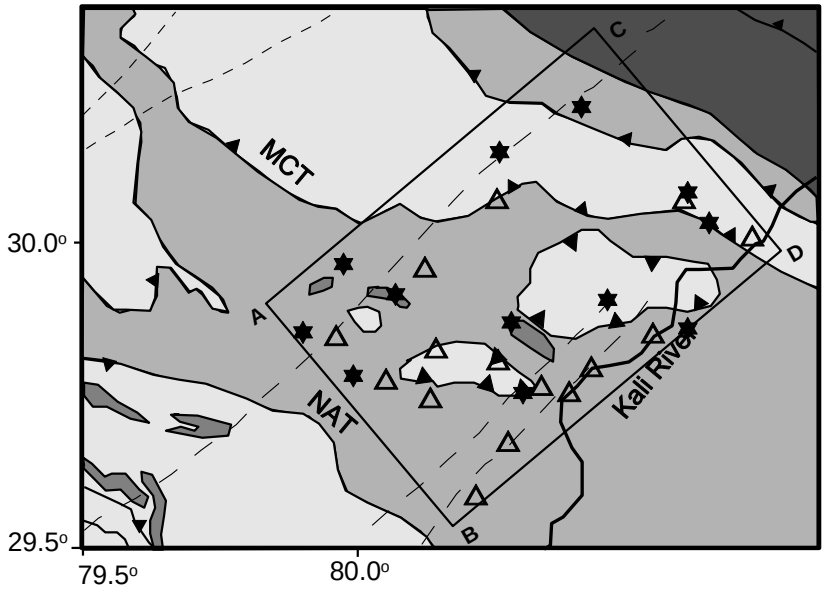

Figure 6.11: Location of events and recording stations for block 1. The recording stations and epicenters of the events are denoted by hollow triangle and solid star, respectively.

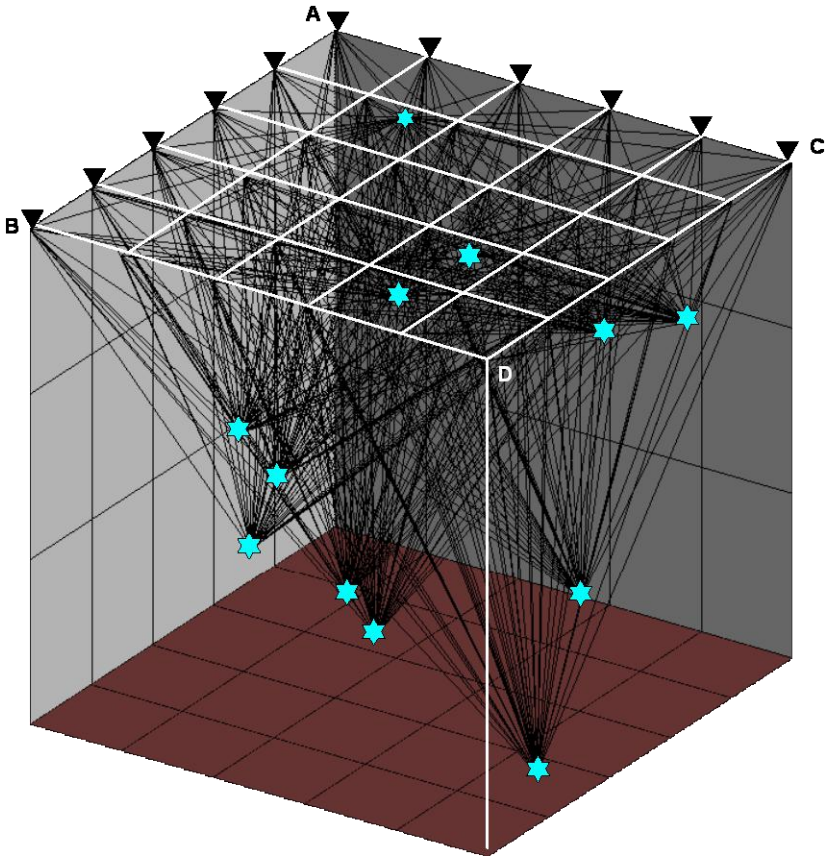

Figure 6.12: Projection of ray path of different events at observation points for block 1. Star denotes the epicenters of earthquakes and triangle denotes the observation points.

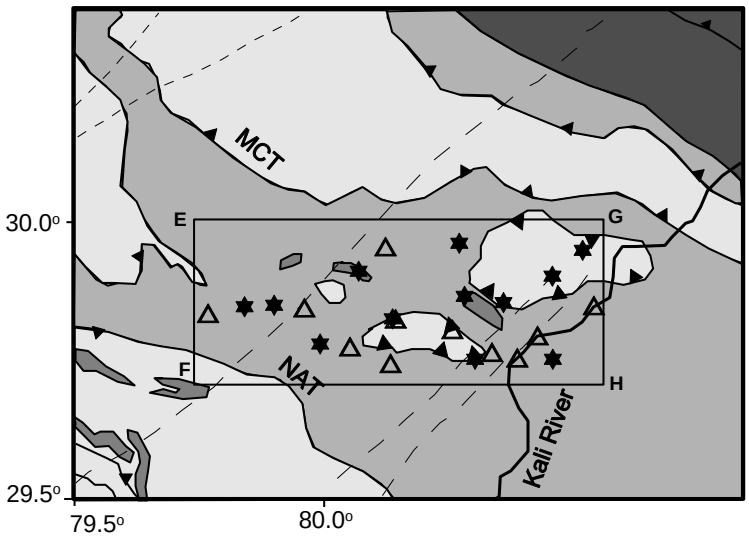

Figure 6.13: Location of events and recording stations for block 2. The recording stations and epicenters of the events are denoted by hollow triangle and solid star, respectively.

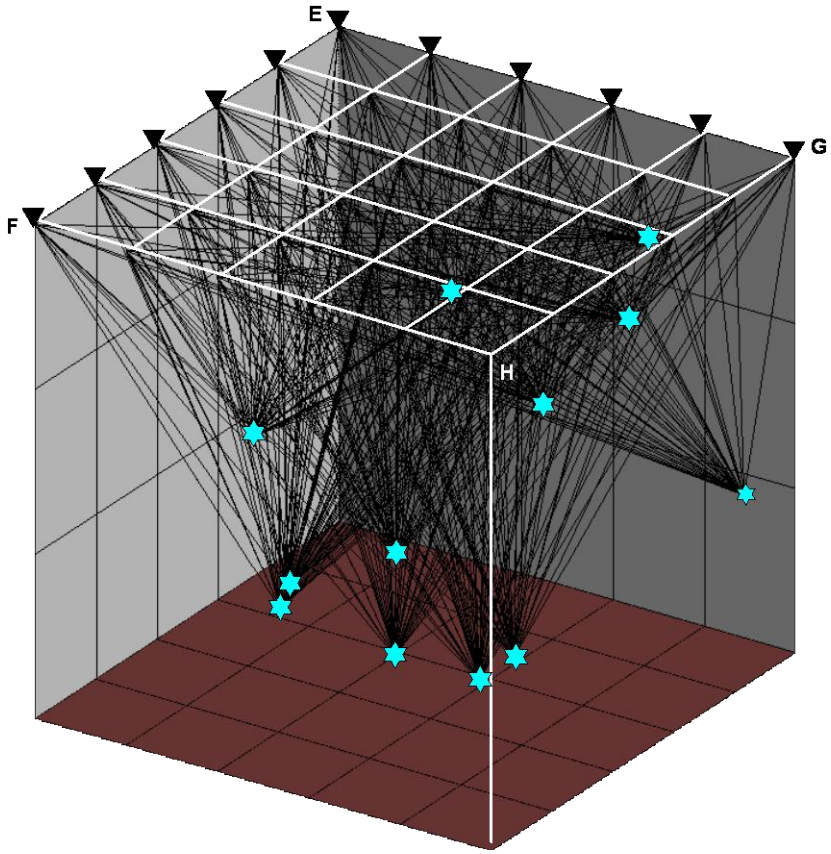

Figure 6.14: Projection of ray path of different events at observation points for block 2. Star denotes the epicenters of earthquakes and triangle denotes the observation points.

An acceleration spectrum of S-phase is the major requirement of this inversion algorithm. Spectrum of S-phase of each event is selected on the basis of visual inspection. Inversion algorithm developed in Chapter 2 requires spectral acceleration data of S-phase free from site effects. The three dimensional attenuation structure of Central Honshu region has earlier obtained using strong motion data recorded at rock site. The KiK net network has installed sensors at both rock and soil site. However the Kumaon network of strong motion recorders is placed only at surface. Most of the sites are at hard rock but site effects from weathered rock and low soil cover cannot be ruled out. An algorithm has been developed in present work where frequency dependent shear wave quality factor ($Q_\beta(f)$) and site effects have been obtained at each station of Kumaon network. Results of this inversion algorithm using strong motion data from Kumaon network is given in Chapter 5. In the present work site effects obtained at each station is used for correcting acceleration spectra of S-phase. Acceleration spectrum at each station used as input to inversion algorithm is corrected for site effects. Value of corrected acceleration spectra at selected frequency

is used to prepare the contour map of spectral acceleration. Various steps used to prepare the contour map of spectral acceleration are shown in Fig. 6.15. Value of spectral acceleration from the contour in each block is used as input to the inversion algorithm. Input point in the block is shown in Fig. 6.15.

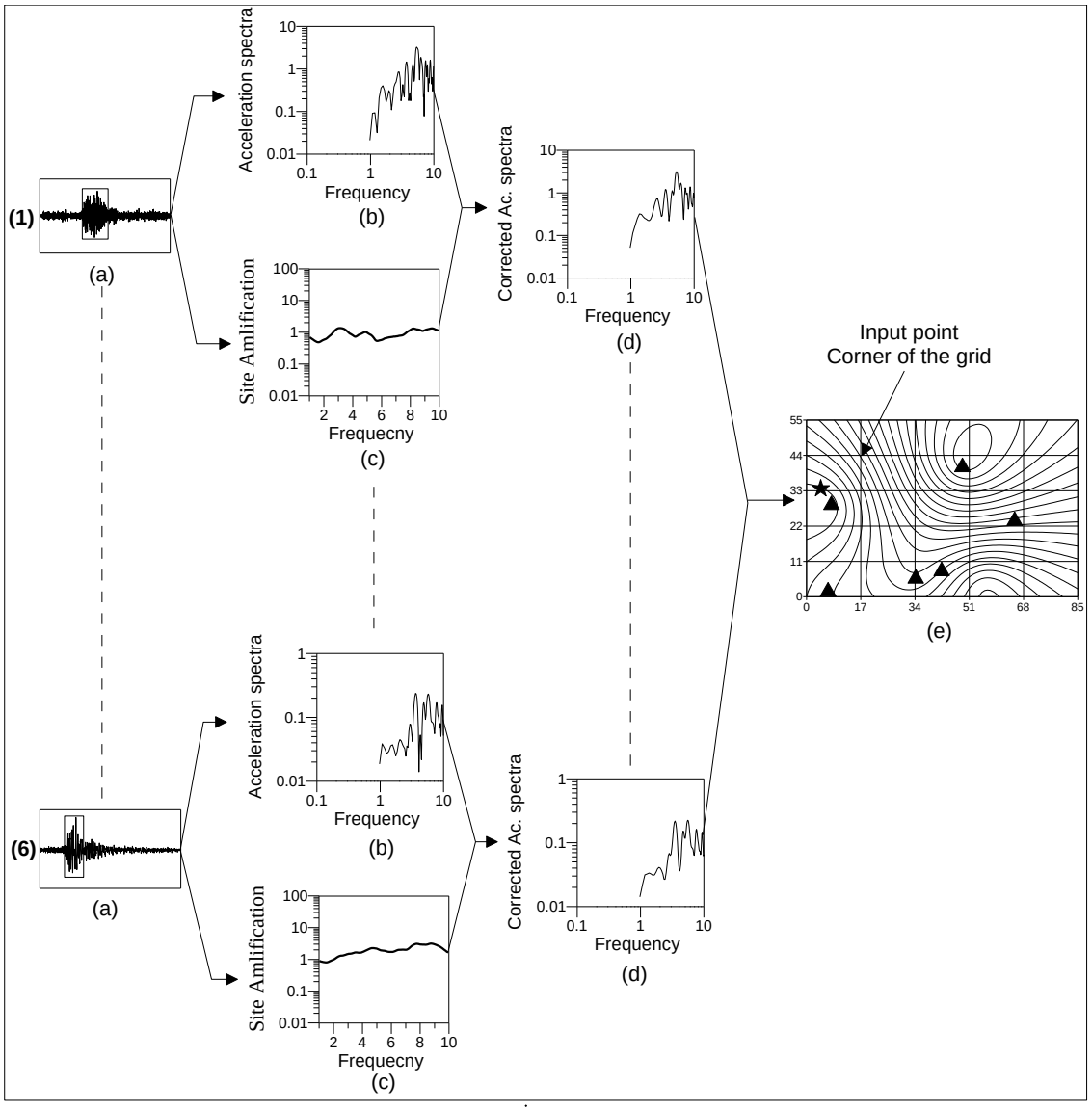

Figure 6.15: (a) The acceleration record of earthquake with S-phase identified by the rectangular block, (b) source acceleration spectrum computed from the S-phase without correction of site effect, (c) site amplification obtained using the inversion technique discussed in Chapter 3, (d) source acceleration spectrum computed from the S-phase after correction of site effect and (e) contour map of acceleration spectra obtained using the corrected acceleration spectra values, respectively. Triangles and star denote the location of recording stations and events, respectively.

6.4 Results

In the present work three-dimensional attenuation structure of the region is determined by using data from two different blocks named as block 1 and block 2. Three-dimensional attenuation structure has been determined at 1.5 Hz, 5.0 Hz and 10.0 Hz frequency, respectively. The values of quality factor at different depth are obtained for the block 1 of surface dimension 85×55 km using data set from earthquakes listed in Table 6.2. Three dimensional distributions of shear wave quality factor and tectonic map at frequency 1.5 Hz, 5.0 Hz and 10.0 Hz at different depth is shown in Fig. 6.16, 6.17 and 6.18, respectively. These figures revealed that the upper most layer (0-5km) has the low value of quality factor as comparison to deepest layer. This trend is seen in all section for each frequency considered in this work. It is seen that the deeper layers contour of quality factor values is parallel to the major tectonic unit of the area.

Table 6.2: Parameters of the events used to determine the attenuation tomography for block 1.

Date (dd/mm/yy)	**Origin time (hr:min:sec)**	**Epicenter**		**Depth (km)**
		Latitute (Degree)	**Longitude (Degree)**	
01/04/06	19:42:52.10	30.212	80.402	11
30/05/06	18:25:18.03	29.902	80.449	03
05/02/07	07:57:35.08	29.866	80.276	31
03/04/07	03:39:14.77	29.753	80.296	25
04/09/08	12:53:10.14	30.139	80.255	15
17/09/08	16:59:09.12	30.075	80.594	25
05/05/11	07:15:22.18	30.026	80.632	37
15/06/11	00:59:22.15	29.959	79.973	4
18/11/11	09:50:37.56	29.85	79.900	31
09/01/12	10:41:15.17	29.856	80.594	25
16/01/12	05:01:50.15	29.780	79.991	25
16/03/12	19:35:50.36	29.847	79.842	20

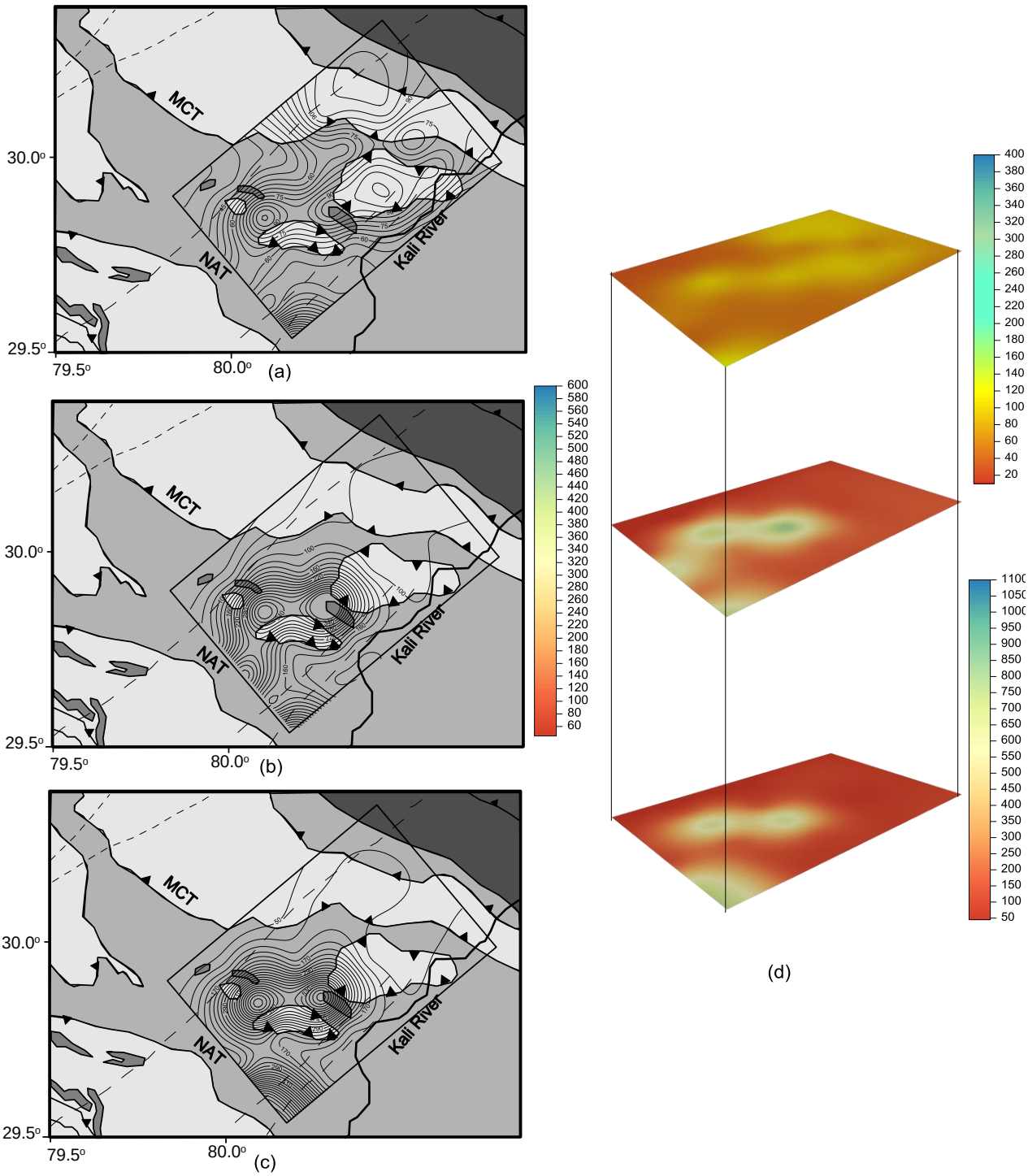

Figure 6.16: Contour of shear wave quality factor at 1.5 Hz for block 1 superimposed on the geological map of the region at (a) 0-5 km, (b) 5-10 km and (c) 10-15 km depth. (d) three- dimensional distribution of shear wave quality factor at 1.5 Hz for block 1.

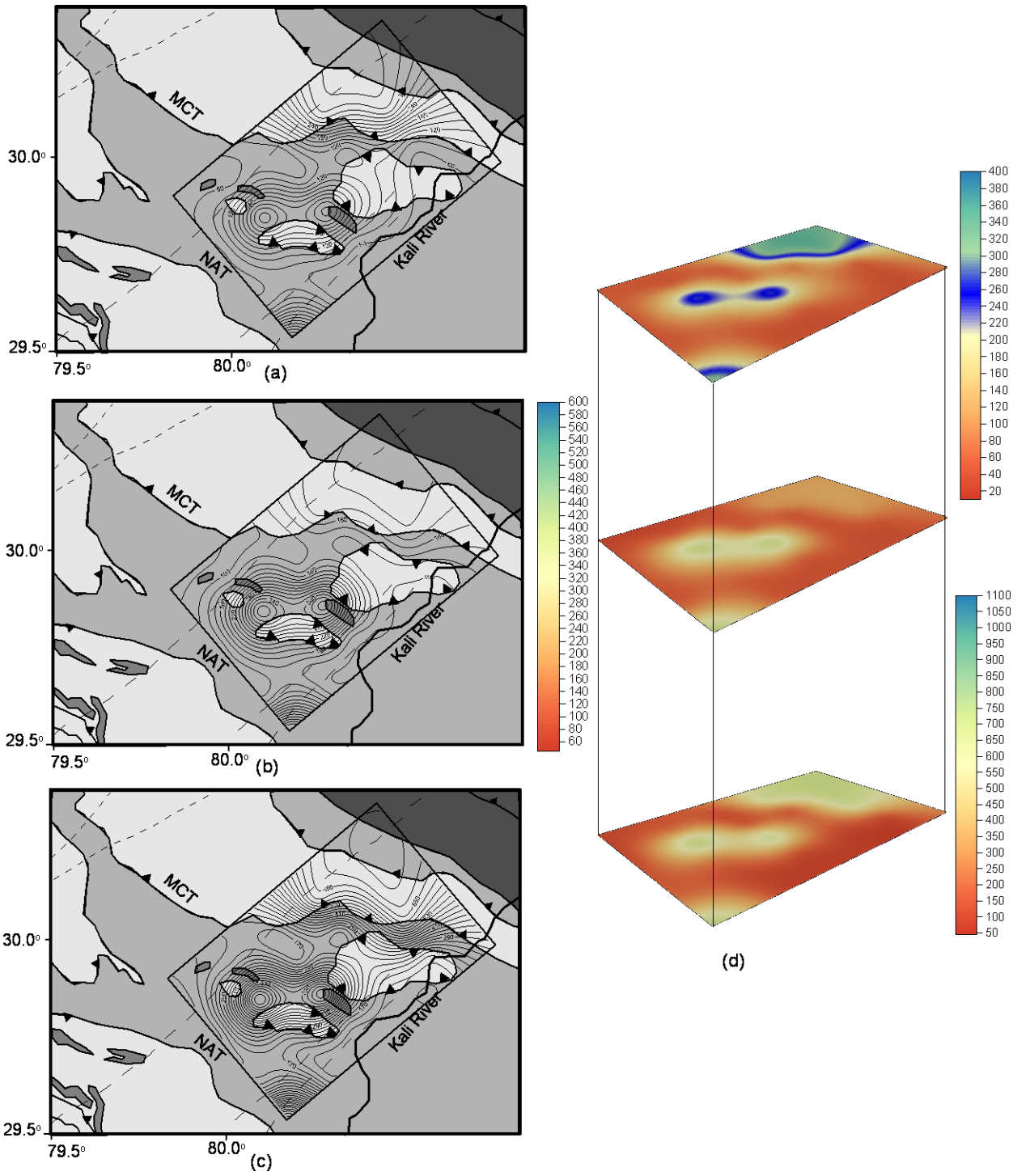

Figure 6.17: Contour of shear wave quality factor at 5 Hz for block 1 superimposed on the geological map of the region at (a) 0-5 km, (b) 5-10 km and (c) 10-15 km depth. (d) three- dimensional distribution of shear wave quality factor at 5 Hz for block 1.

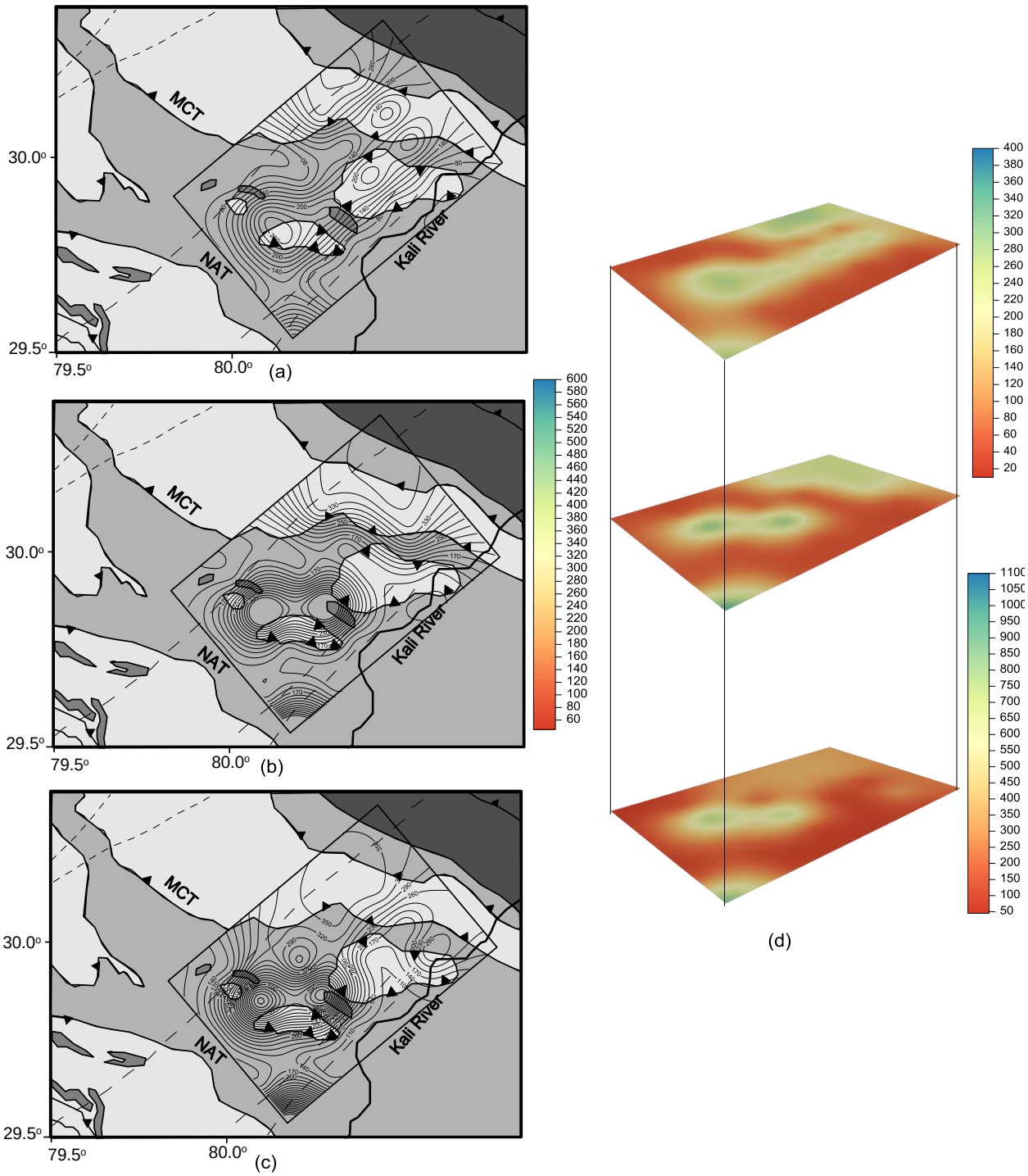

Figure 6.18: Contour of shear wave quality factor at 10 Hz for block 1 superimposed on the geological map of the region at (a) 0-5 km, (b) 5-10 km and (c) 10-15 km depth. (d) three- dimensional distribution of shear wave quality factor at 10 Hz for block 1.

Spectral acceleration data of twelve earthquakes has been used to determine three-dimensional attenuation structure for block 2. The surface dimension of block 2 is 90×30 km. The data set of twelve earthquakes used for block 2 is given in Table 6.3. Three dimensional distributions of quality factor value and tectonic map at frequency 1.5 Hz, 5.0 Hz and 10.0 Hz at different depth is shown in Fig. 6.19, 6.20 and 6.21, respectively. It is observed from Fig. 6.19 to 6.21 that the top most layer (0-5 km) have low quality factor values as compare to the deepest layer. The attenuation distribution for block 2 reflects almost the same result as block 1 in the common overlapping area. It is seen that the distribution of quality factor value for block 2 is almost similar as obtained for block 1.

Table 6.3: Parameters of the events used to determine the attenuation tomography for block 2.

Date (dd/mm/yy)	**Origin time (hr:min:sec)**	**Epicenter**		**Depth (km)**
		Latitute (Degree)	**Longitude (Degree)**	
30/05/06	18:25:18.03	29.902	80.449	03
05/02/07	07:57:35.08	29.866	80.276	31
03/04/07	03:39:14.77	29.753	80.296	25
04/07/10	02:35:57.50	29.857	80.352	13
15/12/10	05:33:02.45	29.753	80.45	25
09/10/11	07:34:55.69	29.949	80.509	22
18/11/11	09:50:37.56	29.85	79.900	31
16/01/12	05:01:50.15	29.780	79.991	25
16/03/12	15:22:42.07	29.911	80.067	12
16/03/12	19:35:50.36	29.847	79.842	20
08/04/12	07:38:14.81	29.962	80.266	14
19/07/12	22:36:51.30	29.826	80.134	24

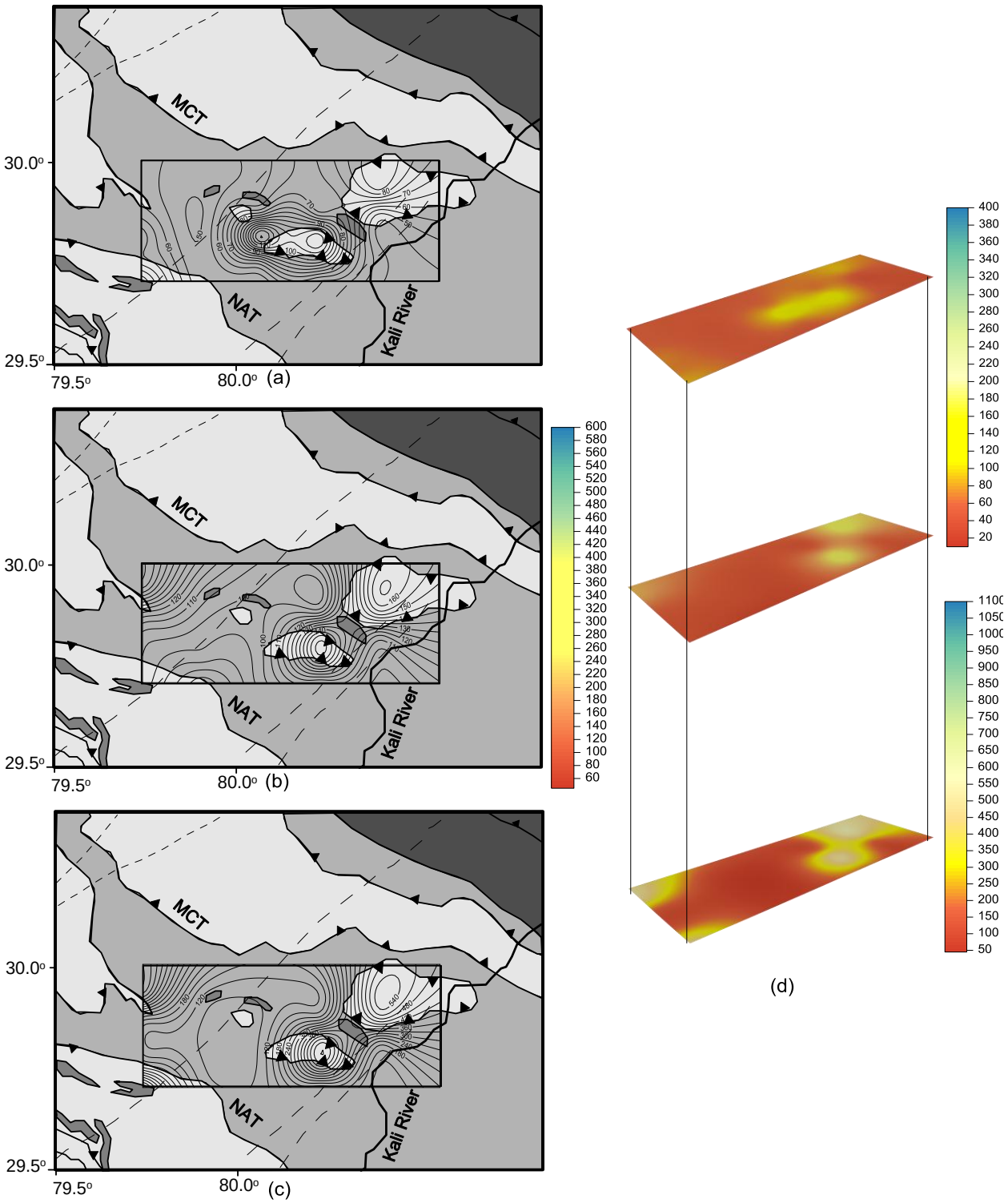

Figure 6.19: Contour of shear wave quality factor at 1.5 Hz for block 2 superimposed on the geological map of the region at (a) 0-5 km, (b) 5-10 km and (c) 10-15 km depth. (d) three- dimensional distribution of shear wave quality factor at 1.5 Hz for block 2.

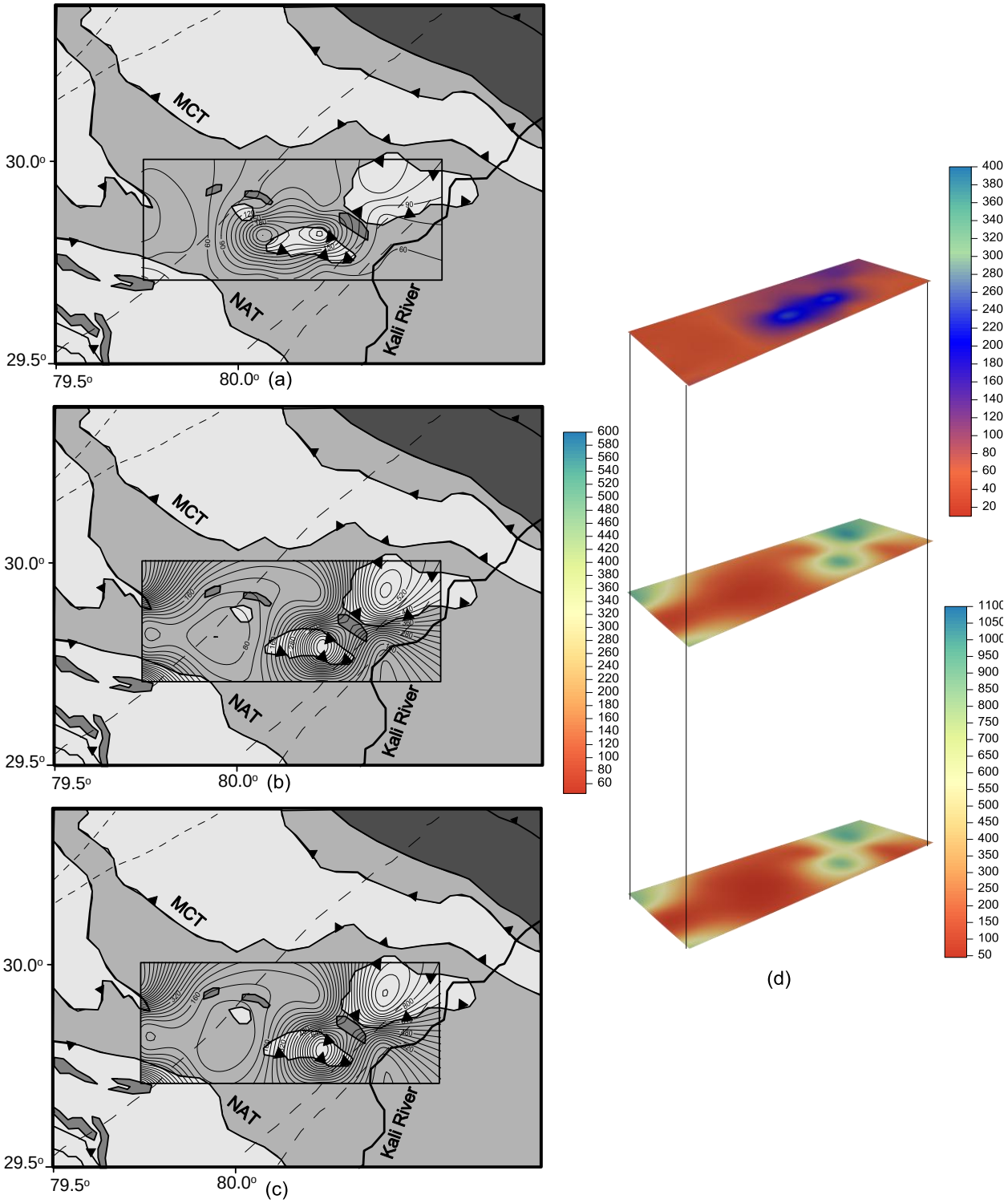

Figure 6.20: Contour of shear wave quality factor at 5 Hz for block 2 superimposed on the geological map of the region at (a) 0-5 km, (b) 5-10 km and (c) 10-15 km depth. (d) three- dimensional distribution of shear wave quality factor at 5 Hz for block 2.

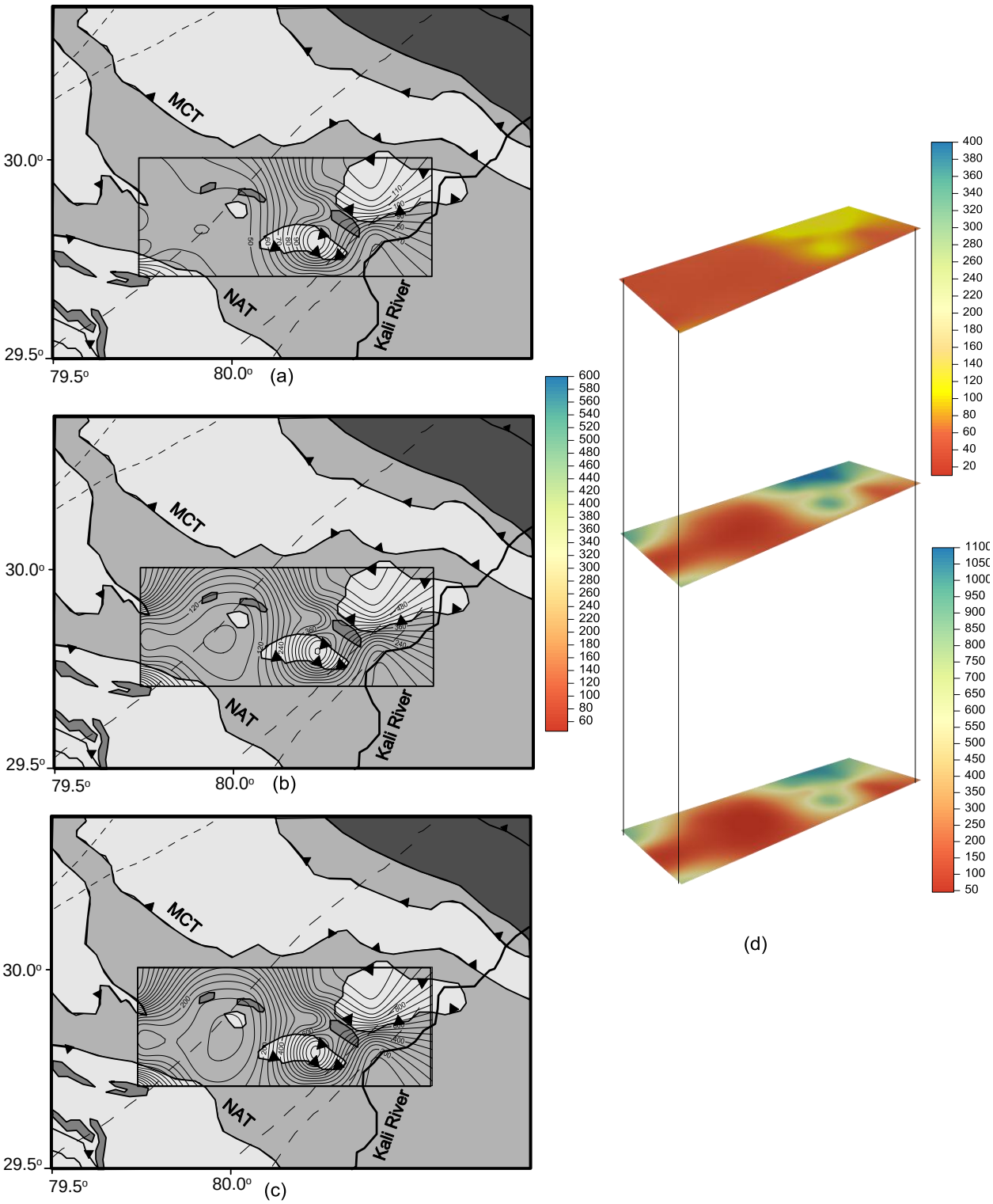

Figure 6.21: Contour of shear wave quality factor at 10 Hz for block 2 superimposed on the geological map of the region at (a) 0-5 km, (b) 5-10 km and (c) 10-15 km depth. (d) three- dimensional distribution of shear wave quality factor at 10 Hz for block 2.

Discussion

In the present work attenuation structure has been obtained at low (1.5 Hz), intermediate (5.0 Hz) and high (10.0 Hz) frequencies. It is observed that attenuation structure obtained at different frequencies matches with the available geological and tectonic unit. Although it is seen that attenuation structure obtained for intermediate frequency give close match with the major tectonic unit present in the region. The three dimensional distribution of quality factor value of block 1 and block 2, explained that the attenuation contours at 5.0 Hz frequency follows the trend of the geological and tectonic units present in the region. It is seen that corner frequency of earthquake of small magnitude may coincide with the low frequency cut off used in the processing of record and this may influence the attenuation structure obtained at low frequency i.e. 1.5 Hz. Also it is seen that f_{max} effects present in strong motion record explain by Hanks (1982) may influence the high frequency cutoff used in the processed record and hence this may influence the attenuation structure obtained at high frequencies. Therefore the attenuation structure obtained at intermediate frequency is supposed to be free from effect of corner frequency of earthquake and f_{max} effects.

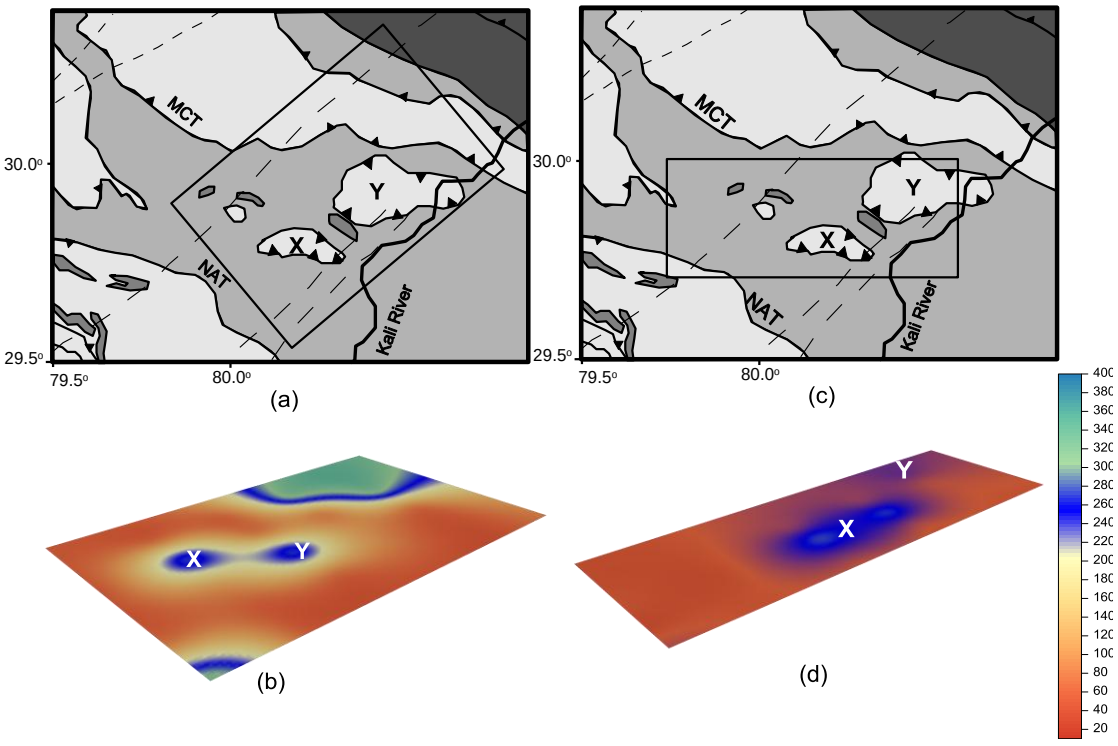

Figure 6.22: Geology of the study area for (a) block 1 and (c) block 2. Three- dimensional distributions of shear wave quality factor at 0-5 km for (b) block 1and (d) block 2 at 5.0 Hz frequency.

The distributions of shear wave quality factor at 0-5 km for block 1 and block 2 at frequency of 5.0 Hz is shown in Fig. 6.22. It is seen from Fig. 6.22 that two point 'X' and 'Y' falls in common region of two blocks used in present work. These two points fall in the same geology formation that is different from surrounding. It is seen that attenuation structure obtained from data in block 1 and 2 clearly differentiate points 'X' and 'Y' on the basis of high shear wave quality factor. The point 'X' and 'Y' having same type of geology and have nearly the same value of quality factor in each block. This confirms reliability of obtained attenuation structure from two different blocks in same region.

High values of quality factor accounts for low attenuation and hence high seismic hazard. The contour of quality factor value at 0-5 km for both blocks at 5.0 Hz is shown in Fig. 6.23. It is observed that both blocks give almost similar results in terms of contour of quality factor values. Ten stations lie in both blocks. The value of quality factor at each of these stations obtained from present inversion of data from block 1 and block 2 separately are given in Table 6.4. Table 6.4 shows that nearly similar values of quality factor have been obtained in each block at same stations although different input data events have been used in the inversion algorithm. Similar values of quality factor obtained from two different data sets confirm the stability and reliability of results from inversion algorithm.

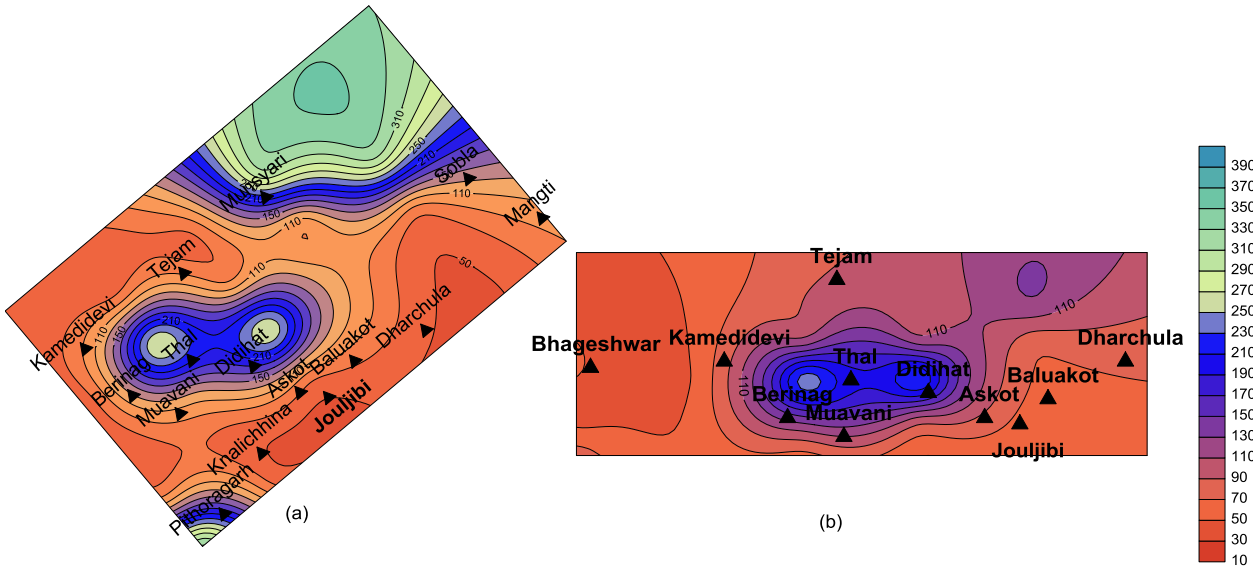

Figure 6.23: Contour map of shear wave quality factor value at 0-5 km with recording stations for (a) block 1 and (b) block 2 at 5.0 Hz frequency. Locations of recording stations are denoted by solid triangles.

Table 6.4: Obtained Q_β values for 5.0 Hz frequency at 0-5 km for block 1 and block 2.

Recording stations	Q_β values in block 1	Q_β values in block 2
Tejam	90	100
Didihat	190	195
Muavani	100	110
Askot	70	80
Jouljibi	55	60
Kamedidevi	95	80
Berinag	130	140
Thal	210	200
Dharchula	55	75
Baluakot	75	65

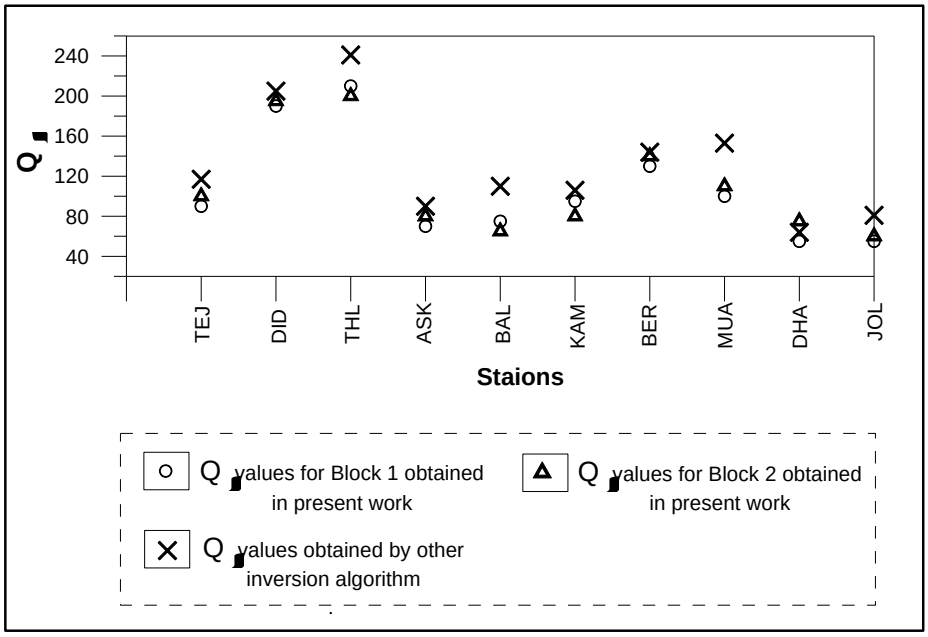

Figure 6.24: Comparison of obtained Q_β at 5.0 Hz frequency for block 1 and 2 with the Q_β values calculated by using other inversion algorithm given in Chapter 5.

Table 6.5: Comparison of $Q_\beta(f)$ values developed in present work with the frequency dependent shear-wave quality factor ($Q_\beta(f)$) calculated in Chapter 5.

Stations Name	Stations code	Present Q_β values at 5.0 Hz for block 1	Present Q_β values at 5.0 Hz for block 2	$Q_\beta(f)$ at 5.0Hz obtained by other inversion algorithm
Tejam	TEJ	90	100	117
Didihat	DID	190	195	205
Thal	THL	210	200	241
Askot	ASK	70	80	90
Baluakot	BAL	75	65	110
Kamedidevi	KAM	95	80	106
Berinag	BER	130	140	144
Muavani	MUA	100	110	153
Dharchula	DHA	55	75	64
Jouljibi	JOL	55	60	81

The frequency dependent shear-wave quality factor ($Q_\beta(f)$) has been already calculated at different stations in Chapter 5 using the inversion algorithm discussed in Chapter 3. The shear wave quality factor values (Q_β) obtained using three dimensional's inversion algorithm have been compared with the ($Q_\beta(f)$) of the region obtained in Chapter 5 by using the different algorithm. The Q_β values at the frequency of 5.0 Hz for the different stations which lie in both blocks, have been used for this comparison given in Table 6.5 and shown in Fig. 6.24. Comparison revealed that the calculated values of Q_β from present work are almost similar with the values of $Q_\beta(f)$ obtained by other inversion algorithm using different data set.

6.5 Conclusion

In this chapter three-dimensional attenuation structure has been obtained for the Kumaon Himalaya using the inversion technique discussed in Chapter 2. Attenuation tomography has been estimated for two different blocks using the strong motion data recorded by the Kumaon network at different frequencies. Similar attenuation structure obtained for two different blocks using different input confirm the stability of the inversion algorithm. It is observed that obtained attenuation structure follows the trend of major tectonic unit in the region. The final attenuation structure revealed that various stations like Thal, Berinag and Didihat lies in the zone of high shear wave quality factor which represent less attenuating earth medium and hence carry high seismic hazard potential zone.

Chapter – 7

Determination of Source Parameters of the Sikkim Earthquake of 18 September, 2011

7.1 Introduction

Acceleration spectrum contains valuable information regarding the source and medium characteristics. The source spectrum of an earthquake can be defined by the omega-square model (Brune 1970). The source acceleration spectrum from the recorded motion is estimated from an acceleration record after correcting it with diminution function, which accounts for the geometrical spreading and anelastic attenuation term. It is seen that at large epicentral distance, the term representing anelastic attenuation and site amplifications plays an important role in shaping the acceleration spectrum. The anelastic attenuation is represented by shear wave quality factor. The Sikkim earthquake (M_w = 6.9) occurred on 18 September 2011 was recorded at six stations of strong motion network in Kumaon region. The frequency dependent shear wave quality factor and site amplification at each station of Kumaon network has been determined using strong motion data and is discussed in Chapter 5. This chapter present method to obtain source acceleration spectra of the Sikkim earthquake using obtained values of shear wave quality factor and site amplification at different stations.

7.2 Geology

Sikkim Himalaya is tectonically and seismically active region. The province of Sikkim in the Eastern Himalaya is bounded by Nepal in the west, Bhutan in the east, and the Tibetan Plateau in the north and is shown in Fig. 7.1. This region comprises the lesser active part of the 2500 km stretch of the active Himalayan belt. The major tectonic features traversing the Sikkim Himalaya are the well-defined Main Boundary Thrust (MBT) and the circular overturned Main Central Thrust (MCT) in the north (Raju et al., 2007). Seismic activity in the Sikkim Himalaya is confined between the MBT and MCT (De, 2000). The seismicity of the Sikkim region including earthquakes between 1973 to 2011 is shown in Fig. 7.1. The most significant earthquake that occurred in its neighbourhood is the 1934 Bihar–Nepal border earthquake of magnitude 8.3 (M_w) that caused high damage in Sikkim Himalaya (Dunn et al., 1939). Earlier, an earthquake of

magnitude 8.0 (M_w) was reported in 1833 (U.S. Geological Survey catalogue). More recently an earthquake of magnitude 6.6 (M_w) was reported in Gangtok in 1988 (Raju et al., 2007).

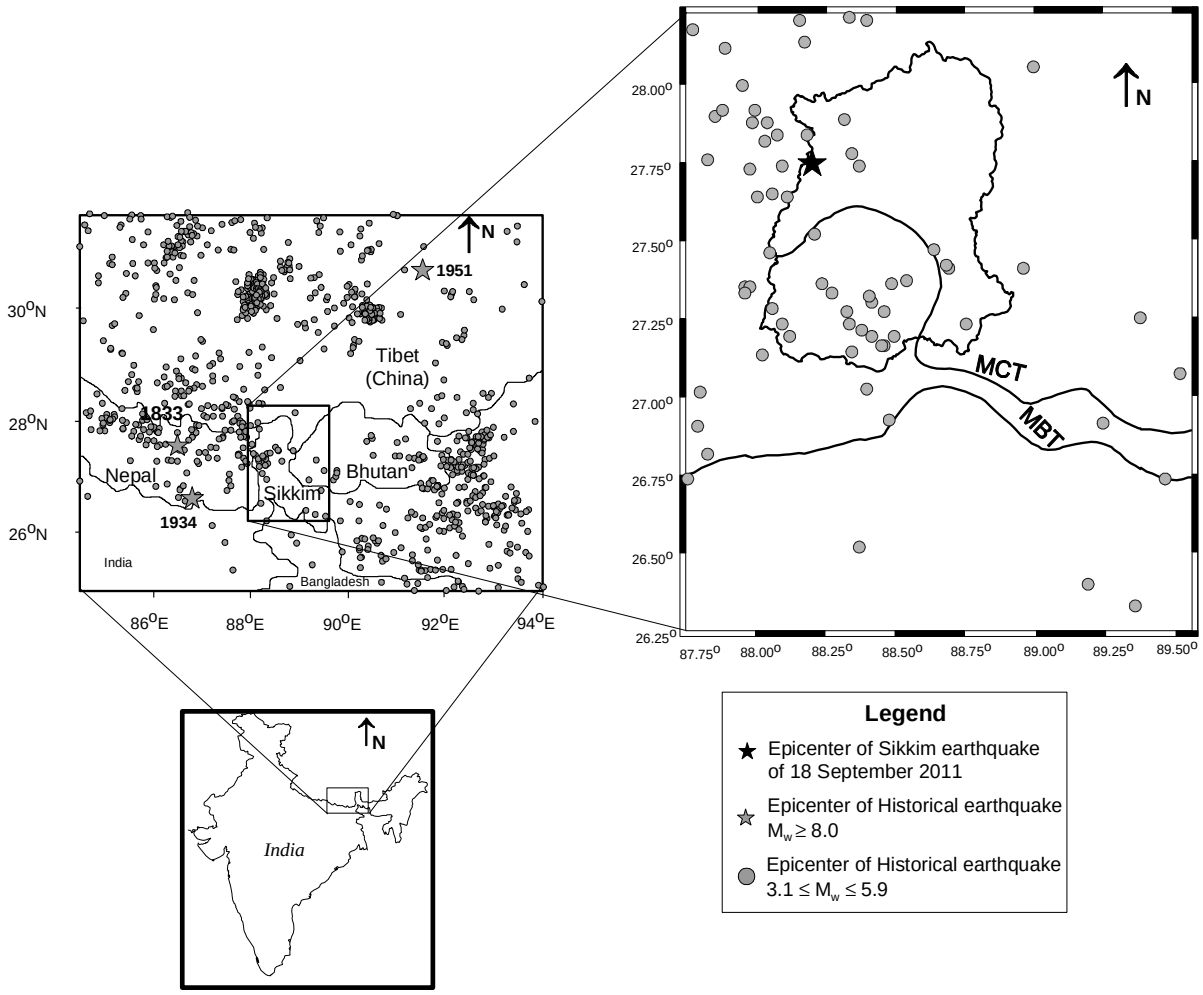

Figure 7.1: Seismicity map of the eastern Himalaya region indicating seismicity around the Sikkim. Location of historical earthquakes occurred during 1973 to 2011. The tectonic of the region is after Nath et al. (2000).

7.3 Data

An earthquake of magnitude 6.9 (M_w) visited the Sikkim region of eastern Himalaya on 18 September, 2011. This earthquake was recorded at six stations of strong motion network installed in the Kumaon array that lies at epicentral distance of about 887 to 944 km. The Kumaon array consists of network of fourteen stations having three-component force balance short period accelerometer. This network has recorded several small earthquakes occurred in the vicinity of the

recording stations. Location of recording stations which have recorded this earthquake and epicenter of this earthquake is shown in Fig. 7.2. This network has first time recorded strong ground motion due to an earthquake originating at such large epicentral distance.

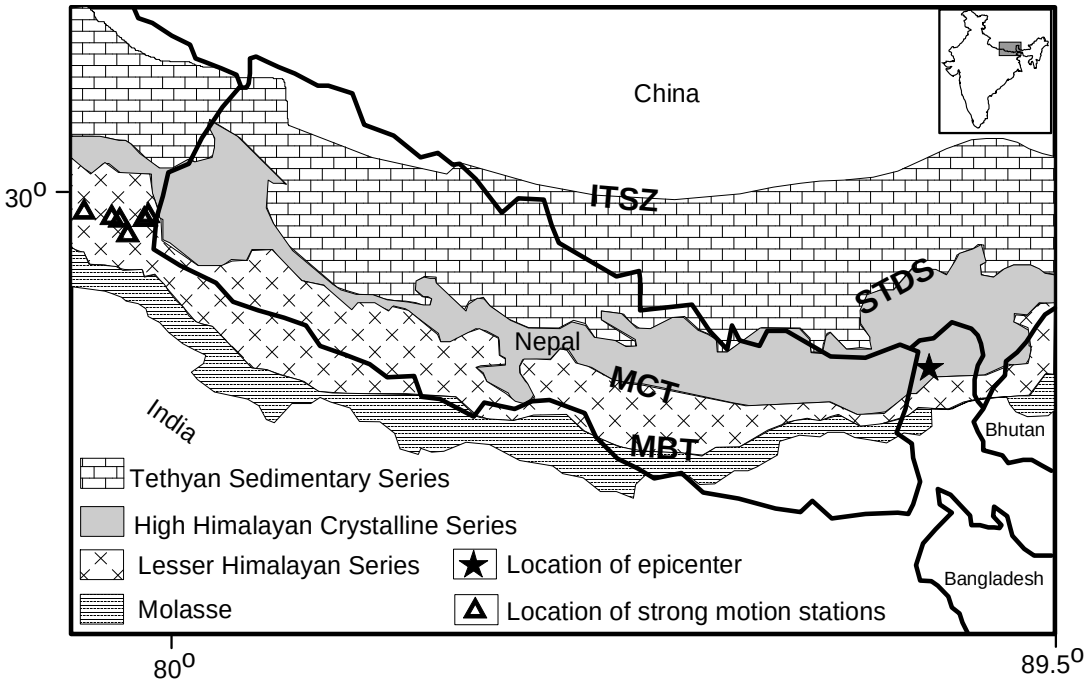

Figure 7.2: Location of strong motion recording stations of the Kumaon array that has recorded the Sikkim earthquake. The strong motion stations of local network and epicenter of the event are denoted by triangle and star, respectively. ITSZ, STDS, MCT and MBT represents Indus–Tsangpo suture zone, South Tibetan Detachment System, Main Central Thrust and Main Boundary Thrust, respectively (Figure modified after Harris, 2007).

This strong motion network lies in Lesser Himalaya which comprising various thrust sheets and nappes being sandwiched between the Main Boundary Thrust (MBT) and Main Central Thrust (MCT) at the base of great Himalaya. In general, the Lesser Himalayan Precambrian sedimentary succession is covered by vast low to medium grade metamorphic thrust sheets of Ramgarh and Almora groups (Paul et al., 2003). Epicenter of the Sikkim earthquake lies in the Sikkim Himalaya. Geologically this region exhibit a vast terrain of proterozoic continental crust on the Indian plate, which is remobilized into vast slab-like Higher Himalayan crystallines (HHC) due to Himalayan collision tectonics. This unit is (occurring as a doubly plunging dome) bounded by the Main Central Thrust (MCT) at the base and the South Tibetan Detachment System (STDS) at the top. The Lesser Himalayan Sedimentary Zone (Buxa, Permian Ranjit Pebble Slate/Damuda Formation) occurs in the Ranjit window and the Outer Lesser Himalayan Belt, as well. The whole sequence

overrides the outermost Sub-Himalayan siwalik Belt along the MBT (Neogi et al., 1998 and Dasgupta et al., 2004).

The Sikkim earthquake of 18 September, 2011 was localized using the arrival time of primary and secondary phases from six records using HYPO71 program originally developed by Lee and Lahr (1972). The obtained hypocentral parameters of this event are given in Table 7.1. The records collected from the accelerograph have been processed using the procedure suggested by Boore and Bommer (2005). The processing steps involve baseline correction, instrument scaling, padding and frequency filtering as discussed in detail in Chapter 4. In the present work processed records that are used for estimation of source parameters at different stations are shown in Fig. 7.3.

Table 7.1: Hypocentral parameters of event obtained from recorded data at six stations of the Kumaon array. ERH and ERZ define the error of epicenter and focal depth, respectively.

Date	**Origin time**	**Epicenter**	**Depth (km)**	**No. of Stations**	**RMS error**	**ERH (km)**	**ERZ (km)**
18/09/11	12:41:00.56	27º45.16',88º 12.00'	30	06	0.52	4.1	3.2

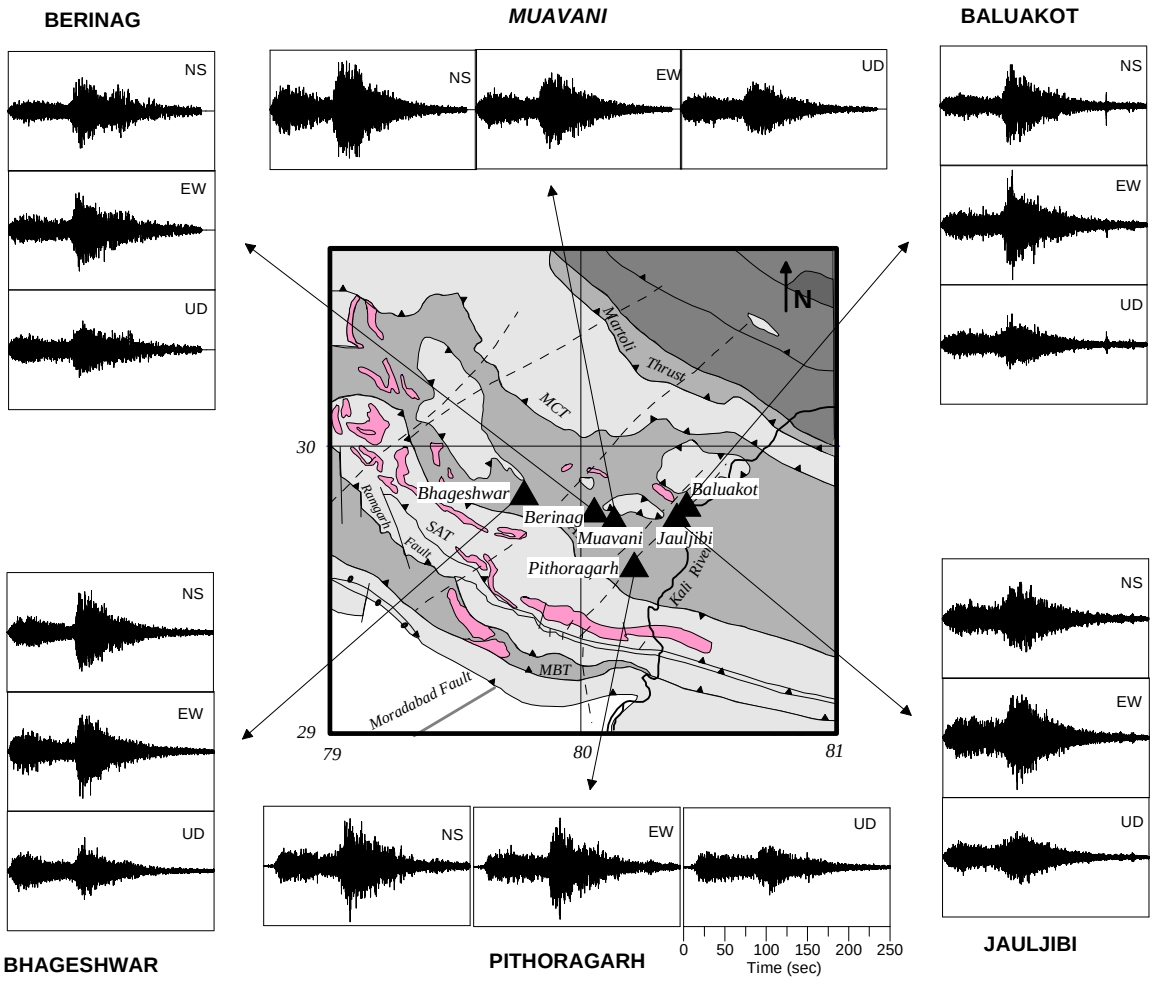

Figure 7.3: Processed normalize NS, EW and vertical components of accelerograms of the Sikkim earthquake of 18 September, 2011 recorded at different stations. Triangle shows the location of recording station. The tectonics of the region is taken after GSI (2000).

7.4 Methodology

The acceleration spectra of shear waves recorded at a distance R due to an earthquake of seismic moment M_o can be given as (Boore, 1983 and Atkinson and Boore, 1998):

$$A(f) = S(f)\, D(f) \tag{7.1}$$

where, the S(f) represents the source acceleration spectra and D(f) denotes a frequency-dependent diminution function which takes into account the anelastic attenuation and attenuation due to geometrical spreading and is given as (Boore and Atkinson, 1987):

$$D(f) = [e^{-\pi f R/Q_\beta(f)\beta} G(R)] P(f, f_m) \tag{7.2}$$

In the above equation $P(f,f_m)$ is a high-cut filter that accounts for the observation that acceleration spectra often show a sharp decrease with increasing frequency, above some cutoff frequency f_m, that cannot be attributed to whole path attenuation (Boore 1983). Due to rapid fall of acceleration spectra after 25 Hz in most of the acceleration records used in the present work, f_m is used as 25 Hz in the analytical form of $P(f,f_m)$ suggested by Boore (1983). The function G(R) represent geometrical attenuation term and is taken to be equal to 1/R for R < 100 km and equal to $1/\left(10\sqrt{R}\right)$ for R > 100 km (Singh et al., 1999). The term $e^{-\pi fR/Q_\beta(f)\beta}$ represent anelastic attenuation term and in this term $Q_\beta(f)$ is the frequency-dependent shear wave quality factor. Using equation (7.1) the source acceleration spectra $S_A(f)$ can be calculated as:

$$S(f) = A(f)/D(f) \tag{7.3}$$

The source displacement spectra '$S_D(f)$' can be calculated from source acceleration spectra 'S(f)' by using differential property of Fourier transform. This gives following equation:

$$S_D(f) = S(f)/ (2\pi f)^2 \tag{7.4}$$

The seismic moment (M_o) which determines the source strength is calculated using long term flat level (Ω_o) and corner frequency (f_c) from source displacement spectra. Source displacement spectra obtained from equation 7.4 give idea about 'f_c' and 'Ω_o'. The source displacement spectra '$S_D(f)$' can be theoretically computed from following expression given by Brune (1970):

$$S_D(f) = 1/(1+(f/f_c)^2) \tag{7.5}$$

In the above expression 'f_c' is corner frequency. Seismic moment (M_o) and radius of rupture (r_0) are related by following relations (Brune 1970, 1971):

$$M_o = 4\pi\rho\beta^3 \Omega_o R/ FS.R_{\theta\varphi} \tag{7.6}$$

where, ρ and β are the density and the S-wave velocity of the medium, respectively, FS is the free surface effect, Ω_o is the long term flat level of the source displacement spectrum at a hypocentral distance of R and $R_{\theta\varphi}$ is the radiation-pattern coefficient. The value of density and shear wave velocity as 2.7 gm/cm^3 and 3.5 km/sec, respectively have been used. The radiation pattern coefficient '$R_{\theta\varphi}$' was approximately taken as 0.63 for S wave (Atkinson and Boore, 1995). The

corner frequency 'f_c' of the source spectra is related to the radius 'r_o' of the equivalent circular crack, which is used to model the earthquake. The relation between 'r_o' and the corner frequency 'f_c' is given as (Brune 1970, 1971):

$$r_o = 2.34\beta/2\pi f_c \tag{7.7}$$

Stress drop ($\Delta\sigma$) is one of the important parameters of an earthquake source and it is the difference between the average shear stress on the fault zone before and after the earthquake (Ruff, 1999). For a circular crack of radius 'r_o' the stress drop '$\Delta\sigma$' is given as (Papageorgiou and Aki, 1983):

$$\Delta\sigma = 7M_o /16\, r_o^3 \tag{7.8}$$

The strong motion data of the Sikkim earthquake is recorded at various stations of Kumaon network which are nearly 900 km away from the source. In order to determine source parameters of this earthquake using records at a distance of 900 km, the effect of anelastic attenuation in the source as well as recording station needs to be removed from spectra of shear wave recorded at various stations. It is seen that the source region and the region of recording station have different attenuation property. In order to include these different attenuation properties the shear wave quality factor for the source region as well as region of recording station has been included in present work. The frequency dependent diminution function has been modified to include the shear wave quality factor of the source region and that for the region of the recording station. Following modifications has been made in the frequency-dependent diminution function:

$$D(f) = \exp\left[-\pi f\left(\frac{R-100}{Q_{\beta 2}.\beta_2} + \frac{100}{Q_{\beta_1}.\beta_1}\right)\right] \tag{7.9}$$

where, $Q_{\beta 1}$, β_1 and $Q_{\beta 2}$, β_2 are the quality factors and shear wave velocities of source and site regions, respectively. In this equation the source zone is defined upto hypocentral distance less than 100 km and for the distance more than 100 km anelastic attenuation of the site zone is used for anelastic attenuation. This is shown in Fig. 7.4. Since the energy reaching at recording stations is travelling mostly through lesser Himalaya sequence the shear wave quality factor estimated at the recording station which lies in the lesser Himalaya is used for correcting anelastic attenuation for far field distances given in equation (7.9). The shear wave quality factor at the source region is used as $Q_\beta(f)=167f^{0.47}$ which is given by Nath and Thingbaijam (2009) for the Sikkim region. The

spectral acceleration data need to be correct for site amplification terms. The site effects and shear wave quality factor at different stations of Kumaon network has been calculated in Chapter 5 using inversion algorithm defined in Chapter 3. The spectral acceleration of shear wave is corrected for site amplification term at each station for determination of source spectra.

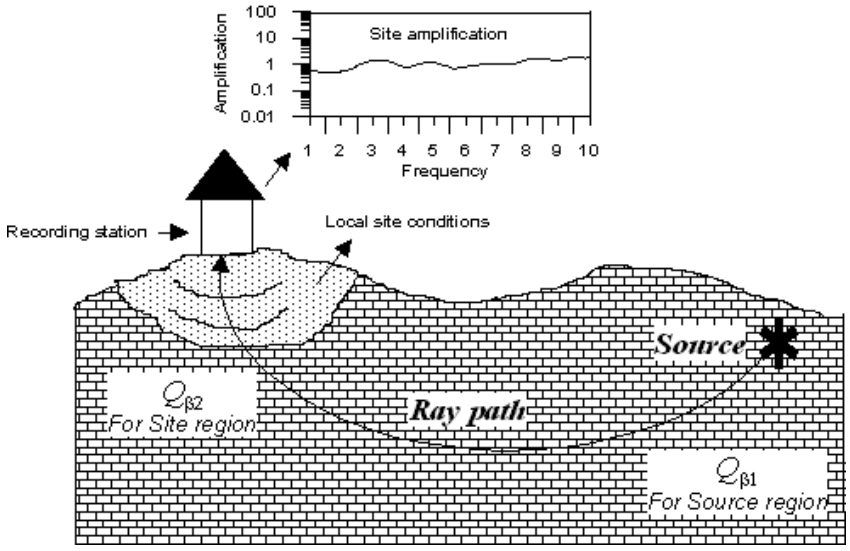

Figure 7.4: Geometry of ray path between source and recording station. The shear wave quality factor at source and the site of recording station is shown by $Q_{\beta 1}$ and $Q_{\beta 2}$, respectively.

7.5 Results

The horizontal component of accelerograms recorded at six stations of the Kumaon array has been used in present work for estimation of the source parameters of the Sikkim earthquake. The first step in this process is the identification of S-phase in the available records. The records used in the present work are mostly far field records with epicentral distance more than 800 km. The S-phase is clearly visible in the records because of the low threshold set in the recorders. The S-phase from the record has been identified on the basis of visual inspection. A time window of length which covers entire S-phase has been applied to the corrected accelerogram. The sampled window is cosine tapered with 10% taper at both end (Sharma and Wason 1994). The spectrum of this time series is calculated using FFT algorithm. This spectrum has been corrected for anelastic attenuation as well as site amplification. All recording stations are located in the mountainous terrain of Himalaya which consists of mostly sedimentary and metamorphic rocks. Site amplification plays the important role in shaping of ground motion recorded at stations having prominent site effects. Since stations are located very far away from the source the shear wave

quality factor in the earth medium surrounding the region of recording station have also important role in shaping the record together with shear wave quality factor surrounding the source region.

The value of quality factor used for source region is $Q_\beta(f)=167f^{0.47}$ given by Nath and Thingbaijam (2009). The values of quality factors for different recording stations are determined in Chapter 5 using the inversion scheme discussed in Chapter 3 and given in Table 7.2. Shear wave quality factor of the source region has been extensively studied by many workers (Nath et al., 2005 and Nath and Thingbaijam, 2009). However, limited information about $Q_\beta(f)$ at recording station is available. Therefore, in the present work $Q_\beta(f)$ estimated at the recording stations using the strong motion data of Kumaon network has been used. Since large difference is obtained between $Q_\beta(f)$ values at source and recording station; so both $Q_\beta(f)$ values are used to correct the path effect between source and receiver. The travel path of seismic wave is comparatively large and the medium characteristics are totally different at source and at recording stations. The various study in the source and receiver region regarding the Q values revealed that source region is having high $Q_\beta(f)$ values as comparison to the receiver area.

A numerical experiment has been performed to check the dependency of source spectra on shear wave quality factor of source and receiver area. This numerical experiment has been used to check the effect of variable shear wave quality factor and site amplification term in the source spectra of the NS component of acceleration record of the Sikkim earthquake recorded at Pithoragarh station. The recorded NS component of acceleration record at Pithoragarh station is shown in Fig. 7.5. The rectangular block in this record shows portion of S-phase used for obtaining source spectra. Source acceleration spectra from the record at Pithoragarh is calculated using correction of the shear wave quality factor at source region give by Nath and Thingbaijam (2009) and is shown in Fig. 7.5. This has been compared with theoretical source spectrum given by Brune (1970). The comparison shows that low frequency in the source spectra does not match correctly with theoretical spectra. This may be due to large epicentral distance of the recording station and use of anelastic attenuation of the source region in computation. In other experiment Source acceleration spectrum is calculated after correcting the effect of the shear wave quality factor at Pithoragarh station. The obtained source spectrum is shown in Fig. 7.6.

Table 7.2: The average $Q_\beta(f)$ relation and RMS error obtained at different stations from the inversion of spectral acceleration data of the NS and EW component of acceleration records of different events.

Stations	Location (Degree)		For NS component		For EW component	
	Lat.	Long.	$Q_\beta(f)$	RMS error	$Q_\beta(f)$	RMS error
Pithoragarh	29.58	80.21	$(40\pm5.0)f^{(0.8\pm0.10)}$	0.0134	$(33\pm8.3)f^{(1.3\pm0.10)}$	0.0478
Bhageshwar	29.83	79.77	$(34\pm4.1)f^{(1.2\pm0.10)}$	0.0328	$(41\pm5.1)f^{(1.2\pm0.12)}$	0.0212
Berinag	29.77	80.05	$(15\pm2.1)f^{(1.3\pm0.15)}$	0.0566	$(23\pm2.2)f^{(1.2\pm0.09)}$	0.0360
Baluakot	29.79	80.42	$(16\pm2.6)f^{(1.1\pm0.11)}$	0.0697	$(13\pm2.8)f^{(1.3\pm0.20)}$	0.0881
Jauljibi	29.75	80.38	$(10\pm0.8)f^{(1.3\pm0.12)}$	0.0425	$(8\pm1.1)f^{(1.3\pm0.12)}$	0.0597
Muavani	29.74	80.13	$(17\pm2.9)f^{(1.4\pm0.14)}$	0.1946	$(24\pm4.5)f^{(1.3\pm0.17)}$	0.3576

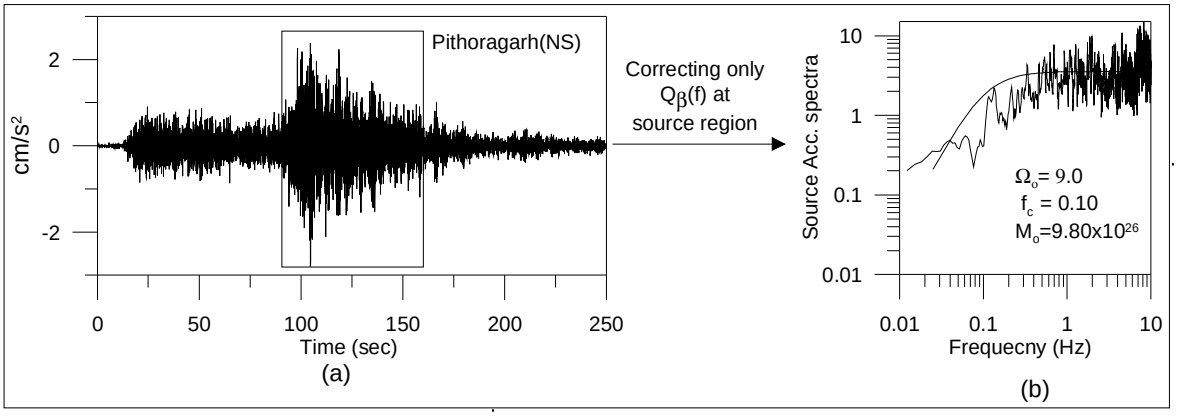

Figure 7.5: (a) North South component of acceleration record recorded at Pithoragarh station rectangular box indicate the S-phase of the record and (b) Comparison of theoretical source spectra and obtained spectra from NS component of acceleration record at Pithoragarh station using correction for anelastic attenuation using $Q_\beta(f)$ at source region given by Nath and Thingbaijam (2009). The parameters M_o, Ω_o and f_c describe the seismic moment, long term flat level and corner frequency, respectively.

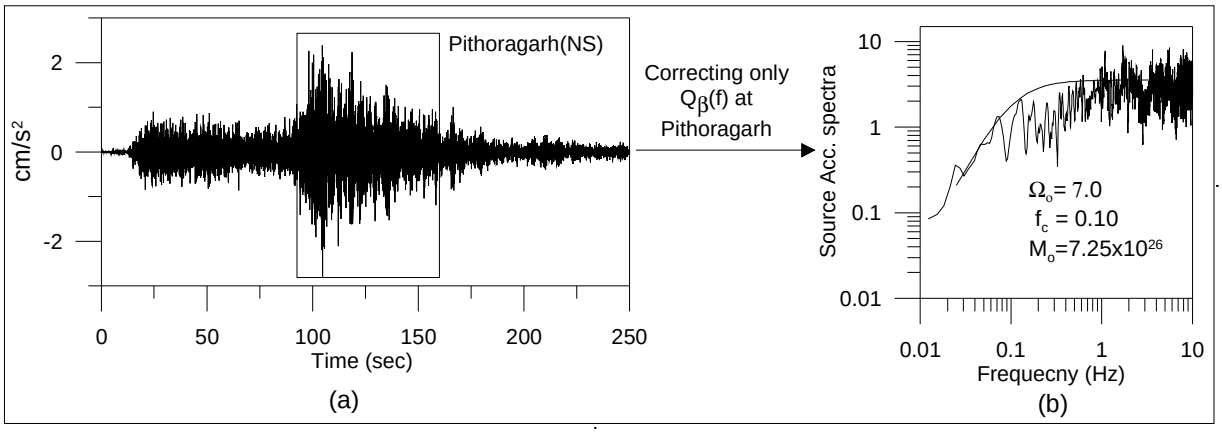

Figure 7.6: (a) North South component of acceleration record recorded at Pithoragarh station rectangular box indicate the S-phase of the record and (b) Comparison of theoretical source spectra and obtained spectra from NS component of acceleration record at Pithoragarh station using correction for anelastic attenuation using $Q_\beta(f)$ at Pithoragarh station obtained from inversion technique. The parameters M_o, Ω_o and f_c describe the seismic moment, long term flat level and corner frequency, respectively.

In a next attempt acceleration spectrum of Pithoragarh is corrected for shear wave quality factor at source as well as recording site without correcting site amplification term. The near source region is defined as the region which lies at a distance less than 100 km and for this near source zone the shear wave quality factor give by Nath and Thingbaijam (2009) has been used. It is seen that correction for anelastic attenuation term using variable shear wave quality factor tends to make source acceleration spectra closer to the theoretical Brune's spectra in low frequencies as shown in Fig. 7.7. Numerical experiment is also performed to check the effect of correction of variable shear wave quality factor and site amplification term. The source acceleration spectrum is computed by correcting effect of variable shear wave quality factor and site amplification at Pithoragarh station. The obtained source spectrum in Fig. 7.8 shows that the obtained source spectrum gives better match with theoretical spectrum when corrections for site amplifications together with variable shear wave quality factor are included in the calculation.

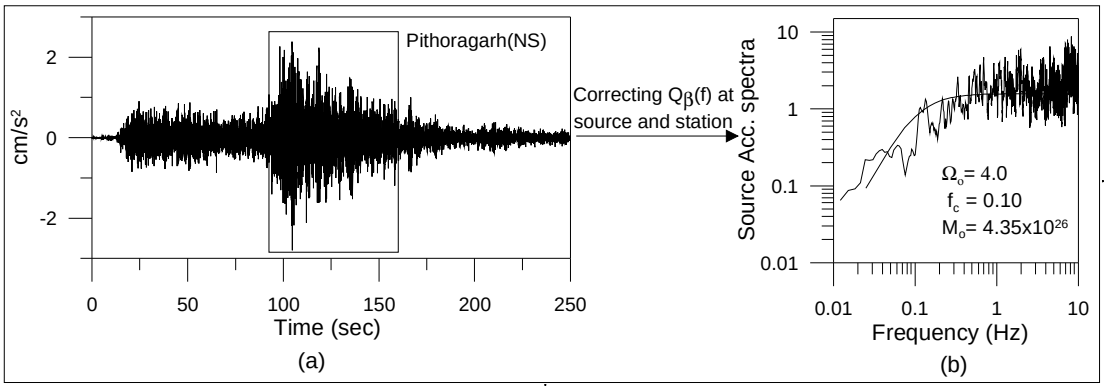

Figure 7.7: (a) North South component of acceleration record recorded at Pithoragarh station rectangular box indicate the S-phase of the record and (b) Comparison of theoretical source spectra and obtained spectra from NS component of acceleration record at Pithoragarh station using correction for shear wave quality factor at source and receiver. The parameters M_o, Ω_o and f_c describe the seismic moment, long term flat level and corner frequency, respectively.

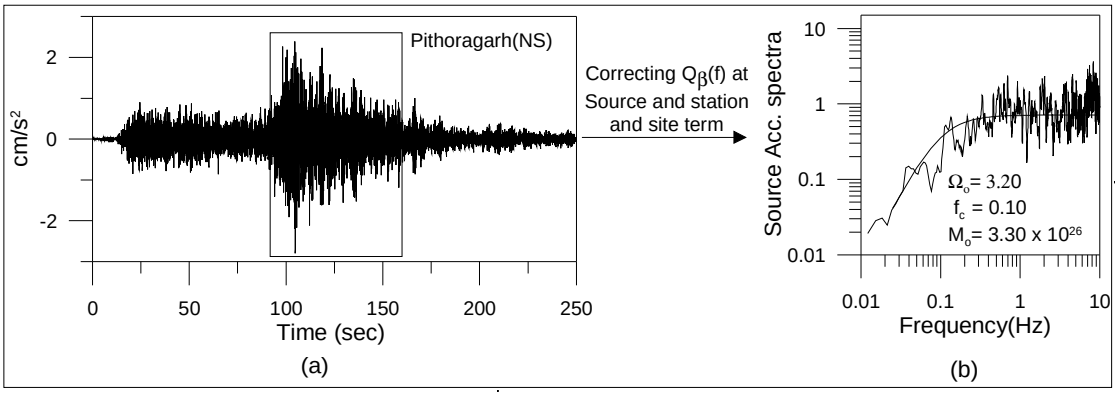

Figure 7.8: (a) North South component of acceleration record recorded at Pithoragarh station rectangular box indicate the S-phase of the record and (b) Comparison of theoretical source spectra and obtained spectra from NS component of acceleration record at Pithoragarh station using both shear wave quality factor at source and site as well as site amplification term. The parameters M_o, Ω_o and f_c describe the seismic moment, long term flat level and corner frequency, respectively.

Source acceleration spectra from NS and EW component of different accelerograms of the Sikkim earthquake recorded at six stations after correction for variable shear wave quality factor and site amplification term is shown in Fig. 7.9 and 7.10, respectively. The obtained acceleration spectra are compared with theoretical spectra by iterative forward modeling technique. The iterative forward modeling is done by considering several possibilities of long term flat level and corner frequency in the theoretical Brune's (1970) spectra. The obtained value of long term flat level (Ω_o) and corner frequency (f_c) is further used to calculate seismic moment, source radius and

stress drop by using the formula given by Brune (1970, 1971) and Papageorgiou and Aki (1983), respectively. The shear wave velocity and density of the medium for this calculation is used as 3.5 km/s (Hazarika et al., 2010) and 2.7 g/cm^3 (De, 2000), respectively which are the values used for the Sikkim region. Estimation of seismic moment, source radius and stress drop from obtained long term flat level and corner frequency at different stations is given in Table 7.3. The average value of seismic moment, stress drop and source radius for the Sikkim earthquake from all six stations using both components is obtained as (3.2 ±0.8) × 10^{26} dyne-cm, 59.2 ±8.8 bars and 13.3 ±0.8 km, respectively.

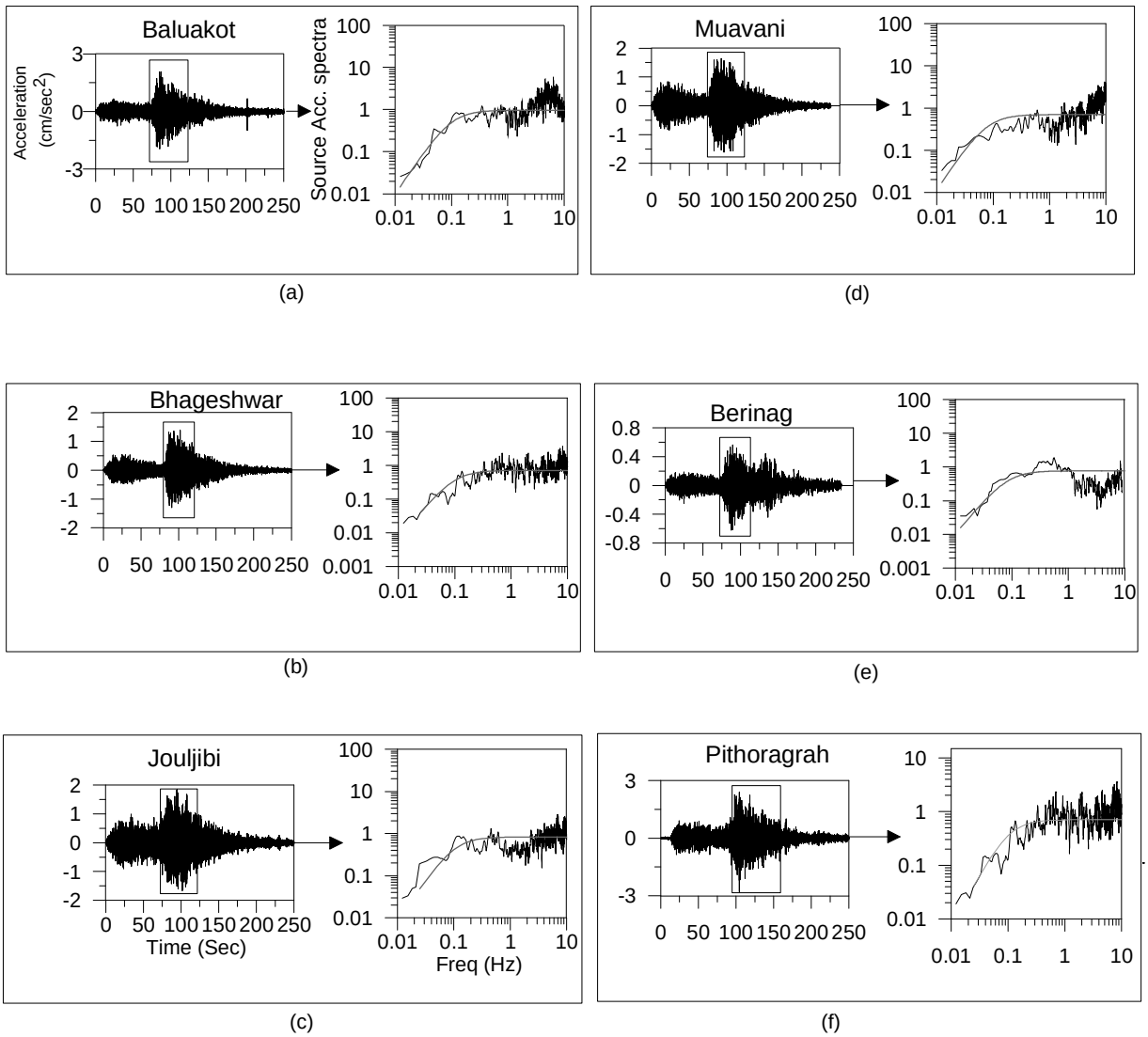

Figure 7.9: The NS component of the acceleration record and source acceleration spectra computed from the S-phase identified by the rectangular block at (a) Baluakot, (b) Bhageshwar, (c) Jouljibi, (d) Muavani, (e) Berinag and (f) Pithoragarh stations, respectively.

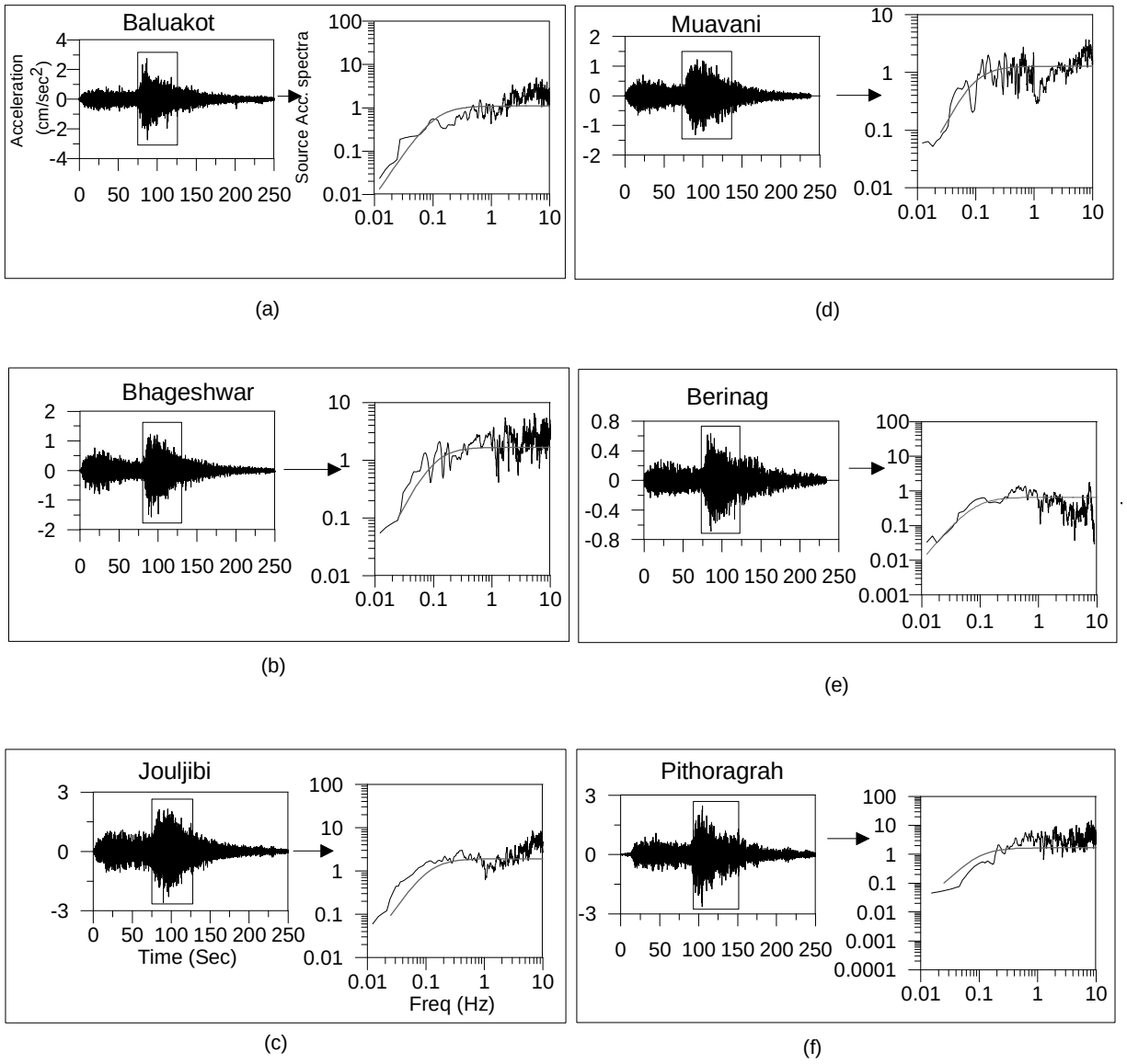

Figure 7.10: The EW component of the acceleration record and source acceleration spectra computed from the S-phase identified by the rectangular block at (a) Baluakot, (b) Bhageshwar, (c) Jouljibi, (d) Muavani, (e) Berinag and (f) Pithoragarh stations, respectively.

Table 7.3: Strong motion parameters determined from the source spectra computed from both NS and EW component of horizontal record at six stations.

Station		Corner freq (Hz)	Long term flat level	Seismic moment (dyne-cm)	Stress drop (bars)	Source radius (km)
Baluakot	EW	.110	2.30	2.35×10^{26}	62.15	11.8
	NS	.099	2.50	2.56×10^{26}	49.24	13.1
Berinag	EW	.097	2.60	2.75×10^{26}	49.80	13.4
	NS	.098	2.70	2.85×10^{26}	53.33	13.3
Bhageshwar	EW	.093	4.40	4.79×10^{26}	76.46	14.0
	NS	.10	2.80	3.05×10^{26}	60.49	13.0
Jauljibi	EW	.096	4.00	4.10×10^{26}	71.92	13.5
	NS	.110	2.10	2.15×10^{26}	56.80	11.8
Muavani	EW	.090	4.00	4.19×10^{26}	60.66	14.5
	NS	.093	3.00	3.14×10^{26}	50.20	14.0
Pithoragarh	EW	.100	3.20	3.30×10^{26}	65.47	13.0
	NS	.095	3.10	3.14×10^{26}	54.38	13.7

The estimated values of seismic moment, stress drop and source radius obtained at different stations for both NS and EW component is shown in Fig. 7.11. It shows that most of the values are within the limit $\mu \pm \sigma$ obtained at different stations. The value of stress drop calculated for this earthquake by Joshi et al. (2012b) is 61.5 bars and this value of stress drop is comparable with the stress strop calculated in the present work. The values of stress drop in the Himalaya region for the Uttarkashi earthquake of 20th October 1991 (M_s = 7.0) are 77 and 53 bars calculated by Joshi (2006c) and Kumar et al. (2005a), respectively and for the Chamoli earthquake of 28th March 1999 (M_s = 6.6) 98 and 65 bars calculated by Joshi (2006c) and Kumar et al. (2005a), respectively. Hence the value of stress drop calculated in this work lies within the range of observed values of stress drop of earthquakes occurring in the Himalayas region. The calculated rupture area for this earthquake using the source radius 13.3 ±0.8 km lies between 489 to 626 sq km. The empirical relation of Wells and Coppersmith (1994) gives the rupture area as 616.6 sq km for this earthquake of magnitude 6.9 (M_w). The comparison has been made and given in Table 7.4. This matches closely with estimation of rupture area of source in present work.

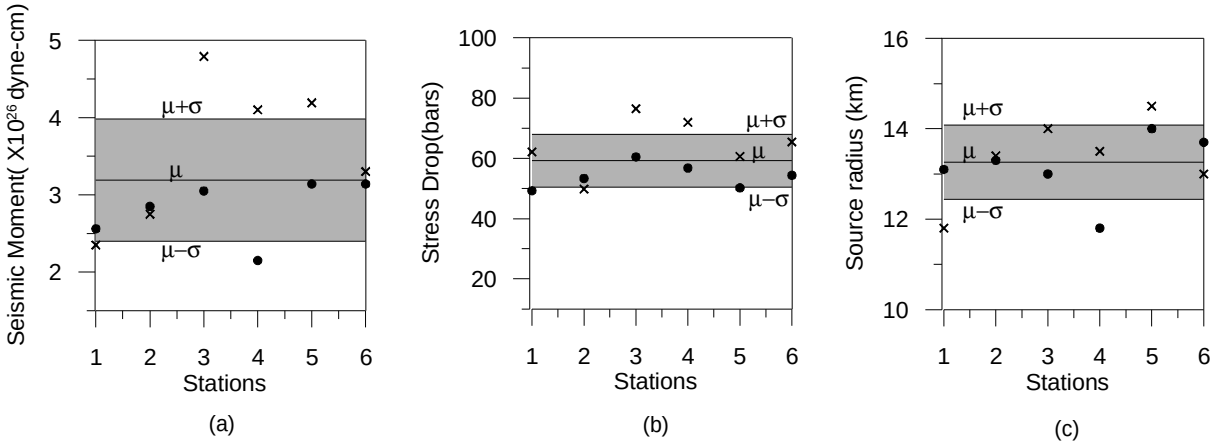

Figure 7.11: (a) Seismic moment, (b) stress drop and (c) source radius obtained at different stations.The shaded area denote the region between (μ+σ) and (μ-σ). The parameters 'μ' and 'σ' denote mean and standard deviation, respectively. Solid circle and cross indicate source parameters obtained from NS and EW component, respectively.

Table 7.4: Parameters determined from the empirical relations and source spectra.

Parameters	**Estimated from Empirical relations**	**Estimated from Source spectra in the present work**
Rupture area	616.6 Sq km [Relation after Wells and Coppersmith (1994)]	489 to 626 Sq km
Seismic moment	2.6×10^{26} dyne-cm [Relation after Wells and Coppersmith (1994) and Hanks and Kanamori (1979)]	$(3.2 \pm 0.8) \times 10^{26}$ dyne-cm

Following relation of calculating moment magnitude given by Wells and Coppersmith (1994) has been used in present work. The obtained value of moment magnitude calculated using the empirical relations of Wells and Coppersmith (1994) for the Sikkim earthquake is 6.9 (M_w). The seismic moment (M_o) can be estimated using the following formula given by Hanks and Kanamori (1979):

$$M_o = 10^{3/2[M_w + 10.71]} \tag{7.10}$$

The value of moment magnitude obtained from relation given by Wells and Coppersmith (1994) is used to calculate seismic moment of this earthquake. The value of seismic moment obtained from equation (7.10) is 2.6×10^{26} dyne-cm. A comparison of computed values of the

parameters from source spectra with the values computed from empirical relations has been made and given in Table 7.4. The values of seismic moment for this earthquake obtained by CMT Harvard and USGS are 2.78×10^{26} dyne-cm and 2.7×10^{26} dyne-cm, respectively. These values of seismic moment match closely with estimation of seismic moment made in this present work. Therefore establishing the utility of corrections of quality factor at source and receiver and site amplification term.

7.6 Conclusion

This chapter explains utility of obtained shear wave quality factor and site amplification terms of the stations of Kumaon network determined in Chapter 5. Various source parameters of the Sikkim earthquake of magnitude 6.9 (M_w) that occurred on 18 September, 2011 has been estimated in this chapter. The source spectra have been calculated using six far field strong motion acceleration records of station of Kumaon network. The corrections for anelastic attenuation at near site and source region have been made together with site amplification terms at each station for estimation of source spectra at different stations. Present studies give estimation of seismic moment, stress drop and source radius for the Sikkim earthquake as $(3.2 \pm 0.8) \times 10^{26}$ dyne-cm, 59.2 ±8.8 bars and 13.3 ±0.8 km, respectively which matches closely with values obtained by other studies. This confirms utility of applying corrections of anelastic attenuation at source and receiver and site amplification term.

Chapter – 8

Summery and Conclusions

8.1 Summery

Propagation of seismic wave through a medium is affected by the three factors viz., source characteristics, travel path and local site effect. The amplitude of seismic wave at observing site is strongly dependent on the attenuation characteristic of medium present between the source and receiver. Different types of propagation material affect differently the amplitude of seismic wave. The effects of the propagation material on earthquake ground motion are associated with the attenuation property of medium. The damage distribution during earthquake is strongly controlled by local site conditions of the observing sites and the attenuation characteristics of the medium. Therefore estimation of attenuation property and site effect is an important task for hazard analysis and subsurface studies. Present research work is an effort to understand and quantify the attenuation property of earthquake ground motions using strong motion data. Main objectives of this study are:

- Development of an algorithm and software for inversion of strong motion data for determination of frequency dependent shear wave quality factor and site effect simultaneously at given site.
- Use of determined site effect for understanding the source characteristics of strong motion earthquakes in the region.
- Development of an algorithm and software for inversion of strong motion data to determine the three dimensional attenuation tomography of a region.
- Application of developed algorithm for determination of three dimensional attenuation structure of well studied region and comparison of obtained results with the available tectonic features of the region.
- Application of algorithm developed in the present work for determination of attenuation structure of the Kumaon Himalaya using strong motion data from a dense network installed in this region.

Strong motion data includes valuable high-frequency near-field data which is considered to be suitable for engineering use. Strong motion data is one of the most useful data which is directly used in the practice of designing earthquake resistant structures. Hence strong motion data having major advantages regarding the engineering point of view. In the present work strong motion data has been used to fulfill the objectives of research work presented in this thesis.

In the present work, attenuation properties have been determined for two regions viz., Kumaon Himalaya, India and the Central Honshu region, Japan. Availability of sufficient strong motion data in this region is main reason for choosing these two study area. In the Kumaon Himalaya region very few studies have been done regarding the attenuation properties. The strong motion data recorded on the Kumaon network consisting of fourteen stations, installed in the highly mountainous terrain of Kumaon Himalaya, India have been used for study related to Kumaon Himalaya. The average interspacing distance of station in Kumaon Himalaya region is 11 km. The strong motion data from 27 stations of KiK-net (KIBAN kyoshin network) network installed in Central Honshu region have been used in present study. The average interspacing distance of station in Central Honshu region is 18 km.

First part of the present study is to determine the three dimensional attenuation structures using the strong motion data. Determination of three dimensional attenuation structure of any region using the algorithm developed in present work depends strongly on availability of strong motion data free from site effect. The strong motion network operating in the Honshu region managed by KiK net provide an opportunity to obtain strong motion data recorded at rock site in borehole. The method of inversion of strong motion data to obtain three dimensional distributions of attenuation coefficients is discussed in details in the Chapter 2. Twenty one earthquakes recorded on 27 strong motion stations at rock site have been used in this work. The magnitude of these earthquake ranges from 3.1 to 4.2 and depth ranging from 5 km to 20 km, respectively. The borehole data having high signal to noise ratio and minimum site effect have been used in the present work. The attenuation structure is determined by dividing the entire area into twenty-five three-dimensional blocks of uniform thickness of 5 km having different frequency-dependent shear wave quality factor. Shear wave quality factor values have been determined at different frequencies from record in a rectangular grid defined by 35.4° N to 36.4° N and 137.2° E to 138.2° E. The observed attenuation structure gives comparable trends with the geological structure of the region. The obtained attenuation structure has been also compared with the available Probabilistic seismic hazard map of the region and shows some remarkable similarity.

The frequency dependent Shear-wave quality factor ($Q_\beta(f)$) has been computed for the Pithoragarh region of the Kumaon Himalaya, India. In this study, forty local events recorded during 2006 to 2012 at sixteen stations have been used. The inversion algorithm works iteratively and final result is determined on the basis of minimum root mean square error between obtained and observed data. The final $Q_\beta(f)$ at each station is calculated by using both the North South (NS) and East West (EW) component of the acceleration records as input to the developed inversion algorithm. The final $Q_\beta(f)$ values is calculated using both North South (NS) and East West (EW) component at each station. The computed final $Q_\beta(f)$ at each station is given in Table 8.1. The final $Q_\beta(f)$ values obtained at different stations have been used to compute a regional relationship for the Pithoragarh region of Kumaon Himalaya of form $Q_\beta(f) = (28\pm2.1)f^{(1.2\pm0.09)}$ which represent the shear wave attenuating property of rocks present in this region. The developed inversion algorithm used for calculation of shear wave quality factor also determined site effects simultaneously at each of 16 stations.

Table 8.1: The $Q_\beta(f)$ relationship at different stations using NS and EW component data. Final $Q_\beta(f)$ relation at each station is developed by using the value of $Q_\beta(f)$ obtained from NS and EW component separately.

Stations	**Final $Q_\beta(f)$ relation using value of $Q_\beta(f)$ obtained from NS and EW component separately**	**Stations**	**Final $Q_\beta(f)$ relation using value of $Q_\beta(f)$ obtained from NS and EW component separately**
Dharchula	$(21\pm5.0)f^{(0.7\pm0.23)}$	Jouljibi	$(10\pm2.9)f^{(1.3\pm0.12)}$
Didihat	$(35\pm7.0)f^{(1.1\pm0.15)}$	Muavani	$(19\pm3.5)f^{(1.3\pm0.07)}$
Pithoragarh	$(39\pm3.5)f^{(1.1\pm0.15)}$	Knalichhina	$(22\pm3.0)f^{(1.3\pm0.09)}$
Thal	$(35\pm8.0)f^{(1.2\pm0.21)}$	Kamedidevi	$(25\pm5.4)f^{(0.9\pm0.06)}$
Tejam	$(20\pm2.6)f^{(1.1\pm0.22)}$	Askot	$(25\pm5.3)f^{(0.8\pm0.09)}$
Bhageshwar	$(39\pm4.7)f^{(1.2\pm0.11)}$	Munsyari	$(44\pm5.6)f^{(1.3\pm0.07)}$
Berinag	$(21\pm5.7)f^{(1.2\pm0.11)}$	Sobla	$(27\pm2.4)f^{(1.1\pm0.05)}$
Baluakot	$(16\pm3.0)f^{(1.2\pm0.12)}$	Mangti	$(33\pm3.7)f^{(1.1\pm0.07)}$

The three dimensional distribution of shear wave quality factor for Kumaon region, India have been estimated using the modified algorithm given in Chapter 2. The obtained site effects at sixteen stations from inversion algorithm given in Chapter 3 have been used in this part of inversion to correct the spectral amplitude of acceleration record for site effect at all sixteen stations. Inversion algorithm described in Chapter 2 has been used for determination of three

dimensional attenuation structures. Eighteen events recorded on strong motion Kumaon network at sixteen stations have been used for this work. Shear wave quality factor at different frequencies have been estimated for two different rectangular blocks of surface dimension 85×55 km and 90×30 km, respectively in this region. Both blocks are divided into twenty-five three-dimensional blocks of uniform thickness of 5 km having different $Q_\beta(f)$ values. The three dimensional distributions of frequency dependent shear wave quality factor in two different blocks expose the attenuation property of the region. The observed contours of attenuation coefficient present comparable trends with the geological structure of the region. It is seen that the contour of quality factor value at deeper depth are remarkably parallel to the main central thrust present in the study region. This shows the strong relation of attenuation property with the available tectonic of the region.

The site amplification and frequency dependent shear wave quality factor determined at 16 stations have been used to compute the source parameter of Sikkim earthquake. The Sikkim earthquake (M_w=6.9) occurred on 18 September, 2011 in Sikkim region, India. This earthquake has been recorded at six stations of strong motion network installed in Uttarakhand Himalaya. In the present work the spectrum of S-phase recorded at these far field stations has been corrected for anelastic attenuation using shear wave quality factor at source and site. Site amplifications at different stations and near site shear wave attenuation factor determined in Chapter 5 by using the technique discussed in Chapter 3 have been used to correct the spectra. The obtain source spectrum from six acceleration records is compared with the theoretical source spectrum defined by Brune (1970) at each station for both horizontal component of the records. Iterative forward modeling of the theoretical source spectrum give an average estimate of seismic moment (M_o), source radius (r_o) and stress drop ($\Delta\sigma$) as (3.2 ±0.8) $\times 10^{26}$ dyne-cm, 13.3 ±0.8 km and 59.2 ±8.8 bars, respectively for the Sikkim earthquake of 18 September, 2011.

8.2 Conclusions

The research work carried out in this thesis revealed that the inversion technique used in this work provide a basic tool to determine detailed shear wave quality factor of the region using strong motion data. The objectives recognized for the present research work have been fulfilled by determining the frequency dependent shear wave quality factor in the Kumaon Himalaya and Central Honshu, Japan region. Major conclusions of the present thesis are listed below:

1. Modification in the method of inversion given by Joshi (2006a, 2007) and Joshi et al. (2010) has been made in the present work to determine three dimensional attenuation structures using strong motion data. Earlier method of inversion given by Joshi (2006a, 2007) and Joshi et al. (2010) considers limited number of events. The restriction of limited number of events has been removed in the modified algorithm.

2. The inversion algorithm developed for three dimensional attenuation structures is numerically tested for its dependency on number of input event. This experiment clearly shows that obtained attenuation structure is strongly dependent on number of input events and root mean square error increases as number of input events decreases provided the data set has similar depth range.

3. The inversion algorithm developed for three dimensional attenuation structures is numerically tested for its dependency on depth range of input events. It is observed that due to difference in the ray path of energy released from earthquake to the observation point with different depth range, different attenuation structures can be obtained for different input data set. The attenuation structure corresponding to minimum root mean square error is obtained for the data set having large depth range. This experiment also shows that present algorithm tend to give similar attenuation structure for input data having events of similar depth range.

4. Numerical experiment on the inversion algorithm regarding data from earthquakes of similar depth range shows that obtained attenuation structure does not depends on order of input data and is a stable algorithm.

5. Shear wave quality factor are strongly influenced by heterogeneity of the medium and tectonic activity in the region. The obtained three dimensional distribution of shear wave quality factor is expected to provide important information regarding both heterogeneity and tectonic of the region. The obtained three dimensional distributions from strong motion data have been

compared in this work with available tectonics of the study region. The comparison of obtained structure with tectonic of the region shows remarkable similarity of distribution of attenuation coefficient with the tectonic of the region.

6. Three dimensional attenuation structures have been obtained by using the modified inversion algorithm in the central Honshu region, Japan. Twenty one earthquakes digitally recorded at 27 stations of KiK-net network have been used for this work. The obtained attenuation structure is compared with the available tectonic features of the region and comparison shows that the obtained attenuation structure is capable of resolving important tectonic features present in the area.

7. Another algorithm based on the least-square inversion technique modified by Joshi (2006b) is used to determine the frequency dependent shear wave quality factor ($Q_\beta(f)$) using seismic moment as an input parameter from independent sources. Modifications in this inversion algorithm have been made to compute seismic moment from input record in an iterative manner.

8. Developed algorithm has been tested for its dependency on input data sets. Results from inversion of different input data indicate that similar shear wave quality factor can be obtained for different data sets from same region. Thereby establishing the fact that inversion results are independent of input data set and clearly reflects the subsurface property as long as the travel path of input events is similar.

9. Strong motion data are rich in high frequencies. Dependency of maximum frequency data on inversion algorithm has been tested in the present work. It is seen that minimum root mean square error is obtained at cut off frequency of 25 Hz at various stations.

10. Developed algorithm has been tested for both North South (NS) and East West (EW) component of acceleration records separately. It has been seen that similar frequency dependent attenuation relation and site effect is obtained by using either NS or EW component. Thereby confirming the fact that same frequency dependent quality factor is sufficient to describe the attenuating property in NS and EW component of acceleration records.

11. Frequency dependent S-wave quality factor ($Q_\beta(f)$) and site amplification have been obtained in the Kumaon Himalaya, India using the modified inversion algorithm. Total forty events recorded at sixteen stations located in this region have been used in this work. The final $Q_\beta(f)$ relation is determined by using all values of $Q_\beta(f)$ obtained from inversion of NS and EW component of acceleration record at each station. A regional regression relation of form $Q_o f^n$ is obtained as $Q_\beta(f) = (28\pm2.1)f^{(1.2\pm0.09)}$ in this study. This relation defines the attenuation property of the Kumaon Himalaya. Low value of 'Q_o' and high value of 'n' obtained in the present $Q_\beta(f)$ relation shows that the region is seismically active and characterized by local heterogeneities. Comparison of the obtained relation with the other relation in the seismically active worldwide area revealed that Kumaon is tectonically active region.

12. The three dimensional attenuation structures have been estimated for two different blocks in the Kumaon region using the strong motion data recorded by the Kumaon network at different stations. Attenuation structures have been obtained at different frequencies. These two blocks are overlapping at certain region. The obtained attenuation structures from two different data sets for these two blocks also show similar structures in overlapped section. The study shows that the complete picture of attenuation tomography in the long stretch can be obtained in a region having limited data.

13. The comparison of obtained attenuation structures of Kumaon region is made with the available geological and tectonic units of the region and it is seen that attenuation structures are capable of explaining major tectonic structures of the region.

14. Very few studies have been carried out in the Kumaon Himalaya regarding the attenuation properties of this region. Hence, the present work gives the essential information required for determination of the earthquake source parameters and simulation of strong ground motions.

15. Source parameters of the Sikkim earthquake of magnitude 6.9 (M_w) that occurred on 18 September, 2011 have been computed using the far field strong motion data recorded by Kumaon network. The present study gives seismic moment, stress drop and source radius of the Sikkim earthquake as $(3.2 \pm 0.8) \times 10^{26}$ dyne-cm, 59.2 ±8.8 bars and 13.3 ±0.8 km, respectively.

References

[1] Abdel-Fattah, A. K., 2009, Attenuation of body waves in the crust beneath the vicinity of Cairo Metropolitan area (Egypt) using coda normalization method, Geophys. Jour. Int., 176, 126-134.

[2] Aki, K. and Chouet, B., 1975, Origin of Coda waves: Source, Attenuation and Scattering Effects, J. Geophys. Res., 80, 3322-3342.

[3] Aki, K., 1967, Scaling law of seismic spectrum, Journal of Geophysical Research, 72, 1217-1231.

[4] Aki, K., 1969, Analysis of seismic coda of local earthquakes as scattered waves, J. Geophys. Res., 74, 615–631.

[5] Aki, K., 1980, Attenuation of shear waves in the lithosphere for frequencies from .05 to 25 Hz, Phys. Earth Planet Interiors., 21, 50-60.

[6] Akinci, A., Taktak, A. G. and Ergintav, S., 1994, Attenuation of coda waves in Western Anatolia, Phys. Earth Planet Inter, 87, 155-165.

[7] Anderson, D. L. and Archambeau, C. B., 1964, The anelasticity of the earth, J Geophys., 69, 2071–2084.

[8] Anderson, D. L., Ben-Menahem, A. and Archambeau, C. B., 1965, Attenuation of seismic energy in the upper mantle, J Geophys Res., 70, 1441–1448.

[9] Archambeau, C. and Anderson, D. L., 1963, Inversion of surface wave dispersion data, Intern. Unioun Geod. And Geophys., XIII General Assembly, Berkeley.

[10] Atkinson, G. M. and Mereu, R. F., 1992, The shape of ground motion attenuation curves in Southeastern Canada, Bull. Seismol. Soc. Am., 82, 2014-2031.

[11] Atkinson, G.M. and Boore, D.M., 1995, Ground-Motion Relation for Eastern North America, Bull. Seism. Soc. Am., 85, 17-30.

[12] Atkinson, G.M. and Boore, D.M., 1998, Evaluation of models for earthquake source spectra in eastern North America, Bull. Seism. Soc. Am., 88, 917-934.

[13] Bhattacharya, A.R., 2008, Basement Rocks of the Kumaun - Garhwal Himalaya: Implications for Himalayan Tectonics, I(I), 1-10.

[14] Bilham, R., Gaur, V. K. and Molnar, P., 2001, Himalayan seismic hazard. Science, 293, 1442–1444.

[15] Bindi, D., Parolai, S., Grosser, H., Milkereit, C. and Karakisa, S., 2006, Crustal attenuation characteristics in Northwestern Turkey in the range from 1 to 10 Hz, Bull. Seismol. Soc. Am., 96, 200-214.

[16] Boatwright, J., 1978, Detail spectral analysis of two small New York State earthquakes, Bull. Seism. Soc. Am., 68, 1117–1131.

[17] Boatwright, J., Fletcher, J. B. and Fumal, T. E., 1991, A general inversion scheme for source, site, and propagation characteristics using multiply recorded sets of moderate-sized earthquakes, Bull. Seism. Soc. Am., 81, 1754–1782.

[18] Boore, D. M. and Akkar, S., 2003, Effect of causal and acausal filters on elastic and inelastic response spectra, Earthquake Eng. and Structural Dyn., 32, 1729-1748

[19] Boore, D. M. and Bommer, J. J., 2005, Processing of strong motion accelerograms: needs, options and consequences, Soil Dyn. Earthq. Eng., 25, 93–115.

[20] Boore, D.M. and Atkinson, G.M., 1987, Stochastic prediction of ground motion and spectral response parameters at hard-rock sites in eastern North America, Bull. Seism. Soc. Am., 77, 440-467.

[21] Boore, D.M., 1983, Stochastic simulation of high-frequency ground motions based on seismological models of the radiated spectra, Bull. Seism. Soc. Am., 73, 1865-1894.

[22] Brahma, J., 2012, Estimation of coda wave attenuation quality factor from digital seismogram using statistical approach, Science and Technology, 2(1): 1-7.

[23] Brune, J.M., 1970, Tectonic stress and spectra of seismic shear waves from earthquakes, J. Geophys. Res., 75, 4997-5009.

[24] Brune, J.N., 1971, Correction, J.Geophys. Res., 76, 5002.

[25] Burchfiel, B.C. and Royden, L.H., 1985, North- South extension within the Convergent Himalaya region, Geology, 13, 679-682.

[26] Campbell, K.W., 2001, Strong motion attenuation relations (Draft, Personnel communication).

[27] Canas, J. A., Pujades, L., Badal, J., Payo, G., de Miguel, F., Alguacil, G., Ibanez, J. and Morales, J., 1991, Lateral variation and frequency dependence of coda–Q in the Southern part of Iberia, Geophys. J. Inter., 107, 57-66.

[28] Cantore, L., Oth, A., Parolai, S. and Bindi, D., 2011, Attenuation, source parameters and site effects in the Irpinia-Basilicata region (south Apennines, Italy), J. Seismol., 15, 375-389.

[29] Castro, R. R., Monachesi, G., Trojani, L., Mucciarelli, M. and Frapiccini, M., 2002, An attenuation study using earthquake from 1997 Umbria Marche sequence, J. seismol., 6, 43-59.

[30] Chandra, U., 1978, Seismicity, Earthquake Mechanisms and Tectonics along the Himalayan Mountain Range and Vicinity, Phys. Earth Planet. Int., 16, 109-131.

[31] Chung, T. W. and Sato, H., 2001, Attenuaiton of high frequency P and S waves in the crust of Southeastern South Korea, Bull. Seismol. Soc. Am., 91(6), 1867-1874.

[32] Cooley, J.W. and Tukey, J.W., 1965, An algorithm for machine calculation of complex Fourier series, Math. Comp., 19, 297–301.

[33] Cruz-atienza, V. M., Pacheco, J. F., Singh, S. K., Shapiro, N. M., Valdés, C and Iglesias Mendoza, C., 2001, Size of popocatépetl volcano explosions (1997-2001) from waveform inversion, Geophys. Res. Lett., 28, 4027-4030.

[34] Dasgupta, S., Ganguly, J. and Neogi, S., 2004, Inverted metamorphic sequence in the Sikkim Himalayas: Crystalline history, P-T gradient and implications, Journal of Metamorphic Geology, 22, 395-412.

[35] De, R., 2000, A microearthquake survey at the MBT zone: Sikkim Himalaya, J Geophys. Res., 21, 1–8.

[36] Demets, C., Gordon, R.G., Argus, D. F. and Stein, S., 1990, Current Plate Motions, Geophys. J. Iner., 101, 425-478.

[37] Dimri, V. P., 1992, Deconvolution and inverse theory: application to geophysical problems. Elsevier Science, Amsterdam. 230.

[38] Douglas, J., 2001, A comprehensive worldwide summary of strong-motion attenuation relationships for peak ground acceleration and spectral ordinate (1969 to 2000), Engineering seismology and Earthquake engineering report no. 01-1.

[39] Dunn, J. A., Auden, J. B., Ghosh, A. M. N. and Roy, S. C., 1939, The Bihar–Nepal earthquake of 1934, Geol Surv India Mem., 73, 280.

[40] Dutta, U., Biswas, N. N., Adams, D. A. and Papageorgiou A., 2004, Analysis of S-wave attenuation in South Central Alaska, Bull. Seismol. Soc. Am., 94, 16-28.

[41] Fitch, T.J., 1970, Earthquake Mechanisms in the Himalayan, Burmese and Andaman Regions and Continental Tectonics in Central Asia, J. Geophys. Res., 75, 2699-2709.

[42] Fletcher, J. B., 1995, Source parameters and crustal Q for four earthquakes in South Carolina, Seism. Res. Lett., 66, 44–58.

[43] Ford, S. R., Dauglas, S. D., Mayeda, K., Walter, R. W., malagnini, L. and Philips, S. W., 2008, Regional attenuation in Northern California; A comparision of five IDQ methods, Bull. Seismol. Soc. Am., 98(4), 2033-2046.

[44] Frankel, A., McGarr, A., Bicknell, J., Mori, J., Seeber, L. and Cranswick, E., 1990, Attenuation of high frequency shear waves in the crust: measurements from New York State, South Africa and Southern California, J. Geophys. Res., 96, 6269–6289.

[45] G.S.I., 2000, Seismotectonic atlas of India and its environs. In: Dasgupta, S., Pande, P., Ganguly D., Iqbal, Z., Sanyal, E., Venkatraman, N.V., Dasgupta S., Sural, B., Harendranath, L., Mazumdar, K., Sanyal, S., Roy, A., Das, L.K., Mishra, P.S. and Gupta, H.K (eds) Geol. Soc. India, vol., 43.

[46] Gahalaut, V.K., 2011, M 6.9 September 18, 2011 Sikkim earthquake, Geomatics, Natural Hazards and risk, 2 (4), 325-328.

[47] Gansser, A., 1964, Geology of the Himalayas-Interscience Publishers John Wiley and Sons Ltd., pp. 1—289, London, New York, Sydney.

[48] Geiger, L., 1912, Probability method for the determination of earthquake epicenters from the arrival time only (translated from Geiger's 1910 German article), Bull. St. Louis Univ., 8, 56-71.

[49] Giampiccolo, E., D'Amico S., Patane D. and Gresta S., 2007, Attenuation and source parameters of shallow microearthquakes at Mt. Etna Volcano, Italy. Bull Seimol. Soc. Am., 97, 184-197.

[50] Gitis, V., Yurkov, E., Arora, B. R., Chabak, S., Kumar, N. and Baidya, P., 2008, Analysis of seismicity in North India, Russ. J. Earth. Sci., 10, ES5002, doi: 10.2205/2008ES000303.

[51] Gupta, A. K., Sutar, A. K., Chopra, S., Kumar, S. and Rastogi, B. K., 2012, Attenuation characteristics of coda waves in Mainland Gujarat (India), Tectonophysics, 530–531, 264–271.

[52] Gupta, S. C. and Kumar A., 2002, Seismic wave attenuation characteristics of three Indian regions: a comparative study, Curr. Sci., 82, 407–413.

[53] Gupta, S. C., Singh, V.N. and Kumar, A., 1995, Attenuation of Coda Waves, in the Garhwal Himalaya, India, Phys. Earth Planet. Interiors, 87, 247-253.

[54] Gupta, S. C., Teotia, S. S., Rai, S. S. and Gautam, N., 1998, Coda Q estimates in the Koyna region, India, Pure Appl. Geophys., 153, 713-731.

[55] Hadley, D. M., Helmberger, D. V. and Orcutt, J. A., 1982, Peak acceleration scaling studies, Bull. Seism. Soc. Am., 72, 959–979.

[56] Hanks, T. C. and Kanamori, H., 1979, A moment magnitude scale, J Geophys. Res., 84(B5), 2348-2350.

[57] Hanks, T. C., 1982, f_{max}, Bull. Seism. Soc. Am., 72(6), 1867-1879.

[58] Harris, N., 2007, Channel flow and the Himalayan-Tibetan orogen: a critical review, Jou of Geological soc. London, 164, 511-523.

[59] Hashida, T. and Shimazaki, K., 1984, Determination of seismic attenuation structure and source strength by inversion of seismic intensity data: method and numerical experiment, J. phys. Earth, 32, 299-316.

[60] Hashida, T. and Shimazaki, K., 1985, Seismic tomography: 3-D image of upper mantle attenuation beneath the Kanto district, Japan, Earth and Planet. Science letters, 75(4), 403-409.

[61] Hashida, T. and Shimazaki, K., 1987, Determination of seismic attenuation structure and source strength by inversion of seismic intensity data: Tohoku district, the northeastern Honshu, J. Phys. Earth, 35, 57-92.

[62] Havskov, J., Malone S., McClurg D. and Crosson R., 1989, Coda Q for the state of Washington, Bull. Seis. Soc. Am.,79, 1024-1038.

[63] Haydar, J., Shukri, A. l. and Mitchell, B. J., 1990, Three dimensional attenuation structure in and around the new Madrid seismic zone, Bull. Seismol. Soc. Am., 80, 615–632.

[64] Hazarika, P., Kumar, M. R., Srijayanthi, G., Raju, P. S., Rao, N. P. and Srinagesh, D., 2010, Transverse tectonics in the Sikkim Himalaya: Evidence from seismicity and focal-mechanism data, Bull. Seism. Soc. Am., 100, 1816-1822.

[65] Heim, A. A. and Gansser, A., 1939, Central Himalaya; Geological Observations of the Swiss Expedition 1936, (New Delhi: Hindustan Publishing Corporation), 73, 245.

[66] Hermann, R., 1980, Q estimates using coda of local earthquakes, Bull. Seismol. Soc. Am., 70, 447–468.

[67] Honda, R., Aoi, S., Sekiguchi, H., Morikawa, N., Kunugi, T. and Fujiwara, H., 2005, Ground motion and rupture process of the 2004 mid Niigata Prefecture earthquake obtained from strong motion data of K-NET and KiK-net (from website http://www.k-net.bosai.go.jp/k-net).

[68] Hough, S. E., 1997, Empirical Green's function analysis: taking the next step, J. Geophys. Res., 102, 5374–5384.

[69] Hough, S., Anderson, J. G., Brune, J., Vernon, F., Berger, J., Fletcher, J., Haar, L., Hanks, T. and Baker, L., 1988, Attenuation near Anza, California, Bull. Seism. Soc. Am., 78, 672–691.

[70] Ibanez, J. M., Del Pezzo, E., De Miguel, F., Herraiz, M., Alguach, G. and Morales J., 1990, Depth dependent seismic attenuation in the Granada zone (southern Spain), Bull. Seismol. Soc. Am., 80, 1222–1234.

[71] Ji-chang, F., Song-lin, L., Xiao-ling, L. and Hong-zhao, D., 2001, Three-dimensional Q structure in Jiashi earthquake region of Xinjiang, Acta Seismologica Sinica, 14(6), 611-619.

[72] Jin, A. and Aki, K., 1988, Spatial and temporal correlation between coda Q and seismicity in China. Bull. Seismol. Soc. Am., 78, 741-769.

[73] Johnston, D. H. and Toksöz, M. N., (eds), 1981, Seismic wave attenuation, Society of Exploration Geophysicists, 1– 5.

[74] Joshi, A. and Midorikawa, S., 2004, A simplified method for simulation of strong ground motion using rupture model of the earthquake source, J Seismol, 8, 467–484.

[75] Joshi, A., 2006a, Three dimensional attenuation structure of the central seismic gap region of Himalaya obtained from inversion of seismic intensity data, Curr Sci., 90, 581–585.

[76] Joshi, A., 2006b, Use of acceleration spectra for determining the frequency dependent attenuation coefficient and source parameters, Bull. Seismol. Soc. Am., 96, 2165-2180.

[77] Joshi, A., 2006c, Analysis of strong motion data of the Uttarkashi earthquake of 20th October 1991 and the Chamoli earthquake of 28th March 1999 for determining the mid crustal Q value and source parameters, J Earth Tech., 43, 11–29.

[78] Joshi, A., 2007, Inversion of seismic intensity data for the determination of three-dimensional attenuation structures in the central gap region of Himalayas, Nat Hazards, 43, 129–146.

[79] Joshi, A., Kumar, A., Castanos, H. and Lomnitz, C., 2013, Seismic hazard of the Uttarakhand Himalaya, India, from deterministic modeling of possible rupture planes in the area, International Journal of Geophysics, Vol. (2013), Article ID 825276, 12 pages http://dx.doi.org/10.1155/2013/825276.

[80] Joshi, A., Kumar, P., Mohanty, M., Bansal, A. R., Dimri, V. P. and Chadha, R. K., 2012a, Determination of $Q_\beta(f)$ at different places of Kumaon Himalaya from the inversion of spectral acceleration data, Pure and Applied Geophysics, 169, 1821-1845.

[81] Joshi, A., Kumari, P., Singh, S. and Sharma, M. L., 2012b, Near-field and far-field simulation of accelerograms of Sikkim earthquake of September 18, 2011 using modified semi-empirical approach, Nat Hazards, 64, 1029-1054.

[82] Joshi, A., Mohanty, M., Bansal, A. R., Dimri, V. P. and Chadha, R. K., 2010, Use of spectral acceleration data for determination of three dimensional attenuation structure in the Pithoragarh region of Kumaon Himalaya, J Seismol., 14, 247-272.

[83] Joshi, A., Mohanty, M., Teotia, S.S., Bansal, A. R., Dimri, V. P. and Chadha, R. K., 2009, Crustal Attenuation of Shear waves in Pithoragarh region, J. Ind. Geophys. Union, 13, 137-146.

[84] Kato, H., 1992, Fossa Magna-A masked border region separating southwest and northeast Japan, Bull. Geol. Sur. Jpn., 43, 1–30.

[85] Keilis-Borok, V. I., 1959, On the estimation of the displacement in an earthquake source and of source dimensions, Ann. Geof., 12, 205-214.

[86] Khattri, K. N. and Tyagi, A. K., 1983, Seismicity patterns in the Himalayan plate boundary and identification of the areas of high seismic potential. Tectonophysics, 96, 281–297.

[87] Kim, K. D., Chung, T. W. and Kyung, J. B., 2004, Attenuation of high frequency P and S waves in the crust of Choongchung Provinces, Central South Korea, Bull. Seismol. Soc. Am., 94(3), 1070-1078.

[88] Knopoff, L., 1964, Q, Reviews of Geophysics, 2, 625-660.

[89] Kobayashi, Y., 1983, Initiation of plate subduction, Earth-Monthly, 5, 510–514 (in Japanese).

[90] Kumar, C. H. P., Sharma, C. S. P., Sekhar, M. and Chadha, R. K., 2007, Attenuation studies based on local earthquake coda waves in the Southern Indian Peninsular shield, Natural Hazard, 40(3), 527-536.

[91] Kumar, D., Sarkar, I., Sri Ram, V. and Khattri, K. N., 2005a, Estimation of the source parameters of the Himalaya earthquake of October 19, 1991, average effective shear wave attenuation parameter and local site effects from accelerograms, Tectonophysics, 407, 1–24.

[92] Kumar, N., Parvez, I. A. and Virk, H. S., 2005b, Estimation of coda wave attenuation for NW Himalayan region using local earthquakes, Physics of the earth and planetary interiors, 151, 243-258.

[93] Kuo, C. H., Wen, K. L., Hsieh, H. H., Lin, C. M., Chang., T. M. and Kuo, K. W., 2012, Site classification and V_s30 estimation of free-field TSMIP stations using the logging data of EGDT, Engineering Geology, 129-130, 68-75.

[94] Lancose, C., 1961, Linear differential operators, D. Van Nostrand Co., Landon.

[95] Langston, C. A., 1979, Structure under mount Rainer, Washington, inferred from teleseismic body waves, J Geophys Res, 84, 4749–4762.

[96] Latchman, J. L., Ambeh, W. B. and Lynch, L. L., 1996, Attenuation of seismic waves in the Trinnidad and Tobago area, Tectonophysics, 253, 111-127.

[97] Lee, W. H. K., and Stewart, S. W., 1981, Principles and applications of microearthquake networks. Academic, New York, 293.

[98] Lee, W. K. H. and Lahr, J. C., 1972, HYPO71: A computer program for determination of hypocenter, magnitude, and first motion pattern of local earthquakes, Open File Report, U.S. Geological Survey 100pp.

[99] Lermo, J. and Chávez-García, F., 1993. Site effect evaluation using spectral ratios with only one station, Bull. Seismol. Soc. Am., 83, 1574–1594.

[100] Levenberg, K., 1944, A method for the solution of certain non-linear problems in least squares, Q Appl. Math., 2, 164–168.

[101] Luzon, F., Gil-Zepeda, S. A., Sanchez-Sesma, F. J. and Ortiz-Aleman, C., 2004, Three-dimensional simulation of ground motion in the Zafarraya Basin (Southern Spain) up to 1.335 Hz under incident plane waves, Geophys. Journal International, 156(3), 584-594.

[102] Maeda, T. and Sasatani, T., 2006, Two layer Q_s structure of the slab near the Southeren Kurlie trench, Earth Plants space., 58, 544-553.

[103] Maeda, T., Ichiyanagi M., Takahashi H., Honda R., Yamaguchi T., Kasahara M. and Sasatani T., 2008, Source parameters of the 2007 Noto Hanto earthquake sequence derived from strong motion records at temporary and permanent stations, Earth Planets space, 60, 1011-1016.

[104] Mamada, Y. and Takenaka, H., 2004, Strong attenuation of shear waves in the focal region of the 1997 northwestern Kagoshima earthquakes, Japan, Bull. Seismol. Soc. Am., 94(2), 464-478.

[105] Mandal, H. S., Khan, P. K. and Shukla, A. K., 2013, Shear wave attenuation characteristics over the central India tectonic zone and its surroundings, Jou. of Asian Earth Sciences, 73, 440-451.

[106] Mandal, P. and Rastogi B. K., 1998, A frequency-dependent relation of coda Q_c for Koyna Warna region, India, Pure Appl. Geophys., 153, 163-177.

[107] Mandal, P., Padhy, S., Rastogi, B. K., Satyanarayana, V. S., Kousalya, M., Vijayraghavan, R. and Srinvasa, A., 2001, Aftershock activity and frequency dependent low coda Qc in the epicentral region of the 1999 Chamoli earthquake of Mw 6.4, Pure Appl. Geophys., 158, 1719–1735.

[108] Matsunami, K., 1991, Laboratory tests of excitation and attenuation of coda waves using 2-d models of scattering media, Phys. Earth planet. Inter., 67, 36-47.

[109] Midorikawa, S., 1980, Prediction of intensity distribution due to major earthquakes with regard to fault rupture and site ground conditions. In: Proc. 8th symposium on ground vibration, architectural institute of Japan, pp. 59–64 (In Japanese).

[110] Mitchell, B. J., 1995, Anelastic structure and evolution of the continental crust and upper mantle from seismic surface wave attenuation, Rev Geophys, 33, 441–462.

[111] Molnar, P. and Chen, W. P., 1983, Focal depths and Fault-Plane Solutions of Earthquakes under the Tibetian Plateau, J. Geophys. Res., 88, 1180-1196.

[112] Mukhopadhyay, S., Sharma, J., Massey, R. and Kayal, J. R., 2008, Lapse time dependence of Coda Q in the source region of the 1999 Chamoli earthquake, Bull. Seismol. Soc. Am., 98(4), 2080-2086.

[113] Nakamura, K., 1983, Possible nascent trench along the eastern Japan Sea as the convergent boundary between Eurasian and North American plates, Bull. Earthq. Res. Inst. Univ. Tokyo, 58, 711–722 (in Japanese).

[114] Nakamura, R. and Uetake, T., 2004, Three dimensional attenuation structure beneath the Tohoku district by using seismic strong motion records, J. of the Seismol. Soc. of Japan, 56(4), 447-455.

[115] Nakamura, R., Satake, K., Toda, S., Uetake, T. and Kamiya, S., 2006, Three-dimensional attenuation (Qs) structure beneath the Kanto district, Japan, as inferred from strong motion records. Geoph. Research Lett., 33, L21304, doi:10.1029/2006GL027352.

[116] Nakamura, R., Shimazaki, K. and Hashida, T., 1994, 3-D attenuation structure beneath the Japanese islands by tomographic inversion of seismic intensity data and predicting JMA seismic intensity distributions in a broad arca. Zisin (J. Seism. Soc. Japan), 47, 21-32.

[117] Nakamura, R., Shimazaki, K. and Hashida, T., 1995, Effects of 3-D attenuation structure on seismic ground motions in Japan, Proceedings of the 10th European Conference on Earthquake Engineering, Balkema, 393-398.

[118] Nakamura, Y., 1988, Inference of seismic response of surficial layer based on microtremor measurement. Quarterly Report on Railroad Research 4, Railway Technical Railway Institute, 18-27 (In Japanese).

[119] Nakata, T., 1989, Active faults of the Himalaya of India and Nepal. In Tectonics of the Western Himalaya (Malinconico, L. L., Jr, and Lillie, R. J., eds.) pp. 232, 243-264. Geol. Soc. America Spl. Paper (Geological Society of America, Colorado, 1989).

[120] Nath, S. K. and Thingbaijam, K. K. S., 2009, Seismic hazard assessment-a holistic microzonation approach, Natural hazards and earth system sciences, 9, 1445-1459.

[121] Nath, S. K., Sengupta, P., Sengupta, S. and Chakrabarti, A., 2000, Site response estimation using strong motion network : A step towards microzonation of the Sikkim Himalayas, Current science, 79, 1316-1326.

[122] Nath, S. K., Vyas, M., Pal, I., Singh, A. K., Mukherjee, S. and Sengupta, P., 2005, Spectral attenuation models in the Sikkim Himalaya from the observed and simulated strong motion events in the region, Current science, 88 (2), 295-303.

[123] Neogi, S., Dasgupta, S. and Fukuoka, M., 1998, High P-T polymetamorphic, dehydration melting and generation of migmatites and granites in the Higher Himalayan Crystalline, Sikkim, India, Journal of Petrology, 39, 61-99.

[124] Ni, J., and Barazangi, M., 1984, Seismotectonics of the Himalayan Collision Zone: Geometry of the Underthrusting Indian Plate beneath the Himalaya, J. Geophys. Res., 89, 1147-1163.

[125] Novelo-Casanova, D. A. and Martinez-Bringas, A., 2005, A seismic attenuation zone below Popocatepetl vocano inferred from coda waves of local earthquakes, Geofisica Internacional, 44(2), 177-186.

[126] Padhy, S., 2009a, Characteristic of body wave attenuations in the Bhuj crust, Bull. Seismol. Soc. Am., 99(6), 3300-3313.

[127] Padhy, S., 2009b, Inversion of seismogram envelopes using a multiple isotropic scattering model in Garhwal Himalaya, Bull. Seismol. Soc. Am., 99(2A), 726-740.

[128] Padhy, S., Subhadra N. and Kayal, J., R., 2011, Frequency dependent attenuation of body and coda waves in the Andaman Sea Basin, Bull. Seismol. Soc. Am., 101(1), 109–125.

[129] Papageorgiou, A. and Aki, K., 1983 A specific barrier model for the quantitative description of inhomogeneous faulting and the prediction of strong ground motion, Part 1. Description of the model, Bull. Seismol. Soc Am., 73, 693-722.

[130] Paul, A., Gupta, S. C. and Pant, C. C., 2003, Coda Q estimates for Kumaon Himalaya, Proc. Ind. Acad. Sci. (Earth Planet. Sci.), 112, 569–576.

[131] Phinney, R. A., 1964, Structure of the earth's crust from spectral behavior of long period body waves, J Geophys Res., 69, 2997–3017.

[132] Polatidis, A., Keratzi, A, Hatzidimitriou, P. and Margaris B., 2003, Attenuation of shear-waves in the back arc region of the Hellenic arc for frequencies from 0.6 and 16 Hz, Tectonophysics, 367(1-2), 29-40.

[133] Press, W. H., Teukolsky, S. A., Vetterling, W. T. and Flannery, B.P., 1992, Numerical Recepies, Cambridge University Press.

[134] Pujades, L., Canas, J. A., Egozcue, J. J., Puigvi, M. A., Pous, J., Gallart, J., Lana, X. and Casas, A., 1991, Coda Q distribution in Iberian Peninsula, Geophys. J. Int., 100, 285–301.

[135] Pulli, J. J., 1984, Attenuation of coda waves in New England, Bull. Seismol. Soc. Am., 74, 1149-1166.

[136] Raghukanth, S. T. G. and Somala, S. N., 2009, Modelling of strong motion data in Northeastern India; Q, stress drop and site amplification, Bull. Seismol. Soc. Am., 99(2A), 705-725.

[137] Rahimi, H., Hamzehloo, H. and Kamalian, N., 2009, Estimation of Coda and Shear wave attenuation in the volcanic area in SE Sabalan Mountain, NW Iran, Acta Geophysica, 58(2), 244-268.

[138] Raju, P. S., Rao, N. P., Singh, A. and Kumar, M. R., 2007, The 14 February 2006 Sikkim earthquake of magnitude 5.3, Current Science, 93, 6.

[139] Rastogi, B. K., 1974, Earthquake Mechanisms and Plate Tectonics in the Himalayan Region, Tectonophysics, 21, 47-56.

[140] Rautian, T. G. and Khalturin, V. I., 1976, Spectral structure of the coda of local earthquakes as an instrument of investigation of the source radiation, Doklady Acad. Sci. USSR 226, (in Russian), 566-569.

[141] Rautian, T. G., 1976, Role of source and medium in the formation of seismic oscillations near local earthquakes, Investigations of the Physics of Earthquakes, Nauka Publishing House, Moscow, (in Russian), 27-55.

[142] Rautian, T.G. and Khalturin, V.I., 1978, The use of coda for determination of the earthquake source spectrum. Bull. Seismol. Soc. Am., 68: 923—948.

[143] Roecker, S.W., Tucker, B., King, J. and Hartzfeld, D., 1982, Estimates of Q in central Asia as a function of frequency and depth using the coda of locally recorded earthquakes, Bull. Seismol. Soc. Am., 72, 129-149.

[144] Ruff, L. J., 1999, Dynamic stress drop of recent earthquakes: Variations within subduction zones, Pure and applied Geophysics, 154(1999), 409-431.

[145] Sahin, S., 2008, Lateral variations of coda Q and attenuation of Seismic waves in Southwest Anatolia, J. of Seismol., 12, 367-376.

[146] Sarker, G. and Abers, G. A., 1998a, Comparison of seismic body wave and coda wave measures of Q, Pure Appl. Geophys., 153, 665–683.

[147] Sarker, G. and Abers, G. A., 1998b, Deep structures along the boundary of a collisional belt: attenuation tomography of P and S waves in the Greater Caucasus, Geophys. J. Int., 133, 326-340.

[148] Sato, H., 1977, Energy propagation including scattering effects single isotropic scattering approximation, J. Phys. Earth, 25, 27-41.

[149] Satoh, T., Kawase, H. and Sato, T., 1997, Statistical spectral model of earthquakes in the eastern Tohoku district, Japan, based on the surface and borehole records observed in Sendai, Bull. Seism. Soc. Am., 87, 446–462.

[150] Satyabala, S. P. and Gupta, H. K., 1996, Is the Quiescene of Major Earthquakes ($M \geq 7.5$) since 1952 in the Himalaya and Northeast India real?, Bull. Seismol. Soc. Am., 86, 1983-1986.

[151] Schlotterbeck, B. A. and Abers, G. A., 2001, Three-dimensional attenuation variations in southern California, J. Geophys. Res., 106(B12), 30,719-30,735.

[152] Seeber, L. and Armbruster, J. G., 1984, Some Elements of Continental Subduction along the Himalayan Front, Tectonophysics, 92, 335-367.

[153] Seeber, L., Armbruster, J. G. and Quittmeyer, R.C., 1981, Seismicity and continental collision in the Himalayan arc. In Geodynamics Series: Zargos, Hindukush, Himalaya, Geodynamic Evolution, (Gupta, H. K., and Delany, F. M., eds.) American Geophysical Union, Washington, 3, 215-242.

[154] Sekiguchi, S., 1991, Three-dimensional Q structure beneath the Kanto-Tokai District, Japan, Tectonophysics, 195, 83–104.

[155] Shakal, A. F., Huang, M. J. and Graizer, V. M., 2004, CSMIP strong motion data processing, Proc. International workshop on strong motion record processing, May 26-27, 2004, COSMOS, Richmond California.

[156] Shapiro, N. M., Singh, S. K., Iglesias-mendoza, A., Cruz-atienza, V. M. and Pacheco, J. P., 2000, Evidence of low q below popocatépetl volcano, and its implication to seismic hazard in Mexico City, Geophys. Res. Lett., 27, 2753-2756.

[157] Sharma B., Teotia S.S., Kumar, D. and Raju, P. S., 2009, Attenuation of P- and S- waves in the Chamoli Region, Himalaya, India, Pure and Applied Geophysics, 166, 1949-1966.

[158] Sharma B., Teotia, S. S. and Kumar, D., 2006, Frequency Dependent attenuation of high frequency P S waves in the upper crust of Garhwal, Himalaya, 6th International conference and Exposition on Petroleum Geophysics, Kolkata 2006.

[159] Sharma, B., Gupta, A. K., Devi, K., Kumar, D., Teotia, S. S. and Rastogi, B. K., 2008, Attenuation of high frequency seismic waves in Kachchh region, Gujrat, India, Bull. Seism. Soc. Am., 98, 2325-2340.

[160] Sharma, B., Teotia, S. S. and Kumar, D., 2007, Attenuation of P, S and coda waves in Koyna region, India, J. Seismol., 11, 327-344.

[161] Sharma, M. L. and Wason, H. R., 1994, Occurrence of low stress drop earthquakes in the Garhwal Himalaya region, Phys. Earth Planet Interior, 34, 159-172.

[162] Singh, C., Bharathi V. K. S. and Chadha, R. K., 2012a, Lapse time and frequency-dependent attenuation characteristics of Kumaun Himalaya, Jour. Of Asian Earth sciences, 54-55, 64-71.

[163] Singh, C., Singh, A., Bharathi V. K. S., Bansal, A. R. and Chadha, R. K., 2012b, Frequency-dependent body wave attenuation characteristics in the Kumaun Himalaya, Tectonophysics, 524-525, 37-42

[164] Singh, P., Tripathi, J. N. and Kumar, S., 2012c, Quality factor of seismic coda waves in Garhwal Himalayas, International journal of civil engineering and Technology, 3(2), 279-291.

[165] Singh, S. K., Ordaz, M., Dattatrayam, R. S. and Gupta, H. K., 1999, A spectral analysis of the 21 May 1997, Jabalpur, India, earthquake (M w = 5.8) and estimation of ground motion from future earthquakes in the Indian shield region, Bull. Seism. Soc. Am., 89, 1620-1630.

[166] Stephens, C. D. and Boore, D. M., 2004, ANSS/NSMP strong motion record processing and procedures, Consortium of Organization from Strong Motion Observation Systems, International workshop proceeding.

[167] Takeuchi, A., 2008, Duplex Stress Regime in the North Fossa Magna, Central Japan, Bull. Earthq. Res. Inst. Univ. Tokyo, 83, 155-162.

[168] Teng, T. L., 1968, Attenuation of body waves and the Q structure of the mantle, J Geophys Res, 73, 2198–2208.

[169] The Headquarters for Earthquake Research Promotion, 2005, National Seismic Hazard Maps for Japan, pp44.

[170] Tripathi, J. N., Singh, P. and Sharma, M. L., 2012, Variation of seismic coda wave attenuation in the Garhwal region, Northwestern Himalaya, Pure appl. Geophys., 169 (2012), 71-88.

[171] Tsumura, N., Hasegawa, A. and Horiuchi, S., 1996, Simultaneous estimation of attenuation structure, source parameters and site response spectra application to the northeastern part of Honshu, Japan, Physics of the Earth and Planetary Interiors, 93, 105-121.

[172] Tsumura, N., Matsumoto, S., Horiuchi, S. and Hasegwa, A., 2000, Three dimensional attenuation structure beneath the northeastern Japan arc estimated from spectra of small earthquakes, Tectonophysics, 319, 241-260.

[173] Umino, N. and Hasegawa, A., 1984, Three dimensional Qs structure in the northeastern Japan arc, Zisin (J Seismol Soc Jpn), Ser 2 37, 217–228.

[174] Valdiya, K. S., 1980, Geology of Kumaun Lesser Himalaya, Interim Record: Dehradun, Wadia Institute of Himalayan Geology, 289p.

[175] Valdiya, K.S., 1981, Tectonics of the central sector of the Himalaya. In Geodynamic series: Zargos, Hindukush, Himalaya, Geodynamic evolution, (Gupta, H. K., and Delany, F. M., eds.) American Geophysical Union, Washington, 3, 87-110.

[176] Valdiya, K.S., 1999, Fast uplift and geomorphic development of the western Himalaya in quaternary period. In Geodynamics of NW Himalaya Gondwana Research Group Memoir (eds) A. K. Jain and Manickavasagam, 179-18.

[177] Ward, R. W. and Young, C. Y., 1980, Mapping seismic attenuation within geothermal systems using teleseismics with application to the Geysers-Clear Lake region, J Geophys Res, 85, 5227–5236.

[178] Wells, L. D. and Coppersmith, K. J., 1994 New Empirical Relationships among Magnitude, Rupture Length, Rupture Width, Rupture Area and Surface Displacement, Bull. Seismol Soc. Am., 84, 974–1002.

[179] Wen, K. L., 1994, Non-linear Soil Response in Ground Motions, Earthq. Eng. Struct. Dyn., 23(6), 599-608.

[180] Wiggins, R. A., 1972, The general linear inverse problem: implication of surface waves and free oscillations for earth structure, Rev Geophys. Space Phys., 10, 251–285.

[181] Wilson, T. and Kato, H., 1995, Gravity Model studies of the Northern Fossa Magna: Central Honshu, Japan, Bull. of Geological Survey of Japan, 46(1), 1-22.

[182] Wu, R. S., 1985, Multiple scattering and energy transfer of seismic waves-seperation of scattering effect from intrinsic attenuation-I. Theoretical modeling, Geophys. J.R. Astr. Soc., 82, 57-80.

[183] Yabe, H., 1918, Itoigawa-Shizuoka Tectonic Line, Gendai-no-Kagaku, 6, 147– 150 (in Japanese).

[184] Yoshimoto, K., Fujisawa, H., Okada, T., Umino, N., Hasegawa, A., Obara, K., Shiomi, K., Tsukahara, H., Okamoto, S., Kawanaka, T., Sato, H., Nishimura, T., Sato, H. and

Ohtake, M., 2004, Moho and Philippine Sea plate structure beneath central Honshu Island, Japan, from teleseismic receiver functions, Earth Planets Space, 56, 1271-1277.

[185] Young, C. Y. and Ward, R. W., 1980, Three dimensional Q model of the Coso Hot springs known geothermal resource area, J Geophys Res., 85, 2459–2470.

[186] Yu, G., Khattri, K. N., Anderson, J. G., Brune, J. N. and Zeng, Y., 1995, Strong ground motion from the Uttarkashi earthquake, Himalaya, India, earthquake: comparison of observations with synthetics using the composite source model, Bull. Seism. Soc. Am., 85, 31–50.

[187] Zelt, B. C., Dotzev, N. T., Ellis, R. M. and Roger, G. C., 1999, Coda Q in Southwestern British Columbia, Canada, Bull. Seismol. Soc. Am., 89, 1083-1093.

Websites used:

http://earthquake.usgs.gov
http://www.globalcmt.org
http://www.glgarcs.net
http://www.kik.bosai.go.jp